1988

Electromechanical modeling, performance testing, and design of piezoelectric polymer film ultrasound transducers

Lewis Frederick Brown
Iowa State University

Order Number 8825903

Electromechanical modeling, performance testing, and design of piezoelectric polymer film ultrasound transducers

Brown, Lewis Frederick, Ph.D.

Iowa State University, 1988

U·M·I
300 N. Zeeb Rd.
Ann Arbor, MI 48106

Electromechanical modeling, performance testing, and design of piezoelectric polymer film ultrasound transducers

by

Lewis Frederick Brown

A Dissertation Submitted to the
Graduate Faculty in Partial Fulfillment of the
Requirements for the Degree of
DOCTOR OF PHILOSOPHY

Departments: Electrical Engineering and Computer Engineering
Biomedical Engineering
Co-majors: Electrical Engineering
Biomedical Engineering

Approved:

Signature was redacted for privacy.
In Charge of Major Work

Signature was redacted for privacy.
For the Major Departments

Signature was redacted for privacy.
For the Graduate College

Iowa State University
Ames, Iowa

1988

TABLE OF CONTENTS

I. INTRODUCTION

The theory and application of ultrasound for characterizing structure is becoming an increasingly important tool in medicine and engineering. The purpose of this research was to provide new insight into the electromechanical performance of a new class of ultrasound transducer materials--piezoelectric polymer films. Although piezoelectricity was discovered in certain polymer films nearly twenty years ago, it hasn't been until recently that their material properties have been enhanced for broadband ultrasound applications of special interest in medicine and engineering.

A. Transducer Requirements for Ultrasound Characterization

Whether a doctor wishes to use ultrasound to characterize the tissue of a patient's liver, or a materials scientist wishes to characterize defects in a metal casting, the basic requirements for the ultrasound transducer are similar. Although the frequencies of interest may differ slightly, both applications typically require a transducer which is capable of producing short pulses of acoustic energy. A target of interest can be better characterized by using a short, ring-free acoustic pulse. Thus, one requirement of transducers for such applications is that they must have a broadband frequency response. That is, they must be

capable of producing and responding to acoustic waveforms over a broad frequency range.

A simple experiment can be used to demonstrate the advantage of short acoustic pulses over long pulses for measuring the thickness of a layer. The layer of interest in this example was a 0.8 mm thickness copper plate submerged in an ultrasound scanning tank, however, it could have been a layer of fat or connective tissue in a patient. In this demonstration, two different ultrasound transducers were submerged and focussed on the copper plate, and the return echoes were acquired with a high speed data acquisition system. Probe A was a narrowband transducer which produces only "long" acoustic pulses, where as probe B was capable of producing very short pulses. Figure 1.1 shows a comparison of the return echoes obtained with the two transducers.

The figure shows that the return echo from probe A appears to be a single very long waveform and contains no useful information concerning the thickness of the copper plate. However, the entire acoustic pulse produced by probe B was reflected back from the front surface of the plate before the reflection from the opposite side of the plate was returned. Thus, a set of returning echoes is seen. By knowing the speed of sound in copper, the thickness of the

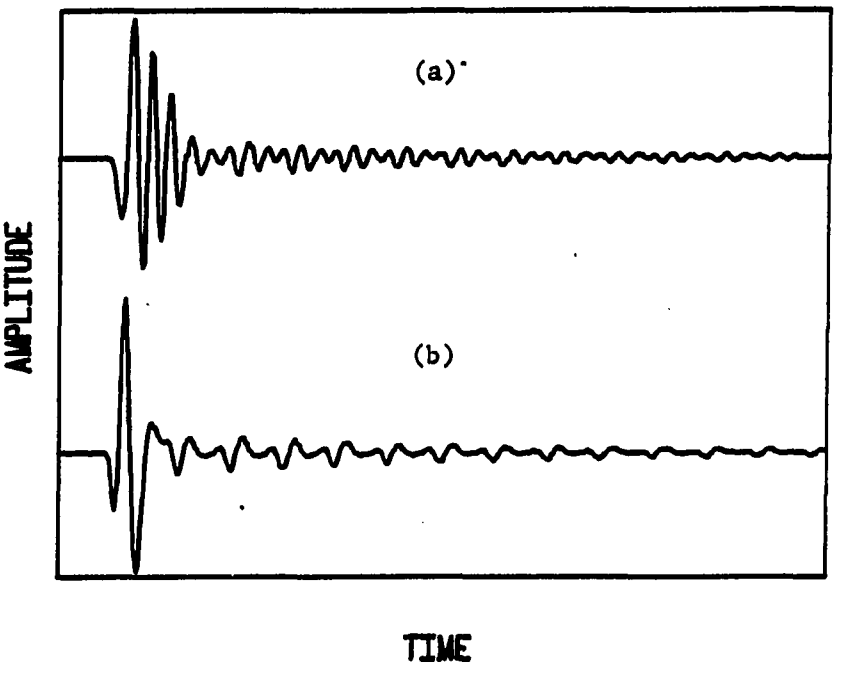

FIGURE 1.1. Return echoes from the thin copper plate for (a) narrowband transducer probe A, and (b) broadband transducer probe B

layer could be easily computed. Notice from Figure 1.1 that the acoustic pulse produced by probe A actually propagates over a longer distance than the thickness of the copper layer of interest. It is therefore impossible to accurately detect or measure thin layers unless the acoustic waveform is much shorter than the layer of interest.

Another important requirement for ultrasound transducers is a close match of the acoustic properties (sound velocity and density) of the transducer material and the medium in which the ultrasound measurements are made.

Ideally, a "perfect" transducer for analyzing biological tissue would be made from a piezoelectric material of the same density and sound velocity as the tissue. Under such matched conditions there would be lossless transmission and reception of acoustic waves into the tissue. Any acoustic mismatch in the properties results in energy losses and thus, inefficient coupling of the acoustic pulse to and from the target. If the mismatch is severe, nearly all of the acoustic energy produced by the transducer may be "wasted". It is apparent then that a second requirement for a useful transducer is a close match of its acoustic properties to the medium in which it is used. Until recently, most of the piezoelectric materials available for ultrasound transducers had neither a natural broadband frequency response nor acoustic properties that closely match tissue or water.

B. A New Class of Piezoelectric Materials

Virtually all of the naturally occurring piezoelectric transducer materials (i.e., quartz) have properties that are not ideally suited for characterizing structure in tissues and water. Manmade piezoelectric ceramic materials are the most frequently used ultrasound transducer materials today. However, these ceramics present many transducer design problems since they have an inherently narrowband frequency

response and offer poor acoustic matching to tissue and water.

Recently however, a newly developed class of piezoelectric materials is gaining an increasing scientific interest. Manmade piezoelectric polymer films can be made which have a "natural" broadband frequency response and closer acoustic property matching to tissue and water, than any previously known materials. Although the new polymer films possess some exciting properties for ultrasound transducers, relatively little research attention has been given to modeling the electromechanical acoustic behavior of these materials so little is known about developing their full potential. Because their piezoelectric and material properties are so unlike previously studied transducer materials, new research is necessary to fully exploit their future role in ultrasound.

Some obvious scientific questions come to mind concerning these polymer films because of their broadband frequency response and close acoustic matching to tissue and water. What physical properties of the polymers are responsible for these "natural" desired transducer characteristics? Is it possible to develop a model for a piezoelectric polymer film transducer that accurately predicts its theoretical acoustic performance? Given such a model, how well can one simulate

actual ultrasound transducer performance under controlled experimental conditions? Could new piezoelectric polymer film transducers permit ultrasonic characterization that is equal or better than the presently used ceramics? Could advances in polymer film technology lead to new innovations in ultrasound transducer applications? The answers to these questions were the heart of this research work.

C. The Scope of This Work

In the interest of learning more about the new piezoelectric films and their possible role in ultrasound, this research focussed on three main topics. Those topics are (1) electromechanical modeling, (2) computer simulation of acoustic performance, and (3) design of broadband ultrasound transducers with piezoelectric polymer films. This research represents new engineering work with a class of exciting new transducer materials that the author believes will alter the future course of ultrasound as a tool in medicine and engineering. For that reason, every effort has been made to construct this dissertation as a "self-contained" reference for the subject. Not all of the background physics and related theory are discussed, but a sufficient review of the most relevant background material is presented in Chapter II.

Chapter III discusses the development of electromechanical circuit models for the piezoelectric polymer films. This chapter discusses a derived method for determining the frequency dependent lossy properties of the polymers--an important consideration for any meaningful understanding of their theoretical performance. Several circuit models are then derived for use in predicting electrical input impedance and acoustic performance of piezoelectric polymer film transducers.

Chapter IV describes a method for implementing the electromechanical models in an interactive design/simulation computer program. Analysis and design applications of such a program are discussed.

The actual design and testing of broadband piezoelectric polymer film transducers is presented in Chapter V. The experimental development of high performance ultrasound probes is detailed. Test results are given which compare the predicted and actual acoustic performance of the probes.

Chapter VI demonstrates the power of this research by applying the results to the design of piezo film ultrasound transducers with enhanced bandwidth and sensitivity.

Copies of all computer programs used in this research are contained in the final chapters (appendices) of this dissertation.

II. REVIEW OF ULTRASOUND PHYSICS AND CLASSICAL WORK

The study of the physics of ultrasound transducers has been of great interest since early sonar research. This chapter will review the most relevant background material needed to understand the development and significance of this research work. A review of the basic physics of piezoelectricity and ultrasound transducers is presented in the first two sections. Next, a review of classical transducer modeling techniques is discussed. A section is also devoted to describing the development, theory of operation, and properties of piezoelectric polymer films. In the last section, limitations of previous electromechanical modeling techniques and the need for this research are presented.

A. Review of Basic Ultrasound Transducer Physics

To understand the need for this research, it is necessary to review some of the fundamentals of piezoelectricity, transducer theory, and ultrasonic fields. Some typical applications for ultrasound transducers are also discussed.

1. Piezoelectricity

The piezoelectric (pressure-electric) effect is the most significant physical principle involved in ultrasound theory. Pierre and Jacques Curie are credited with the

discovery of piezoelectricity in the 1880s (Pennwalt, 1983). The piezoelectric effect is the name given to the phenomenon whereby certain crystalline materials physically deform when subjected to an electric field, and conversely, become electrically polarized when subjected to a mechanical stress. From their discovery, early transducers were constructed from natural piezoelectric crystals such as quartz, tourmaline, and Rochelle salt. Wilhelm Einthoven's famous electrocardiograph recorder, invented at the turn of the century, used a quartz piezoelectric transducer for the recording device--a string galvanometer (Cromwell et al., 1980).

Most crystalline materials are isotropic. That is, their atomic structure is symmetric in all directions and there is no net electric dipole moment. Piezoelectric crystallines, on the other hand, are nonisotropic. There is at least one axis in the crystal whereby the atomic arrangement varies with position. These materials possess a net electric dipole moment which, in the presence of an external electric field, can react causing mechanical deformation.

A significant event occurred in 1955 when piezoelectricity was discovered in polarized solid solutions of manmade ceramics (Wells, 1969). When properly prepared, the ceramics (lead zirconate titanates, or PZTs) possess very

strong piezoelectric properties. These manmade piezoelectric ceramics are ferroelectric. Their net electric dipole moment and thus, piezoelectric properties, are lost at temperatures greater than a threshold value called the Curie Temperature. When heated above the Curie temperature their crystalline structure undergoes an atomic rearrangement and the piezoelectric properties are then destroyed. PZTs have a high Curie temperature (typically greater than 300°C) making them well suited for many harsh environments (Wells, 1977).

In their "raw" form, PZTs have no piezoelectric properties--they must be properly polarized to be left with piezoelectric activity. In the unpolarized state, the many electric dipoles within the atomic crystalline structure are randomly oriented as shown in Figure 2.1.

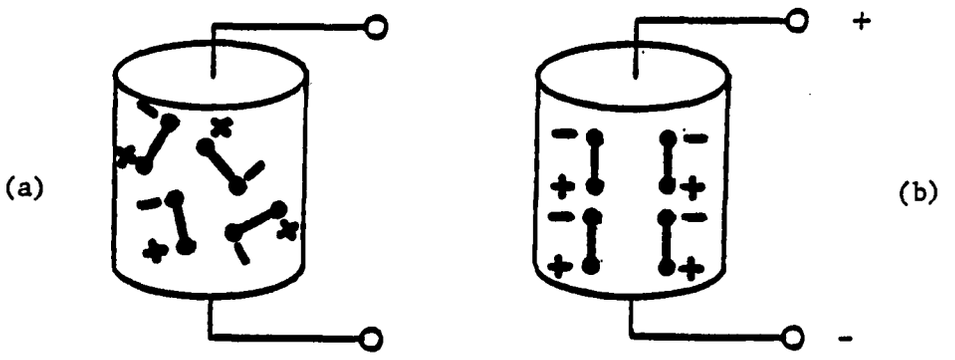

FIGURE 2.1. Cylinders of PZT material: (a) unpolarized and (b) polarized

The random orientation of the dipoles in the unpolarized material gives a net electric dipole moment of zero. To impart a nonzero net dipole moment, the material is polarized (poled) by heating it to near its Curie temperature in the presence of a strong electric field. The presence of the electric field causes the internal dipoles to line up as seen in the previous figure. If the electric field is maintained while the ceramic is slowly cooled, the dipoles have great difficulty returning to their original random orientation and a net electric dipole moment is thus maintained. As long as the temperature of the poled material is maintained below the Curie temperature, the piezoelectric properties will remain intact for many years.

If a cylindrical disk of piezoelectric material is stressed, the crystal structure is distorted, giving rise to a shift of the dipole moment and redistribution of the charged elements of the crystalline lattice. The result is the deposition of charge on the surface of the material which causes a voltage potential to appear across the crystal. The polarity of the voltage depends on the relationship between the material's polarization axis and the direction of the applied stress. If such a disk is compressed, the polarity of the developed surface voltage will be the same as that of the material's poling voltage. If elonga-

tion of the material occurs, a voltage of opposite polarity will be developed. Conversely, the presence of an electric field of the same/reverse polarity as the material's poling voltage will cause the disk to elongate/compress. The effects are shown in Figure 2.2 where V represents the applied (or produced) terminal voltage across the disk.

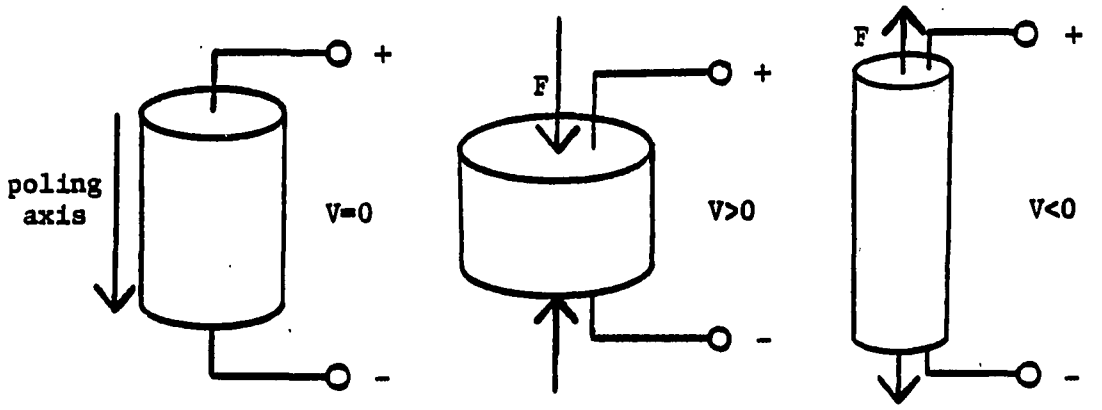

FIGURE 2.2. The effects of electric field polarity on a cylinder of piezoelectric material

In the presence of a time-varying electric field, the disk will likewise elongate/compress with time. Thus, a piezoelectric material is capable of converting (transducing) electrical/mechanical energy to mechanical/electrical energy.

2. Transducers

To make use of the properties of a piezoelectric material, a device (transducer) must be constructed which permits the desired conversion of electromechanical energy.

Electrode layers are usually deposited on opposite faces of the material to permit either the application of a desired electric field, or the means for measuring the voltage resulting from an applied stress. The conductive layers are typically applied by means of vacuum deposition, evaporation, or sputtering.

Most ultrasound transducers are fabricated from disk-shaped piezoelectric ceramic elements. The thin electrode layers at the ends of the disk are used for electrical connection to measuring devices. Normally only one end of the transducer is used for measurements (front) while the other end (rear) is bonded to a desirable backing material.

When a time-varying voltage is applied to the electrodes, the ends of the transducer move inward and outward, causing longitudinal sound waves to be launched. It is usually desirable to absorb those waves that leave the back of the transducer element to prevent unwanted reflections from interfering with the activity at the front face of the transducer. Thus an acoustic absorbing material is typically placed over the rear face of the transducer. The study of appropriate backing materials has been of great interest to many researchers (Kossoff et al., 1965; Kossoff, 1966). Figure 2.3 shows a sketch of the cross section of a typical PZT ultrasound transducer probe.

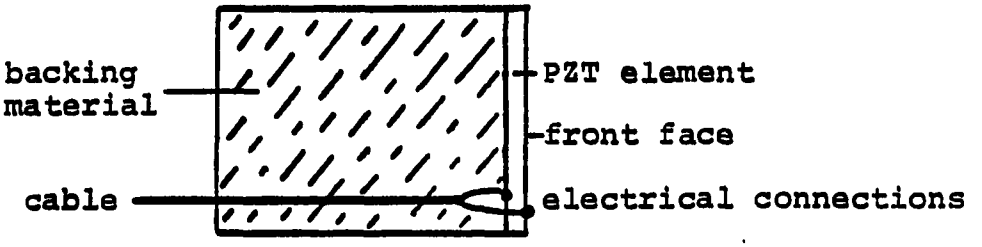

FIGURE 2.3. Cross section of a typical PZT ultrasound transducer

A great deal of technical detail must be given for the design of useful ultrasound transducer probes. The criteria for the design varies widely, depending on the particular application.

3. Ultrasound fields and propagation

The ultrasound waves of interest in tissues and water are longitudinal (compressional) waves (Silk, 1984). The acoustic energy propagates from the front face of the transducer through fluids, whereby the supporting particles of the fluid oscillate back and forth in the same direction as that which the wave is traveling in. As a result, such a propagating wave is essentially composed of moving compactions and rarefactions of the fluid.

The acoustic waves that are radiated from the front face of an ultrasound transducer probe will propagate

through a homogeneous medium in a coherent manner for only a finite distance and will then spread out. In this coherent region the acoustic energy is confined to a cylinder. Eventually, a distance is reached where the acoustic energy spreads out (diffracts) and is no longer contained within the cylinder. The cylindrical field is called the near field or Freznel zone. It is highly transient and the cross-sectional acoustic intensity distribution (acoustic beam profile) is a function of the distance from the front face and off-axis position within the cylindrical acoustic field. At a known distance from the front face, the acoustic field approaches a steady state as it spreads out due to diffraction. This marks the beginning of the far field or Fraunhofer Zone (Wells, 1969). Figure 2.4 illustrates these two distinct acoustic field regions.

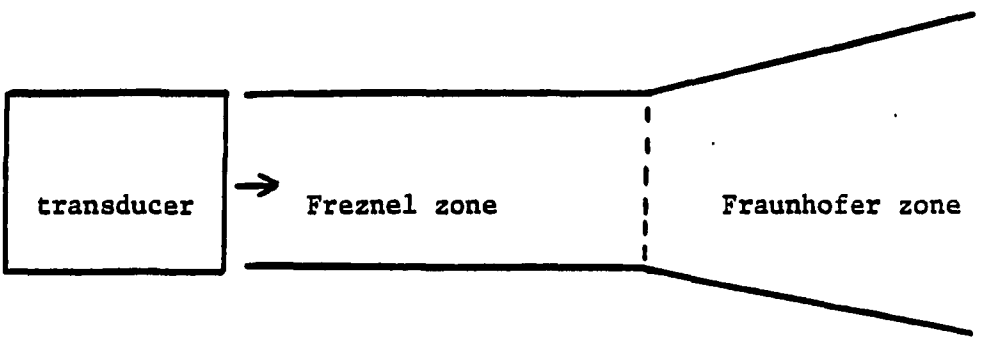

FIGURE 2.4. Ultrasound field for a disk transducer

Within the near field, the on-axis acoustic intensity is a function of distance from the radiating face and has many zeros and maxima in this region, making focussing on a target often extremely sensitive. The boundary between the near and far fields is the location of the last maxima of on-axis acoustic intensity. The acoustic field and on-axis intensity slowly decay as the distance from the radiating face is increased beyond this boundary. Focussing is thus easier in this part of the acoustic field and most quantitative nondestructive evaluation (NDE) analysis is performed there.

The location of the near/far field boundary is a function of the transducer's diameter and frequency. If the radius of the transducer, r, is much greater than the acoustic wavelength, λ, then the boundary is given by:

$$D = \frac{r^2}{\lambda} \tag{2.1}$$

where D = distance from transducer to boundary

r = radius of transducer face

λ = acoustic wavelength in the medium

Since λ is inversely proportional to frequency, Equation 2.1 shows that the near/far field boundary is close to the transducer for low frequencies, and far from the trans-

ducer for high frequencies. The acoustic wavelength is given by:

$$\lambda = v/f \qquad (2.2)$$

where v = sound velocity in the medium

f = frequency of the acoustic wave

Sound velocity varies from material to material and can even vary depending on the direction that sound waves propagate through a medium. Sound travels at about 331 m/s in air but much faster in denser mediums. Table 2.1 lists some propagation velocities of sound in various materials (from Wells, 1969).

TABLE 2.1. Sound velocities in various materials

Material	Velocity (m/s)
Air at S.T.P.	331
Water	1480
Fat	1450
Liver	1549
Muscle	1585
Brass	4490
Aluminum	6400

Sound waves are attenuated as they propagate through a medium. The attenuation is a result of diffraction and loss

of energy due to scattering caused by elastic discontinuities in the medium. Any scattering of impinging acoustic energy causes attenuation. Some energy is also removed by absorption of the energy which can be converted to heat and/or vibrations. Acoustic attenuation is often frequency dependent and can also be dependent on the direction of propagation through a medium (Wells, 1977). Table 2.2 shows some acoustic attenuation values for a frequency of 1 MHz.

TABLE 2.2. Acoustic attenuation of various materials

Material	Attenuation (dB/cm)
Air	12.0
Fat	0.63
Liver	0.94
Brass	0.02

When a propagating acoustic wave impinges on the boundary between two different structures, a portion of the wave is reflected while the remainder is transmitted across the boundary. The amount of reflection and transmission depends on the angle of incidence and acoustic impedances of the two structures. Acoustic impedance, Z, is defined as:

$$Z = \rho v \tag{2.3}$$

where Z = acoustic impedance of the material (Rayl)

ρ = density of material (kg/m^3)

v = sound velocity of material (m/s)

The unit of measurement for acoustic impedance is the Rayl, named after Lord Rayleigh. For a longitudinal wave propagating in medium 1, impinging at normal incidence on a boundary in medium 2, the pressure of the reflected wave is given by:

$$P_r = P_i \cdot \Gamma = P_i \cdot \frac{Z_2 - Z_1}{Z_2 + Z_1} \qquad (2.4)$$

where P_r, P_i = Pressure of reflected wave, incident wave

Γ = reflection coefficient

Z_1, Z_2 = acoustic impedance of medium 1,2

The pressure of the transmitted wave in medium 2 is given by:

$$P_t = P_i \cdot \frac{2Z_2}{Z_2 + Z_1} \qquad (2.5)$$

where P_t = pressure of transmitted wave

The equations clearly show that if $Z_1=Z_2$, there is no reflection and thus, perfect transmission, (i.e., $P_t=P_i$). The results imply that the intensity of the echo returned from a target will be larger if the target's acoustic impedance is much higher or lower than that of the medium.

Thus, detecting boundaries between similar media is difficult since little reflection occurs. Table 2.3 gives reflection coefficients for targets submerged in water.

TABLE 2.3. Reflection coefficients for various media in water

Target Material	Γ
Water	0.0
Fat	-0.04
Liver	0.05
Aluminum	0.85
Brass	0.92

Acoustic impedance and reflection are directly analogous to effects encountered in electrical transmission line theory. Just as every transmission line has a characteristic impedance that is dependent on its physical properties, every material has a characteristic acoustic impedance that is dependent on its density and sound velocity. The reflection equations, 2.4 and 2.5, are also valid for electrical transmission lines that have characteristic impedances Z_1 and Z_2. Transmission line theory is thus extremely useful as will be shown in future sections.

4. Transducer Applications

Ultrasound transducers are used in a variety of applications for medical and NDE analyses. The required transducer design depends on the type of ultrasound analysis which may vary from simple ranging measurements to complex imaging techniques. Many applications require a single transducer while most imaging applications require an array of transducers.

The simplest transducer application in ultrasound, called pulse-echo operation, involves the use of a single transducer which acts as both transmitter and receiver. Typically, a brief pulse of acoustic energy is launched from the transducer and time is measured until the arrival of a return echo. By knowing the acoustic velocity in the medium, distance may be computed from the time measurement. Additional details concerning the nature of the target can often be determined from spectral analysis of the return pulse-echo waveform and a wealth of mathematical theory has been derived for single transducer pulse-echo analysis.

Another transducer application in ultrasonics, the pitch-catch method, involves using a pair of transducers; one acts as a transmitter and the other as a receiver. The pitch-catch method is commonly used for measuring blood flow through in vivo arteries (Webster, 1978) or industrial chem-

icals through pipes. The pitch-catch method can also be used for ultrasonic Bragg scattering applications for tissue, similar to X-ray diffraction used in crystallography (Haumschild and Carlson, 1983). By knowing the angles of incidence of ultrasound on "homogeneous" tissue structure, like healthy liver, pitch-catch Bragg scattering techniques can be used to detect changes in normal tissue structure.

The most complicated transducer applications are probably those used for ultrasonic imaging. Such applications may involve a large array of miniature phased transducers, as in medical imaging applications, or a small array of larger transducers used for NDE applications.

It will be shown in this dissertation that the successful construction of a transducer for even the simplest pulse-echo application demands careful scientific design.

B. Review of Basic Piezoelectric Equations

This section will briefly review the fundamental piezoelectric equations that govern the electromechanical behavior of ultrasound transducers. No attempt is made to derive the equations, but rather to present those fundamental relationships that this research is based on. The basic piezoelectric constants, fundamental equations, and mathematical terminology are presented.

1. The piezoelectric constants

The electromechanical energy conversion that takes place in an ultrasound transducer may be described in terms of its piezoelectric constants.

The piezoelectric transmission (or charge) constant, d, describes the relationship between strain (relative deformation) and an applied electric field. The relationship is given by:

$$S = dE \tag{2.6}$$

where S = resulting strain, $\Delta l/l$

d = piezoelectric transmission constant

E = applied electric field, volt/meter

Since strain is dimensionless, the piezoelectric d constant has the reciprocal units of electric field, m/V. A large d constant implies high electromechanical conversion for ultrasound transmission.

Similarly, the piezoelectric receiving constant, g, describes the relationship between an applied stress (force per unit area) and the resulting electric field. Thus, the relationship is:

$$E = -gT \tag{2.7}$$

where E = resulting electric field

g = piezoelectric receiving constant

T = applied stress (N/m^2 or Pa)

The piezoelectric constant, g, thus has the units Vm/N or V/mPa, and a large value for g implies good ultrasonic receiver operation.

The two piezoelectric constants, d and g, are related by the unclamped (constant stress) dielectric permittivity, ϵ^T, where $\epsilon^T = d/g$. Thus, the unclamped permittivity represents a ratio of the transmission-to-receiver performance of a piezoelectric material.

Another important piezoelectric coefficient is the deformation constant, h. It describes the relationship between the change in plate thickness (due to an applied force), Δl, and the resulting electric field. The relationship is given by:

$$E = h \cdot \Delta l \tag{2.8}$$

Virtually all of the piezoelectric constants for a material are directionally dependent. To make relevant comparisons between piezoelectric materials, a set of standards was established.[1] The adopted standards follow the same conventions used in crystallography.

For piezoelectric materials, the direction of positive polarization is chosen to correspond to the Z axis of a conventional crystallographic axes. The xyz axes are

---

[1]Committee on Piezoelectric Crystals, 1949.

numbered 123 as shown in Figure 2.5. The poling voltage axis is assumed to have the same direction as the Z (or 1) axis.

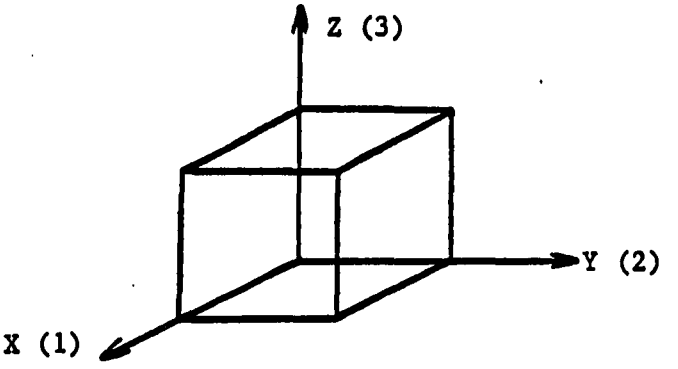

FIGURE 2.5. Conventional piezoelectric axes

Anytime a stress is applied to a solid, that stress can be resolved into 6 components--3 tensile stress and 3 tangential components, each acting orthogonally along the xyz (123) axes. These stress components are not vectors but tensors. Each tensor component is given a double subscript where the first number refers to the electrical direction and the second refers to the mechanical direction. Thus, a piezoelectric constant of d_{31} refers to the resulting strain developed in the 1 direction when an electric field is applied in the 3 direction. Most ultrasound transducers involve electrical and mechanical operation in the 33 direction, called thickness-mode operation.

2. The piezoelectric equations

The piezoelectric effect involves both electrical and mechanical activity. The relationship between these two quantities may be described by a pair of linear equations involving two variables, one electrical and one mechanical. The freedom of choice of independent electrical or mechanical variables gives one the opportunity to describe piezoelectric activity with more than one set of equations. Four pairs of derived equations, known as the piezoelectric equations, describe the fundamental electromechanical activity of a piezoelectric transducer. These 4 pairs of equations are given below:

$$\begin{aligned} S &= s^E T + dE \\ D &= dT + e^T E \end{aligned} \tag{2.9}$$

$$\begin{aligned} E &= -gT + D/e^T \\ S &= s^D T + gD \end{aligned} \tag{2.10}$$

$$\begin{aligned} E &= -hS + D/e^S \\ T &= c^D S - hD \end{aligned} \tag{2.11}$$

$$\begin{aligned} D &= eS + e^S E \\ T &= c^E S - eE \end{aligned} \tag{2.12}$$

In these equations, the superscripts represent the quantity held constant under boundary conditions. For instance, ϵ^T represents dielectric permittivity under constant stress (unclamped). It is from these fundamental equations that electromechanical models for ultrasound transducers are derived.

C. Review of Mason's Classical Work

Most electromechanical modeling of piezoelectric ultrasound transducers is based on classical work by W. P. Mason in the 1940s. Since the transducer models used in this research were based on Mason's classical work, it is necessary to review the derivation of the classical Mason's model for a piezoelectric resonator.

1. Electromagnetic field considerations

Mason's work came as a result of studying electromechanical transducers and wave filters (Mason, 1948). The starting point for his derivation involved fundamental electromagnetic field relationships. The task of his derivation was to develop an electromechanical circuit model that accurately portrayed the piezoelectric performance of a lossless one-dimensional thickness-mode resonator. Consider the lossless piezoelectric resonator shown in Figure 2.6.

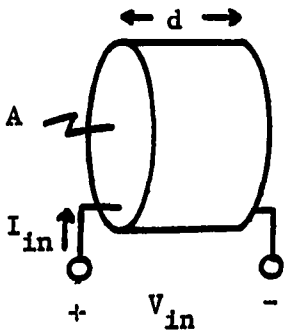

FIGURE 2.6. Lossless piezoelectric resonator

To begin the derivation, note that the electric field within the resonator is given by:

$$E = V/d \tag{2.13}$$

An expression for the input current may be derived by either applying Maxwell's version of Ampere's Law (Plonus, 1978) or by noting that since the resonator is lossless, I_{in} will be strictly due to displacement current, I_D. In the frequency domain, the current through a dielectric (i.e., capacitor) is given by:

$$I_{in} = \frac{V}{1/j\omega C} \tag{2.14}$$

$$I_{in} = j\omega CV \tag{2.15}$$

$$I_{in} = j\omega(\epsilon A/d)(Ed) \tag{2.16}$$

$$I_{in} = j\omega\epsilon EA \tag{2.17}$$

$$I_{in} = j\omega AD \tag{2.18}$$

The input voltage can be expressed by integrating the electric field across the resonator, thus:

$$V = \int_0^d E dx \tag{2.19}$$

With the electrical quantities defined, it is now necessary to relate the piezoelectric quantities.

2. Mason's derivation

Mason began by dividing Equations 2.18 and 2.19 to express the input electrical admittance of the resonator, Y_{in}:

$$Y_{in} = \frac{I_{in}}{V_{in}} \tag{2.20}$$

$$\Rightarrow Y_{in} = \frac{j\omega AD}{\int_0^d E dx} \tag{2.21}$$

Next, the electrical quantities, D and E, of Equation 2.21 may be substituted by the relevant piezoelectric equations, 2.9. The results, after considerable algebraic manipulation, are:

$$Y_{in} = j\omega C_o + \frac{1}{\frac{1}{-j\omega C_o} + \frac{Z_m}{\phi^2}} \tag{2.22}$$

The terms Z_m and ϕ^2 represent complex electromechanical expressions. Mason recognized that Equation 2.22 could be represented by an electric circuit with the same admittance, as shown in Figure 2.7.

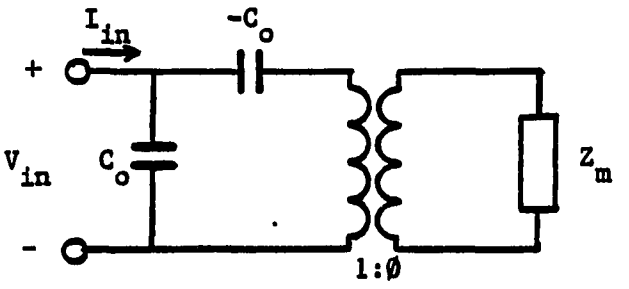

FIGURE 2.7. A circuit which has the same input admittance as Equation 2.22

Mason's circuit derivation was completed when he then represented ϕ and Z_m in greater detail. His final circuit result is shown in Figure 2.8.

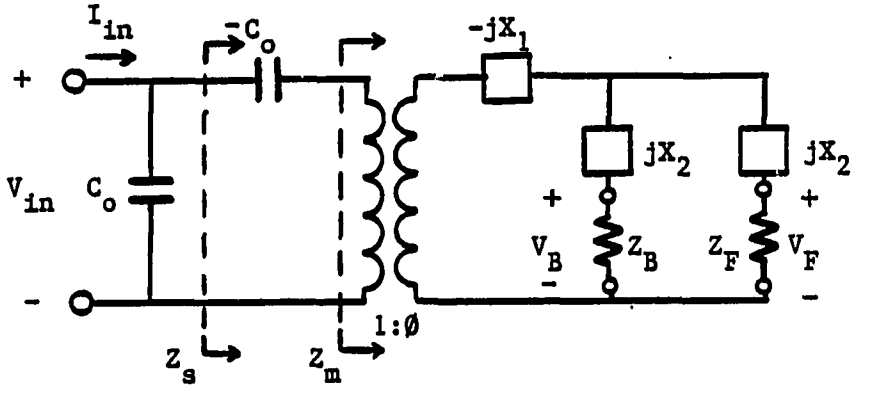

FIGURE 2.8. Mason's classical circuit

The remaining component values of the circuit are given by:

$$C_o = \epsilon A/d \quad (2.23)$$

$$X_1 = Z_o/\mathrm{Sin}(\theta) \quad (2.24)$$

$$X_2 = Z_o\mathrm{Tan}(\theta) \quad (2.25)$$

$$Z_F, Z_B = \text{acoustic impedance of front, rear face} \quad (2.26)$$

$$V_F, V_B = \text{force present at front, rear face.} \quad (2.27)$$

$$\phi = k_t[v_o C_o Z_o/d]^{1/2} \quad (2.28)$$

where:

$$\rho = \text{density of piezoelectric material} \quad (2.29)$$

$$v_o = \text{acoustic velocity in the material} \quad (2.30)$$

$$Z_o = \text{acoustic impedance of the material} \quad (2.31)$$

$$\theta = 2\pi fd/v_o \quad (2.32)$$

$$f = \text{frequency (Hz)} \quad (2.33)$$

$$k_t = \text{electromechanical coupling coefficient} \quad (2.34)$$

The real power of Mason's circuit lies in the fact that it is an electric circuit and thus, all of the well known theorems regarding circuit analysis may be applied. The terminating resistors, Z_F and Z_B, represent the loading on the faces of the resonator by the front and back mediums. The voltage developed across these resistors, due to an applied input voltage, represents the force (or stress) produced across the faces of the transducer.

One of the most interesting aspects of Mason's model is the ideal transformer which represents electromechanical energy transfer. The input impedance of the mechanical portion of the circuit, Z_m, is real at the parallel resonant frequency, f_p. This frequency is determined by the material's sound velocity and the thickness of the resonator, d. Parallel resonance occurs at the frequency where the thickness of the resonator is equal to half of the acoustic wavelength, λ:

$$d = \lambda/2 \tag{2.35}$$

where $$\lambda = v/f \tag{2.36}$$

Thus, $$f_p = v/2d \tag{2.37}$$

3. Applications of Mason's model

Mason's model has been used extensively in the 40 years since its derivation. Some researchers have developed slightly different representations of the original circuit (Rhyne, 1978; Filipczynski, 1975).

The study of matching layers and backing materials for ultrasound transducers has been greatly enhanced by studying such modifications with Mason's model. Any additional layer added to the face(s) of a piezoelectric transducer may be accounted for in Mason's model by coupling the front/rear ports of the model to the appropriate loads, Z_F and/or Z_B, through the network shown in Figure 2.9.

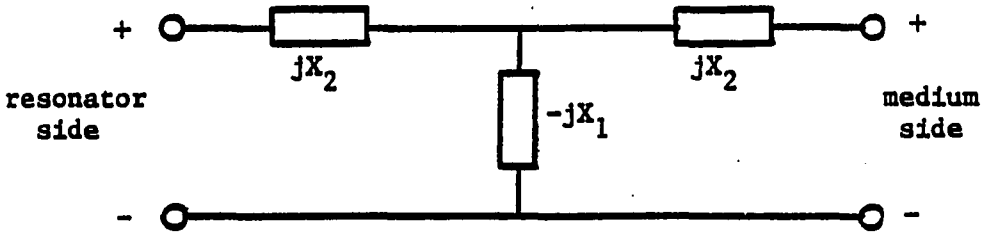

FIGURE 2.9. Network for representing an acoustic layer

The components X_1 and X_2 are given by Equations 2.24 and 2.25, except that the thickness, d, and velocity, v, are those for the particular layer material. This approach can be used to account for the electrode layers.

To prevent unwanted reflections due to severe acoustic mismatches at the ports (faces) of an ultrasound transducer, a quarter-wavelength matching layer is often added to reduce the effects of the mismatch. The two-port network model for an acoustic layer appears "invisible" at a frequency that corresponds to the quarter-wavelength thickness of the matching layer, if the acoustic impedance of the matching layer is carefully chosen. If the acoustic impedance of the matching layer is chosen as the geometric mean of the resonator material and the desired medium, a perfect match is achieved at the particular frequency. Thus, for matching:

$$Z_L = (Z_o \cdot Z_F)^{1/2} \qquad (2.38)$$

where Z_L = required acoustic impedance of matching layer

Z_F = acoustic impedance of desired medium

Z_O = acoustic impedance of the resonator

Mason's model has been used extensively for including the effects of matching layers on ultrasound transducers (Saitoh et al., 1985; Lancee et al., 1985; Persson and Hertz, 1985; Highmore, 1973; Seitchik, 1972). Other applications of Mason's model for transducer design and evaluation include Morris and Hutchens, 1986; Hunt et al., 1983; Swartz and Plummer, 1980a; Meeker, 1972; Sittig, 1967.

Additional circuit modeling techniques have been used by Persson and Hertz, 1985; Houze et al., 1985; Selfridge and Gehlbach, 1985; Hutchens and Morris, 1984; Hue et al., 1980; Desilets et al., 1978; Filipczynski, 1975; Dotti, 1975; Ballato et al., 1974; Leedom et al., 1971; and Krimholtz et al., 1970. Still other investigators have used systems models to evaluate piezoelectric resonators: Hayward, 1986; Hayward, 1984; Hayward and Jackson, 1984; Hayward et al., 1984; Hayward and Jackson, 1983. Mathematical models, with no circuit representation, have been used by Alais et al., 1980; Lewis, 1978; and Bui et al., 1977.

Electromechanical modeling techniques have thus played an important role in the design and evaluation of piezoelectric resonators for ultrasound.

D. Review of the Simplified Electrical Impedance Model

Another commonly used circuit model is limited to modeling the electrical input impedance of an acoustic resonator. Although such a model may at first seem to have only limited value, it is a powerful aid for both the design of ultrasound transducers and analysis of their acoustic performance.

The electrical input impedance of a piezoelectric resonator operating near resonance may be represented by the circuit given in Figure 2.10. In this circuit, the capacitor C_o represents the same bulk capacitance as that used in Mason's model (see Equation 2.23).

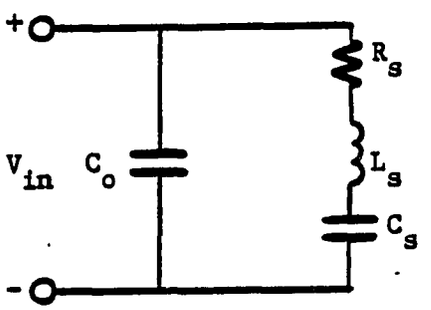

FIGURE 2.10. Simplified electrical input impedance model

The series branch of R_s, L_s, and C_s represents the mechanical-acoustic effects of series resonance on the input impedance. The resonant frequency of this branch,

$1/(L_S C_S)^{1/2}$, is the same as the series resonant frequency, f_S, of Mason's model (see Figure 2.8). A great deal of classical circuit theory is known about series resonant circuits (Nilsson, 1983). For instance, the acoustic Q of the resonator can be computed from:

$$Q = 1/\omega_S R_S C_S \qquad (2.39)$$

where $\omega_S = 2\pi f_S$

The air-loaded acoustic Q is a parameter that is commonly specified for various piezoelectric materials since it describes how "peaked" the unloaded acoustic response is.

In 1949, the Institute of Radio Engineers (IRE) Committee on Piezoelectric Crystals released a report entitled Standards on Piezoelectric Crystals: Recommended Terminology, (Committee on Piezoelectric Crystals, 1949). The report established standard symbols and terminology to be used thereafter. These standards were updated at later dates (Committee on Piezoelectric Crystals, 1957) and in 1959, the simplified electrical impedance model was described. In those standards, numerous characteristic parameters for a piezoelectric resonator were defined in terms of the four components of the circuit model and its resonant frequencies.

Also included in the 1949 IRE Standards were circular input impedance and admittance diagrams for the simplified circuit model. The resonance frequencies and other quantities of interest may be determined from the diagrams as shown in Figure 2.11.

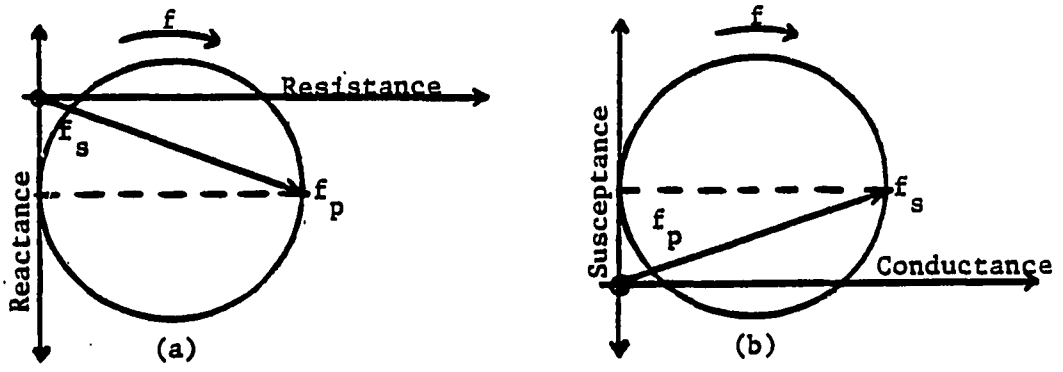

FIGURE 2.11. Circular (a) impedance and (b) admittance diagrams for a piezoelectric resonator

The diagrams show that both the series and parallel resonant frequencies may be determined from the diagrams, however some caution must be applied in using this approach. As the IRE Standards clearly pointed out, (Committee on Piezoelectric Crystals, 1957) the validity of these diagrams is limited to nearly lossless piezoelectric resonators whose dielectric properties are independent of frequency. As the next section points out, these are hardly the properties of the piezoelectric polymers.

The real power in using the simplified impedance model is in its use in designing tuned circuits to enhance the bandwidth and sensitivity of ultrasound transducers. Many investigators have used the simplified impedance model for this purpose--Hue et al., 1980; Ravinet et al., 1980; Augustine and Andersen, 1979; Committee on Piezoelectric Crystals, 1957; and Mason, 1964. Some specific design applications using this approach will be presented in Chapter V.

E. Review of Piezoelectric Polymer Films

The discovery of piezoelectricity in natural occurring organic materials became of great interest in the 1950s and 1960s when Japanese physicists discovered piezoelectricity in wood, silk, bone, and collagen (Silk, 1984). For the most part, the piezoelectric properties of these materials were so weak that they hardly warranted any significance for ultrasound transducers. However, a significant discovery by the Japanese physicist, Kuwai, occurred in 1969. Kuwai discovered strong piezoelectric properties in uniaxially stretched polarized films of poly vinylidenefluoride (PVDF or PVF_2). The impact of his discovery may only now be seriously affecting medical and NDE ultrasound applications.

1. Production of the polymer films

Unpoled PVF_2 has been produced in this country for commercial plastic applications for more than 20 years.[2] Manufactured under the trade name Kynar, it is a clear, compliant film that has had numerous industrial applications. PVF_2 is highly chemically resistant which makes it useful for lining industrial pipes and pumps (Chatigny, 1984). Because it has excellent dielectric properties, it is also widely used as insulation for electrical wires. Thus, PVF_2 was already processed in great quantities in this country before Kuwai's discovery in 1969. Pennwalt Corporation, the leading supplier of PVF_2 resin, began research into piezoelectric polymers in the 1970s. Since that time, their newly developed films have become of great interest for ultrasound transducer applications.

PVF_2 is a long-chain semi-crystalline polymer. Its monomer units, $CH_2{=}CF_2$, give high head-to-tail configuration during polymerization, (...-CH_2-CF_2-CH_2-CF_2-...). Thus, under proper production conditions, the polarized material exhibits a high net electric dipole moment.

The PVF_2 resin has two common crystalline phases of interest: alpha and beta. Under normal cooling conditions of the PVF_2 resin, the alpha (nonpolar) phase results.

---

[2]Pennwalt Corporation, King of Prussia, PA.

Deformation of the alpha structure produces the beta (polar) phase. The nonpolar alpha phase is extruded, causing the unit cells to be arranged in the parallel planes of the beta polar phase.

Metal electrode layers are sputtered onto the film surfaces and a high DC polarizing potential is applied at a temperature slightly below the Curie point. After slowly cooling (approximately 1 hour) significant piezoelectric and pyroelectric properties result. Virtually every step of the process can influence the final properties and performance of the films.

More recently, a new copolymer has been discovered which has even stronger piezoelectric properties than polarized PVF_2 (Kimura and Ohigashi, 1983). The material is a copolymer of vinylidenefluoride and trifluoroethylene, poly(vinylidenefluoride-trifluoroethylene), P(VDF-TrFE) or $P(VF_2\text{-}VF_3)$.

Pennwalt Corporation now also produces this new material which has much stronger piezoelectric properties. The copolymer is much more crystalline, making it more brittle than PVF_2, but still flexible enough for many unique transducer applications. Samples of some of Pennwalt Corporation's first $P(VF_2\text{-}VF_3)$ copolymer films and newest PVF_2 were obtained for this research work.

2. Properties of the piezo films

The piezo films offer both advantages and disadvantages for ultrasound transducer applications. Unlike the rigid PZT ceramics, the films are soft and compliant and possess large acoustic mechanical losses. The films also have dielectric properties that are unique. Their dielectric permittivity, ϵ, is not only very frequency dependent, but much lower that that of the PZTs. The dielectric loss tangent, $\mathrm{Tan}(\delta_d)$, is also frequency dependent, and much higher than for the PZTs. Thus, the mechanical and dielectric properties of the films are extremely lossy.

Actually the lossy properties of the piezo films are not entirely a disadvantage. The inherent lossy properties of the films are responsible for their low-Q broadband acoustic performance. For ultrasound transducers, the piezoelectric films offer excellent bandwidth at the expense of efficiency and sensitivity. A comparison of typical PZT, PVF_2, and $P(VF_2\text{-}VF_3)$ properties is given in Table 2.4. It is obvious from the table that the properties of the piezo films are very unlike those of the PZTs. Also note the significant difference in k_t between PVF_2 and $P(VF_2\text{-}VF_3)$.

Notice the large differences in acoustic impedance between the piezo films and PZT material. The low acoustic impedance of the films makes them much better (more efficient) than the PZTs for operation in water or tissue. The

TABLE 2.4. Comparison of piezoelectric material properties

Property	PZT-5[a]	PVF_2[b]	$P(VF_2-VF_3)$[b]
Density ($10^3 Kg/m^3$)	12	1.78	1.80
Rel. Permittivity, ϵ_r	>1500	6.0	4.5
Acoustic velocity (m/s)	3780	2200	2380
Mechanical Q	75	12	14
Coupling coefficient, k_t (%)	71	13.5	21

[a]Taken from Wells, 1969.
[b]Measured by author at 10 MHz.

larger dielectric losses give the films a lower Q and thus, a broader bandwidth natural response. However, the cost for the low Q is lower sensitivity. Some advantages of the piezo films over the PZTs for ultrasound transducer applications are given below:

1. The low acoustic impedance of the piezo films makes them better suited (more efficient) for use in water and tissue.
2. The lower acoustic Q gives the films an inherent broadband frequency response.
3. A higher dielectric strength allows the piezo films to be excited with much higher voltage potentials (up to 2,000 V for 28 micron film thickness).

4. The films may be used in many harsh environments since they have a higher resistance to wear, most chemicals, and moisture.
5. The film is flexible and may be cut, shaped, and molded to fit many diverse applications.

The material properties of the piezo films also give rise to distinct disadvantages over the PZTs. A few of those are listed below:

1. The much lower dielectric permittivity of the piezo films means very little bulk capacitance for a transducer, causing cable and stray capacitances to significantly affect performance.
2. The much higher electromechanical coupling of the PZTs makes them capable of producing much larger acoustic waveforms from an applied voltage.
3. Electrical connections to the PZTs may be easily made by soldering. However, making reliable connections to the films is more difficult, typically requiring conductive epoxies and shims.
4. The piezo films are particularly sensitive to electromagnetic radiation, thus special design precautions must be taken to minimize noise problems.

5. The maximum operating temperature of the piezo film is 100°C, far below that of the PZTs.

The decision to use either a PZT or piezo film for an ultrasound transducer depends entirely on the specific application. For many narrowband applications there may be no need to consider the piezo films over PZTs. However, as this research will show, there are many broadband ultrasound applications where the piezo films may be viable competitors with the PZTs.

3. Piezo film ultrasound transducer applications

PVF_2 has seen some use in ultrasound transducer applications. Its greatest contribution to ultrasound science has probably been its use for small ultrasound hydrophone probes. Because PVF_2 offers superior acoustic matching to water, many miniature probes have been developed for studying the intensity of underwater ultrasonic fields (Platte, 1985; Lewin, 1984; Lewin, 1981; Schotton et al., 1980). Other applications for broadband NDE ultrasound transducers and medical imaging applications include Hunt et al., 1983; and Swartz and Plummer, 1980b.

The enhanced piezoelectric properties of newly developed $P(VF_2-VF_3)$ copolymers offer the hope for more competition with PZTs for NDE and medical ultrasound applications. Recent improvements in piezo film technology have resulted

in lower acoustic and dielectric losses, a closer acoustic match to tissue, and higher electromechanical coupling coefficients. Broadband ultrasound transducers using these new films are discussed in Chapter V.

4. Piezo films require new modeling techniques

The frequency dependent lossy properties of the piezo films prohibit the direct application of classical electromechanical circuit models for predicting ultrasound transducer performance. Mason's classical circuit model cannot be directly used for piezo film transducers since it does not account for any mechanical losses or frequency dependent dielectric properties. This is no surprise since the first step in deriving Mason's model was based on assuming that the input current was entirely due to displacement and not conduction (see Section C).

The simplified impedance model characteristics described in the IRE Standards are irrelevant since their validity requires negligible mechanical losses and dielectric properties that are independent of frequency (see Section D). It is apparent that new research work is required to accurately model piezo film ultrasound transducers. Nearly all attempts to model the acoustic performance of the piezo films have failed to produce accurate results because of the investigators' failures to properly account

for the frequency dependent properties of the films, (Bui et al., 1977). The next chapter describes the approach used in this research to model the piezoelectric polymer films' acoustic performance.

III. ELECTROMECHANICAL MODELING OF PIEZO FILM ULTRASOUND TRANSDUCERS

The first major objective of this research was to develop circuit models that accurately predict the electromechanical performance of piezo film ultrasound transducers. It was shown in Chapter II that the frequency-dependent lossy properties of the piezo films prohibit the direct application of classical circuit models. This fact presents a distinct disadvantage in studying the design and application of piezo films ultrasound transducers. Electromechanical models are needed to provide the theoretical insight necessary to exploit all of the properties of the piezo films for high performance ultrasound transducer applications. Without such models a designer is unable to predict, let alone achieve, optimum transducer performance.

The first section of this chapter describes a method for determining the frequency-dependent lossy properties of the piezo films. Next, two sections describe the derivation of simplified electrical input impedance and modified Mason's models for the films. Comparisons between actual and predicted performance are included in all three sections. A section is also included which summarizes the modeling results for numerous piezo film samples.

A. Modeling the Frequency Dependent Dielectric Properties

It was pointed out in Chapter II that the frequency-dependent lossy properties of the piezo films offer both advantages and disadvantages for ultrasound transducers. It is the consequence of these losses, both dielectric and mechanical, that give PVF_2 and $P(VF_2-VF_3)$ their low-Q broadband ultrasound performance. No electromechanical model for the piezo films can give accurate broadband prediction of acoustic performance without accurately accounting for these frequency-dependent lossy dielectric properties.

1. Effects of dielectric properties on input impedance

The frequency-dependent dielectric properties of PVF_2 have been reported by other investigators (Hunt et al., 1983; Swartz and Plummer, 1980a; Ravinet et al., 1980). Thus, accurate broadband electromechanical modeling of the piezo films requires knowledge of the dielectric permittivity, ϵ, and the dielectric loss tangent, $\mathrm{Tan}(\delta_d)$. Both ϵ and $\mathrm{Tan}(\delta_d)$ are known to be frequency dependent and to vary with the stretching and poling conditions used (Ravinet et al., 1980). It is these two quantities that are needed to model the electrical impedance of a lossy dielectric. To determine ϵ and $\mathrm{Tan}(\delta_d)$, use was made of the fact that at frequencies far from resonance, the electrical input

impedance of a piezoelectric resonator is essentially due to the properties of its dielectric. It will later be shown why this is the case.

The implication of this fact is that by analyzing the electrical input impedance of the piezo films at frequencies far from resonance, one should be able to derive the required dielectric properties. The first requirement for determining these dielectric properties was to derive the mathematical relationship between the electrical input impedance and the dielectric properties, ϵ and $\mathrm{Tan}(\delta_d)$.

The first step in deriving Mason's model was in assuming that the input current, I_{in}, was strictly due to displacement current, I_D (see Chapter II, Section C). This assumption is only valid for a lossless dielectric. In lossy dielectrics the input current has two components--one of displacement and one of conduction (Plonus, 1978). The circuit for a lossy dielectric can thus be represented as shown in Figure 3.1.

In the figure, a shunt resistance, R_o, is included to account for the conduction current, I_C. The dielectric loss tangent is the ratio of the magnitude of conduction current to displacement current, or:

$$\mathrm{Tan}(\delta_d) = |I_C|/|I_D| \qquad (3.1)$$

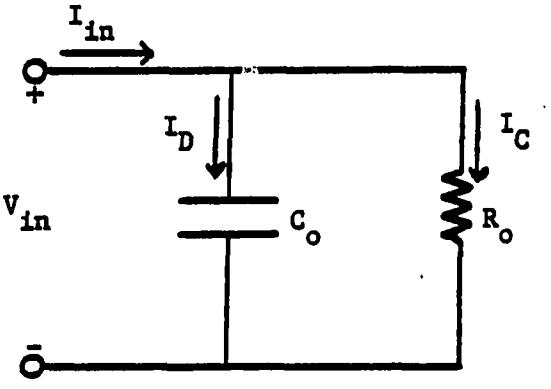

FIGURE 3.1. Schematic of a lossy dielectric

In the frequency domain, I_D is given by Equation 2.14 and I_C is found by simply applying Ohm's Law. Thus, Equation 3.1 may be written as:

$$\text{Tan}(\delta_d) = \frac{V/R_o}{|V/(1/j\omega C_o)|} \tag{3.2}$$

or $$\text{Tan}(\delta_d) = 1/\omega R_o C_o \tag{3.3}$$

Now, by knowing $\text{Tan}(\delta_d)$ one can express the shunt dielectric resistance as:

$$R_o = 1/(\omega C_o \text{Tan}(\delta_d)) \tag{3.4}$$

If one assumes that the input impedance of a lossy piezoelectric resonator is essentially due to the dielectric properties (i.e., at frequencies far from resonance) then the expression for the input impedance, Z_{in}, is:

$$Z_{in} = R_o//C_o = R_o/(1 + j\omega C_o R_o) \qquad (3.5)$$

By solving for the impedance magnitude, $|Z_{in}|$, and phase angle, θ_Z, of Equation 3.5 and substituting Equations 2.23 and 3.4, expressions for the dielectric properties can be written as:

$$Tan(\delta_d) = -1/(Tan(\theta_Z)) \qquad (3.6)$$

and

$$\epsilon = \frac{d}{|Z_{in}|\omega A(Tan^2(\delta_d) + 1)^{1/2}} \qquad (3.7)$$

Equations 3.6 and 3.7 are the needed mathematical tools for determining the lossy dielectric properties of the piezo films. The equations show that at frequencies far from resonance, one can approximate ϵ and $Tan(\delta_d)$ from knowledge of the input impedance and physical dimensions of the film. As will be shown, the accuracy of Equations 3.6 and 3.7 degrades as frequency, ω, approaches resonance. However, the next section will show how it is possible to closely approximate ϵ and $Tan(\delta_d)$ in the neighborhood of resonance.

2. Actual impedance measurements of the films

It was next desired to make actual input impedance measurements of piezo film samples in an effort to apply the

derived equations for ϵ_r and $\text{Tan}(\delta_d)$. Special equipment was required to obtain broadband input impedance measurements of piezo film samples. Obviously, a device was needed for measuring the impedance magnitude and phase angle of the samples. An HP 4815A RF Impedance Meter was used for measuring the impedance magnitude and phase angle of the samples.[3]

One of the major problems encountered in making impedance measurements concerned making electrical connections from the RF impedance meter to the film sample being studied. Since the film cannot be soldered to, and any permanently attached leads would restrict (dampen) the film's movement, a special test fixture was needed. Several unsuccessful fixtures were tested which involved permanently mounting the film sample between clamped electrical connections, leaving the sample suspended in air. The resulting uneven stress across the surface of the films caused undesirable standing waves which produced unwanted resonant peaks and dips in the impedance measurements. What was required was a fixture that freely suspended the film sample in air with no added tension across the surface of the film. It was also desirable to construct a simple fixture that would permit the connection and analysis of many different

---

[3]Loaned by Rockwell International, Cedar Rapids, IA.

samples. A sketch of the successful film fixture is given in Figure 3.2.

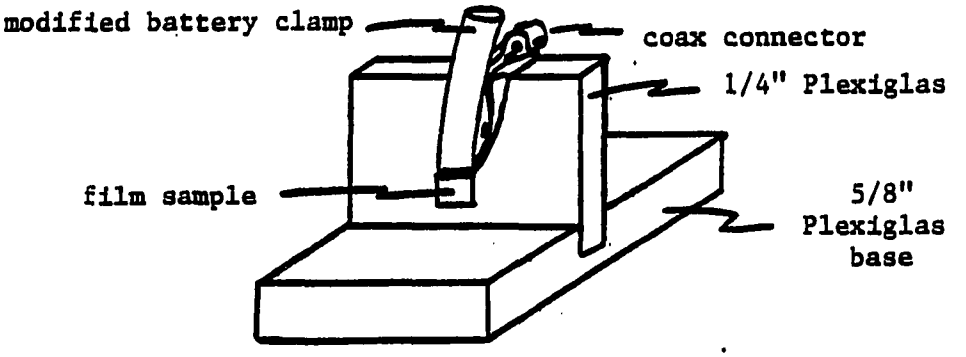

FIGURE 3.2. Sketch of successful piezo film test fixture

The spring-loaded battery clamp was modified so that as it closed on a film sample, its conductive jaws made contact with the metallization on both sides of the film. Leads connected the two sides of the film (jaws) to a coax BNC connector. The clamp was mounted to 1/4" Plexiglas so that a clamped sample hung freely in the air. The film sample under study was clamped as close as possible to one edge and the area of contact of the jaws with the film was much smaller than the area of the film sample so that unwanted damping was negligible. The assembly could be held upright by placing the 1/4" Plexiglas backing into the machined channel of a 5/8" Plexiglas base as shown in the figure.

The film test fixture obviously has electrical properties of its own that must be accounted for. Because the dielectric permittivity, and thus capacitance, of the piezo film is low, the impedance of the test fixture had to be accounted for in deriving meaningful information from the impedance measurements. Figure 3.3 shows a schematic of the test setup for obtaining input impedance measurements of the film samples.

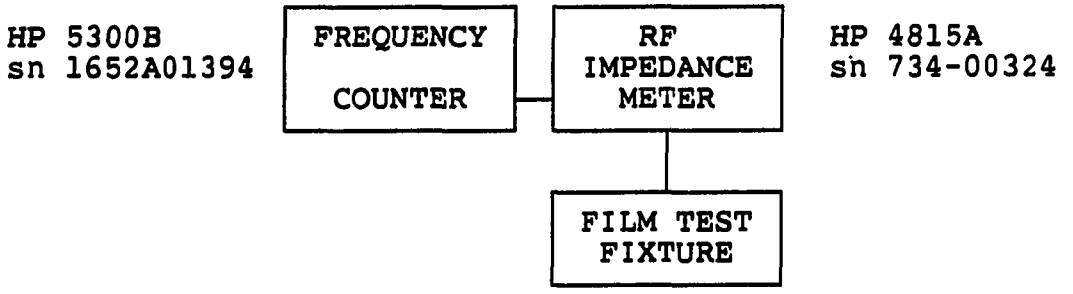

FIGURE 3.3. Test setup for piezo film impedance measurements

For each film sample under study, three 1cm x 1cm samples were cut and analyzed and the resulting impedance measurements averaged to correct for interpolation errors associated with reading the analog meters of the HP 4815A. A broad frequency range, which included resonance, was used for each film sample and a frequency resolution of 0.5 MHz

was used, except near resonance where a resolution of 0.1 MHz was used. Typical frequency ranges for analysis were 0-50 MHz (28 micron films), 0-32 MHz (52 micron films), and 0-24 MHz (110 micron films).

To determine the impedance of the test fixture and connecting coax cable, open-circuit and short-circuit impedance measurements of the test fixture and cable were made at three equally spaced frequencies in the range of interest, both before and after each film sample was analyzed. From these measurements, the impedance of the test fixture was modeled as shown in Figure 3.4.

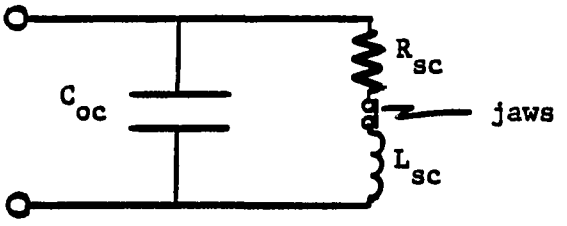

FIGURE 3.4. Impedance model of the test fixture

The open-circuit impedance was capacitive and consisted mainly of cable capacitance from a 3' length of RG58A/U coax cable. The open-circuit impedance, Z_{OC}, was thus used to compute C_{OC} from:

$$C_{OC} = 1/j\omega Z_{OC} \qquad (3.8)$$

The short-circuit impedance consisted mainly of lead inductance and resistance. To minimize the contact resistance of the test fixture jaws, the contacts were cleaned before each calibration and film analysis. The real and imaginary components of the short-circuit impedance were then used to determine R_{SC} and L_{SC} from:

$$R_{SC} = Re\{Z_{SC}\} \tag{3.9}$$

$$L_{SC} = Im\{Z_{SC}\}/\omega \tag{3.10}$$

The influence of the shunt capacitance, C_{OC}, on the short-circuit impedance readings was negligible since at all frequencies below 50 MHz, $Z_{OC} >> Z_{SC}$.

The component values R_{SC}, L_{SC}, and C_{OC} were computed at each of the three equally spaced frequencies and the results taken before and after each film sample were averaged. Thus, for each film sample a unique set of component values was derived for the test fixture and subsequently used to correct the input impedance measurements of the film sample.

3. Processing the actual impedance measurements

After carefully cleaning the jaw contacts and calibrating the test fixture, the film sample under study was clamped into position. The HP 5300B frequency counter was used to maintain frequency within 100 Hz of each nominal value. At the time of the first film analyses there was no

access to a computer to record the readings, so all measurements were recorded in an engineering notebook and later transcribed into computer storage for processing. Several thousand measurements were recorded and transcribed in this way. Later in the research a computer and interactive transcription program, ZTRANSCR.FOR, were used to store the raw film impedance measurements directly into a computer file as they were acquired. A copy of the transcribing program is given in Appendix A.

After a complete set of raw measurements from a film sample was read into a computer file, the measurements were ready for correction. Another computer program, ZCORRECT.FOR, removed the impedance of the test fixture and connecting cable from the raw measurements and stored the corrected results in a new file. The corrected impedance measurements for three film samples were averaged to give a computer file of average corrected input impedances for each film under study. The programs used to correct the raw measurements and average the corrected files, ZCORRECT.FOR and ZFAVERAG.FOR, are contained in Appendices B and C. The computer file of average corrected impedance measurements was then ready for analysis to determine ϵ and $\mathrm{Tan}(\delta_d)$.

4. Computing ϵ and Tan(δ_d)

A FORTRAN computer program was used to evaluate Equations 3.6 and 3.7 to determine the dielectric quantities ϵ and Tan(δ_d). However, these two equations cannot be evaluated unless the area (A) and thickness (d) for the film are known. This presented another problem. The piezo films were too thin to accurately measure with a micrometer, and too thick to measure with the surface profile measurement systems used in local thin film laboratories.

Film thickness was measured on a laboratory microscope (Bausch and Loumb, model 31-32-13, sn 313087). The microscope had an eyepiece scale that was first calibrated against a slide micrometer standard (Bausch and Loumb, 0.01 mm). The 1 cm x 1 cm film samples were viewed under the microscope and their thickness measured at two equally spaced points on three sides of each sample. The side that was clamped was not measured. For each of three film samples, the six thickness measurements were averaged and their sample standard deviation was computed. The thickness of the film under study was then determined by weighting the three average thickness measurements by their sample deviations:

$$d = \frac{\sum_{i=1}^{3} \bar{d}_i S_L / S_i}{\sum_{i=1}^{3} S_L / S_i} \qquad (3.11)$$

where $\bar{d}_i$ = average thickness of i^{th} film sample

S_i = sample standard deviation of i^{th} film sample

S_L = largest sample standard deviation of the 3 film samples

The precise area of each film sample was measured with a caliper (Craftsman, sn 40257). The average area of the three samples, A, and the weighted thickness, d, were used in the computer program to evaluate Equations 3.6 and 3.7 for ϵ and $\text{Tan}(\delta_d)$. A copy of the computer program, ZDIELECT.FOR, is included in Appendix D. The program computed ϵ and $\text{Tan}(\delta_d)$ at each specified frequency and wrote the results in both hardcopy and graphics output files. The graphics files were formatted for use with the Iowa State University campus VAX system's AGRAPH utility.[4]

As discussed earlier, Equations 3.6 and 3.7 are not valid in the neighborhood of resonance. They are, however, valid at frequencies well above or below the neighborhood of resonance, so close approximations for ϵ and $\text{Tan}(\delta_d)$ can be

---

[4]AGRAPH is a graphics package written by Iowa State University professor A. A. Read, Dept. of EE/CpE.

obtained by "smoothly" interpolating the computer results through resonance. The results for a 52 micron PVF_2 film are shown on Figure 3.5.

Solid lines in the plots represent the cubic spline interpolated program results at 16 frequencies in 0.5-32 MHz. These lines show the same characteristic behavior reported by others (Ravinet et al., 1980). This method of smoothly interpolating through resonance provides excellent first-order approximations for ϵ and $\text{Tan}(\delta_d)$. It will be later shown how to further "tune" these values for even better accuracy.

The dielectric circuit model is therefore completed by computing C_o (Equation 2.23) and R_o (Equation 3.4) by using the cubic spline interpolated values for ϵ and $\text{Tan}(\delta_d)$, and using the shunt R_oC_o circuit of Figure 3.1. It can be seen from Figure 3.5 that the dielectric properties are extremely frequency dependent and thus, why failure to account for these properties prevents accurate broadband modeling of piezo film electromechanical performance. With knowledge of the dielectric properties it was then possible to study the effects of mechanical performance on the input impedance.

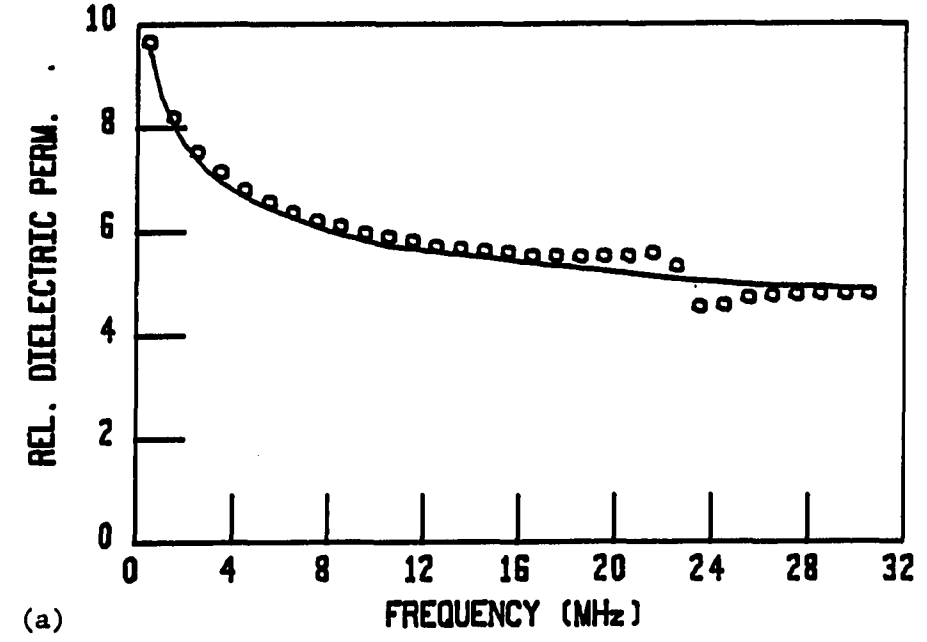

(a)

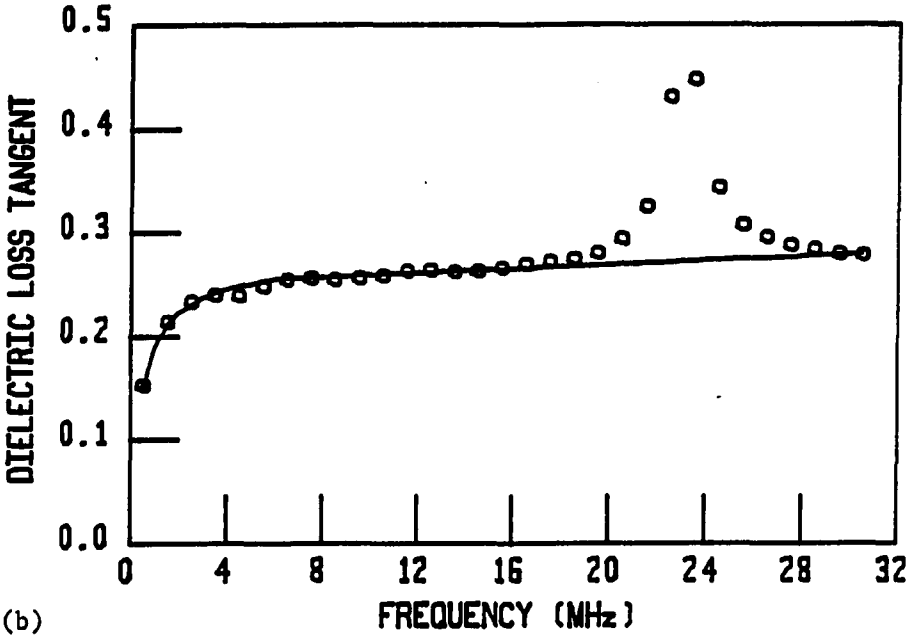

(b)

FIGURE 3.5. Plots of 52 micron PVF_2 (a) ϵ_r and (b) $\text{Tan}(\delta_d)$. The discrete symbols represent the ZDIELECT.FOR program results. The solid lines represent the "smoothly" interpolated values through resonance ($\simeq$23 MHz)

B. Derivation of the Simplified Impedance Circuit Model

It was shown in Chapter II (Section D) that the simplified impedance circuit model is useful for the design of ultrasound transducers. In the design of broadband ultrasound transducers, passive components are used to tune the dielectric response to optimize the acoustic performance. The design of such tuned circuits requires explicit knowledge of the components of the simplified impedance circuit model. The challenge in achieving this research objective was in deriving the components of the circuit model that best fit the actual broadband impedance measurements. This section describes the technique used for deriving accurate broadband impedance circuit models for the piezo films.

1. Deriving the series resonance circuit

The simplified impedance circuit model was introduced in Figure 2.10. Since the dielectric components, R_o and C_o, can be approximated by using the methods of the previous section, it is the series resonant branch which required derivation. It was clear that if the impedance Z_s were available at several frequencies near resonance, the components of the branch could be easily determined.

In principle, the impedance of the series resonant branch, Z_S, is that portion of the electrical input impedance that remains after the shunt impedance of R_O and C_O are removed. It was this fundamental principle that was used in deriving the series resonant components. A computer program (ZF0.FOR) was used to remove the shunt impedance of the previously derived values for R_O and C_O from the corrected input impedance measurements. At each frequency, the FORTRAN program performed the analysis using complex algebra in three steps:

1. The corrected input impedance measurement, Z_{in}, was inverted to give the input admittance, Y_{in}.
2. R_O and C_O were computed from the previously derived values of ϵ and $\text{Tan}(\delta_d)$, and the admittances of R_O and C_O were then subtracted from Y_{in}.
3. The resulting admittance, Y_S, was inverted to give the desired series resonant impedance Z_S.

By analyzing Z_S near resonance, the components R_S, L_S, and C_S may be derived. The program ZF0.FOR (Appendix E) performed the removal of Z_S from the actual impedance measurements and created a hardcopy file of the real and imaginary components, $\text{Re}\{Z_S\}$ and $\text{Im}\{Z_S\}$. Table 3.1 shows a

portion of the output file for a 52 micron PVF_2 sample (MM86005).

TABLE 3.1. ZF0.FOR results for Z_S near resonance--52 micron PVF_2

f (MHz)	$Re\{Z_S\}$ (Ω)	$Im\{Z_S\}$ (Ω)
22.3	407.73	-214.59
22.4	400.54	-172.95
22.5	392.44	-133.46
22.6	393.49	-105.12
22.7	387.35	-62.35
22.8	387.50	-26.04
22.9	388.28	10.48
23.0	384.01	54.75
23.1	381.04	90.26
23.2	379.00	127.84
23.3	376.29	167.46

The series resonant frequency, f_S, is that frequency where $X_S=0$. From the table it can be seen that f_S lies in the range 22.8-22.9 MHz. Linear interpolation of the data gives $f_S=22.87$ MHz. At series resonance, Z_S is real, thus R_S can be found from a linear interpolation of $Re\{Z_S\}$ at f_S From the table, the interpolated value at 22.87 MHz is $R_S=388.0\ \Omega$. Only the reactive components L_S and C_S remain to be derived. Two different methods were used to determine L_S and C_S.

The most "tempting" method for deriving L_S and C_S is to simply equate the imaginary part of Z_S, X_S, to the theoretical value, $\omega L_S + 1/\omega C_S$, at two frequencies near resonance. Thus, two independent equations in L_S and C_S may be solved and the components of the branch derived. This method was applied to several different piezo films and the resulting input impedance of the derived models was compared with the actual impedance measurements. A FORTRAN program, ZDEV.FOR (Appendix F), created both hardcopy and graphics output files for the percent deviation in impedance magnitude and phase. The maximum deviations were typically ±7% over the broadband frequency range of the actual impedance measurements. This was considered unsatisfactory. In all cases, the series impedance of the model quickly diverged from the Z_S values computed from the actual impedance measurements, except at the two frequencies where L_S and C_S were computed. It soon was apparent why this approach was a poor choice for acceptable broadband accuracy.

In the neighborhood of resonance, X_S is linear and has a positive slope since the series reactance is capacitive (negative) below f_S and inductive (positive) above f_S. Since the corrected measurements of Z_{in} are subject to slight uncertainties, selecting two frequencies close to resonance for deriving C_S and L_S can result in poor broadband modeling. Figure 3.6 shows how this can occur.

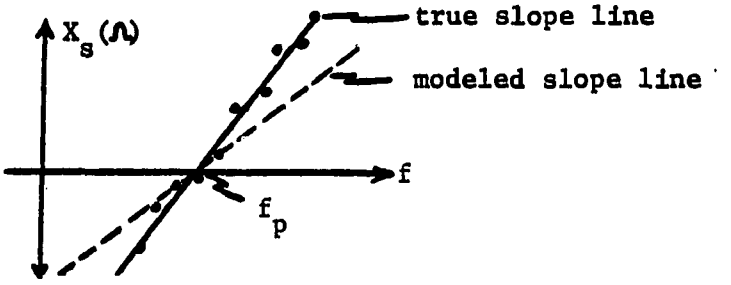

FIGURE 3.6. Analysis of series reactance error

The figure shows an example of how even with perfect correlation of the model's X_S to the corrected measurements at two frequencies, the slope of the model's X_S is clearly in large error. It is thus apparent that the best correlation between the model's X_S and the corrected X_S measurements will occur if the components are selected to produce the same slope, $\Delta X_S/\Delta\omega$.

To better fit the model and actual measured impedances over a broader frequency range, L_S and C_S were chosen to match the slope of X_S over a frequency range symmetric about f_S. This can be done by noting that:

$$\omega_S = 2\pi f_S = 1/(L_S C_S)^{1/2} \tag{3.12}$$

$$\text{Slope of } X_S = \frac{dX_S}{d\omega} = \frac{\Delta X_S}{\Delta\omega} \tag{3.13}$$

$$\text{where } X_S = \omega L_S - 1/\omega C_S \tag{3.14}$$

$$\text{Thus, } \Delta X_S = X(\omega + \Delta\omega) - X_S(\omega) \tag{3.15}$$

$$\text{or } \Delta X_S = [(\omega+\Delta\omega)L_S - 1/(\omega+\Delta\omega)C_S] - [\omega L_S - 1/\omega C_S] \tag{3.16}$$

One can now choose $\omega<\omega_S<\omega+\Delta\omega$, and by substituting Equation 3.12 into Equation 3.16 for L_S, the value of C_S which matches the slope of the model's X_S, $\Delta X_S/\Delta\omega$, to the actual impedance measurements' is:

$$C_S = \frac{\Delta\omega}{\Delta X_S(\omega)}\left[\frac{1}{\omega_S^2} + \frac{1}{\omega(\omega+\Delta\omega)}\right] \qquad (3.17)$$

The value for ω_S is determined from a linear interpolation of the frequency where the corrected X_S measurements equal 0. The inductance L_S is then found by substituting C_S and ω_S into Equation 3.12. To obtain optimum matching of the X_S slopes, one must choose ω and $\Delta\omega$ of Equation 3.16 to be large enough to reduce the effects of the small uncertainties of each measurement as shown in Figure 3.6. A symmetric neighborhood of 1 MHz gives excellent results if the frequency resolution of the actual measurements is 0.1 MHz.

The most accurate matching is thus achieved by considering the slope of $X_S(\omega)$ in the 1 MHz region symmetric about ω_S. This slope is most accurately computed by taking a linear regression of the 11 corrected measurements of X_S that are contained in the 1 MHz neighborhood.

The series resistance, R_S, is determined from a linear interpolation of $Re\{Z_S\}$ at ω_S, or:

$$R_S = Re\{Z_S(\omega_S)\} \qquad (3.18)$$

The mechanical (acoustic) Q of the series resonant branch is found from:

$$Q_S = 1/\omega_S R_S C_S \qquad (3.19)$$

This approach was used to recompute the simplified impedance circuit models for the previously tested films. A computer program, ZSIMP.FOR (Appendix G), was used to evaluate the simplified impedance circuit model. In most cases, the model's maximum deviations of impedance magnitude and phase were less than 2% over the broadband frequency ranges of the actual measurements. The 5% improvement in accuracy verified the value in choosing the reactive components to give optimum matching of their reactive slope, X_S. The completed model results for the 52 micron PVF_2 (MM86005) are shown in Figure 3.7.

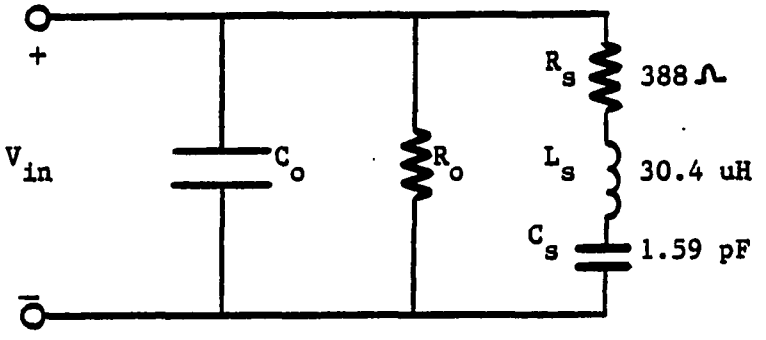

FIGURE 3.7. Completed model for 52 micron PVF_2 (MM86005)

The completed model gave impedance magnitude and phase values that deviated less than 2% from the actual measurements for 0.5-32 MHz.

2. Model simulations

A FORTRAN program, ZPLOT.FOR (Appendix H), was used to read in each set of corrected input impedance measurements and produce output graphics files for input impedance magnitude and phase for (1) the full broadband frequency range, (2) a frequency range symmetric about resonance, and (3) circular impedance and admittance diagrams. Hundreds of plots of actual and modeled impedance results were completed for the many piezo films studied. This section shows some of those plots for the 52 micron PVF_2 film previously mentioned (MM86005).

Figure 3.8 shows the comparisons between the actual and modeled impedance magnitude and phase for the full 0.5-32 MHz frequency range. The scaling of the impedance magnitude was chosen to show the resonant dip at 22-25 MHz. As a result, the impedance magnitude goes off scale below 3 MHz. Notice how the impedance phase angle shows the same characteristic shape as $\mathrm{Tan}(\delta_d)$, (see Figure 3.5). This is intuitive from their mathematical relationship given in Equation 3.6.

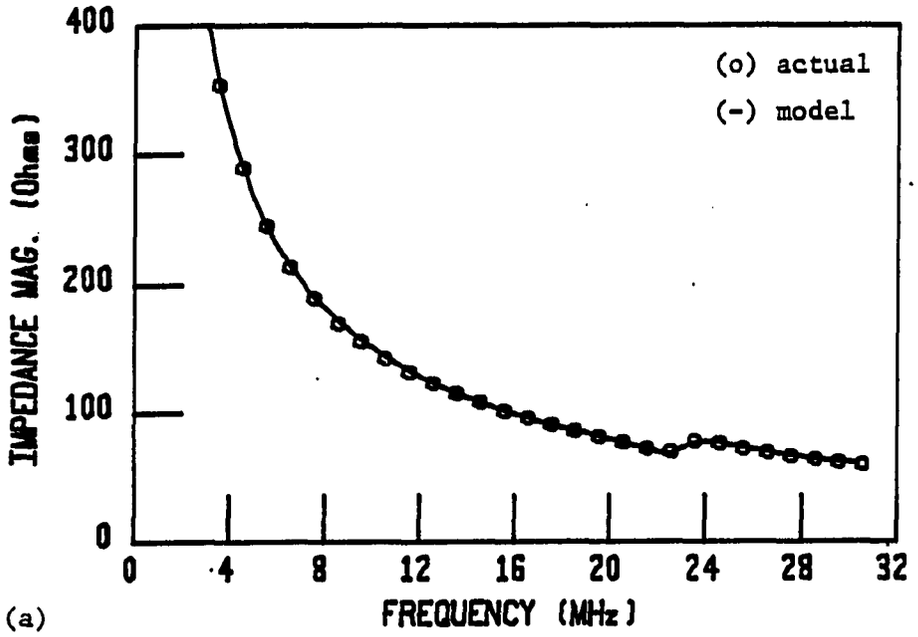

(a)

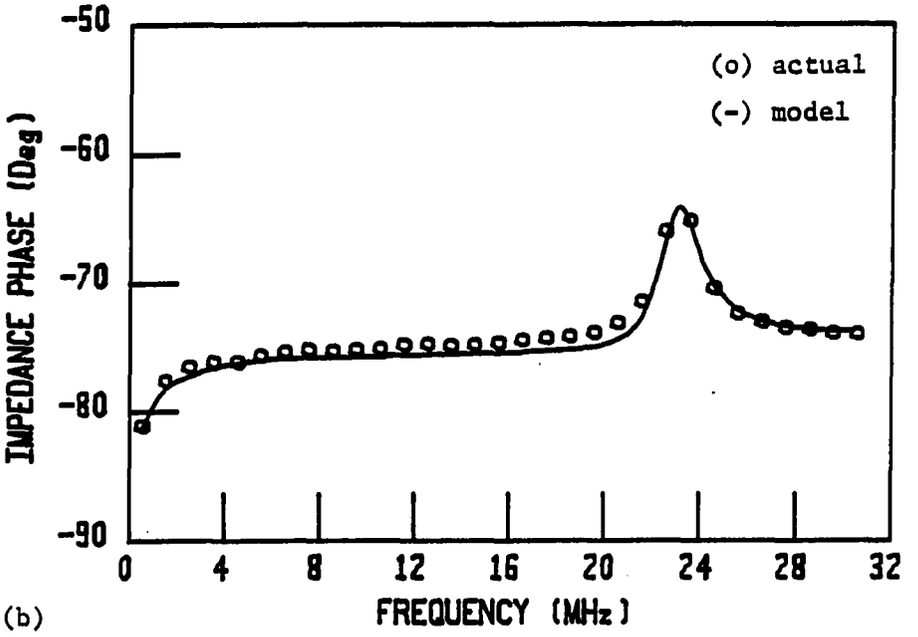

(b)

FIGURE 3.8. Comparison of actual and modeled broadband input impedance (a) magnitude, and (b) phase angle. Results are for 52 micron PVF_2 (MM86005)

The results near resonance are shown in more detail in Figure 3.9. The accuracy of the model near resonance can be better appreciated in this figure.

The real difference in electromechanical behavior between a lossy and near-lossless resonator can be seen by comparing Figure 3.10 with the theoretical circular plots of Figure 2.11. The obvious differences in the plots clearly illustrates the failure of the classical electromechanical modeling techniques which were intended for near-lossless resonators. Note the location of f_s and f_p in the figure for the films.

Figure 3.11 shows the percent deviations in impedance magnitude and phase over the entire 0.5-32 MHz frequency range. The results show good correlation (less than 2% deviation) over the entire range.

3. Improving the approximations for ϵ and Tan(δ_d)

The values for ϵ and Tan(δ_d) were derived by assuming that at frequencies far from resonance, the input impedance is essentially due to C_o shunted by R_o. The model results show that this is indeed the case, however, the mechanical portion of the model always exhibits some, even if negligible, effect on the input impedance. Thus, after computing the wideband deviation of the input impedance of the model and actual measurements, one can "tune" the ϵ and Tan(δ_d)

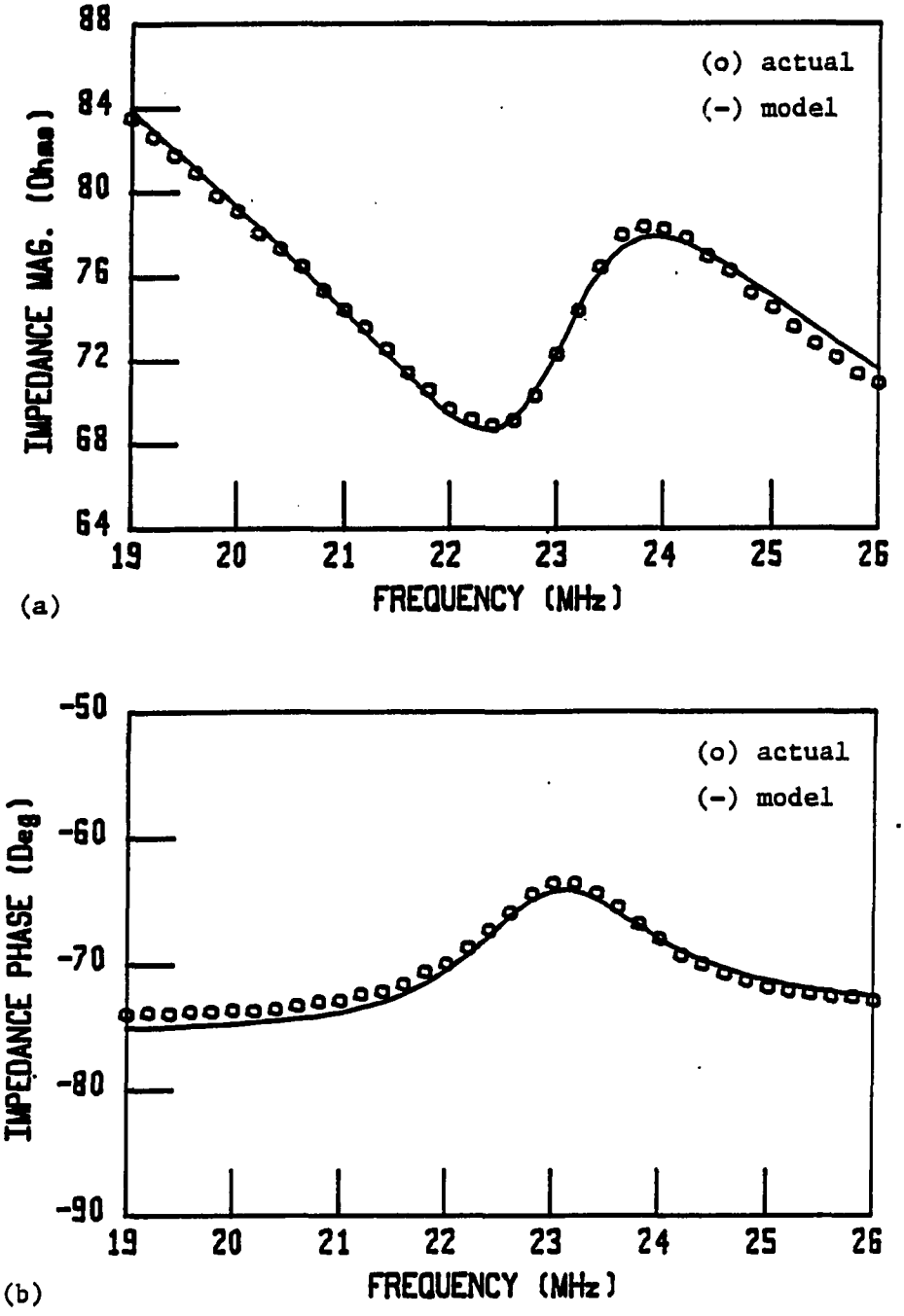

FIGURE 3.9. Comparison of actual and modeled input impedance near resonance for impedance (a) magnitude, and (b) phase angle, PVF_2 (MM86005)

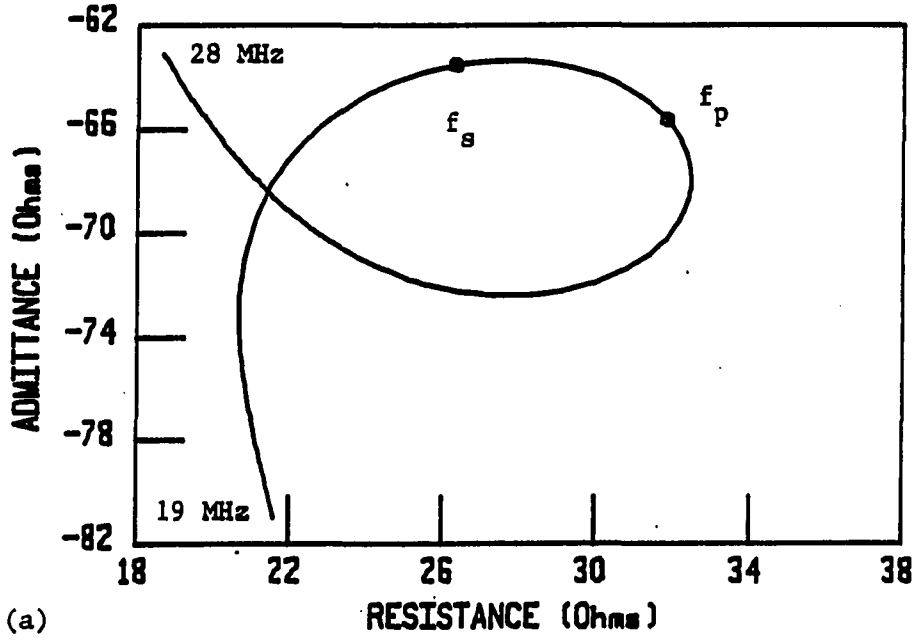

(a)

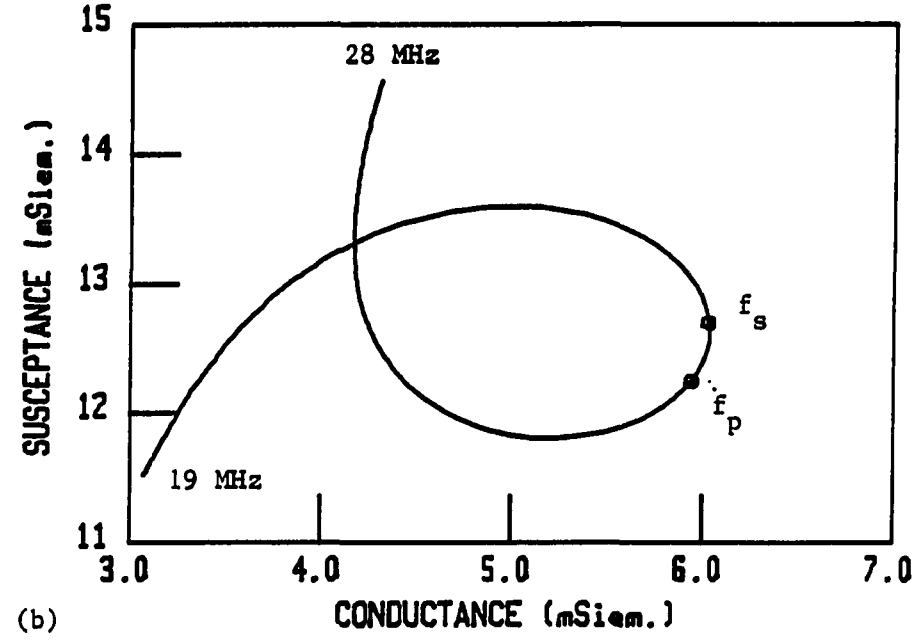

(b)

FIGURE 3.10. Circular plots of 52 micron PVF_2 (MM86005): (a) impedance, and (b) admittance, for 19-28 MHz

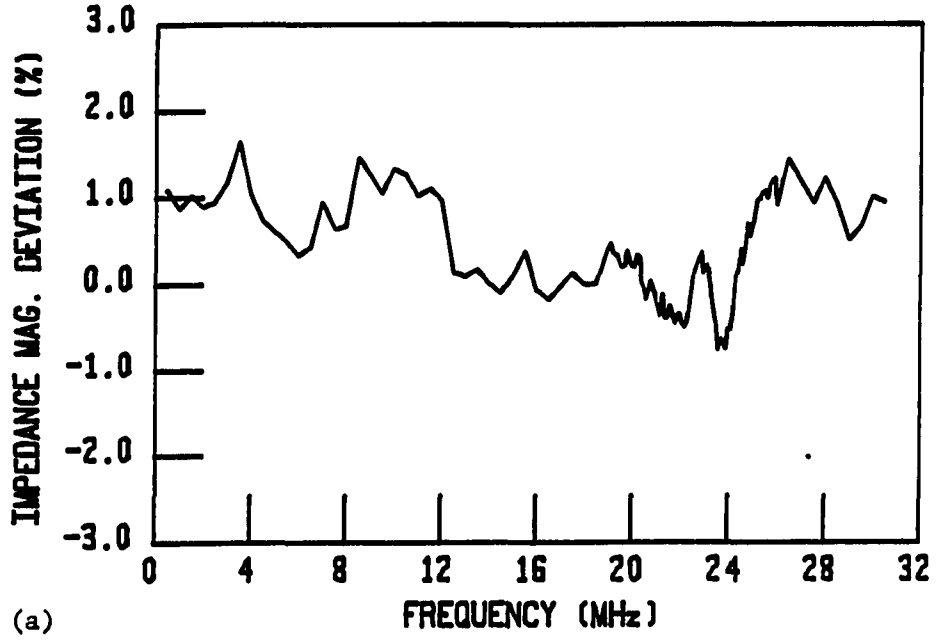

(a)

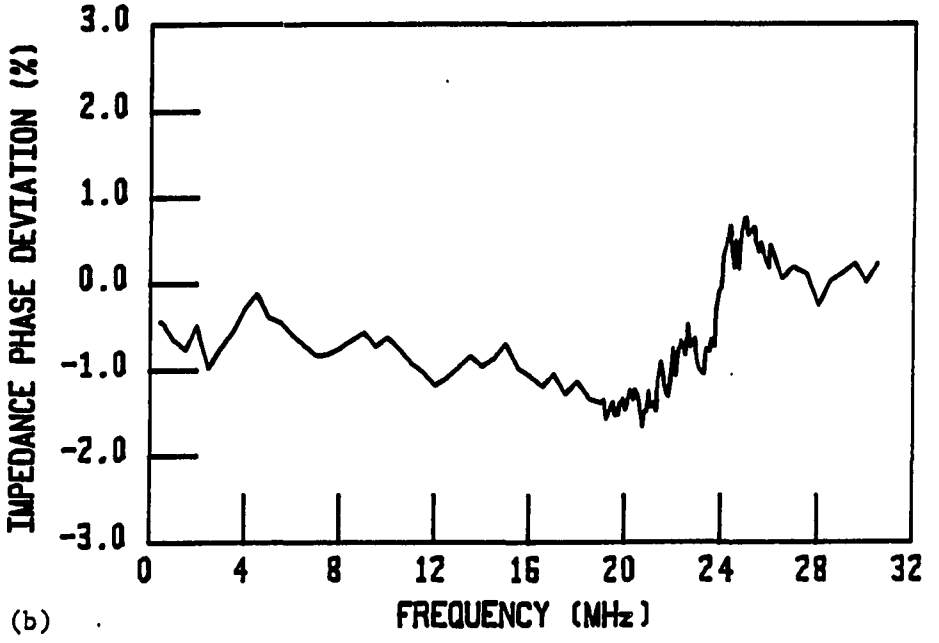

(b)

FIGURE 3.11. Percent deviation of impedance (a) magnitude, and (b) phase angle, for 52 micron PVF_2 (MM86005)

values to shift the deviation to zero, and recompute the circuit components. A computer program can be used to perform such iterations until the magnitude of the impedance deviations lies within the uncertainty of the actual impedance measurements. The result is a model which best fits the measured impedance values.

The previously shown plots of model performance for 52 micron PVF_2 required two iterations. The number of required iterations depends on the degree to which the series (mechanical) resonance portion of the circuit influences the input impedance. Since PVF_2 has a very low electromechanical coupling coefficient (K_t=14.6% for the 52 micron sample), the mechanical branch has little effect on the input impedance at frequencies far from resonance. The copolymer material $P(VF_2-VF_3)$ has a much higher k_t, thus, Z_s will influence the input impedance over a broader frequency range. The degree to which Z_s affects the input impedance also depends on the magnitude of the dielectric losses of the piezo film. Figure 3.12 shows the interpolated ϵ values for a 110 micron $p(VF_2-VF_3)$ sample (VA110G00). The film had much higher electromechanical coupling (K_t=20.69%) and lower dielectric loss tangent ($Tan(\delta_d)$=12.5% at f_s). It can be seen that the lower losses and higher electromechanical coupling cause the first ZDIELECT.FOR approximations for ϵ

and Tan(δ_d) to be in greater error. For this film sample, three iterations were required to give the final estimates for ϵ and Tan(δ_d) that gave impedance deviations of less than 2% over the broadband frequency range.

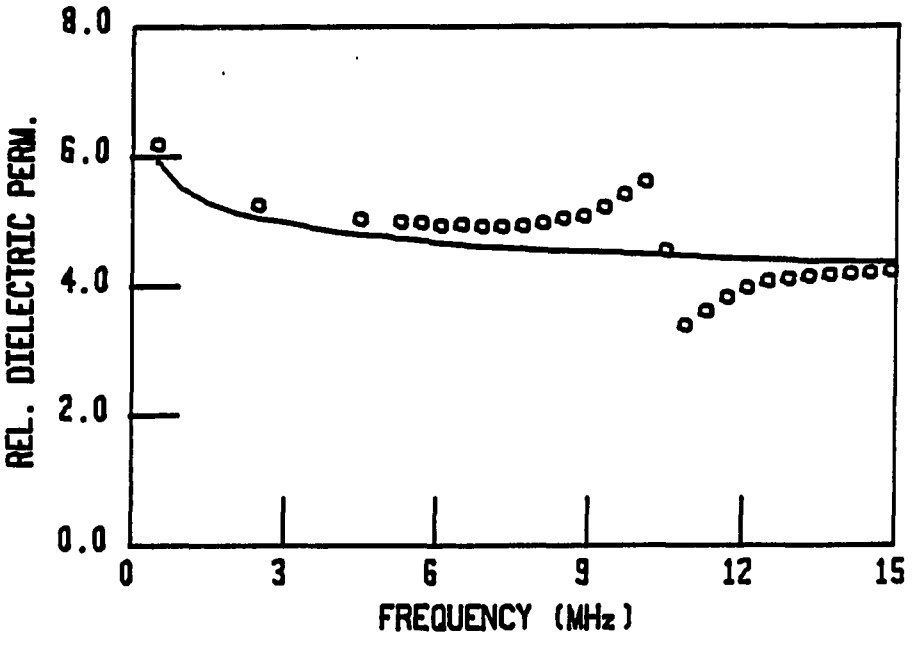

FIGURE 3.12. Final interpolated results of ϵ for 110 micron P(VF_2-VF_3) - (VA110G00). Compare to Figure 3.5

It can be seen from Figure 3.12 that the mechanical impedance, Z_s, exhibits more effect on the input impedance of the copolymer films than with PVF_2, since the ZDIELECT.FOR estimates for ϵ required adjustment (a slight

lowering) even at low frequencies. For the hypothetical case where there is no electromechanical coupling (K_t=0), the final iterated value for ϵ would be the same as the first estimates from the ZDIELCT.FOR program (i.e., no lowering of the initial estimates). After gaining sufficient experience in analyzing both piezo film types, one can soon make better first approximations for both ϵ and Tan(δ_d) so that only two iterations are required for accurate broadband modeling results.

4. Conclusions

It was shown in this section that by correctly modeling the series resonance portion of the simplified impedance circuit model, accurate broadband modeling of the input impedance may be achieved. The keys to this success were in the derivation of the initial estimates of the dielectric properties ϵ and Tan(δ_d), and choosing L_s and C_s to match $dX_s/d\omega$ of the model and actual results. The entire modeling procedure is now outlined below:

1. Obtain the broadband corrected impedance measurements (magnitude and phase).
2. From knowledge of the physical dimensions of the film (A and d), determine the first estimates of ϵ and Tan(δ_d) from program ZDIELECT.FOR, and

smoothly interpolate the results through resonance.

3. Remove the shunt impedance $R_O//C_O$ from the corrected impedance measurements (program ZF0.FOR) and print out the remaining impedance, Z_S, in the 1 MHz neighborhood symmetric about resonance.
4. Compute the series resonance frequency, f_S, from a linear interpolation of frequency where $Im\{Z_S\}=0$.
5. Compute R_S from a linear interpolation of $Re\{Z_S\}$ at f_S.
6. Compute the slope $\Delta X_S/\Delta\omega$ in the 1 MHz frequency range symmetric about f_S.
7. Compute C_S from Equation 3.17.
8. Compute L_S from Equation 3.12.
9. Compute the broadband deviations in actual and model impedance magnitude and phase. Use these deviations to improve the ϵ and $Tan(\delta_d)$ values until the magnitude of the impedance deviations lies within the uncertainty of the actual impedance measurements.

This approach yields a model that best fits the actual impedance measurements. The procedure was used on nine

different piezo films and in all cases, the simplified impedance models provided broadband results that were within 3% of the actual measurements (most were within 2%). Results for the simplified impedance circuit models for some of these films are provided at the end of this chapter. The use of the circuit models for transducer design will be shown in Chapters V and VI.

After achieving a method for successful broadband impedance modeling of the piezo films, the work next focussed on modeling both acoustic and impedance performance in a single electromechanical circuit model.

C. Derivation of Modified Mason's Models

Mason's classical circuit derivation was presented in Chapter II. It was pointed out in that chapter that since the derivation failed to account for dielectric and mechanical losses, it could not be directly used for the piezo films. However, Mason's model is an extremely important tool for assessing quantitative acoustic performance of suitable low-loss piezoelectric materials (i.e., quartz, PZTs, etc.). Since so many design techniques are already used with Mason's circuit, a method was developed for modifying Mason's model which would allow the application of these techniques for the piezo films. It was also believed

that if only slight modifications to Mason's model were required, the work would not only be easier than starting completely over, but would be better received by investigators who already use the well-recognized circuit model. This section describes how Mason's model was modified to provide accurate broadband modeling of the piezo films.

1. Modifications to Mason's Model

There are three major reasons why Mason's model fails to accurately model the piezo films:

1. Mason's model does not account for the frequency dependence of the bulk capacitance, C_o.
2. Mason's model does not account for the frequency-dependent dielectric losses.
3. Mason's model does not account for the mechanical-acoustic losses.

The first two problems can be addressed by modeling the dielectric circuit with the previously derived shunt combination of R_o and C_o. To account for the mechanical losses required additional thought. The solution to the problem was obvious after studying the series resonance branch, Z_s, for the impedance circuit models that were previously derived for the piezo films. In all cases the resistance component R_s was simply too large to have been accounted for

in Mason's model for air-loaded impedance measurements. The implication of this observation was that a mechanical loss resistance must be added to Mason's model to account for the high acoustic losses of the piezo films. Even though it was not obvious how to scientifically derive the value for this resistance, it was clear that a resistor was needed in series with the mechanical portion of the circuit model. This resistance, R_m, and the dielectric loss resistance, R_o, were added to Mason's model as shown in Figure 3.13.

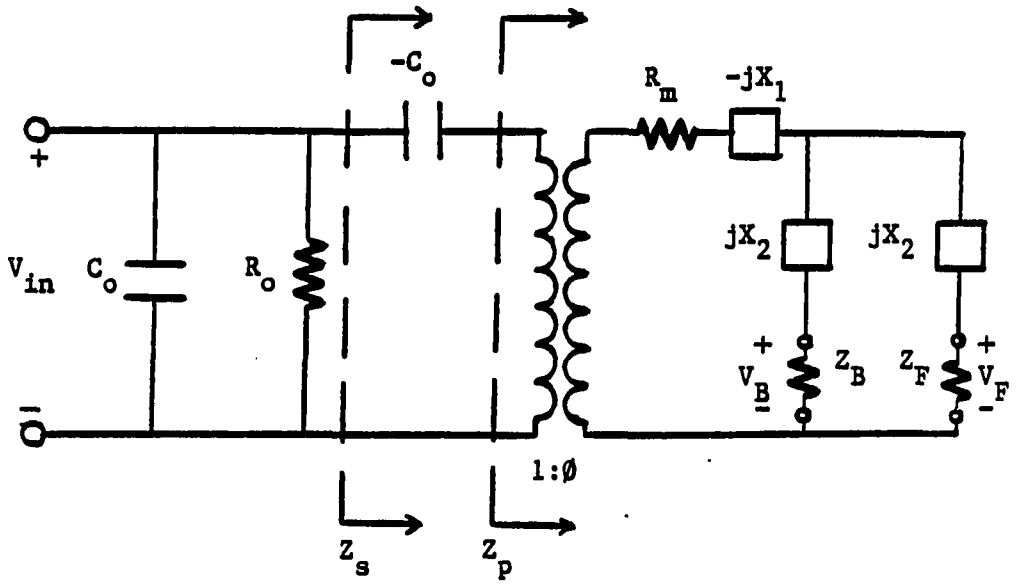

FIGURE 3.13. The modified Mason's model

Another version of the circuit model, Figure 3.14 accounts for the electrode layers as described in Chapter II (Figure 2.9). The subscripts "o" are used for the variables concerning the piezo film and the subscripts "E" are used for the variables concerning the electrode material.

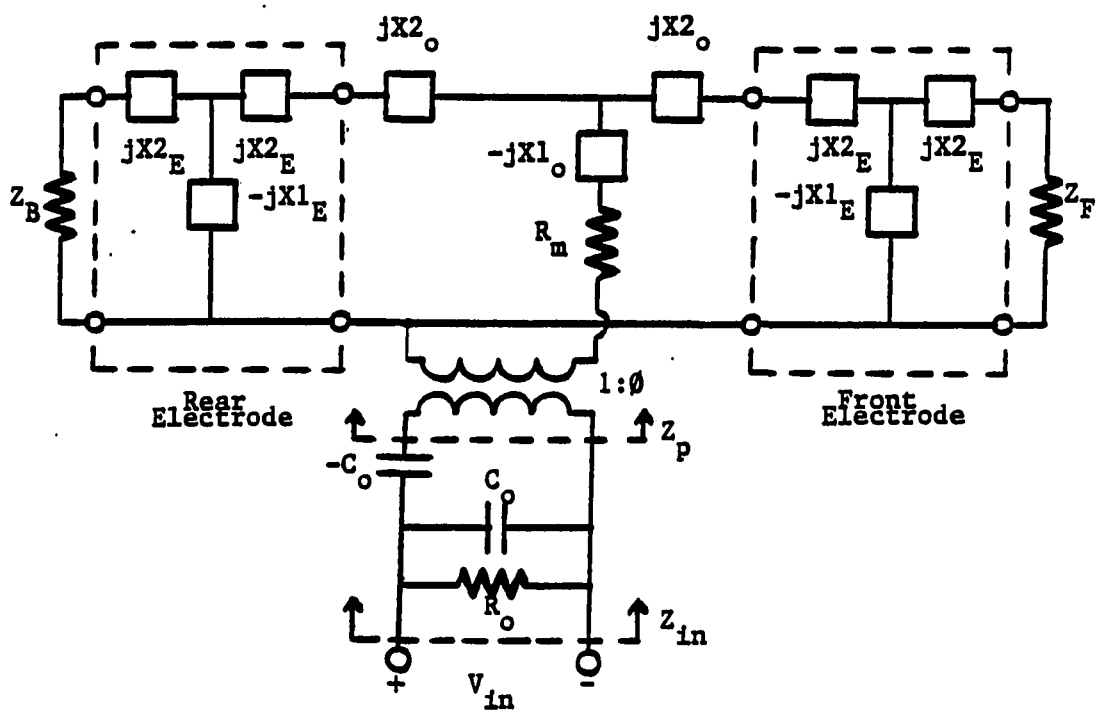

FIGURE 3.14. The modified Mason's model which includes electrode layers

It can be shown that the added mechanical loss resistance can be accurately accounted for by:

1. Placing a resistance of R_m in series with the secondary of the ideal transformer (as shown).
2. Placing resistances of $2R_m$ in series with each acoustic face (port).
3. Placing a resistance of R_m/ϕ^2 in series with the primary of the ideal transformer.

The choice of the location may be made by mathematical convenience for the investigator. Since the ideal transformer provides conversion of electrical (primary side) to/from mechanical (secondary side) energy, the mechanical loss resistance seems more "natural" if placed in the mechanical circuit as shown in the figures.

While it was obvious that the resistance had to be accounted for, it was not immediately obvious how to derive its value.

2. Determining the circuit model components

The circuit model components required for the modified Mason's models are summarized below:

$R_o = 1/(\omega C_o \mathrm{Tan}(\delta_d))$, dielectric loss resistance (3.20)

$C_o = \epsilon A/d$, bulk capacitance (3.21)

ρ = density (3.22)

v = sound velocity (3.23)

R_m = mechanical loss resistance (3.24)

C_m = mechanical capacitance (3.25)

$$Q_m = 1/\omega R_m C_m \text{ , air-loaded mechanical Q} \quad (3.26)$$

$$Z_o = \rho v_o \text{ , acoustic impedance of piezo film} \quad (3.27)$$

$$Z_E = \rho v_E \text{ , acoustic impedance of electrodes} \quad (3.28)$$

$$Z_F, Z_B = \text{acoustic impedance of front/back loads} \quad (3.29)$$

$$X1_n = Z_n/\mathrm{Sin}(\theta_n) \quad (3.30)$$

$$X2_n = Z_n\mathrm{Tan}(\theta_n) \quad (3.31)$$

$$\theta = 2\pi fd/v \quad (3.32)$$

$$f = \text{frequency (Hz)} \quad (3.33)$$

$$\phi = k_t[v_o C_o Z_o/d]^{1/2} \quad (3.34)$$

$$k_t = \text{electromechanical coupling coefficient} \quad (3.35)$$

To compute the model components, the area, thickness, and densities of the piezo film (and electrodes if desired) are required. The film area and thickness are determined as described in Section A (see Equation 3.11). The density of the piezo films was determined by dividing the product of the measured values for A and d, by the weight of the particular sample. All samples were weighed on a precision balance (Mettler Model H31AR, sn 673802). Determining the remaining model components requires knowledge of R_m, C_m, Q_m, v_o, and k_t. After many different approaches to solving for these quantities, a successful method was derived for systematically determining the components.

The key in determining the components is knowing how and where to start first! One must keep in mind that all of

the mechanical circuit must provide approximately the same electrical impedance as the series impedance branch of the simplified impedance circuit model. In that model, only three components had to be derived from the impedance measurements. For the modified Mason's model there are five quantities to derive and most of the values appear to be interactive. For instance, a change in v_o causes ϕ to change, which in turn changes the input impedance to the electromechanical transformer. It is this impedance that determines the mechanical Q! Some investigators, when faced with this situation, have derived a multidimensional family of curves and set criteria for a best-fit derivation of the piezoelectric constants k_t and Q_m (Saitoh et al., 1985).

It will be shown that all of the needed constants and components can be independently derived by following a five-step algorithm. To begin the analysis, an approach similar to that in deriving the components of the simplified impedance circuit model was used. The same computer program (ZF0.FOR) was used to aid the Mason's model derivations.

> In all following discussions, the superscript "$^-$" will be used to denote impedance values derived from the actual impedance measurements.

The program first computed $\bar{Z}_s$ from the actual impedance measurements by removing the shunt impedance of R_o and C_o. Next, the impedance of the negative capacitance, $-C_o$, was subtracted, leaving the parallel impedance, $\bar{Z}_p=(\bar{R}_p+j\bar{X}_p)$. The desired quantities can all be independently determined from analysis of $\bar{Z}_p$.

A computer program ZSEC.FOR (Appendix I) was used to compute the theoretical impedance values of the modified Mason's model for comparison with the actual results of ZF0.FOR. To begin the analysis, a hardcopy of the real and imaginary components of $\bar{Z}_p$ is analyzed. Table 3.2 shows a list of the program results for the 52 micron PVF_2 sample (MM86005).

TABLE 3.2. ZSEC.FOR hardcopy results for Z_p near resonance

f (MHz)	Re{Z_p} (Ω)	Im{Z_p} (Ω)
22.5	392.44	-213.29
22.6	393.49	-184.67
22.7	387.35	-141.61
22.8	387.50	-105.03
22.9	388.28	-68.23
23.0	384.01	-23.69
23.1	381.04	12.09
23.2	379.00	49.95
23.3	376.29	89.84
23.4	379.00	135.34
23.5	371.48	176.07

From the table, the parallel resonant frequency, f_p, can be determined from a linear interpolation of frequency where $\bar{X}_p=0$. This frequency can be used to compute the acoustic velocity from Equation 2.37, thus:

$$v_o = 2df_p \tag{3.36}$$

Next, the slope of $\bar{X}_p$, $\Delta\bar{X}_p(\omega)/\Delta\omega$, is computed in the 1 MHz frequency range symmetric about f_p, and C_m is then computed from Equation 3.17. For this particular film:

$\Delta\bar{X}_p(\omega)/\Delta\omega$ = 389.4 Ω/MHz and C_m = 1.54 pF

Table 3.2 is also important since it is used to compute $\bar{R}_m$ from a linear interpolation of $Re\{\bar{Z}_p\}$ at f_p. After supplying the ZSEC.FOR program with the dielectric data for ϵ and $Tan(\delta_d)$, v_o, and C_m; the program prompts the user for the remaining model values and then prints the resulting impedance values to the screen for analysis. The user is prompted for the value of k_t which is set to match the computer-generated slope, $\Delta X_p(\omega)/\Delta\omega$, with the actual slope, $\Delta\bar{X}_p(\omega)/\Delta\omega$. For the 52 micron PVF_2 (MM86005), a value of K_t=14.66% was needed to match the slopes to 389.4 Ω/MHz.

Finally, the computer-generated impedance Z_p is then compared with $\bar{Z}_p$, and Q_m is set to match $Re\{Z_p\}$ with $Re\{\bar{Z}_p\}$ at f_p. The resistance $Re\{Z_p\}$ is composed of both mechanical

loss resistance and the acoustic impedance of air at the front/rear faces (ports). From the model:

$$R_p = \mathrm{Re}\{Z_p\} = (R_m + Z/2)/\phi^2 \qquad (3.37)$$

where Z = acoustic impedance of air at front/rear ports

Therefore, R_m can be computed from Equation 3.37 and the analysis is complete. In completing the analysis of the 52 micron PVF_2, the results where Q_m=11.76, R_p=382.0 Ω, and R_m=14.45 Ω.

The same procedure is followed for the modified Mason's model that includes the electrode layers. However, instead of determining v_o from Equation 3.36, v_o is set to match the computer-generated f_p with the value determined from a linear interpolation of $\mathrm{Re}\{\bar{Z}_p\}$ at f_p. Another program, ZIN.FOR (Appendix J), is used to evaluate the full model instead of ZSEC.FOR, and the values for v_E and d_E must also be specified. Both models provide nearly identical simulation results since the electrode layers are nearly thin enough to neglect (300 Å). However, slight differences are seen in the model parameters and the results from the full model (with electrodes) are considered more accurate. Table 3.3 shows a comparison between the two models for the same 52 micron PVF_2.

TABLE 3.3. Comparison of modified Mason's model results for the 52 micron PVF_2 (MM86005)

COMPONENT, PROPERTY	NO ELECTRODES	WITH ELECTRODES
f_p (MHz)	23.07	23.16
v_o (m/s)	2380.0	2389.0
C_m (pF)	1.54	1.54
R_p (Ω)	382.0	382.0
Q_m	11.76	11.75
k_t (%)	14.66	14.63

The effects of the 300 Å Ni-Al electrodes are seen to be small from the results in the table. As expected, the added mass of the electrodes slightly dampens the mechanical response and gives a slightly lower value for Q_m. Since sound travels much faster in the metallization than in the piezo film, failure to account for the electrodes results in a slightly lower ($\simeq$0.4%) resonant frequency, f_p, and acoustic velocity, v_o. Just as for the simplified impedance circuit model, the deviations of the broadband impedance of the models and actual results can be used to tune the values for ϵ and $\mathrm{Tan}(\delta_d)$ for increased accuracy. The result is a modified Mason's model that best fits the actual impedance measurements.

After two or three such iterations, the modified Mason's models provided excellent broadband simulation of

input impedance. The models deviated less than 1% from the actual impedance magnitude and phase measurements over the complete broadband frequency range of analysis, (0.5-32 MHz for the 52 micron PVF_2).

3. Model simulations

Both modified Mason's model programs (ZSEC.FOR and ZIN.FOR) produce output graphics files for plotting the computed input impedance values. For each piezo film analyzed, a full set of impedance plots and deviations was recorded. This section contains a full set of plots for the same 52 micron PVF_2 film previously discussed (MM86005). Results are shown from both the simple modified Mason's model (no electrodes) and the full model (300 Å electrodes included). A partial set of plots for a 30 micron $P(VF_2-VF_3)$ film is also included for comparison. Table 3.4 lists the plots found in this section.

Figures 3.15 and 3.16 show excellent broadband correlation in modeled and actual input impedance for the PVF_2. No difference can be "seen" in the full model results in Figures 3.17-3.19. In fact, the percent deviation plots in Figure 3.20 shows that both modified Mason's model deviations are nearly identical. This was because the parameters of the models were set for a best fit of the impedance measurements. As Table 3.3 showed, the slight differences between the two models are apparent in the model parameters.

TABLE 3.4. List of the modified Mason's model results for 52 micron PVF_2 (MM86005) and $P(VF_2-VF_3)$ (MM87070)

FIG. NO.	PIEZO FILM	DESCRIPTION
3.15[a]	52 micron PVF_2	Broadband input impedance
3.16[a]	" "	Input impedance near resonance
3.17[b]	" "	Broadband input impedance
3.18[b]	" "	Input impedance near resonance
3.19[b]	" "	Circular impedance, admittance
3.20[c]	" "	Broadband impedance deviations
3.21[d]	30 micron $P(VF_2-VF_3)$	Dielectric properties
3.22[b]	" "	Broadband input impedance
3.23[b]	" "	Input imped. near resonance

[a] ZSEC.FOR program results (no electrodes).

[b] ZIN.FOR program results (electrodes included).

[c] ZDEV.FOR program results.

[d] ZDIELECT.FOR program results.

The copolymer plots were included to show the differences in the dielectric properties, and how these properties affect the input impedance results. This particular copolymer had a lower dielectric permittivity than the PVF_2 films, and had comparable dielectric losses (see Figure 3.21). Because of the higher electromechanical coupling, k_t, the mechanical performance had more influence over the input impedance. This can be clearly seen in the larger peaks in impedance phase shift shown in Figures 3.22 and 3.23.

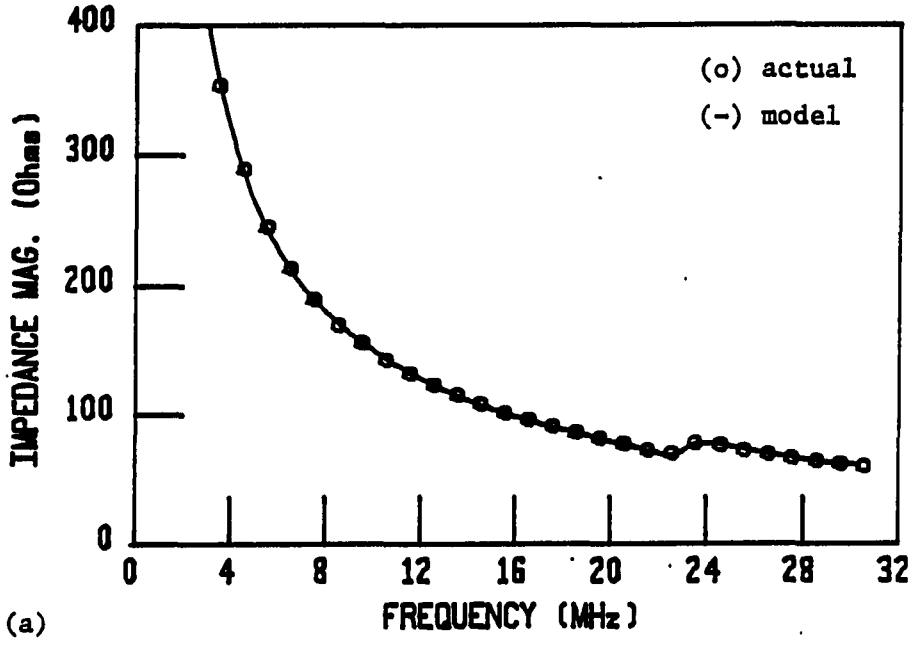

(a)

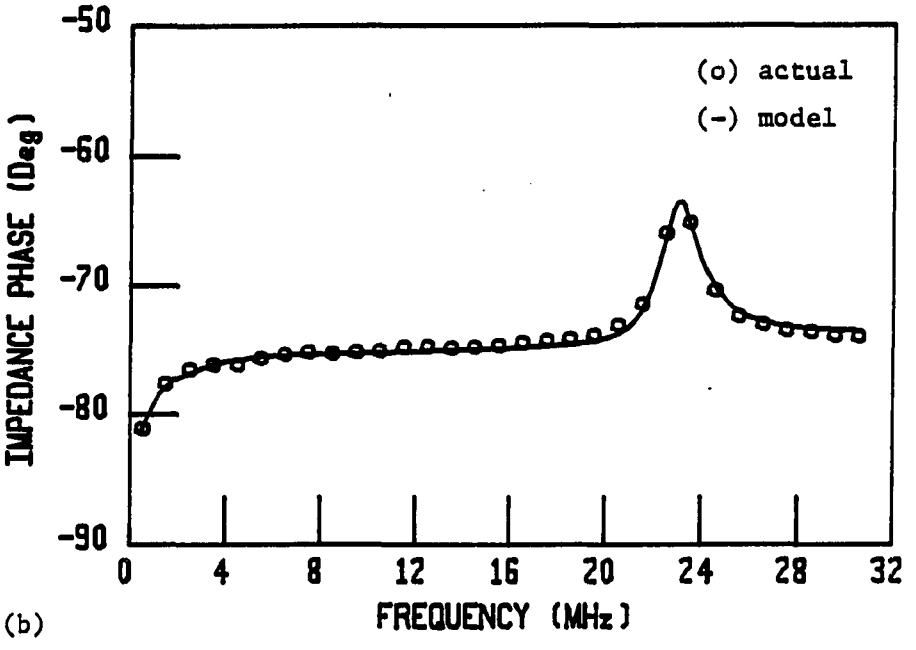

(b)

FIGURE 3.15. Comparison of actual and modeled broadband input impedance (a) magnitude and (b) phase for 52 micron PVF_2--modified Mason's model (no electrodes)

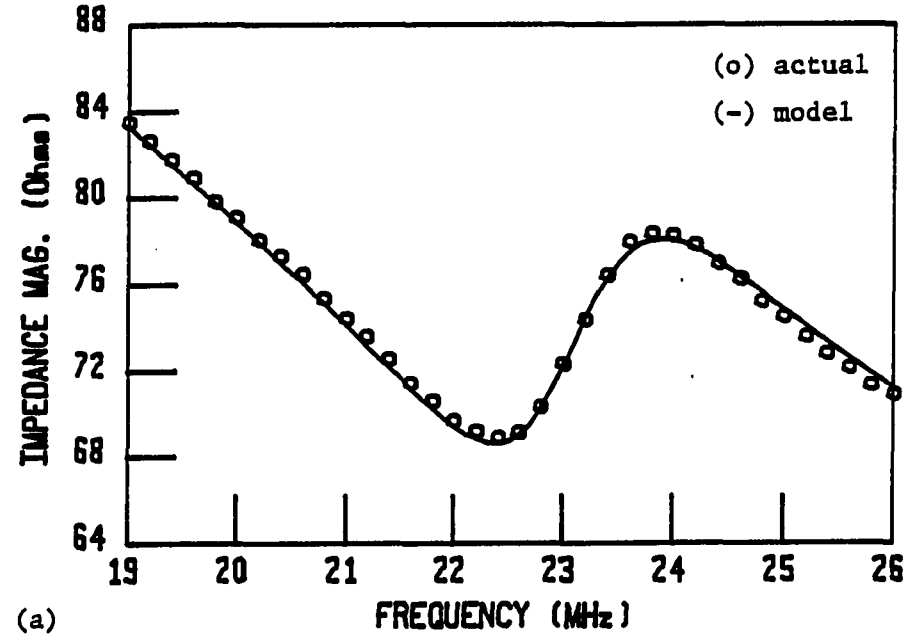

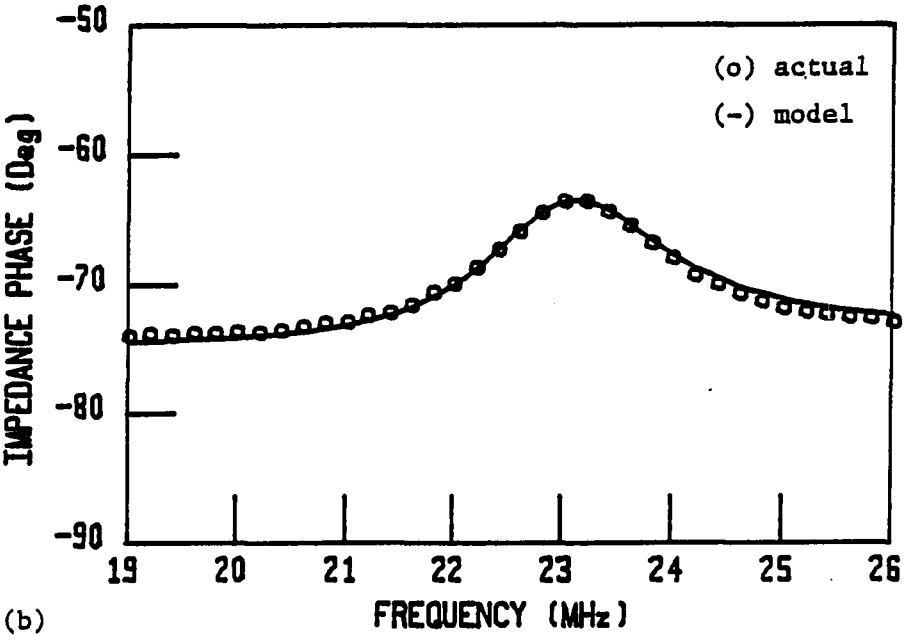

FIGURE 3.16. Comparison of actual and modeled input impedance near resonance: impedance (a) magnitude and (b) phase for 52 micron PVF_2--modified Mason's model (no electrodes)

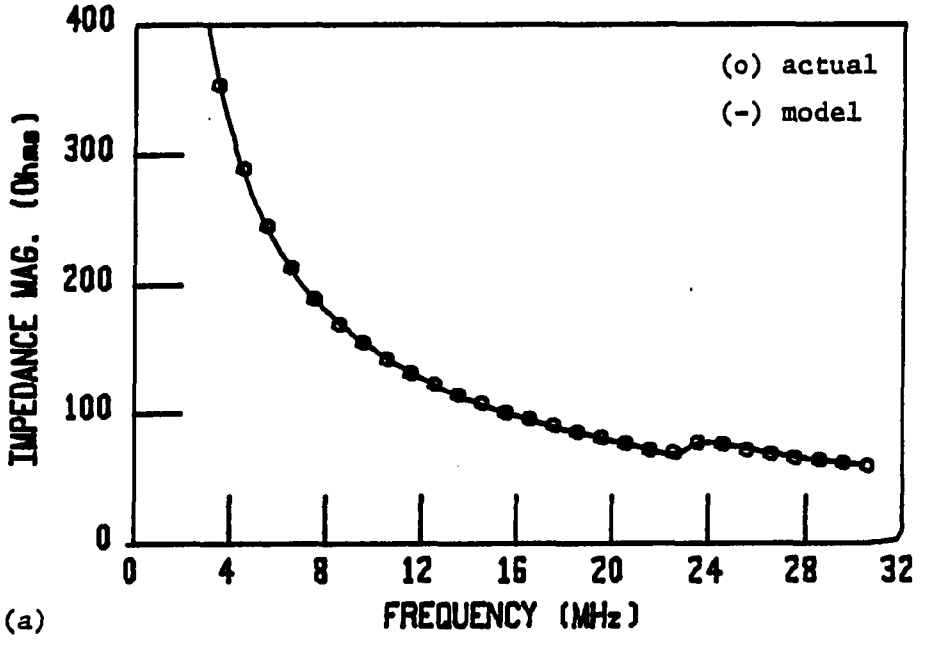

(a)

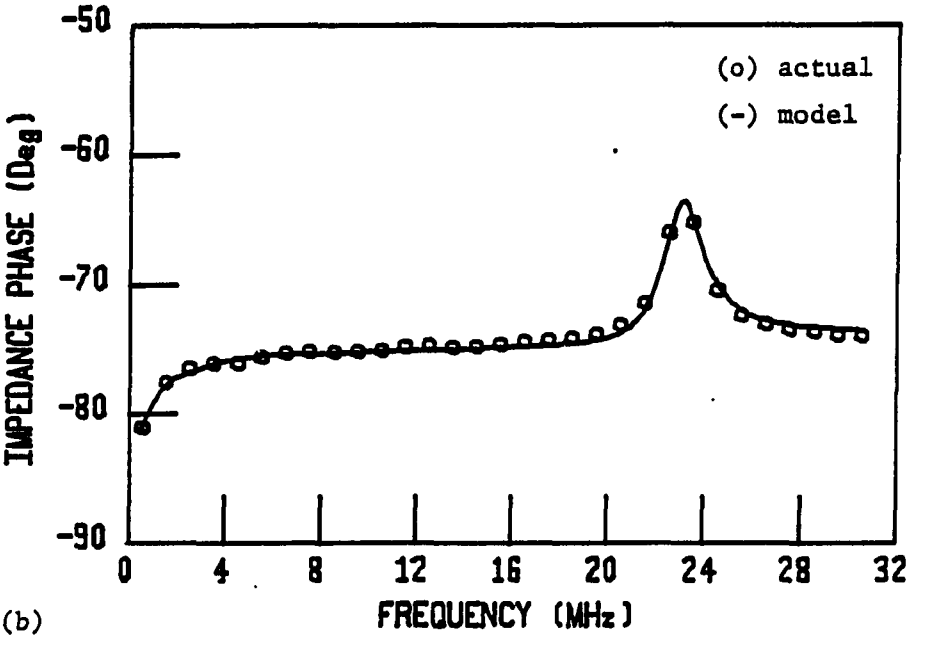

(b)

FIGURE 3.17. Comparison of actual and modeled broadband input impedance (a) magnitude and (b) phase for 52 micron PVF_2--modified Mason's model (with electrodes)

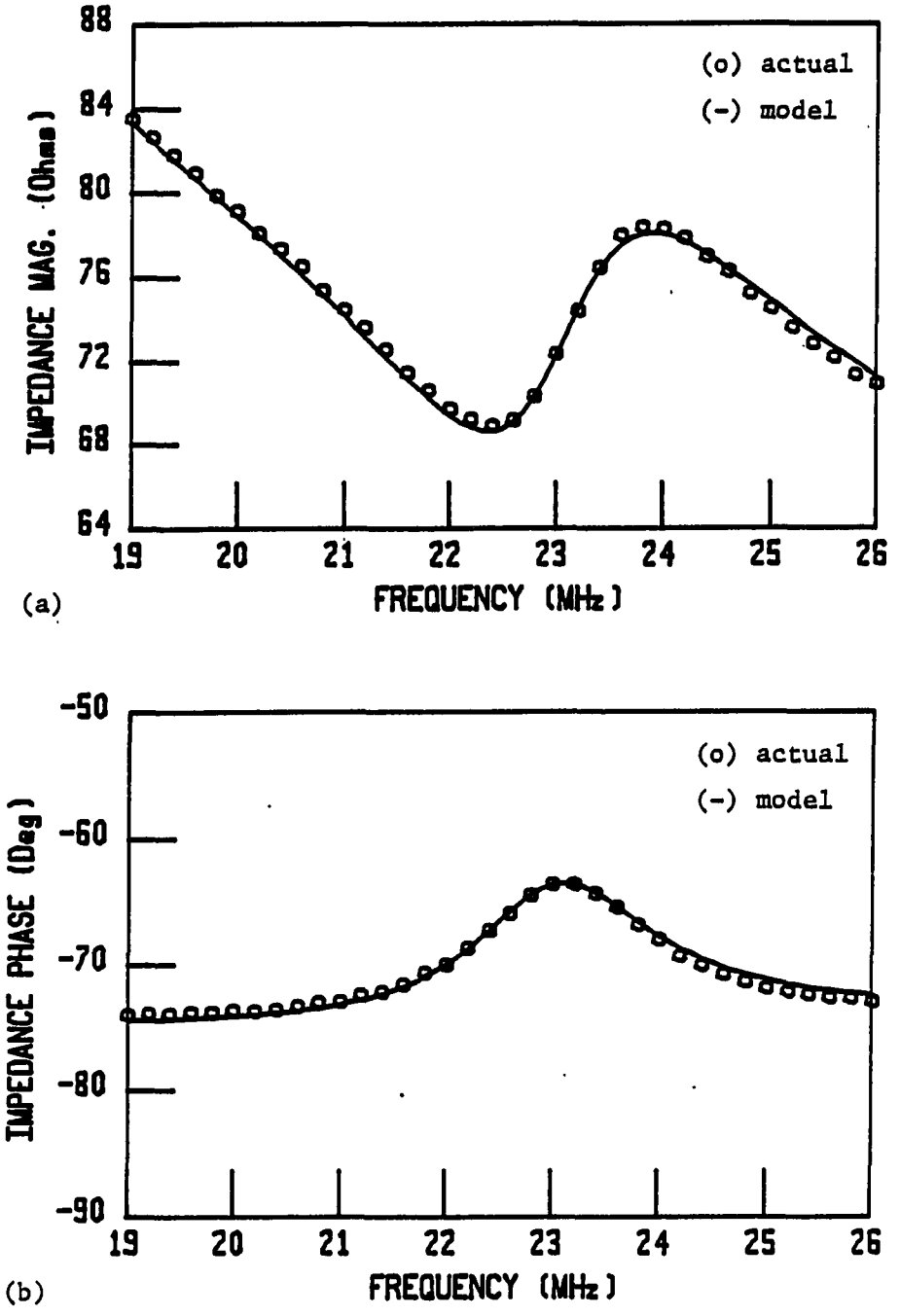

FIGURE 3.18. Comparison of actual and modeled input impedance near resonance: impedance (a) magnitude and (b) phase for 52 micron PVF_2--modified Mason's model (with electrodes)

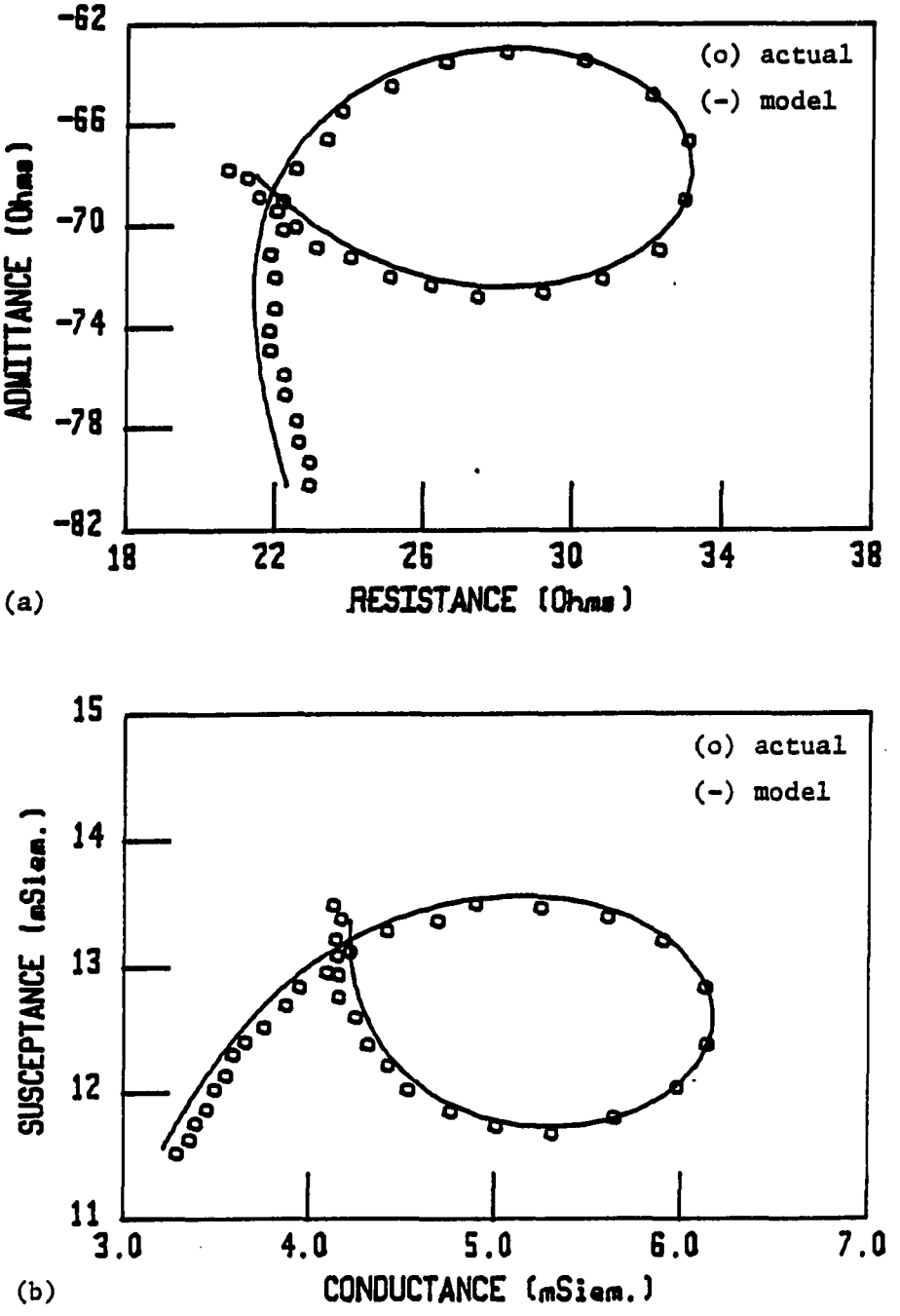

FIGURE 3.19. Comparison of actual and modeled circular (a) impedance and (b) admittance: 52 micron PVF_2--modified Mason's model (with electrodes)

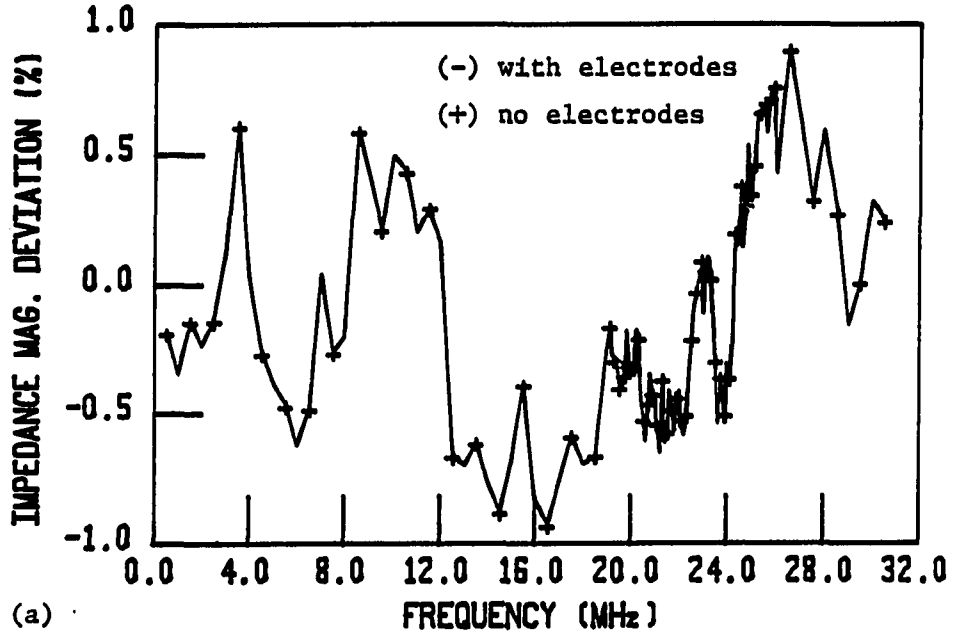

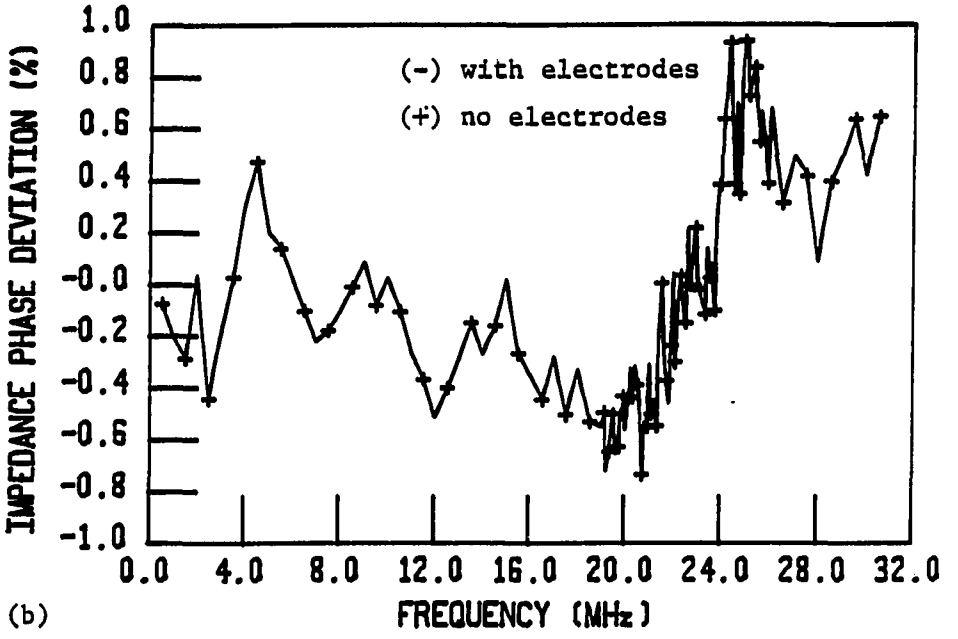

FIGURE 3.20. Comparison of percent deviation in broadband impedance (a) magnitude and (b) phase: 52 micron PVF_2--both modified Mason's models

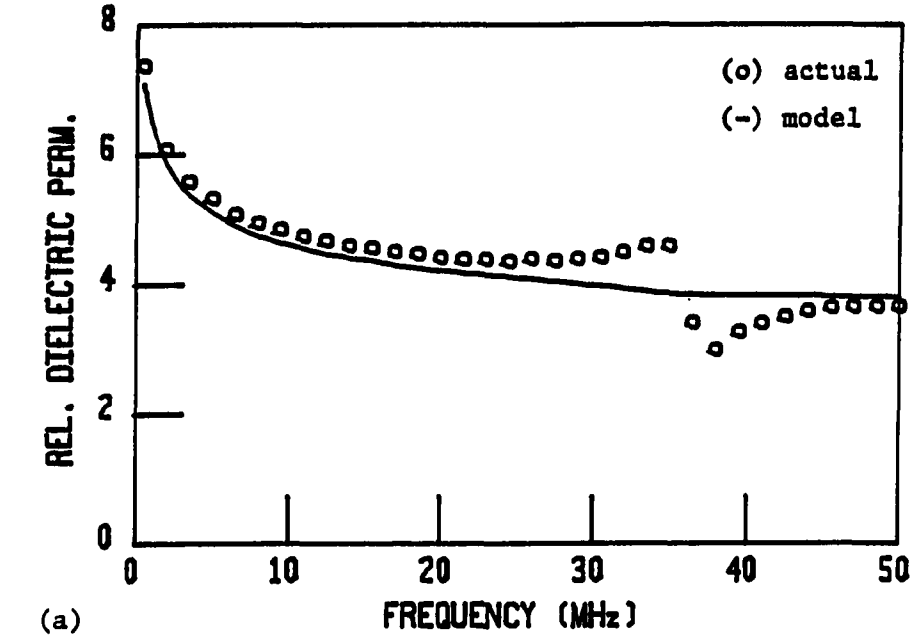

(a)

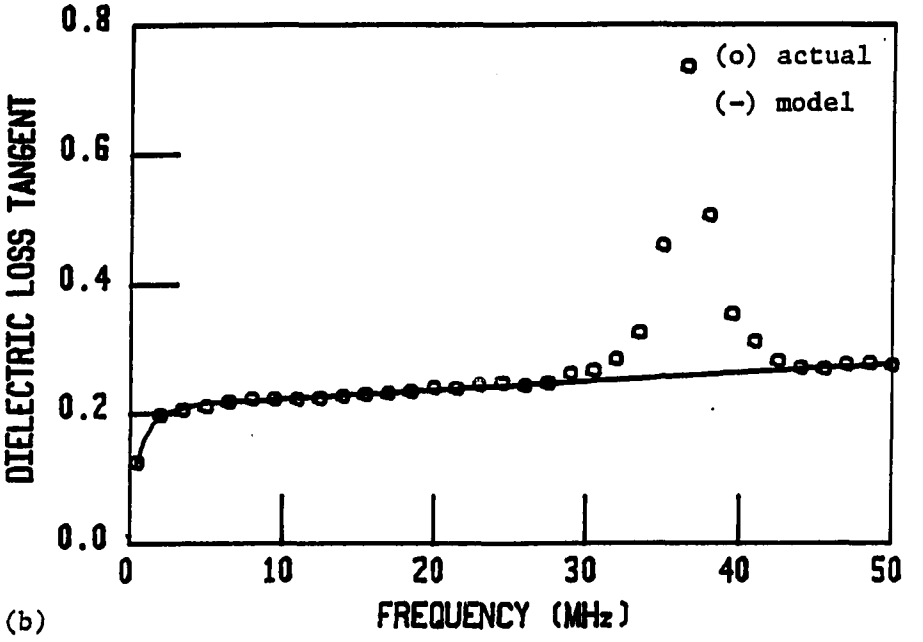

(b)

FIGURE 3.21. Dielectric properties of 30 micron $P(VF_2-VF_3)$: (a) ϵ and (b) $\text{Tan}(\delta_d)$. Compare to results of Figures 3.5 and 3.12

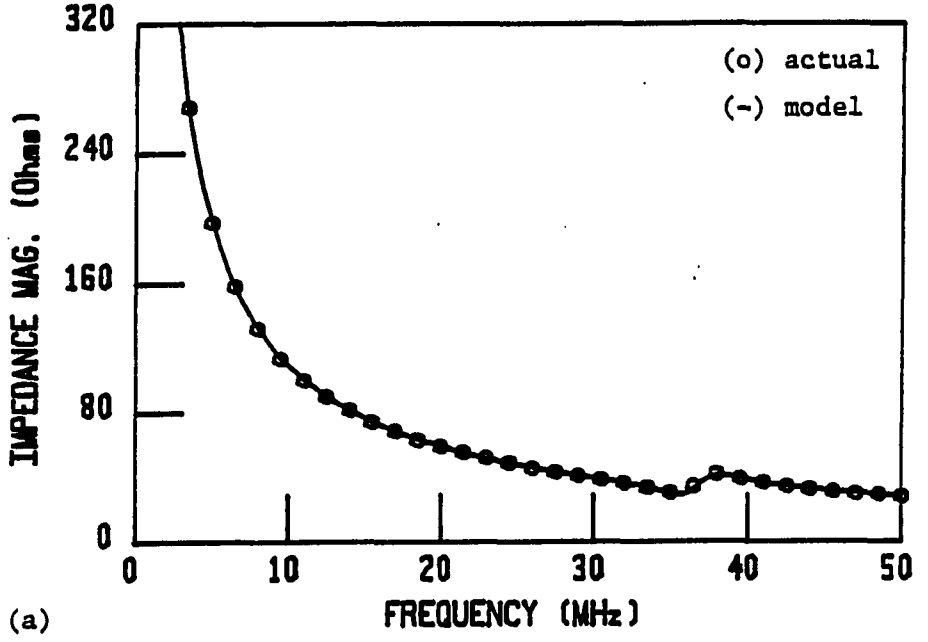

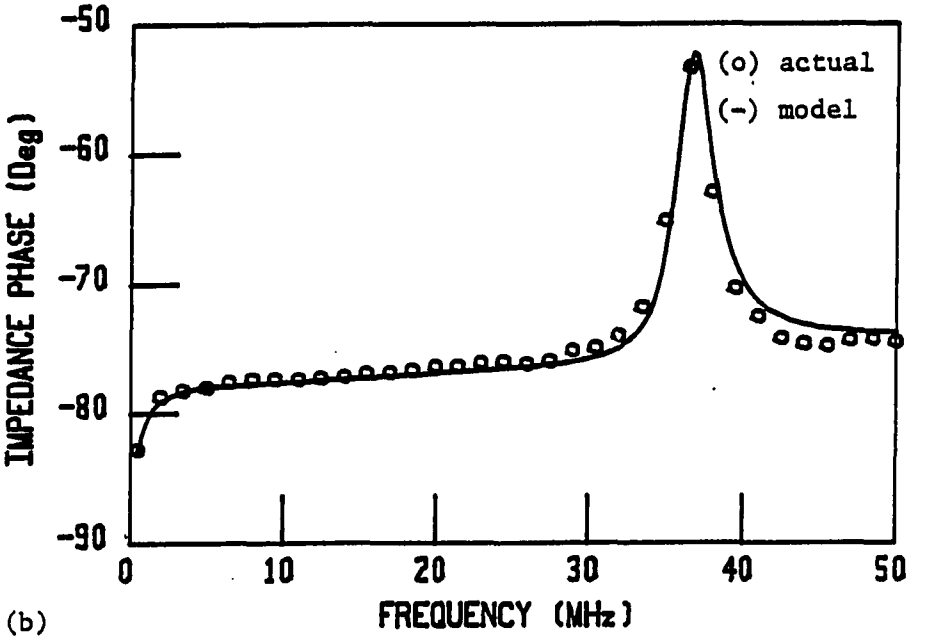

FIGURE 3.22. Comparison of actual and modeled broadband input impedance (a) magnitude and (b) phase for 30 micron P(VF_2-VF_3)--modified Mason's model (with electrodes)

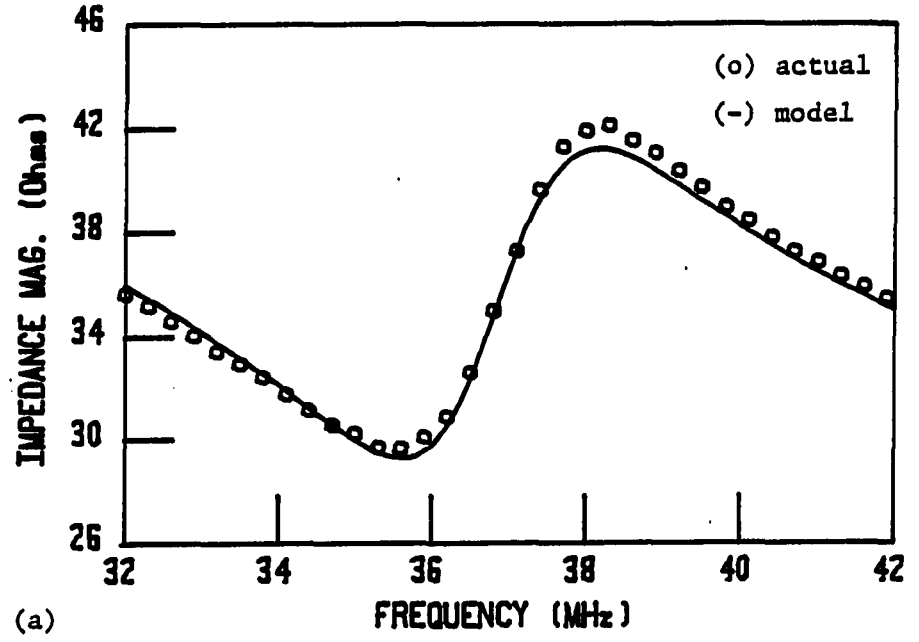

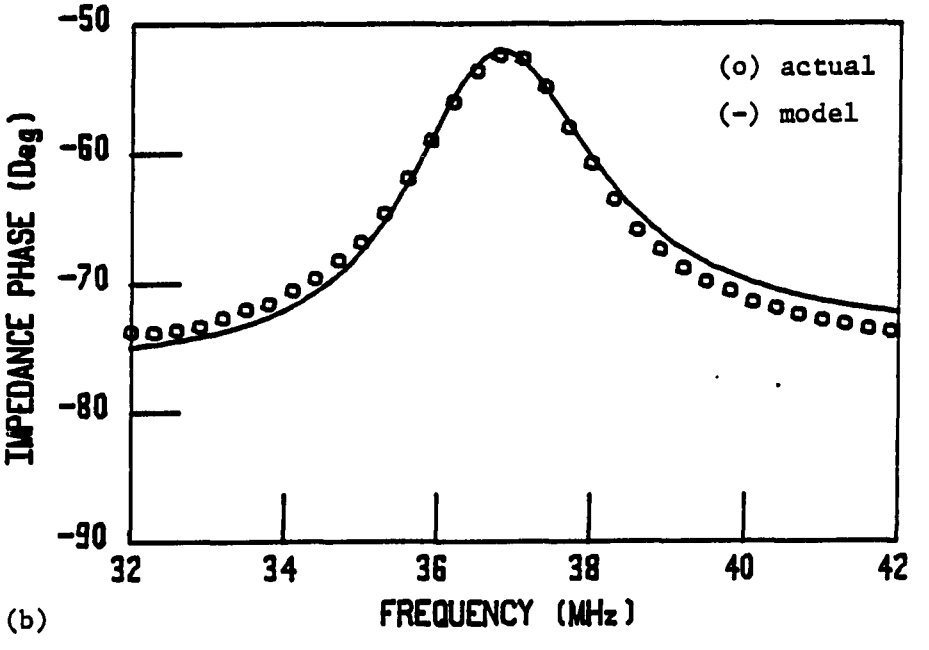

FIGURE 3.23. Comparison of actual and modeled input impedance near resonance: impedance (a) magnitude and (b) phase for 30 micron $P(VF_2-VF_3)$--modified Mason's model (with electrodes)

4. Conclusions

The modified Mason's model provided excellent broadband prediction of electrical input impedance for the piezo films. The modifications to Mason's circuit model developed here, thus appear to be both accurate and justified. As for predicting acoustic performance, the effects of the circuit modifications were not known until later research. But it was clear that the modified circuit models provided impedance results that were as accurate as the actual impedance measurements that the model parameters were determined from.

The key to determining the needed parameters for the models was in discovering how to systematically derive the parameters by following the five-step algorithm. The success of the impedance modeling was proof that by knowing the dielectric properties and physical dimensions of the film, the needed piezoelectric constants and circuit components can be derived from analysis of a film's input impedance near resonance. This approach offers a new, relatively easy method for determining k_t and Q_m for a lossy piezoelectric resonator. The five-step algorithm, based on comparing the mechanical impedance of a film's actual measurements ($\bar{Z}_p=\bar{R}_p+j\bar{X}_p$) to the computer-generated value ($Z_p=R_p+jX_p$) is summarized below:

1. The parallel resonant frequency, f_p, is determined from a linear interpolation of frequency where $X_p=0$. The acoustic velocity is then found from $v_o=2df_p$. If electrodes are included in the model, v_o is set to match f_p of the model with the previously interpolated value.
2. The slope $\Delta\bar{X}_p(\omega)/\Delta\omega$ is computed in the 1 MHz frequency range symmetric about f_p, and C_m is computed from Equation 3.17.
3. $\bar{R}_p$ is determined from a linear interpolation of $Re\{\bar{Z}_p\}$ at f_p.
4. Next, k_t is set to match the circuit model's slope $\Delta\bar{X}_p(\omega)/\Delta\omega$, with the measured value of step (2) in the 1 MHz frequency range symmetric about f_p.
5. Finally, Q_m is set to match $Re\{\bar{Z}_p\}$ with $Re\{Z_p\}$ at f_p, and R_m is then determined from Equation 3.37.

The addition of the mechanical loss resistance, R_m, clearly fits intuition concerning mechanical acoustic losses. Its presence is actually valid in any Mason's model for a piezoelectric resonator. For ceramic PZTs, which have very large Q_m values, the resistance would be so small that it would offer little significance, except to explain the acoustic Q of the material which is always a finite value.

Without the resistor, Mason's model yields an unloaded Q_m of infinity!

It is clear then that valuable new insight has been gained in both electromechanical modeling of piezoelectric resonators, and into the physical properties of the piezo films that give rise to their broadband acoustic performance. Further research strongly supported the accuracy of the modified Mason's models in also predicting acoustic performance. The next section contains a summary of the circuit modeling results for some of the piezo films analyzed in this research.

D. Specifications for Modeled Piezo Films

Many different PVF_2 and $P(VF_2\text{-}VF_3)$ films were analyzed and modeled in this research. For each film, a specification sheet was compiled for documenting its piezoelectric properties and modeling components for all three models: (1) simplified impedance circuit model, (2) simple modified Mason's model (no electrodes), and (3) full modified Mason's model (electrodes included). Copies of some of these specification sheets were sent to Pennwalt Corporation production engineers who were interested in the effects of new film processing techniques on the piezoelectric properties.

It was apparent from the different analyses that each piezo film had distinct properties. This is evident in the specification sheets contained in this section. In consulting with Pennwalt engineers, the production techniques used for the piezo films have been continually varied in an effort to enhance specific properties of the films. Each of the films analyzed in this research was produced under slightly different conditions. Differences in ϵ_r and $\mathrm{Tan}(\delta_d)$ are seen between PVF_2 samples and between individual $P(VF_2\text{-}VF_3)$ samples.

The most stunning properties noted in the films studied were those on the last specification sheet for a 100.5 micron $P(VF_2\text{-}VF_3)$ film. This particular film had an extremely low acoustic impedance. The value, $2.887 \cdot 10^6$ Rayl, could be the lowest of any known piezoelectric material that has any usable electromechanical properties. The use of such a material for medical and NDE applications (especially for hydrophones) would offer superior acoustic matching properties. Human tissue has an acoustic impedance of about $1.63 \cdot 10^6$ Rayl, and water has a value of about $1.54 \cdot 10^6$ Rayl (Wells, 1969). Thus this copolymer offers much closer acoustic matching than any previously used material. The lower acoustic impedance would also make the copolymer a better candidate for air-coupled ultrasound applications.

Summary of Model Data for 31.75 Micron PVF_2 (MM86093)

Er(F) Values		Tan(δ_d) (F) Values	
f (MHz)	Er(F)	f (MHz)	Tan(δ_d)
0.5	8.825	0.5	0.1828
1.0	7.944	1.5	0.2344
1.5	7.403	2.5	0.2540
2.0	7.062	3.5	0.2607
3.5	6.373	4.5	0.2617
5.5	5.900	5.5	0.2618
7.5	5.620	7.0	0.2620
10.5	5.320	8.5	0.2622
12.5	5.191	10.5	0.2624
15.5	5.010	15.5	0.2630
17.5	4.965	20.5	0.2636
20.5	4.893	25.5	0.2642
22.5	4.835	30.5	0.26475
25.5	4.793	35.5	0.2653
27.5	4.749	40.5	0.2659
30.5	4.692	45.5	0.2665
35.5	4.620	50.5	0.2671
40.5	4.500		
45.5	4.456		
50.5	4.450		

$\rho = 1.6952$ g/cm^3

d = 31.75 microns Area = 1.0176 cm^2

Metallization = 300 Å Ni-Al

$Z = 3.9653 \cdot 10^6$ Rayl

Simplified Impedance Circuit Model Values	Simple Mason's Model Values
R_s = 205.2 Ω	v_o = 2324.80 m/s
L_s = 11.663 μH	C_m = 1.615 pF
C_s = 1.643 pF	R_m = 11.24 Ω
Q = 12.981	k_t = 12.37 %
f_s = 36.358 MHz	Q_m = 13.506
	Damped f_p = 36.611 MHz
$\frac{d}{df}\text{Im}\{Z_s\}$ = 146.56 Ω/MHz	$\frac{d}{df}\text{Im}\{Z_p\}$ = 146.86 Ω/MHz

Full Mason's Model Values

True v_o = 2339.14 m/s	Undamped f_p = 36.837 MHz
C_m = 1.615 pF	k_t = 12.33 %
R_m = 11.31 Ω	
Q_m = 13.489	$\frac{d}{df}\text{Im}\{Z_p\}$ = 146.86 Ω/MHz

Summary of Model Data for 51.58 Micron PVF_2 (MM86005)

Er(F) Values f (MHz)	Er(F)	Tan(δ_d) (F) Values f (MHz)	Tan(δ_d)
0.5	9.467	0.5	0.15278
1.0	8.600	1.5	0.2120
1.5	8.046	2.5	0.2300
2.0	7.675	3.5	0.2430
3.0	7.145	4.5	0.2490
4.0	6.789	5.5	0.2535
5.5	6.441	7.0	0.2568
7.5	6.081	8.5	0.2580
10.5	5.713	10.5	0.2600
12.5	5.593	12.5	0.2619
15.5	5.432	15.5	0.2649
17.5	5.328	20.5	0.2698
20.5	5.173	25.5	0.2748
25.5	4.967	32.0	0.2812
30.5	4.866		
32.0	4.785		

ρ = 1.6413 g/cm^3

d = 51.58 microns Area = 1.0172 cm^2

Metallization = 300 Å Ni-Al

$Z = 3.9208 \cdot 10^6$ Rayl

Simplified Impedance Circuit Model Values

R_s = 388.0 Ω
L_s = 30.379 μH
C_s = 1.594 pF
Q = 11.252
f_s = 22.871 MHz

$\frac{d}{df}\text{Im}\{Z_s\}$ = 382.05 Ω/MHz

Simple Mason's Model Values

v_o = 2379.51 m/s
C_m = 1.538 pF
R_m = 14.45 Ω
k_t = 14.66 %
Q_m = 11.763
Damped f_p = 23.066 MHz

$\frac{d}{df}\text{Im}\{Z_p\}$ = 389.36 Ω/MHz

Full Mason's Model Values

True v_o = 2388.84 m/s
C_m = 1.538 pF
R_m = 14.51 Ω
Q_m = 11.752

Undamped f_p = 23.157 MHz
k_t = 14.63 %

$\frac{d}{df}\text{Im}\{Z_p\}$ = 389.36 Ω/MHz

Summary of Model Data for 30 Micron $P(VF_2-VF_3)$ (MM87070)

Er(F) Values		$Tan(\delta_d)$ (F) Values	
f (MHz)	Er(F)	f (MHz)	$Tan(\delta_d)$
0.5	7.070	0.5	0.1255
1.0	6.481	1.5	0.1850
1.5	6.110	2.5	0.2020
2.0	5.837	3.5	0.2100
3.0	5.488	4.5	0.2150
4.0	5.264	5.5	0.2170
5.5	5.013	7.0	0.2190
7.5	4.778	8.5	0.2210
10.5	4.561	10.5	0.2238
12.5	4.457	15.5	0.2306
15.5	4.342	20.5	0.2374
17.5	4.261	25.5	0.2442
20.5	4.187	30.5	0.2510
25.5	4.080	35.5	0.2578
30.5	3.967	40.5	0.2646
35.5	3.845	45.5	0.2714
40.5	3.830	50.5	0.2782
45.5	3.815		
50.5	3.800		

ρ = 1.7580 g/cm^3
d = 30.00 microns Area = 1.0063 cm^2
Metallization = 300 Å Ni-Al
Z = $3.9240 \cdot 10^6$ Rayl

Simplified Impedance Circuit Model Values	Simple Mason's Model Values
R_s = 89.00 Ω	v_o = 2218.22 m/s
L_s = 4.703 μH	C_m = 3.814 pF
C_s = 4.087 pF	R_m = 11.27 Ω
Q = 12.053	k_t = 20.33 %
f_s = 36.301 MHz	Q_m = 13.592
	Damped f_p = 36.970 MHz
$\frac{d}{df}Im\{Z_s\}$ = 59.02 Ω/MHz	$\frac{d}{df}Im\{Z_p\}$ = 61.10 Ω/MHz

Full Mason's Model Values

True v_o = 2232.18 m/s	Undamped f_p = 37.203 MHz
C_m = 3.814 pF	k_t = 20.27 %
R_m = 11.34 Ω	$\frac{d}{df}Im\{Z_p\}$ = 61.10 Ω/MHz
Q_m = 13.589	

Summary of Data for 110.6 Micron P(VF_2-VF_3) (VA110G00)

Er(F) Values		Tan(δ_d) (F) Values	
f (MHz)	Er(F)	f (MHz)	Tan(δ_d)
0.5	5.920	0.5	0.099
1.0	5.500	0.75	0.106
1.5	5.280	1.0	0.109
2.0	5.130	1.5	0.113
3.0	4.970	2.0	0.114
4.0	4.830	3.0	0.115
5.0	4.750	4.0	0.117
6.0	4.660	5.0	0.118
8.0	4.550	6.0	0.120
10.0	4.490	8.0	0.123
12.0	4.410	10.0	0.1255
15.0	4.360	12.0	0.128
20.0	4.080	15.0	0.133
		20.0	0.140

ρ = 1.8140 g/cm^3
d = 110.6 microns Area = 1.0189 cm^2
Metallization = 300 Å Gold
Z = 4.3220·10^6 Rayl

Simplified Impedance Circuit Model Values

R_s = 855.17 Ω
L_s = 175.46 μH
C_s = 1.306 pF
Q = 13.554
f_s = 10.514 MHz

$\frac{d}{df}\text{Im}\{Z_s\}$ = 2198.16 Ω/MHz

Simple Mason's Model Values

v_o = 2368.50 m/s
C_m = 1.263 pF
R_m = 12.34 Ω
k_t = 20.76 %
Q_m = 14.048
Damped f_p = 10.708 MHz

$\frac{d}{df}\text{Im}\{Z_p\}$ = 2187.71 Ω/MHz

Full Mason's Model Values

True v_o = 2382.50 m/s
C_m = 1.263 pF
R_m = 12.39 Ω
Q_m = 14.039

Undamped f_p = 10.771 MHz
k_t = 20.69 %

$\frac{d}{df}\text{Im}\{Z_p\}$ = 2190.21 Ω/MHz

Summary of Model Data for 100.5 Micron $P(VF_2-VF_3)$

Er(F) Values		Tan(δ_d) (F) Values	
f (MHz)	Er(F)	f (MHz)	Tan(δ_d)
0.5	6.14	0.5	0.118
1.0	5.63	0.75	0.129
1.5	5.33	1.0	0.137
2.0	5.12	1.5	0.150
3.0	4.85	2.0	0.158
4.0	4.68	3.0	0.161
5.0	4.53	6.0	0.1643
6.0	4.40	10.0	0.1686
8.0	4.31	15.0	0.174
10.0	4.23	25.0	0.1848
12.0	4.11		
15.0	4.05		
25.0	4.01		

ρ = 1.5425 g/cm^3
d = 100.5 microns Area = 1.0133 cm^2
Metallization = 300 Å Gold
Z = $2.8870 \cdot 10^6$ Rayl

Simplified Impedance Circuit Model Values

R_S = 1433.03 Ω
L_S = 198.36 μH
C_S = 1.557 pF
Q = 7.876
f_S = 9.056 MHz

$\frac{d}{df}\text{Im}\{Z_S\}$ = 2949.45 Ω/MHz

Simple Mason's Model Values

v_o = 1856.50 m/s
C_m = 1.418 pF
R_m = 13.20 Ω
k_t = 21.44 %
Q_m = 8.427
Damped f_p = 9.236 MHz

$\frac{d}{df}\text{Im}\{Z_p\}$ = 2626.92 Ω/MHz

Full Mason's Model Values

True v_o = 1871.50 m/s
C_m = 1.418 pF
R_m = 13.33 Ω
Q_m = 8.418

Undamped f_p = 9.311 MHz
k_t = 21.38 %

$\frac{d}{df}\text{Im}\{Z_p\}$ = 2626.96 Ω/MHz

In consulting with the Pennwalt technical staff it was apparent that there is still much to learn (and gain) in the production of high performance piezo films. The specification sheets show that for thickness-mode ultrasound transducers, the copolymer is superior to PVF_2 since it retains the low-Q broadband response and has much higher electromechanical coupling. Later research confirmed this observation.

E. Conclusions

After completing the modeling analyses of numerous piezo films it was clear that the first objective of this research was achieved. Successful electromechanical circuit models were derived/modified which accurately predicted the electrical input impedance and many of the acoustic parameters of the piezo films.

One of the keys to the success of this modeling was in deriving "simple" methods for determining the dielectric and acoustic properties from impedance measurements of the films. Most of the "work" in applying the modeling analyses is in obtaining accurate measurements of the physical dimensions of the film samples and making the many required impedance readings. Several thousand impedance magnitude and phase measurements had to be read and transcribed. The

use of more modern equipment could greatly reduce much of the burden.

The author later had the opportunity to use a new HP4194A Impedance/Gain Phase Analyzer (sn 2617J00867) at the Center for NDE facilities at Iowa State University. This computer-controlled network analyzer is capable of making 400 measurements of impedance magnitude and phase in a desired frequency range, correcting the measurements, producing plots of the results, and storing the results in a file which can be down-loaded; all in seconds. Thus, the 4 1/2 hours required to read and transcribe three samples per film could have been easily accomplished in less than five minutes. There are also precision thickness-measuring devices available (such as the Sloan Dektak) which can quickly and accurately measure film thicknesses in the range of 10-1000 microns. The point is this--the entire measurement, analysis, and modeling for a piezo film could be accomplished in a few minutes using readily available industrial equipment.

The value of the derived simplified impedance circuit models was greatly appreciated later when actual transducers were designed and tested. Accurate broadband tuning of an ultrasound transducer is simply not possible without knowing the impedance model components. The modified Mason's models

not only provided accurate modeling of the piezo films, but provided new insight into the impact of the dielectric and mechanical losses on input impedance and air-loaded acoustic performance. In addition, the five-step modeling algorithm provided a new method for determining k_t and Q_m for a lossy piezoelectric resonator.

Thus, the first portion of this research was considered a success. Of course one of the reasons for deriving the models was to use them to gain new insight into the theoretical acoustic performance of ultrasound transducers. Therefore, the next task was to use the models to predict the theoretical acoustic performance of piezo film ultrasound transducers.

IV. COMPUTER SIMULATION OF PIEZO FILM ULTRASOUND TRANSDUCER PERFORMANCE

The development of the electromechanical models in the first part of this research would be of little value if one could not use these models to simulate the performance of a desired ultrasound transducer design. Thus, the goal of the second part of this research was to implement the derived models in an interactive design/simulation computer program that allows a user to "see" the theoretical performance of a particular transducer design. Because of the complex nature of the modified Mason's models, the only feasible way to evaluate them is with the use of a computer program. Commercial circuit analysis programs are incapable of evaluating the models so an original approach was required.

This chapter describes all work related to the second part of this research. The first section discusses the circuit analysis techniques that were used to evaluate the electromechanical circuit models. These analysis techniques were implemented in an interactive computer program as discussed in the second section. The third section presents computer simulation results for a $P(VF_2\text{-}VF_3)$ ultrasound transducer. The many graphics plots in that section illustrate the versatility of the computer simulation program. One of the objectives in applying the simulation program was

to compare side-by-side, the theoretical ultrasound performance of PVF_2 and $P(VF_2-VF_3)$. The fourth section details a comparison of ultrasound performance for the two materials that came as a result of running more than 1000 simulations.

Since the objective of the computer program was to allow a user to "see" theoretical performance, this chapter contains many figures that show the computer-generated output graphics results. To prevent "overwhelming" the reader with graphics data, every effort has been made to group the figures in sections to provide the most insight.

A. Analysis of the Modified Mason's Models

Evaluating the electromechanical circuit models for the piezo films is not an easy task. Other investigators have used circuit analysis programs (i.e., SPICE and PCAP) to analyze Mason's models (Morris et al., 1986; Hutchens and Morris, 1984). Since neither SPICE nor PCAP allow the use of ideal transformers or negative capacitance, special "tricks" are needed to construct networks that approximate these theoretical components.

Even with this approach, the circuit analysis programs will not work for the piezo films. The frequency-dependent nonlinear properties of the piezo films do not lend themselves to existing circuit analysis programs. The complex-

ity of the models and nonlinear properties of the components make it necessary to use a "custom" computer program to evaluate the circuit models. Before such a program could be written, the desired analyses had to be defined and outlined.

1. Fourier analysis

Since the modified Mason's models are composed of electrical circuit components, classical circuit analysis techniques were chosen for their evaluation. Because of the nonlinear nature of the component values and the complexity of the circuit models, any attempts to derive transfer function expressions for the circuits were dismissed.

It was shown in Chapter II that the Mason's models have three ports: one electrical and two acoustic. The acoustic ports of the model are terminated with a resistance, Z_F or Z_B, which represents the acoustic impedance of the medium that loads the front or back face of the transducer. To simulate acoustic performance one can apply a voltage waveform to the input electrical port and, using circuit analysis techniques, solve for the time-varying voltage waveform present at the desired acoustic port. The acoustic port voltage waveform is analogous to the mechanical force waveform present at the port. One can derive voltage/force (transmission mode) and force/voltage (receive mode)

frequency domain transfer functions, but these expressions are extremely cumbersome and provide little insight. However, the concept of a frequency domain 2-port representation of a transducer was used to aid the analysis.

To understand the approach, Figure 4.1 shows a 2-port representation of a Mason's circuit model.

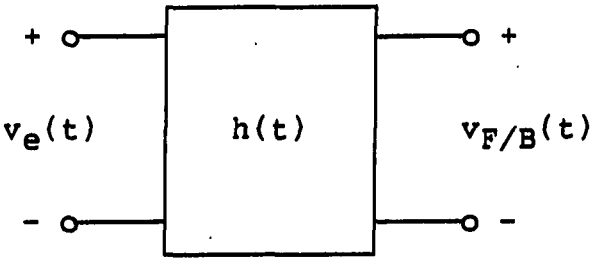

FIGURE 4.1. A 2-port representation of the modified Mason's model

In the figure, $v_e(t)$ represents the voltage waveform across the electrodes of the transducer. The voltage $v_{F/B}(t)$ represents the voltage (force) waveform present at the front/back face of the transducer (port of the circuit model). The system response of the transducer is represented by h(t). By definition then (Nilsson, 1983), $v_{F/B}(t)$ is given by the convolution of $v_e(t)$ with h(t):

$$v_{F/B}(t) = v_e(t)*h(t) \qquad (4.1)$$

Since convolution in the time domain can be accomplished by appropriate multiplication in the frequency domain, the expression may be rewritten through the use of the Fourier transform as:

$$V_{F/B}(j\omega) = V_e(j\omega) \cdot H(j\omega) \qquad (4.2)$$

The upper case variables represent the Fourier transforms of the original lowercase variables. Since $H(j\omega)$ was much too cumbersome to derive, another approach was used to make use of Equation 4.2. Since Equation 4.2 is valid at all frequencies, ω, the author chose to evaluate the equation at discrete frequencies of interest.

The circuit components can be replaced by their sinusoidal-steady state impedances, and the circuit evaluated at desired discrete frequencies. That is,

$$V_{F/B}(j\omega_k) = V_e(j\omega_k) \cdot H(j\omega_k) \qquad (4.3)$$

where $\omega_k = k\Delta\omega$ for $0 \leq k\Delta\omega \leq \omega_m$

and $\Delta\omega$ = desired frequency resolution

$k = 0, 1, 2, \ldots N$

By applying this classical approach to solving for $V_{F/B}(j\omega_k)$ in the sinusoidal steady-state, one obtains a bandlimited (to ω_m) approximation for $V_{F/B}(j\omega)$. The accuracy of the approximation depends on ω_m and $\Delta\omega$.

The resulting values for $V_{F/B}(j\omega_k)$ are complex numbers that are the result of applying the Fourier transform of $v_e(t)$ to the circuit, and using classical circuit analysis techniques. After performing the analysis at N discrete points, as in Equation 4.3, the result is a discrete frequency domain representation of $V_{F/B}(j\omega)$. Of course if $V_e(j\omega_k)=1$, the Fourier transform of a unit impulse function, the voltage $V_{F/B}(j\omega)$ represents $H(j\omega)$, the transfer function of the transducer. One can thus plot the resulting discrete values for $|H(j\omega)|$ and $\text{Arg}\{H(j\omega)\}$, and observe the desired transfer function response. But what about the time domain force waveform $v_{F/B}(t)$?

The discrete values for $V_{F/B}(j\omega_k)$ can be used to approximate $v_{F/B}(t)$ with a discrete Fourier series representation (Patterson and Brown, 1987). The discrete frequency domain results can be transformed to the time domain by the use of an inverse discrete Fourier transform (inverse DFT) or inverse fast Fourier transform (inverse FFT). In using this approach, one obtains time domain sampled values of $v_{F/B}(t)$ which are an accurate representation if the frequency resolution, $\Delta\omega$, and number of points, N, are sufficient. This was precisely the approach used in this research.

For a given transducer design, a frequency range of $0\text{-}2f_p$ was used for the bandlimited analysis at 256 equally spaced points. At each discrete frequency, the Fourier transform of the desired input waveform was derived and applied to the input of the circuit. Circuit analysis, performed in the sinusoidal steady state, was used to derive the desired complex output variable for that particular frequency. These spectral results for the desired variable were written to a graphics file for plotting. The resulting 256 spectral components were then "folded over" onto the $2f_p\text{-}4f_p$ frequency axis to give a two-sided 512-point spectral representation for the desired variable. To increase the plotting resolution of the inverse FFT results, the 512-point representation was zero-padded to eight times its original length (to 4096 points). The 4096-point inverse FFT results thus gave a bandlimited time domain waveform with an apparent sampling rate of $32f_p$. As a result, very "smooth" time domain waveforms were derived. Of course, the zero-padding adds no additional time domain information but it does add "smoother looks" to the time domain graphics plots.

2. The circuit analysis technique

The first step in performing the frequency domain circuit analysis was to compute all of the modified Mason's model components. Cubic spline interpolations of ϵ and $\mathrm{Tan}(\delta_d)$ were computed at each frequency to allow the circuit components to be derived. Rather than apply classical Kirchhoff's circuit analysis techniques, the only circuit analysis principle required was Ohm's Law.

To simplify the analysis and allow easy programming, a set of impedance values was derived for each modified Mason's model circuit for transmit and receive operation. As an example, Figure 4.2 shows the impedance definitions for the simple modified Mason's model (no electrodes) for transmission operation.

The impedance values are derived by beginning at the output port of interest, and working back to the desired input port. For Figure 4.2 the complex impedance values are seen to be:

$$Z_{MF} = Z_F + jX_2 \tag{4.4}$$

$$Z_{MB} = Z_B + jX_2 \tag{4.5}$$

$$Z = Z_{MF}Z_{MB}/(Z_{MF} + Z_{MB}) \tag{4.6}$$

$$Z_1 = Z - jX_1 + R_m \tag{4.7}$$

$$Z_2 = Z_1/\phi^2 \tag{4.8}$$

$$Z_3 = Z_2 - Z_{Co} \tag{4.9}$$

$$Z_{in} = Z_{RoCo}Z_3/(Z_{RoCo} + Z_3) \tag{4.10}$$

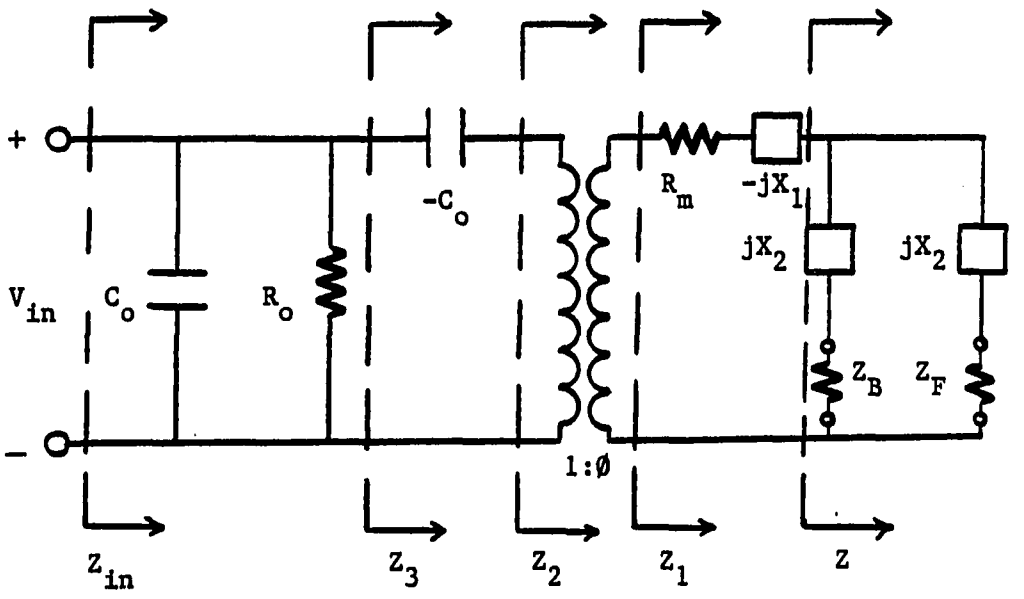

FIGURE 4.2. Assigned impedance values for the simple Mason's model circuit

where $Z_{Co} = 1/j\omega C_o$

and $Z_{RoCo} = R_o//C_o$

It can be seen from these equations that Z_2 is the same as the parallel impedance, Z_p, and that Z_3 is thus the same as the series impedance, Z_s. These seven simple equations provide all of the impedances needed to apply Ohm's Law to evaluate the circuit for any desired voltage or current. Only four additional equations are required to determine v_F from an input voltage, v_{in}:

$$v_{pri} = v_{in} \cdot Z_2/Z_3 \tag{4.11}$$

$$v_{sec} = v_{pri} \cdot \phi \tag{4.12}$$

$$v_Z = v_{sec} \cdot Z/Z_1 \tag{4.13}$$

$$\Rightarrow v_F = v_Z \cdot Z_F / Z_{MF} \qquad (4.14)$$

The same approach was used to evaluate the circuit models for receive operation. The value in using this approach is that the equations are easy to derive and easy to program using complex variables. To evaluate the combined transmit/receive (XMTR/RCVR) performance, one can (1) apply the Fourier transform of the desired waveform to the input port, (2) solve for the output waveform (XMTR operation) and apply this result to the input of the RCVR circuit, and (3) determine the output voltage from analysis of the RCVR circuit. This was the circuit analysis technique implemented in the simulation program.

B. The Computer Simulation Program, XFER.FOR

The previously discussed circuit analysis techniques were implemented in a double-precision FORTRAN program, XFER.FOR (Appendix K). The program, originally intended for simple voltage impulse (transfer function) analysis, was eventually modified to permit many more analyses. The result was a user-friendly interactive design/simulation program that provided great insight into the performance of piezo film ultrasound transducers.

1. Program structure

The main components of the simulation program are the declaration/initialization section, main menu, main frequency loop, inverse FFT sections, and FFT subroutines.

The declaration/initialization section reserves complex variables and arrays for the impedance and voltage values. The voltage variables can be seen to be dimensioned to 4096, which permits 8:1 zero padding of the 512-point frequency domain results. The ϵ and $\mathrm{Tan}(\delta_d)$ values are read into arrays for cubic spline interpolation.

The simulation menu allows the user to select voltage impulse response, voltage step response, current impulse response, or sinusoidal burst response test of the XMTR, RCVR, or XMTR/RCVR performance. The user may also select the simple model (no electrodes), full model (with electrodes), or the full model with an acoustic backing medium of any desired impedance and/or quarter-wavelength matched water-loaded front face. The particular design may be inductively shunt tuned to any desired frequency and if specified, the quarter-wavelength front layer may also be chosen to match at any desired frequency. After supplying the desired number of points (N) and frequency range for the analysis, the evaluation is carried out in the main frequency loop.

The main frequency loop is executed N/2 times, once for each discrete frequency value. Each time, the model components and required impedance values are computed. The remainder of the loop is divided into sections--one for each type of analysis. For instance, if analysis number (1) is selected from the menu (voltage impulse response of XMTR, RCVR, XMTR/RCVR), only that section of the main loop is executed. During each pass through the loop, spectral magnitude and phase results for each analysis are written to AGRAPH graphics files.

At the conclusion of the N/2 analyses, the next section encountered is the inverse FFT section. Each spectral array is zero-padded to eight times its original length before the inverse FFT is used. That is, the spectral magnitude and phase results are padded with zeros to eight times their original length. This zero-padding increases the apparent sampling frequency eight-fold, which gives higher resolution inverse FFT (time domain) results. The time domain results are then written to AGRAPH graphics files. Thus, for analysis number (1), nine graphics files are produced--spectral magnitude, spectral phase, and time domain results for XMTR, RCVR, and XMTR/RCVR performance.

The last section of the program is for the FFT routines. The five-routine package, modified for double

precision and proper amplitude scaling, allows both forward and inverse FFTs in both rectangular and polar coordinates. The cubic spline routines used were linked to the main program from the ISU VAX PORTLIB utility (subroutine CSPIN).

2. Menu options

The user may also elect to create graphics files for ϵ, $\mathrm{Tan}(\delta_d)$, or one of the important impedances Z_p, Z_s, or Z_{in}. It will be shown in Chapter V that these impedance values are required for a particular water-loaded transducer design to permit optimum bandwidth tuning.

Separate menus are invoked, should the user select a sinusoidal burst analysis, or to apply a user-supplied input waveform. Both of these options will be further discussed later.

The menu allows a user to select five different types of tests, on three modes of operation, for one of three types of models, for tuned/untuned, matched/unmatched performance. Thus, for a single transducer, 180 different analyses may be performed, with an infinite number of tuning schemes possible. The user is thus afforded the opportunity to simulate electromechanical performance for nearly any thickness-mode ultrasound transducer, performing nearly any desired test. At the time of this writing, further performance analyses were still being added.

C. Acoustic Performance Simulation Results

The most significant insight from this research came as a result of studying the many computer-generated acoustic simulation results. More than 1000 different simulations were generated, analyzed, and documented. With an infinite number of design simulations possible, a tremendous amount of insight can be gained by using the XFER.FOR simulation program. Every parameter involved in the design of a thickness-mode piezo film ultrasound transducer can be varied, and the resulting effects on performance can be "seen".

This section shows simulation results from each of the five main types of analyses: (1) ideal voltage impulse response, (2) ideal voltage step response, (3) ideal current impulse response, (4) ideal sinusoidal burst response, and (5) quarter-wavelength resonating/tuning response. Each subsection contains a discussion of the relevant analysis and graphs of computer simulated performance for various tuned designs. All results are for a 1 cm x 1 cm area transducer of 110.6 micron $P(VF_2-VF_3)$ (VA110G00) unless otherwise stated.

1. Ideal voltage impulse response simulations

The ideal voltage impulse response of the circuit model is derived by applying the Fourier transform of a unit volt-

age impulse to the input of the circuit. The unit impulse function, $f(t)=\delta(t)$, has a Fourier transform of 1, $F(\omega)=1$. Since the simulations were performed in the frequency range of $0\text{-}2f_p$, the simulation results obviously represent the bandlimited ideal response.

The voltage impulse response was considered the most important analysis since it can be used to determine the voltage/force (XMTR), force/voltage (RCVR), and voltage/force-force/voltage (XMTR/RCVR) transfer functions. It is from the characteristics of these transfer functions that ultrasound transducers are evaluated and compared. Figures 4.3-4.15 show the spectral magnitude, spectral phase, and time domain simulation results for XMTR, RCVR, and XMTR/RCVR performance for the 110.6 micron $P(VF_2\text{-}VF_3)$.

Figures 4.3-4.5 show the voltage impulse XMTR simulation results for various designs. In Figure 4.3, the spectral magnitude and phase response of the XMTR are shown. The results are for water-loaded (unmatched) faces. The graph shows a peaked response at the parallel resonant frequency f_p (10.71 MHz). Note the broadband performance.

Figure 4.4 illustrates the effects of acoustically matching the front and rear faces of the piezoelectric element. The dotted line response is for the case where the piezo film element is bonded to a backing material of iden-

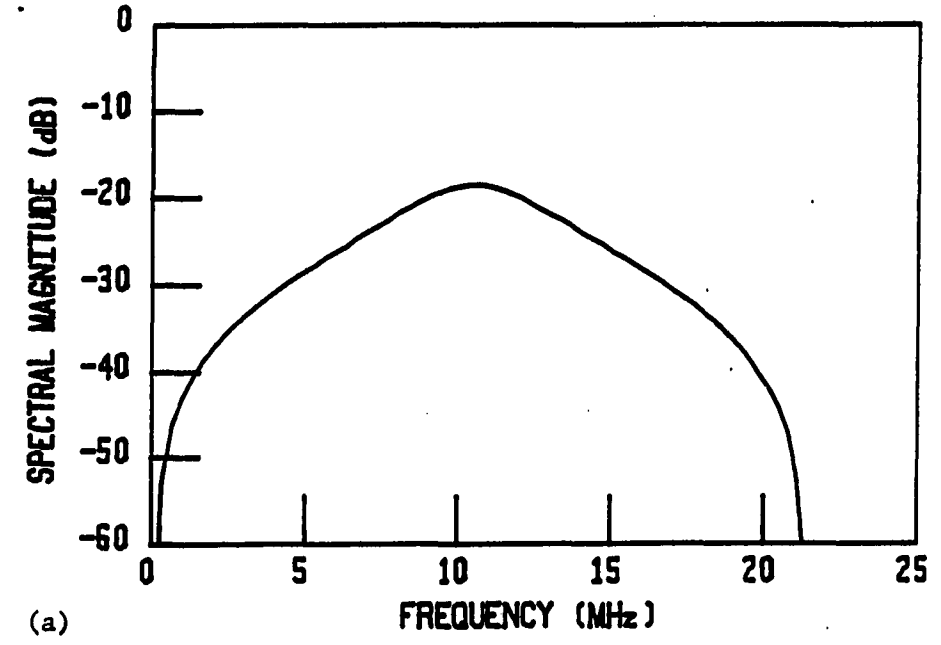

(a)

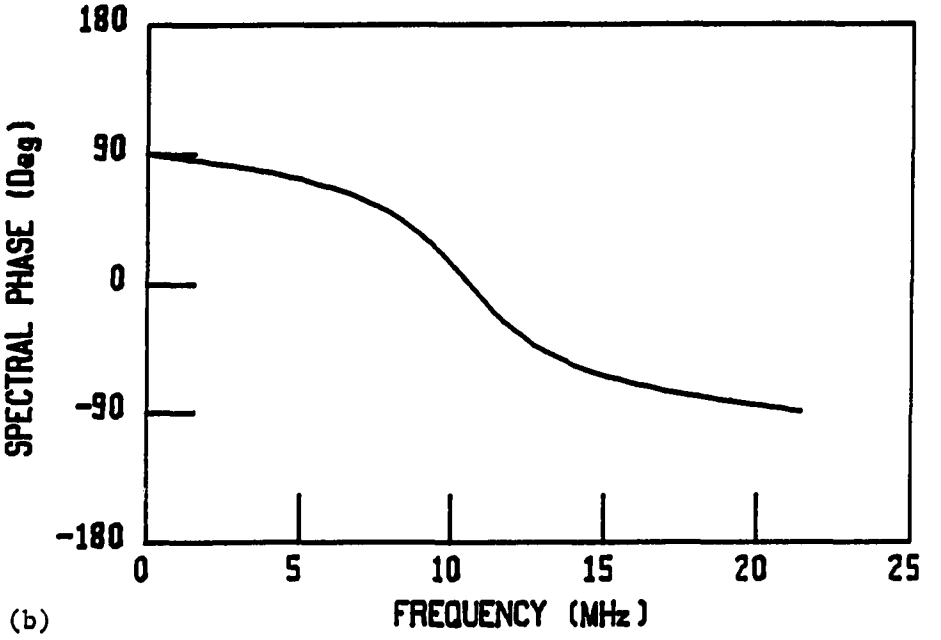

(b)

FIGURE 4.3. Simulated ideal voltage impulse XMTR response: (a) spectral magnitude response, (b) spectral phase response, of untuned, water-loaded transducers

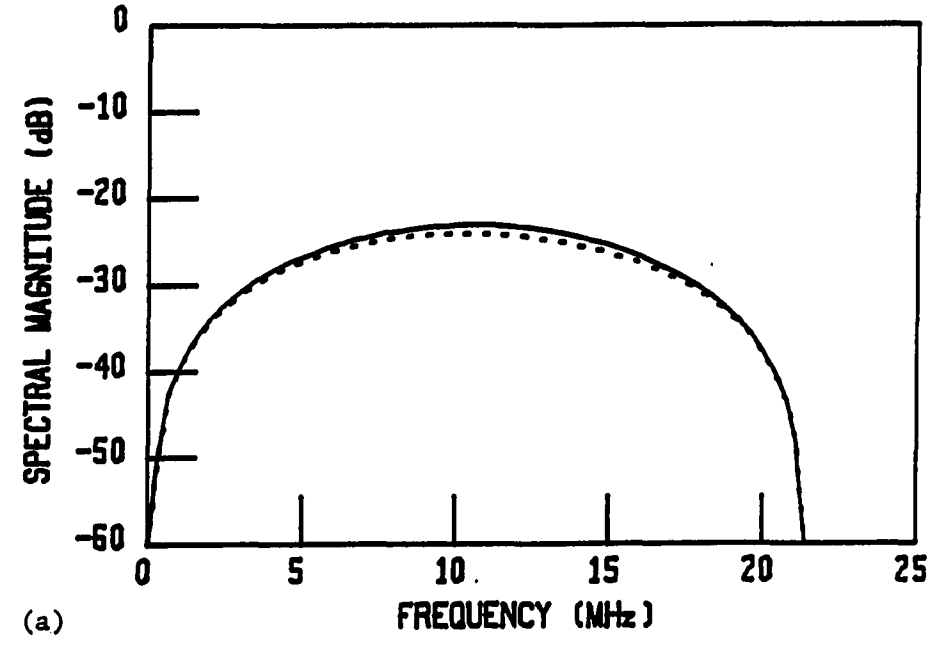

(a)

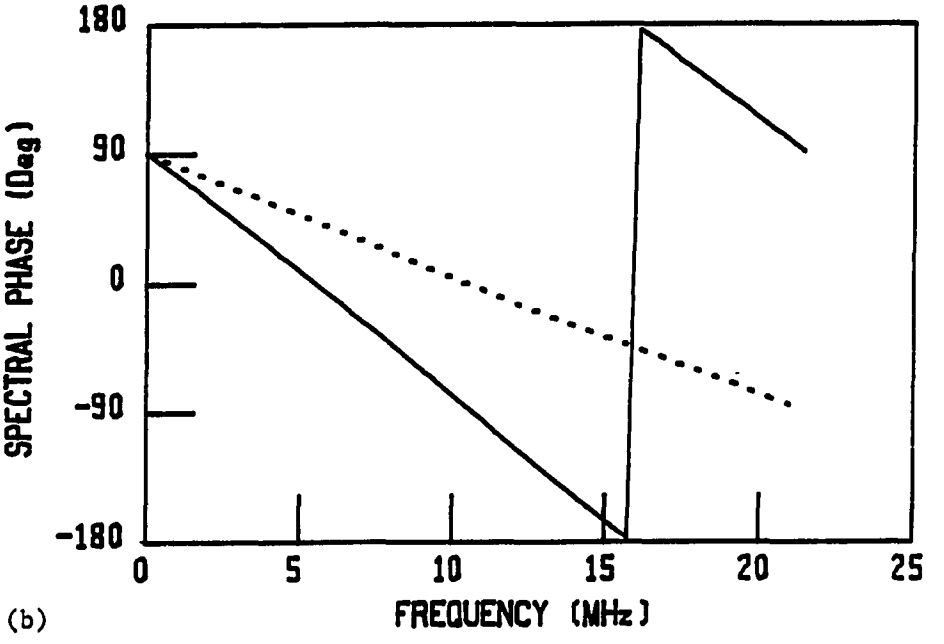

(b)

FIGURE 4.4. Simulated ideal voltage impulse XMTR response: (a) spectral magnitude response and (b) spectral phase response of back-matched shunt-tuned water-loaded transducers. Solid line is for fully matched case

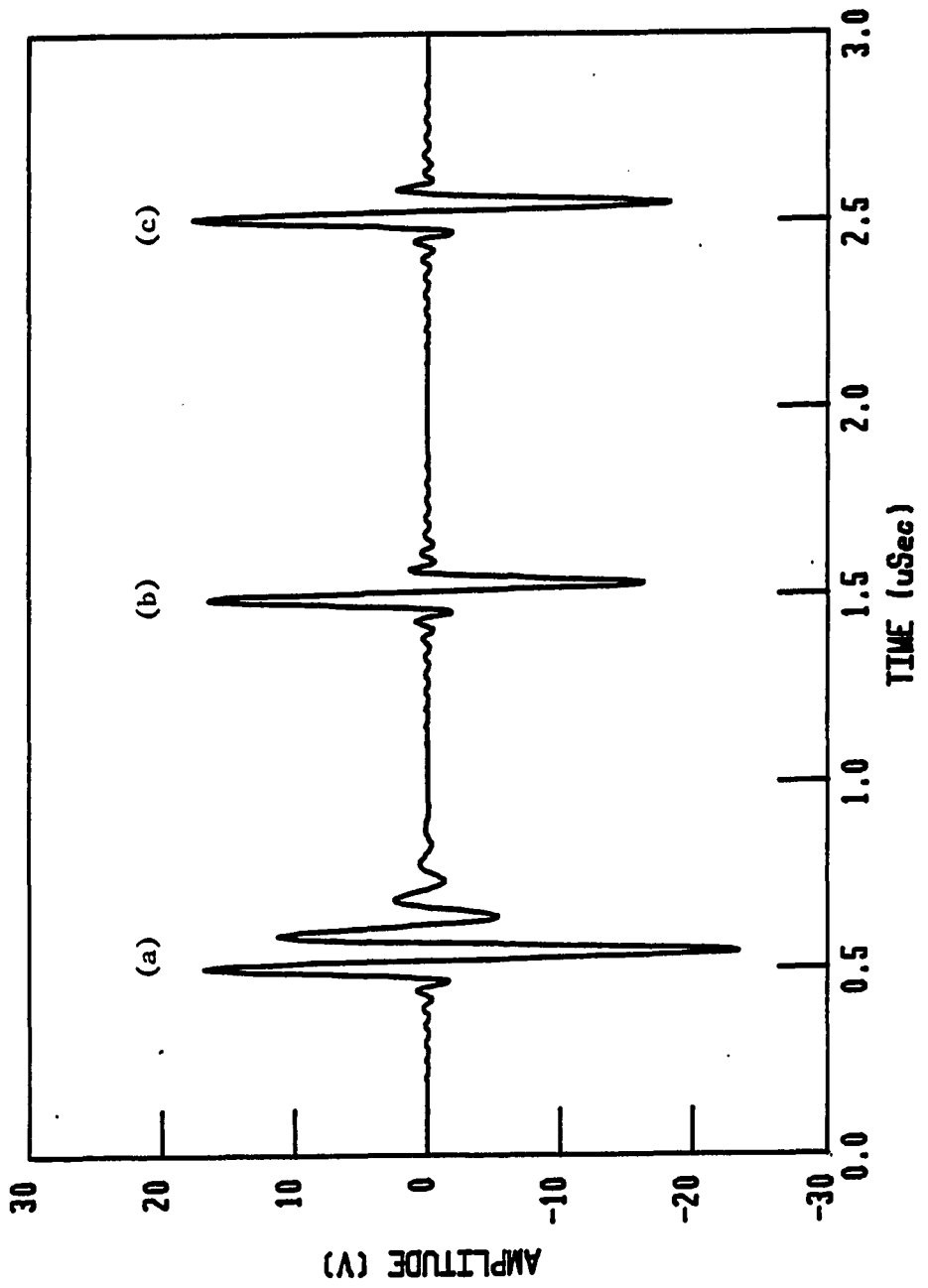

FIGURE 4.5. Simulated ideal voltage impulse (time domain) XMTR response of (a) untuned, (b) back-matched, and (c) fully matched water-loaded transducers

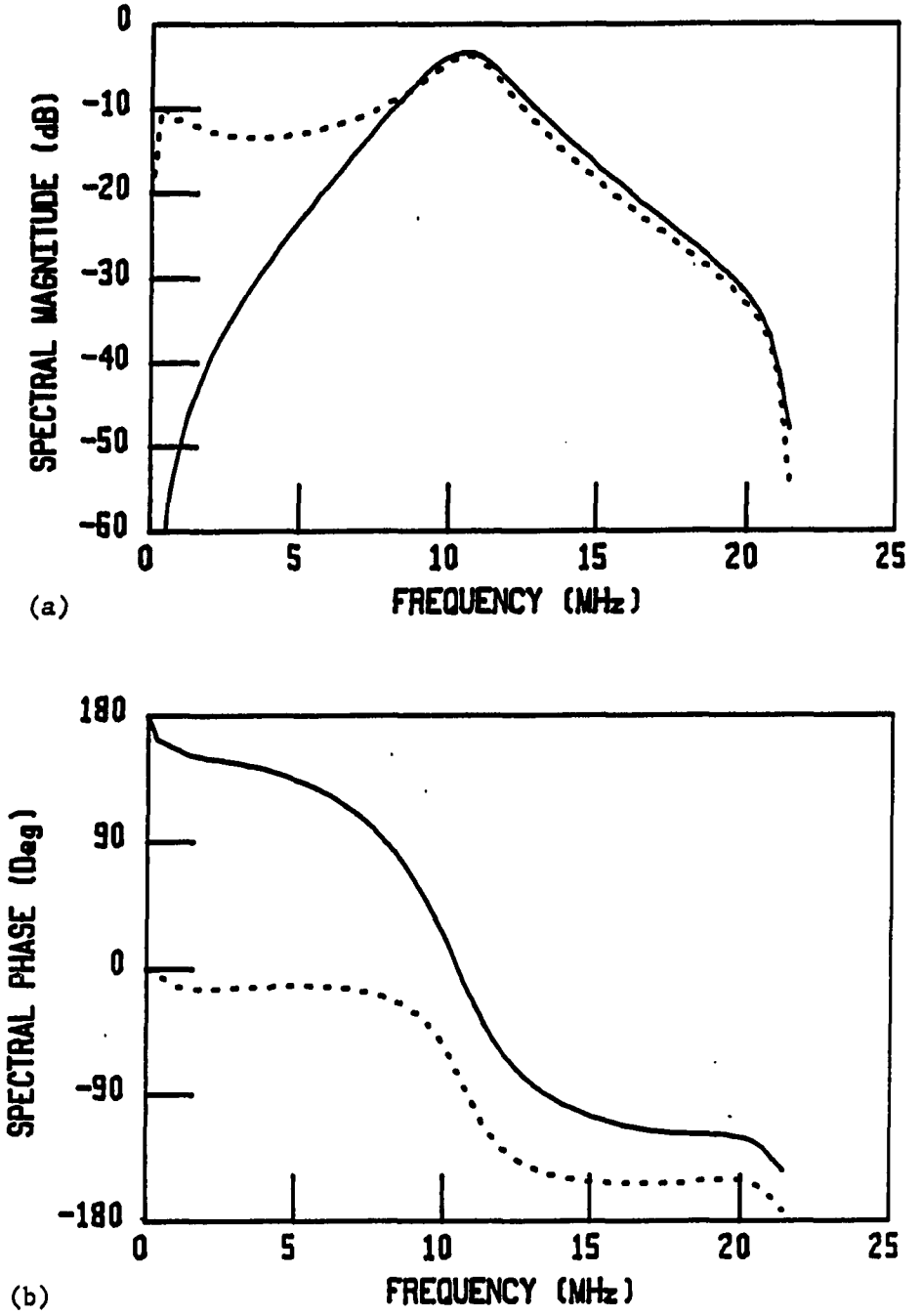

FIGURE 4.6. Simulated ideal voltage impulse RCVR response: (a) spectral magnitude response and (b) spectral phase response of water-loaded transducers. Broken line is for untuned case, solid line is for shunt-tuned case

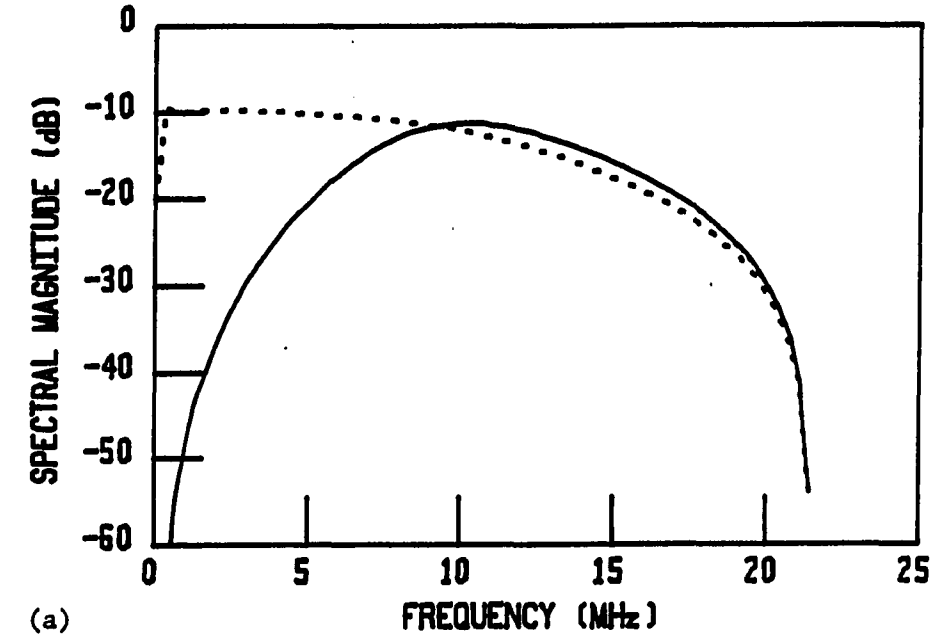

(a)

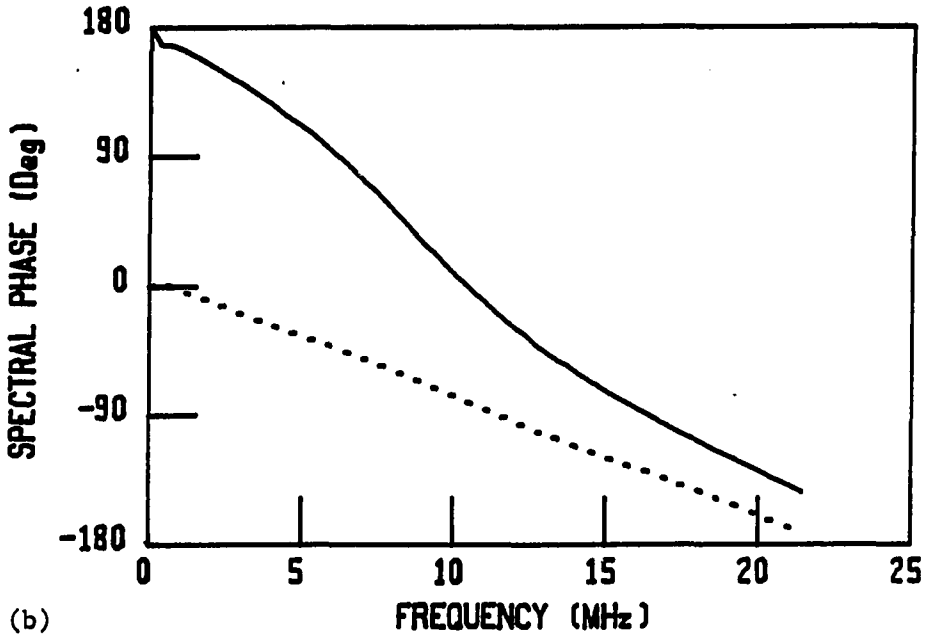

(b)

FIGURE 4.7. Simulated ideal voltage impulse RCVR response: (a) spectral magnitude response and (b) spectral phase response of back-matched water-loaded transducers. Solid line is for shunt-tuned case

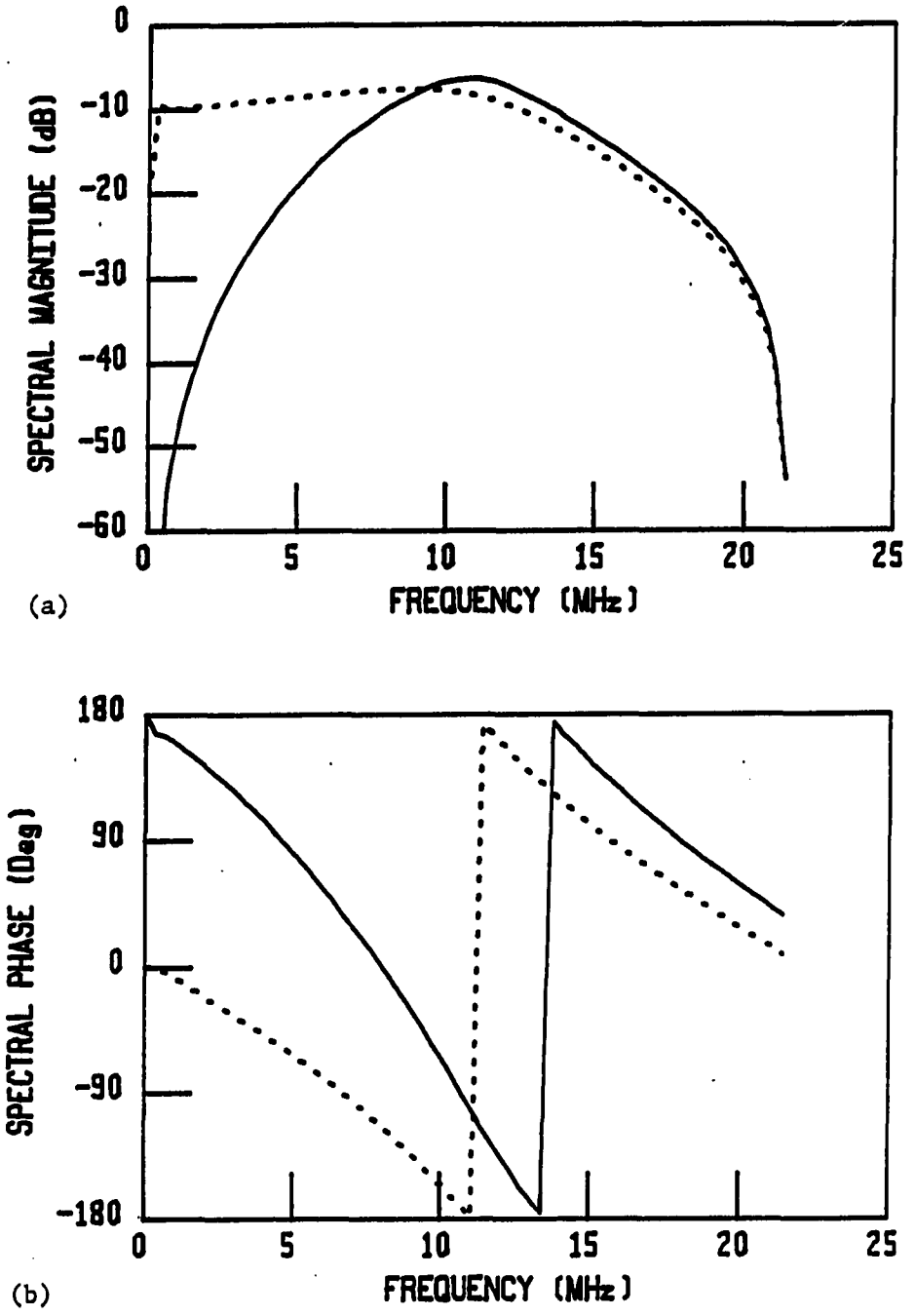

FIGURE 4.8. Simulated ideal voltage impulse RCVR response: (a) spectral magnitude response and (b) spectral phase response of fully matched water-loaded transducers. Solid line is for shunt-tuned case

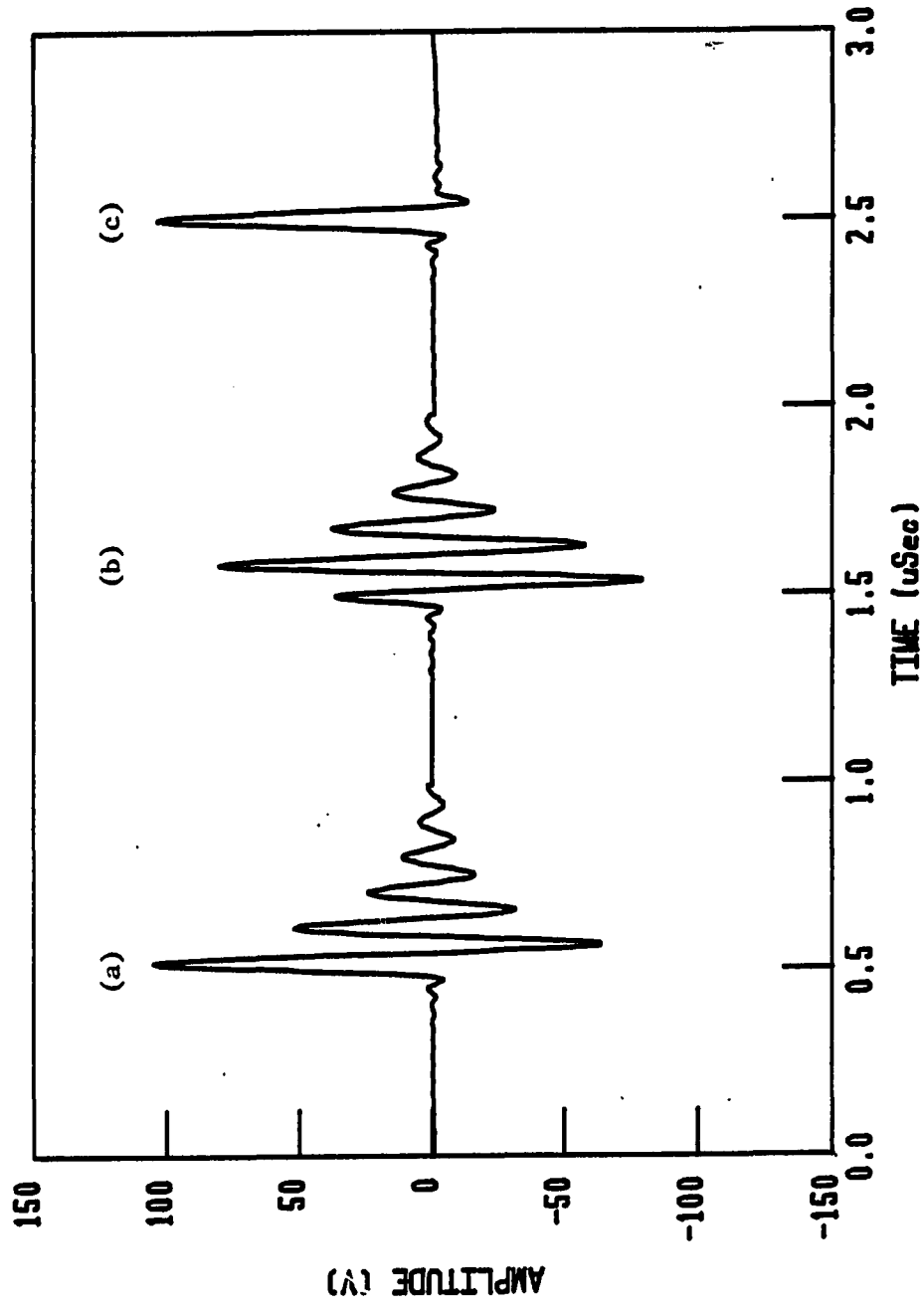

FIGURE 4.9. Simulated ideal voltage impulse (time domain) RCVR response of water-loaded transducers: (a) untuned, unmatched, (b) shunt-tuned, unmatched, and (c) untuned, back-matched case

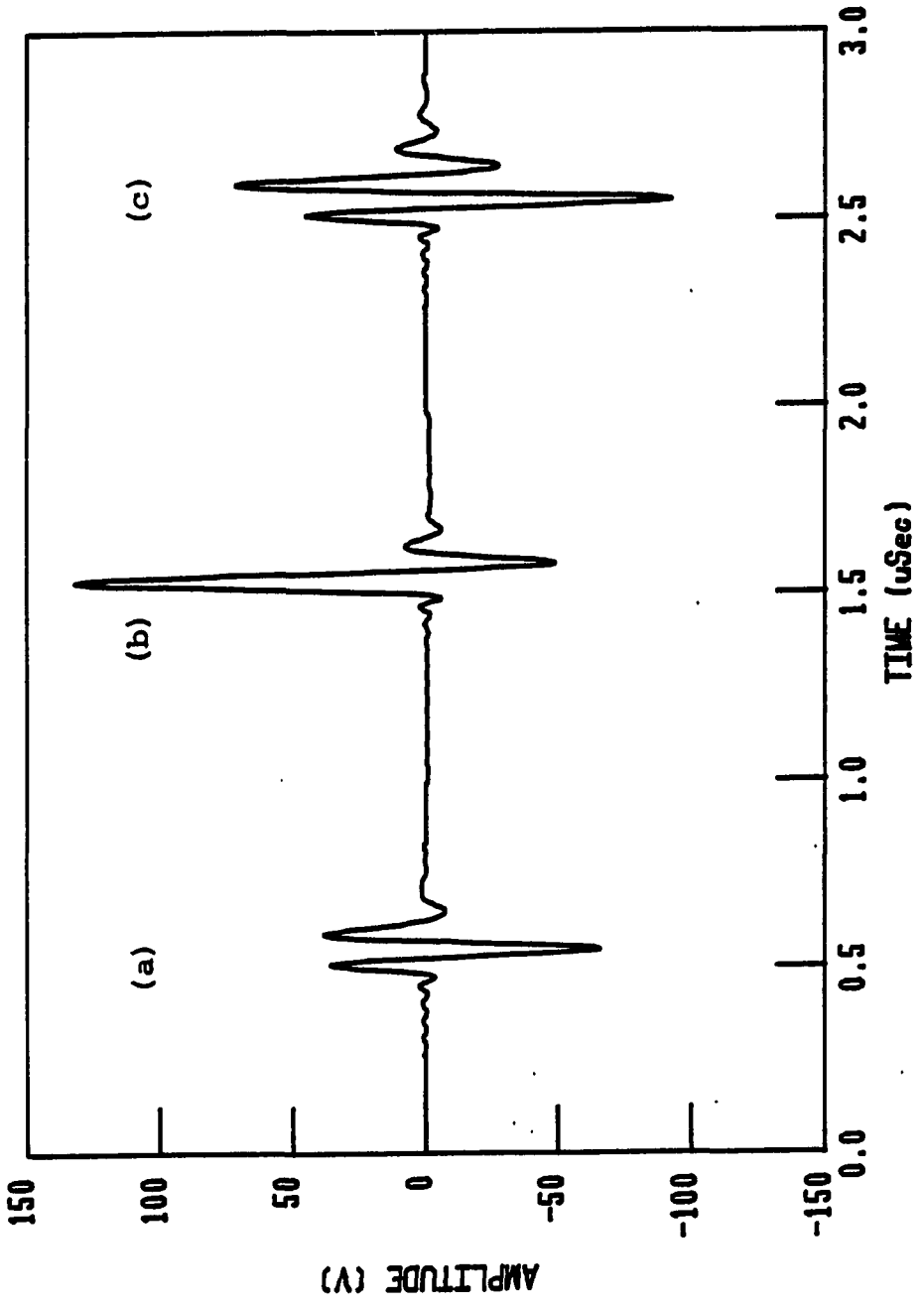

FIGURE 4.10. Simulated ideal voltage impulse (time domain) RCVR response of water-loaded transducers: (a) shunt-tuned, back-matched, (b) untuned, fully matched, and (c) shunt-tuned, fully matched case

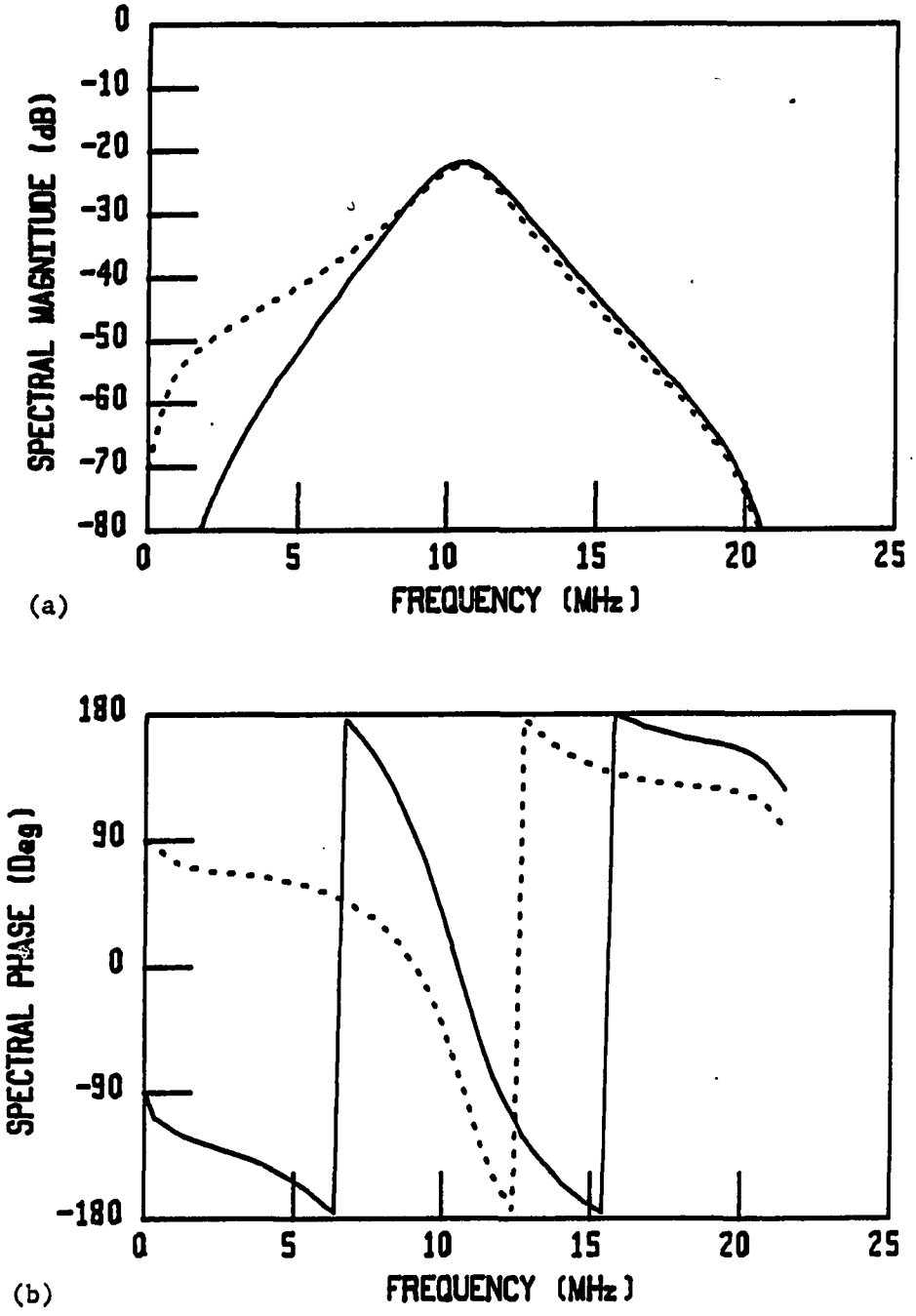

FIGURE 4.11. Simulated ideal voltage impulse XMTR/RCVR response: (a) spectral magnitude response and (b) spectral phase response of water-loaded transducer. Broken line is for untuned case, solid line is for shunt-tuned case

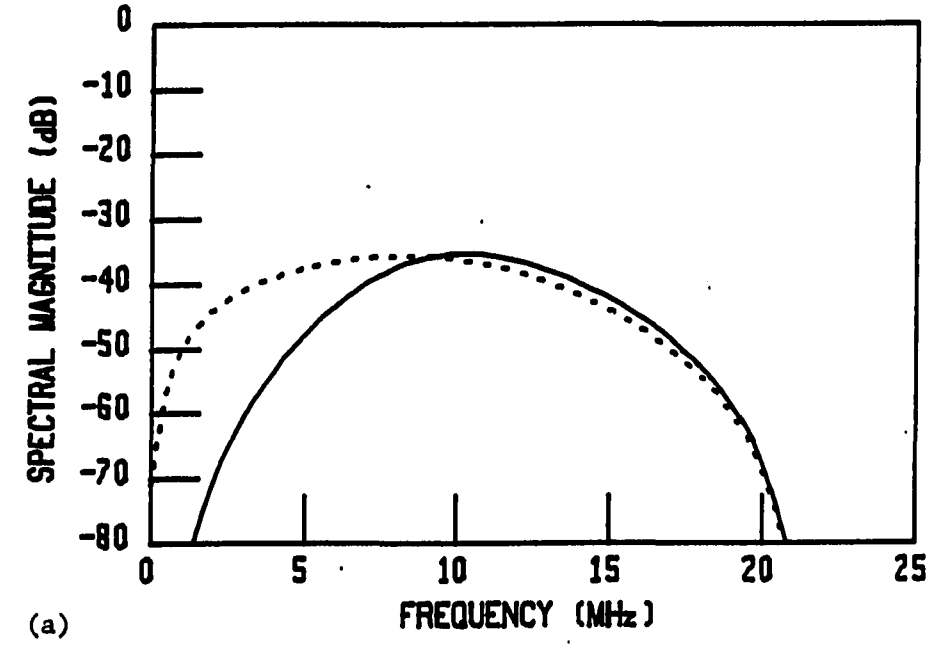

(a)

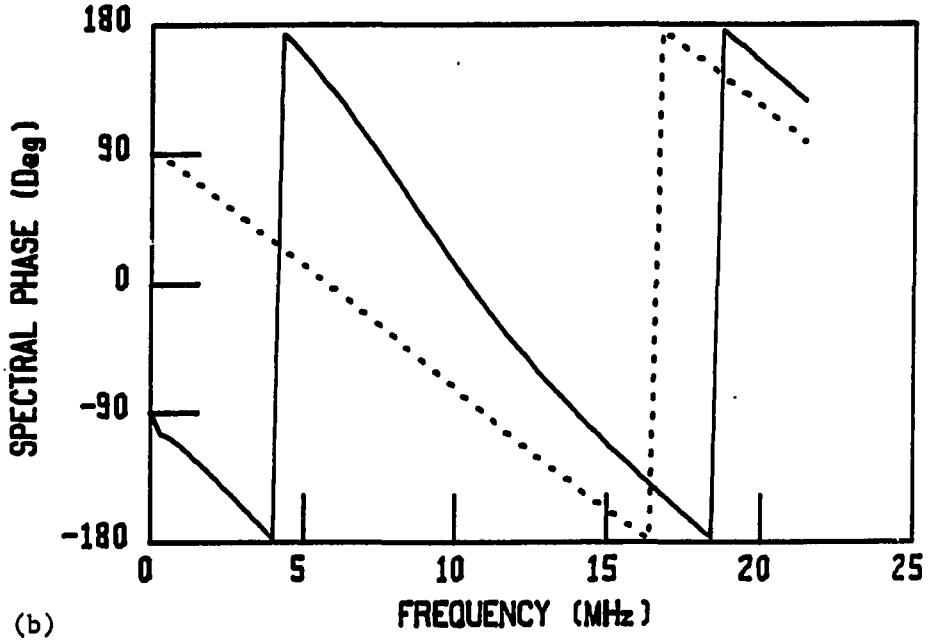

(b)

FIGURE 4.12. Simulated ideal voltage impulse XMTR/RCVR response: (a) spectral magnitude response and (b) spectral phase response of back-matched water-loaded transducer. Solid line is for shunt-tuned case

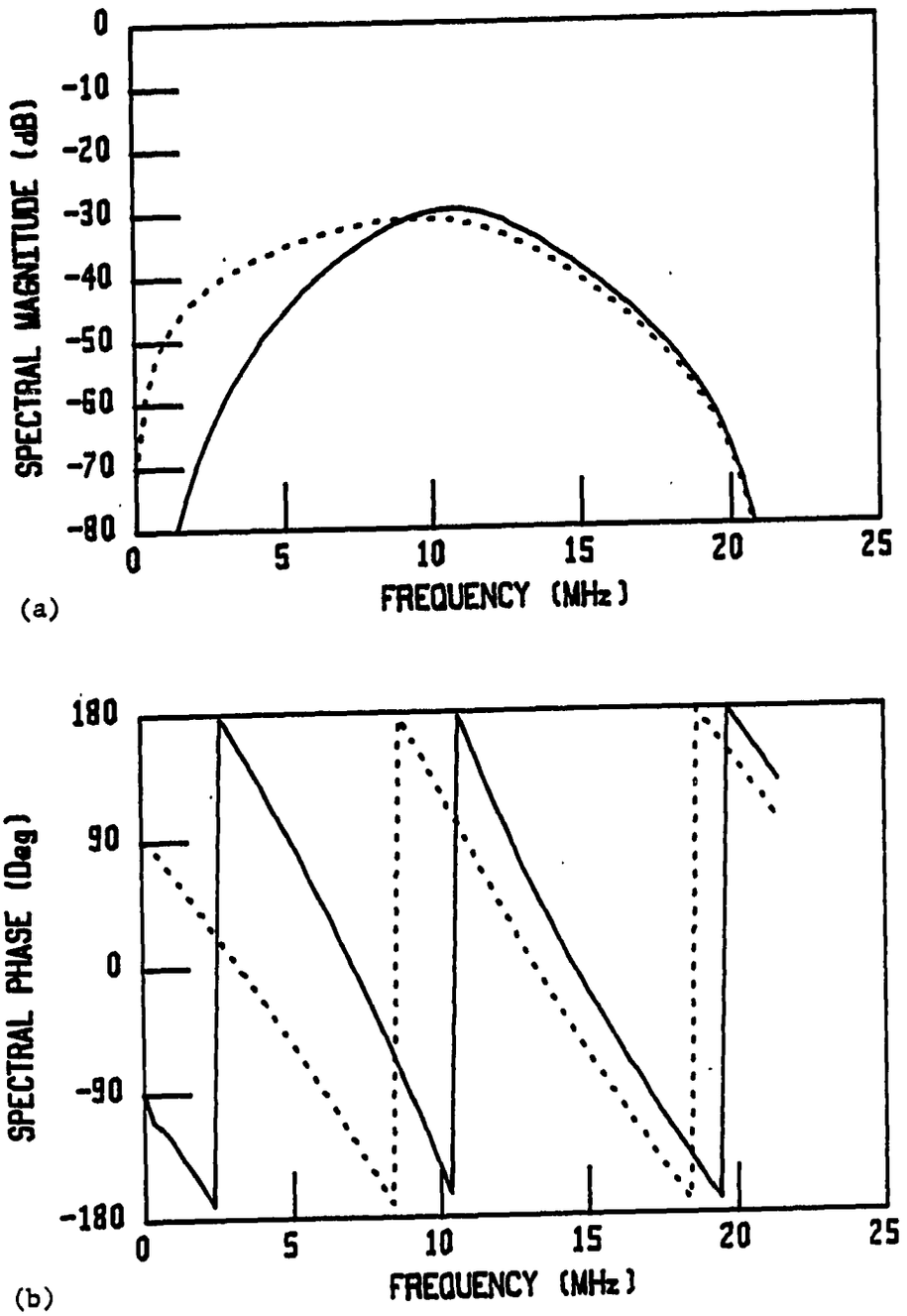

FIGURE 4.13. Simulated ideal voltage impulse XMTR/RCVR response: (a) spectral magnitude response and (b) spectral phase response of fully matched water-loaded transducer. Solid line is for shunt-tuned case

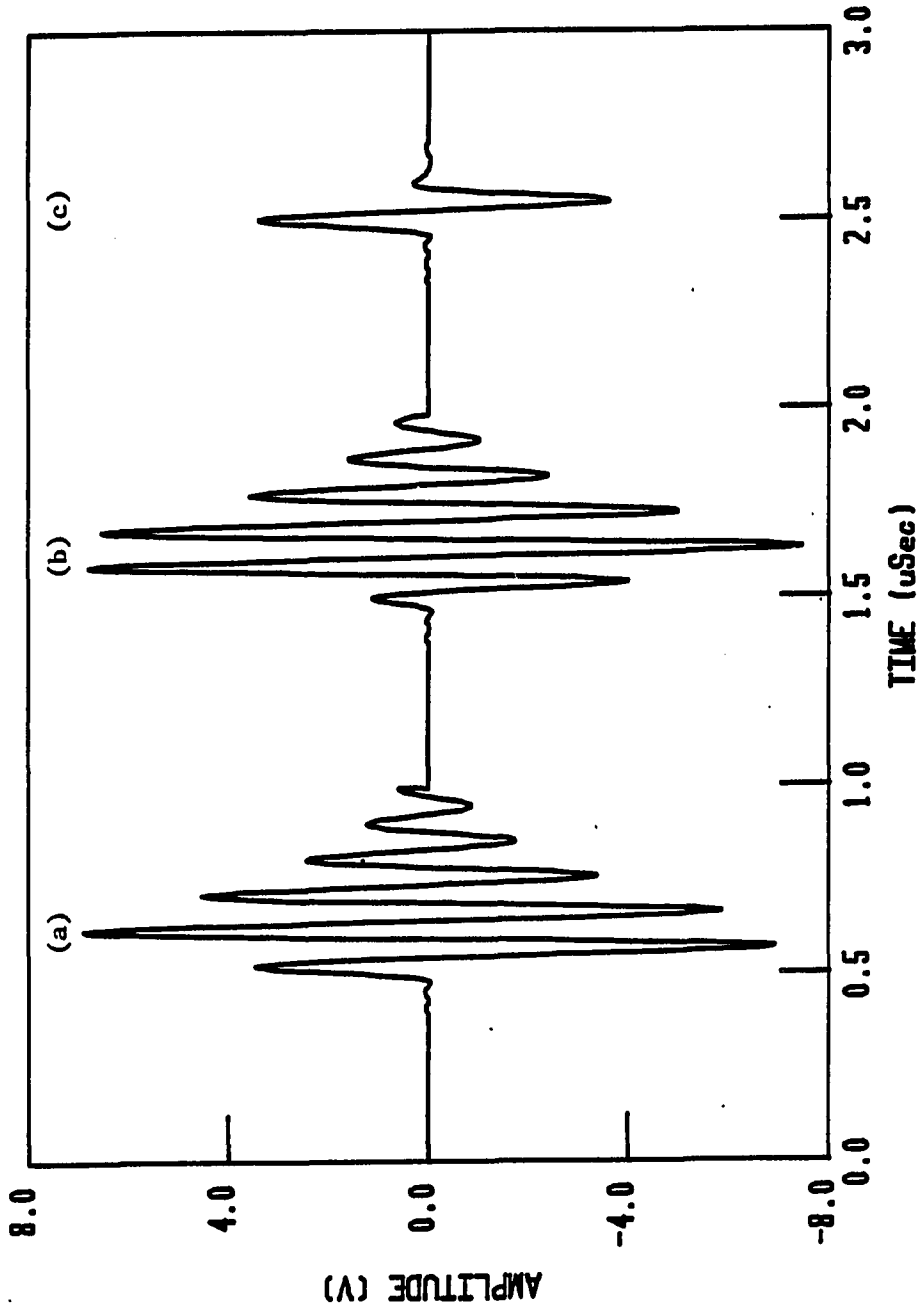

FIGURE 4.14. Simulated ideal voltage impulse (time domain) XMTR/RCVR response of water-loaded transducers: (a) untuned, unmatched, (b) shunt-tuned, unmatched, and (c) untuned, back-matched case

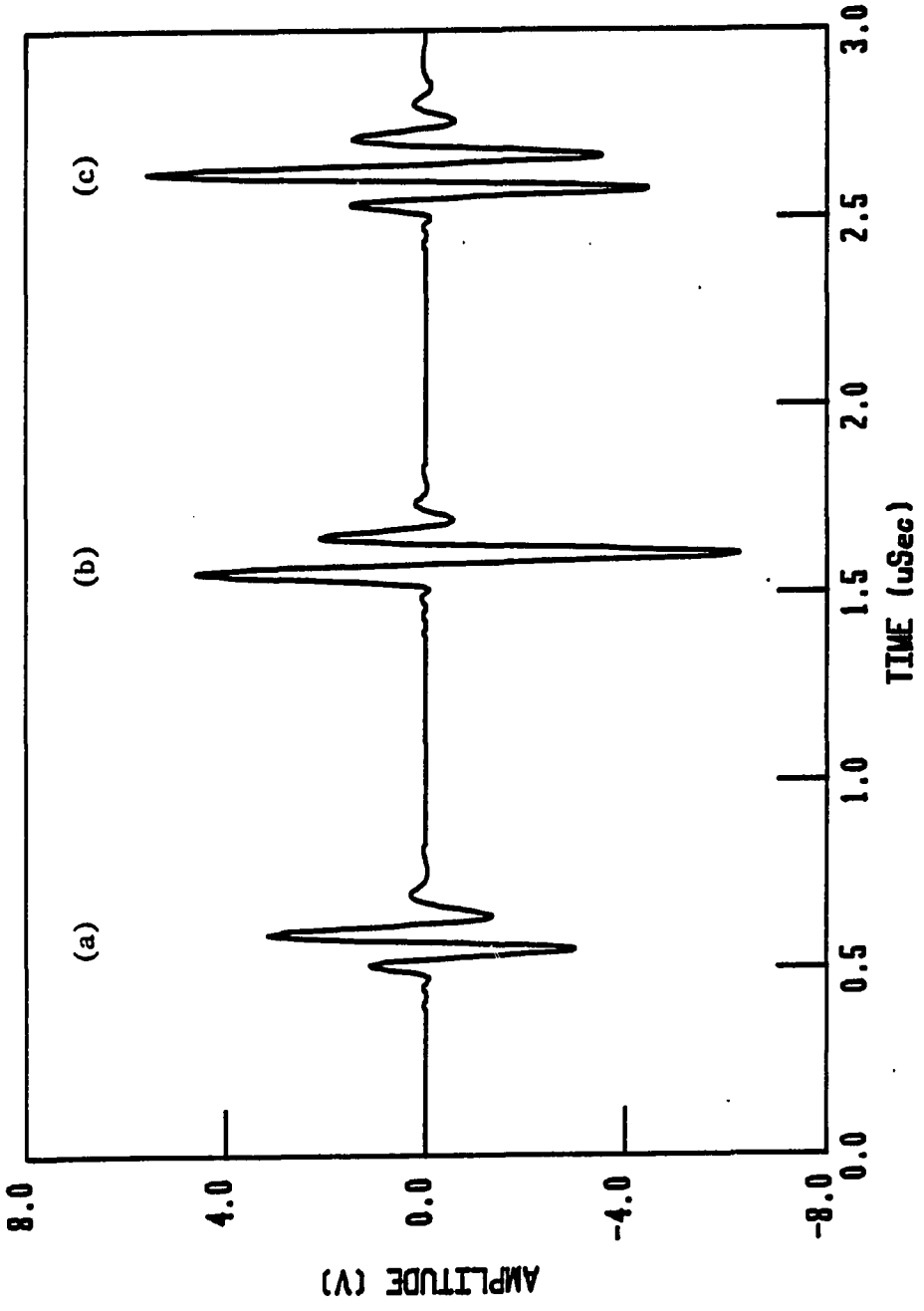

FIGURE 4.15. Simulated ideal voltage impulse (time domain) XMTR/RCVR response of water-loaded transducers: (a) shunt-tuned, back-matched, (b) untuned, fully matched, and (c) shunt-tuned, fully matched case

tical acoustic impedance. The result is a much more broadband, yet less sensitive, response than for the simple water-loaded case of Figure 4.3. The solid lines represent the fully matched case. In this design, the film is not only bonded to an acoustically matched backing material, but a quarter-wavelength matching layer is also incorporated on the front (water-loaded) face of the film element. The results show a slight increase in sensitivity near resonance.

Both matched designs show very linear phase responses. However, the fully matched design shows a total phase change which is twice that of the design that features only back-matching. With a perfect match at the rear face, acoustic waves freely propagate from the rear face without reflection. In the transmission mode, acoustic waves propagate through the front half-thickness of the film to the front (water-loaded) face. Thus, the simulated phase response should show a group time delay which is equal to the acoustic propagation time through half the film thickness. This group delay time can be determined from the phase response by:

$$t_{1/2} = \frac{-d\phi(\omega)}{d\omega} \text{ sec} \qquad (4.15)$$

where $t_{1/2}$ = acoustic propagation time through the

front half-thickness of the film

(i.e., 110.6/2 microns)

$\phi(\omega)$ = phase angle of voltage impulse response

ω = radian frequency

From the figure:

$$t_{1/2} = -(-\pi/2\pi \cdot 21.4 \text{ MHz})$$

$$\Rightarrow t_{1/2} = 0.0233 \ \mu s$$

This propagation time suggests an acoustic velocity of:

$$v_o = (d/2)/t_{1/2} = 55.3 \cdot 10^{-6} m / 0.0233 \cdot 10^{-6} s$$

$$\Rightarrow v_o = 2373 \text{ m/s}$$

---

which is close to the value of 2382 m/s from the piezo film's specification sheet given in Chapter III.

The fully matched phase response of Figure 4.4 shows a linear phase change of 180° (π). The increase in group delay time is due to the added front matching layer. The layer, which has a thickness of $d_{\lambda/4}=v_m/4f_s$ and acoustic velocity of 1875 m/s, gives rise to a propagation time of:

$$t_{1/4} = \frac{d_{\lambda/4}}{v_m} = \frac{v_m}{4f_s v_m} = \frac{1}{4f_s} \text{ sec} \qquad (4.16)$$

where f_s = 10.514 MHz

Thus, $t_{\lambda/4} = 0.0238\ \mu s$

The total propagation time is therefore:

$$\Rightarrow t = t_{1/2} + t_{\lambda/4} = 0.0471\ \mu s \tag{4.17}$$

Now, applying (4.15) to the phase response gives:

$$t_{1/2} = \frac{-d\phi(\omega)}{d\omega}\ \text{sec} = -(-2\pi/\pi \cdot 21.4\ \text{MHz})$$

$$\Rightarrow t = 0.0466\ \mu s \tag{4.18}$$

which is in good agreement with the theoretical value of Equation 4.17.

The time domain responses of Figure 4.5 further illustrate the improvements in performance that can be achieved with front and rear acoustic matching. The unmatched transmitted waveform in (a) shows a long, ringing response. The back-matched (b) and fully matched (c) cases show that a much shorter ring-free pulse can be achieved with correct use of matching layers.

One way to increase sensitivity near the resonant frequency is to shunt tune the transducer with an inductance which resonates the bulk capacitance, C_o, at the series resonant frequency, f_s. Thus, at f_s the dielectric portion of the circuit model appears as an open circuit. This

results in a noticeably larger output voltage developed in receiver operation. The shunt inductance produces no change in the ideal XMTR response, however, for a practical driving source which has a nonzero output impedance, the shunt inductance reduces the loading of the transducer on the driving source at resonance and does improve XMTR performance. Since a real driving source sees an infinite dielectric impedance at f_s, and Z_s is real at this frequency, maximum energy can be delivered to the mechanical portion of the circuit. This matching only occurs at exactly f_s and the result of the tuning is a more peaked (higher sensitivity) response near f_s. A shunt resistance is also included for inductive shunt tuning to match the Q of the dielectric circuit with that of the water-loaded acoustic Q. Further discussion of this technique is covered in Chapter V.

Figures 4.6-4.10 show similar comparisons of RCVR mode performance. A unit impulse voltage (force) was applied to the transducer's front face (port) and the resulting output voltage developed across the electrodes was computed. The effects of inductive shunt tuning are evident in these figures. The shunt tuning clearly reduces the bandwidth of the receiver performance. In the back-matched and fully matched cases, shunt tuning tends to "peak up" the response at a severe cost of bandwidth, especially below the resonant

frequency. It is clear from Figures 4.7 and 4.8 that an untuned matched piezo film ultrasound transducer makes an excellent broadband receiver. The time domain results, shown in Figures 4.9 and 4.10, also reveal the adverse effects of shunt tuning. In all cases, shunt tuning caused more ringing in the ideal impulse response. The untuned back-matched case (4.9c) shows the shortest, most broadband impulse response. The untuned fully matched case (Figure 4.10c) shows a slightly greater sensitivity, but with slightly more ringing.

The final set of figures (4.11-4.15) shows the combined pulse-echo (XMTR/RCVR) performance. Again, the effects of tuning and matching are clear. The results show that the untuned back-matched design provides the most broadband pulse-echo performance. The fully matched case provides slightly more sensitivity, however the time domain response also shows more ringing.

The power of the simulation/design program is clear: one can design many different piezo film ultrasound transducers with the computer and "see" the voltage impulse (transfer function) responses.

2. Ideal voltage step response simulation

Analysis of the ideal voltage impulse response produced knowledge of the desired system transfer functions. The decision to include an option for voltage step response analysis was based on recent scientific interest in producing unipolar acoustic pulses. The use of such pulses can be valuable in detecting "fuzzy" (graded) boundaries (Thompson and Hsu, 1988). Unipolar acoustic pulses are produced by applying a step voltage to the transducer. If the transducer is capable of sufficiently broadband response, the step voltage causes the front face of the transducer to accelerate forward and come to a complete stop. The resulting movement causes the launching of a unipolar acoustic waveform rather than the conventional bipolar waveform encountered in voltage impulse excitation.

It is extremely difficult to design a unipolar ultrasound transducer from high-Q piezoelectric materials like PZTs since they want to vibrate at their natural frequency when excited with a step voltage. Special techniques for matching and damping must be used in order to achieve a true unipolar output waveform. The piezo films, which clearly have low-Q broadband acoustic properties, are well suited for unipolar pulse generation without the need for additional damping.

The purpose of the voltage step response option was to allow the user to study the bandlimited ideal voltage step response of unipolar ultrasound transducer designs. The computer program applies the Fourier transform of a unit step function ($1/j\omega$ for $\omega>0$) to the input of the modified Mason's model and the desired response is then computed in the same manner as for the voltage impulse response. Figures 4.16-4.19 show the simulated voltage step response results.

The untuned, unmatched water-loaded step response is shown in Figure 4.16. The phase response looks the same as for the voltage impulse response except for a downward shift of 90° (see Figure 4.3). This was expected since the step function's Fourier transform is purely imaginary instead of purely real as for the voltage impulse transform. The effects of back-matching are seen in the figures. The untuned back-matched design shows a more broadband transmitted pulse waveform, as expected from analysis of the voltage impulse response results. The time domain results, shown in Figure 4.17, show the lack of ringing for the back-matched case. The result is the transmission of an excellent unipolar acoustic pulse waveform. The width of the pulse (measured at the 50% amplitude points) is seen to be approximately 50 ns from the figure. The theoretical pulse width is given by (Buchler et al., 1987):

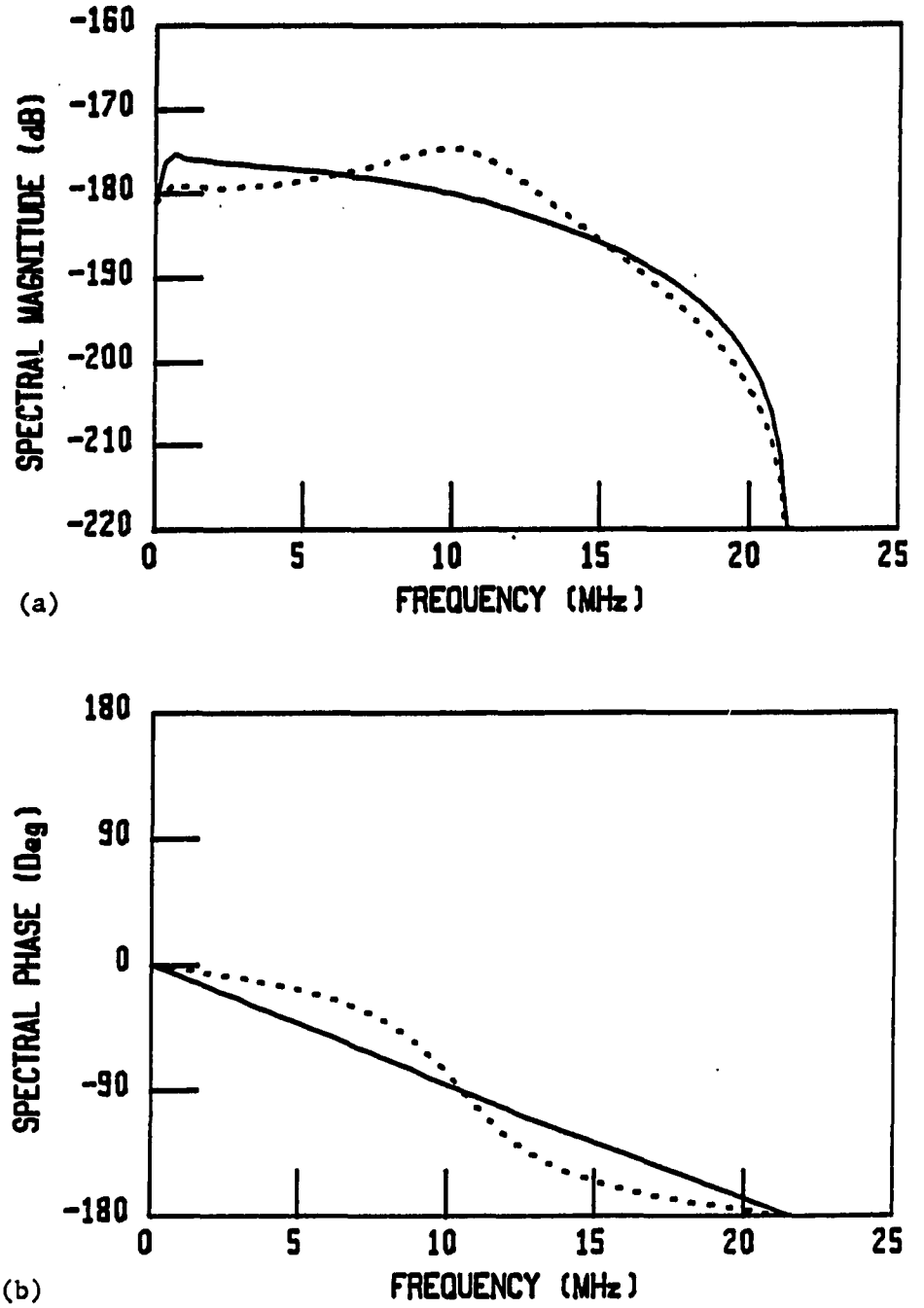

FIGURE 4.16. Simulated ideal voltage step XMTR response: (a) spectral magnitude response and (b) spectral phase response of untuned back-matched water-loaded transducers. Solid line is for fully matched case

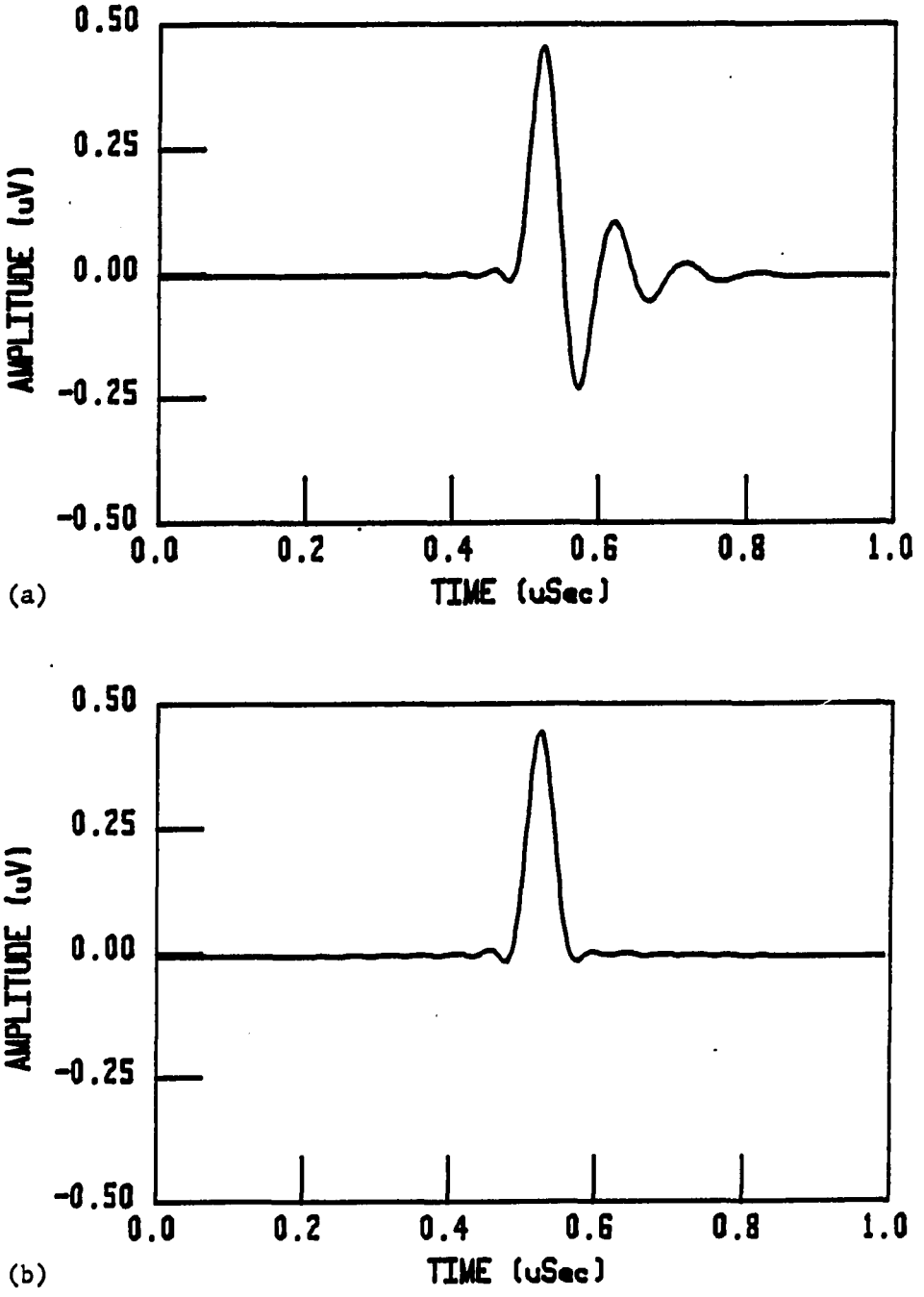

FIGURE 4.17. Simulated ideal voltage step (time domain) XMTR response of (a) untuned unmatched and (b) untuned back-matched, water-loaded transducers

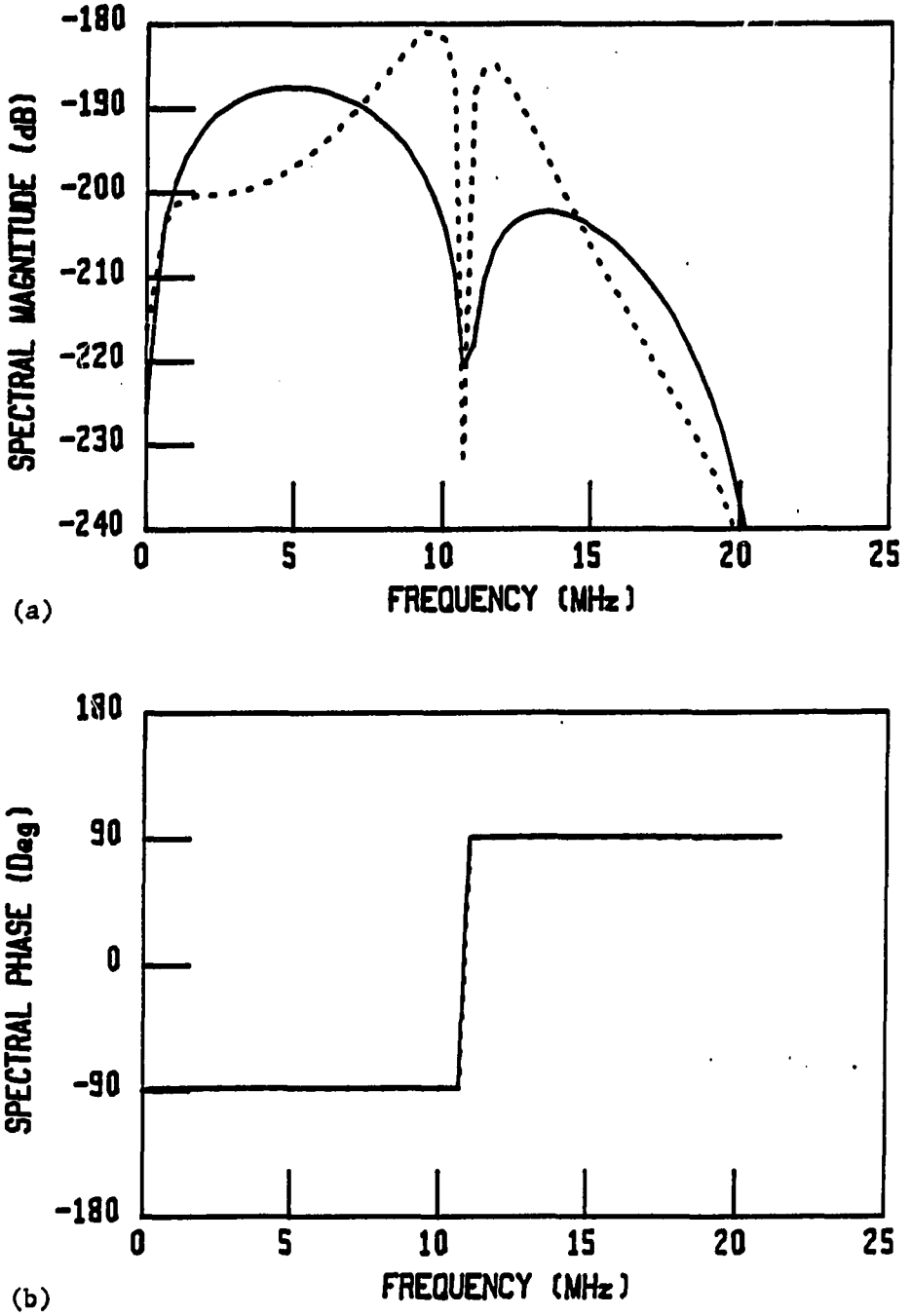

FIGURE 4.18. Simulated ideal voltage step XMTR/RCVR response: (a) spectral magnitude response and (b) spectral phase response of untuned back-matched water-loaded transducers. Solid line is for fully matched case

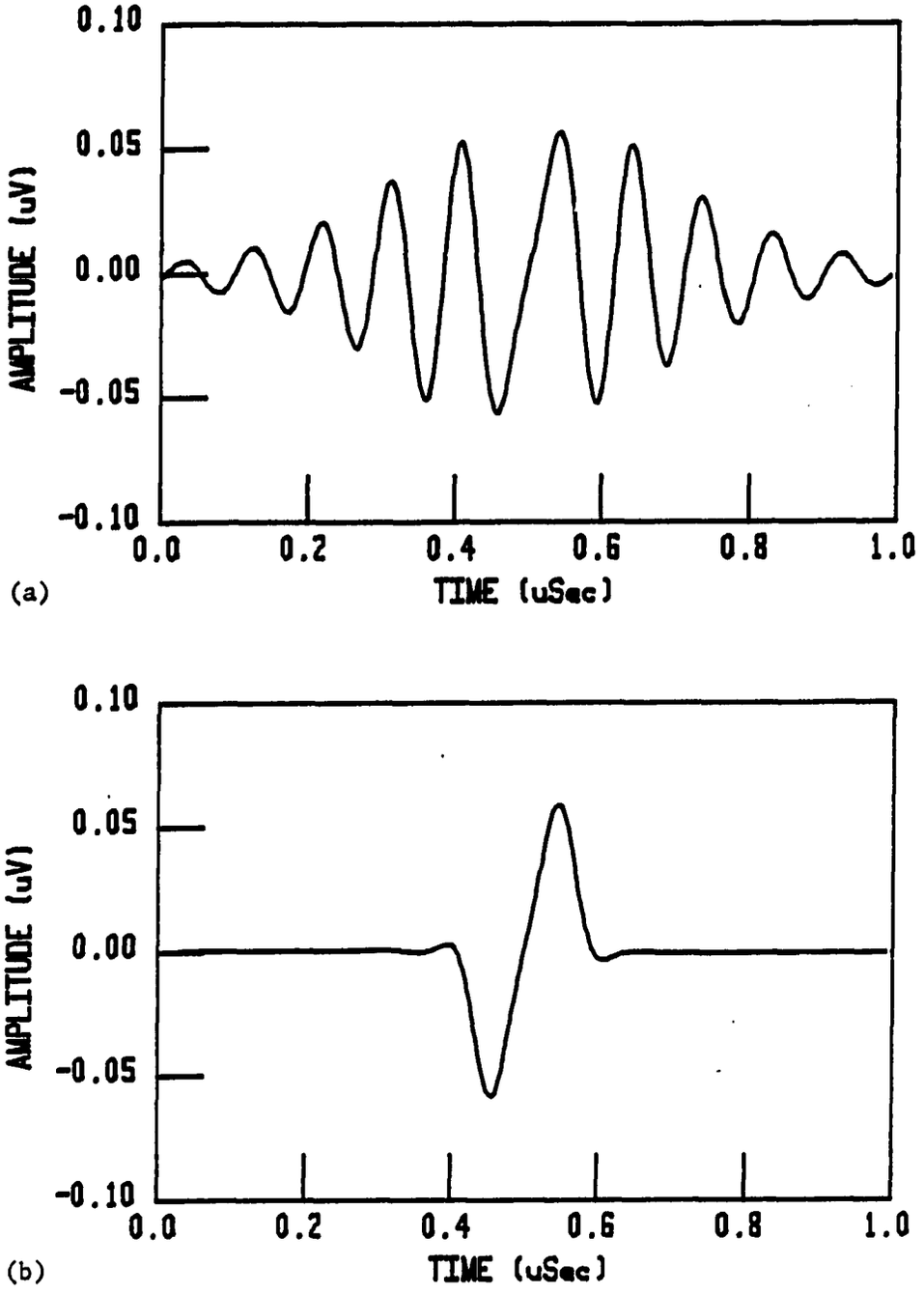

FIGURE 4.19. Simulated ideal voltage step (time domain) XMTR/RCVR response of (a) untuned unmatched and (b) untuned back-matched, water-loaded transducers

$$t_x = d/v_o \qquad (4.19)$$

$$t_x = (110.6 \cdot 10^{-6}\ \text{m})/(2382.5\ \text{m/s})$$

$$\rightarrow t_x = 46\ \text{ns}$$

---

where t_x = 50% amplitude pulse width

d = thickness of resonator

v_o = acoustic velocity in resonator

Thus, the film thickness must be chosen for the desired pulse width. The infinite bandwidth step response gives a transmitted acoustic pulse which is rectangular in shape. Since this simulation program, as well as any practical voltage pulser, is bandwidth limited, the actual pulse will have a "smoothed" appearance.

Figures 4.18 and 4.19 show the pitch-catch XMTR/RCVR response. The unmatched, untuned response is extremely undesirable since it gives the distortion and ringing shown in Figure 4.19a. The XMTR/RCVR waveform for the back-matched case is a bipolar waveform which is similar to the negative of the unipolar waveshape's derivative. Further research is needed to derive the necessary tuning conditions for better reproduction of the unipolar waveform in the receive mode of operation (Chapter VI).

The results of the step response analyses showed that indeed, the piezo films are capable of producing the desirable unipolar acoustic pulses, but that further study was needed to accurately reproduce these pulses in the receive mode. These observations would later be confirmed at the Center for NDE facilities (Chapter VI).

3. Ideal current impulse response simulations

The simplest (first order) model for the electrical input impedance of a lossless piezoelectric transducer is simply its bulk capacitance, C_o. When suddenly connected to a charged capacitance C_p, the result is an impulsive current response. The analogy is more accurate for low-loss piezoelectric materials, however, it was desired to study the ideal current impulse response of the piezo films. Thus, if desired, the simulation program can apply a 1 ampere input current at all frequencies in the prescribed bandwidth, and the bandlimited current impulse analysis performed.

Figures 4.20-4.23 show the simulated current impulse response results. It is clear from these simulation results that as far as waveshape is concerned, the current impulse response is nearly identical to the voltage step response (compare to Figures 4.16-4.19). This is intuitive since the impulse current response caused by the sudden connection of a charged capacitor to a transducer is the result of apply-

ing a step change in the transducer voltage. Thus, the similarity of these simulation results agrees well with intuition concerning circuit theory.

4. Ideal sinusoidal burst response simulations

The sinusoidal burst response was also of practical interest. Short sinusoidal bursts of ultrasound are used in most air-coupled applications and Bragg scattering techniques. A very short burst can also be used for simple ranging measurements, as in tissue. Because tissue has such frequency dependent velocity and attenuation properties (Wells, 1969), simple fat thickness measurements are better made with a very short burst of single frequency energy.

A sinusoidal burst waveform is typically generated by applying a rectangular window (i.e., a gate) to a continuous-wave sinusoid. One of the technical problems associated with generating short sinusoidal bursts is in starting and stopping the burst at 0 volts. Failure to match the endpoints of the burst to 0 volts results in a "smearing" of the burst's frequency spectrum and undesirable sidelobes are produced. Thus, the burst analysis was incorporated in the simulation program with two options: (1) matching endpoints of 0 volts, and (2) mismatched endpoints of +1 volt, -1 volt. This mismatched endpoint case represents the "worst" possible spectral smearing case.

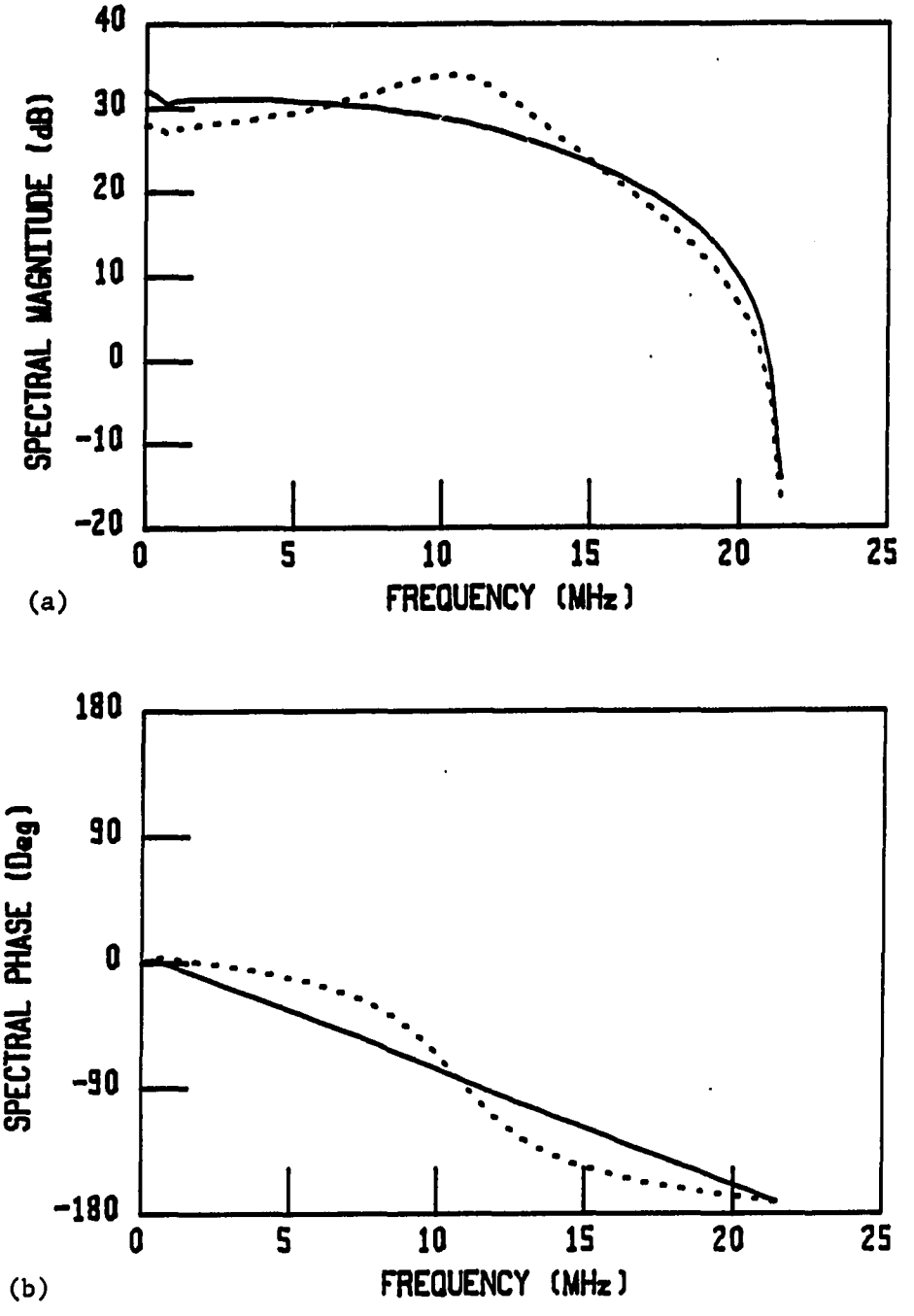

FIGURE 4.20. Simulated ideal current impulse XMTR response: (a) spectral magnitude response and (b) spectral phase response of untuned back-matched water-loaded transducers. Solid line is for fully matched case

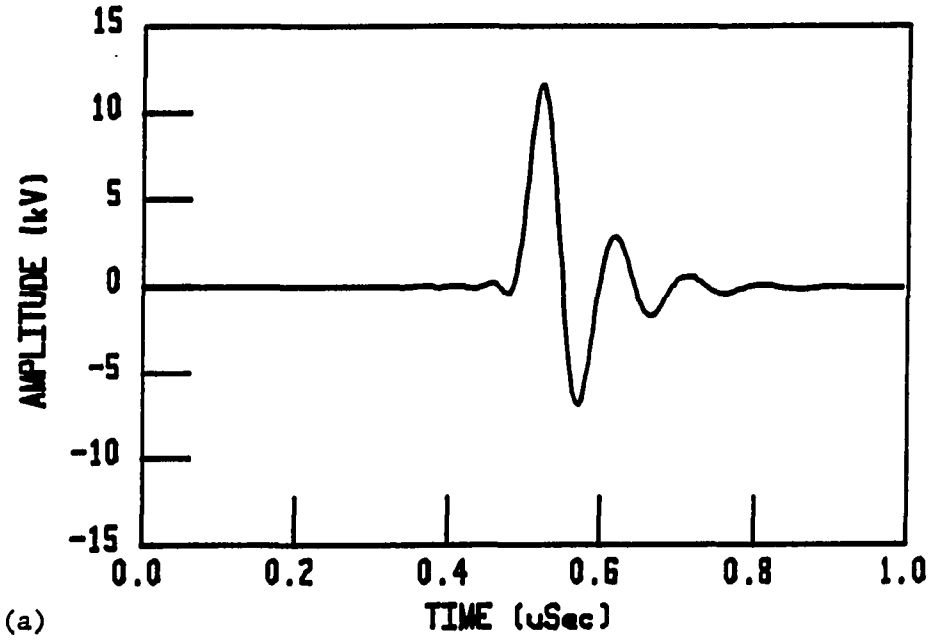

(a)

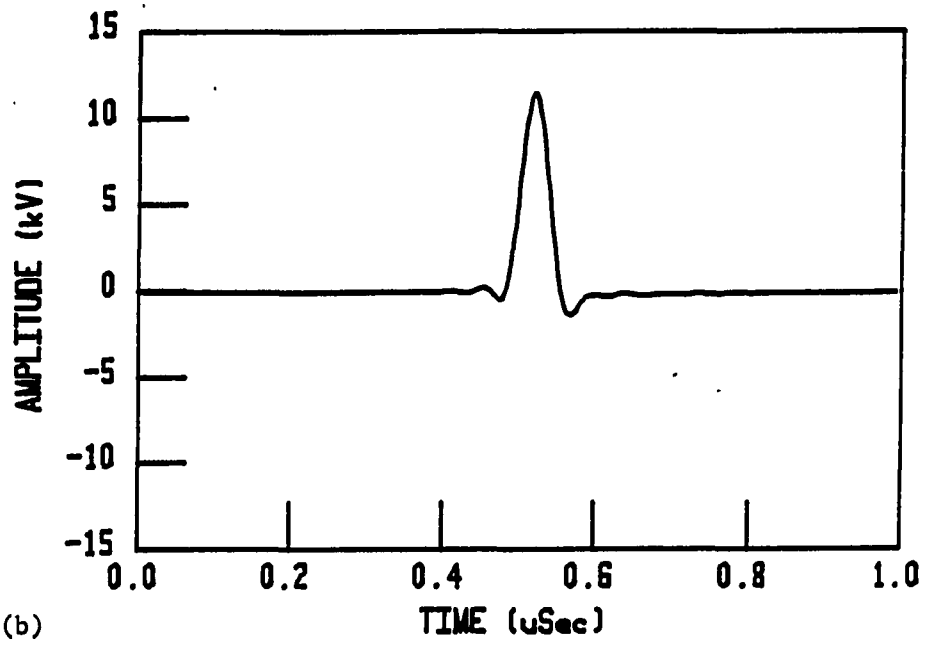

(b)

FIGURE 4.21. Simulated ideal current impulse (time domain) XMTR response of (a) untuned unmatched and (b) untuned back-matched, water-loaded transducers

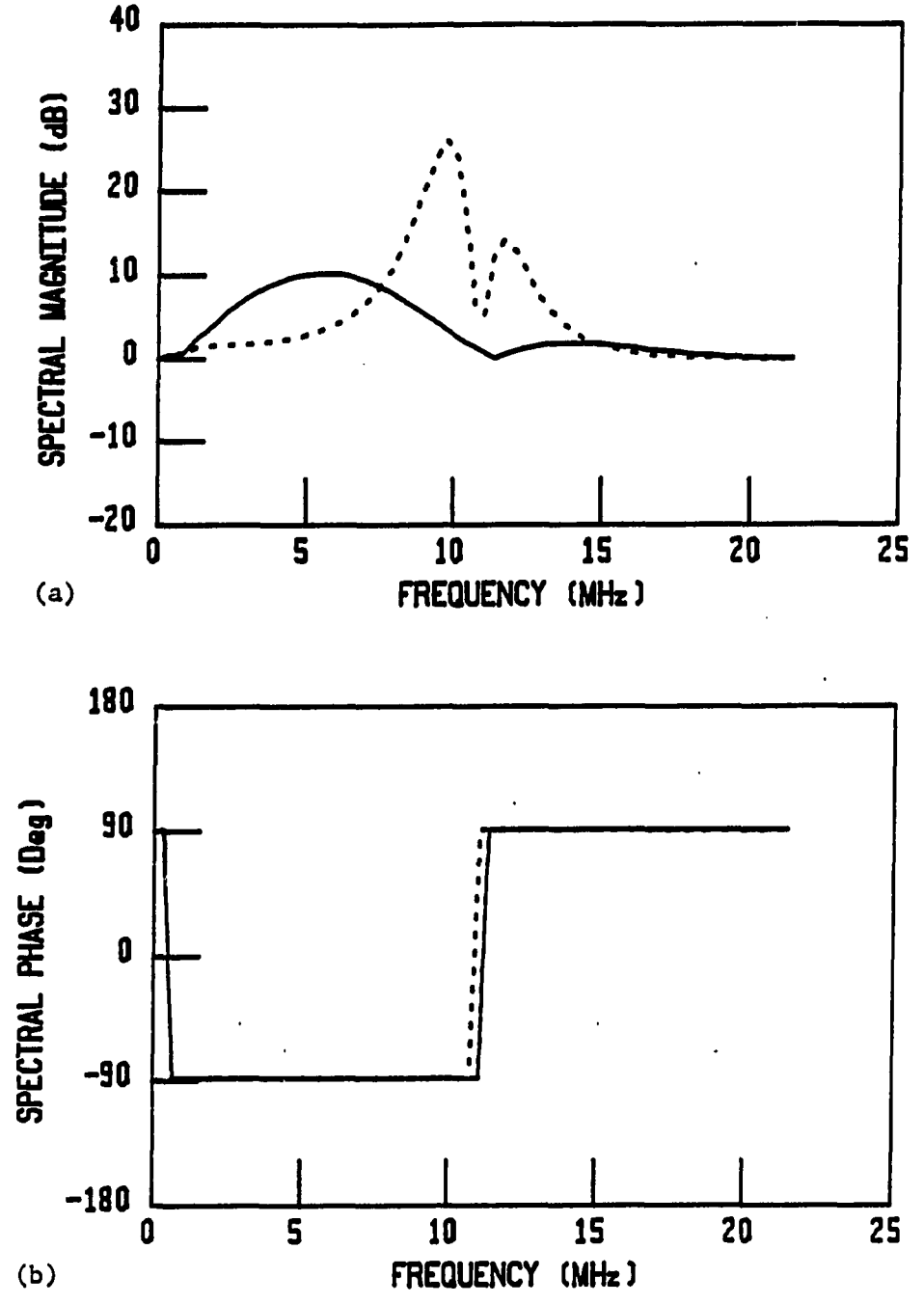

FIGURE 4.22. Simulated ideal current impulse XMTR/RCVR response: (a) spectral magnitude response and (b) spectral phase response of untuned back-matched water-loaded transducers. Solid line is for fully matched case

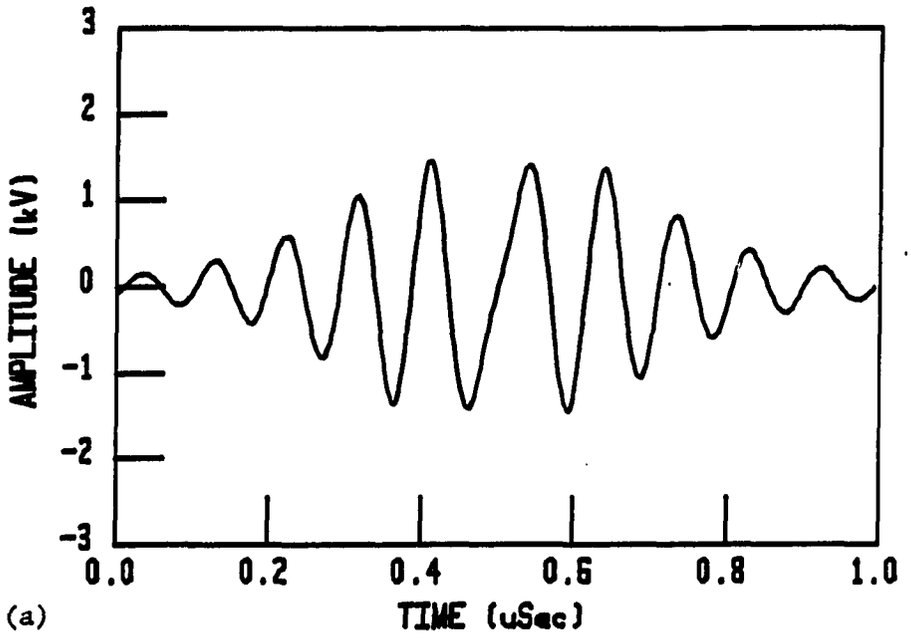

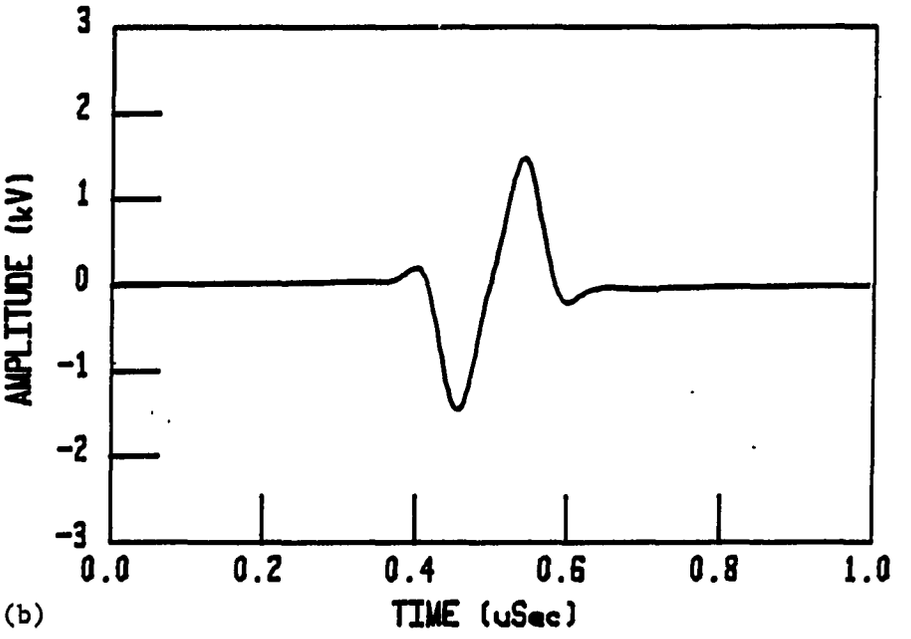

FIGURE 4.23. Simulated ideal current impulse (time domain) XMTR/RCVR response of (a) untuned unmatched and (b) untuned back-matched, water-loaded transducers

After selecting the burst analysis option of the simulation menu, a burst menu is presented on the computer's CRT. The user is prompted for (1) the frequency of the sinusoidal burst, (2) matched or mismatched endpoints, and (3) the number of cycles in the burst. Software protection is included which checks to make sure the entered specifications can be achieved. If they cannot be met (i.e., too many cycles to fit in the sampling period), an error message is printed on the CRT.

The simulation program first computes the sampled input burst waveform and stores it in an array for processing. An FFT is performed on the burst array and the spectral results are applied to the input of the modified Mason's circuit model. The simulation program creates graphics files for:

1. The input burst waveform
2. The FFT spectral magnitude and phase results for the input burst waveform
3. The XMTR response: spectral magnitude, phase, and time domain results
4. The XMTR/RCVR (pulse-echo) response: spectral magnitude, phase, and time domain results

Figures 4.24 and 4.25 show the results of a 2 MHz burst analysis for an untuned back-matched transducer. Figure

4.24 shows the 128-point 2 MHz input burst waveform and its FFT spectral magnitude. As expected, the spectral magnitude response resembles the magnitude of a sinc function ($\mathrm{Sin}(\pi x)/\pi x$). The figure shows spectral smearing (leakage) even with matched endpoints. However, it is evident that there is little energy in the burst spectrum near the resonant frequencies of the 110.6 micron $P(VF_2\text{-}VF_3)$, thus, the "clean" time domain results of Figure 4.25 were expected.

The transmitted burst (Figure 4.25a) shows excellent reproduction of the derivative of the input burst waveform. The broadband response of the untuned back-matched receiver is evident in the faithful reproduction of the waveform in the pulse-echo mode (Figure 4.25b). For the matched-zero endpoints, the copolymer design provides excellent sinusoidal burst performance.

The unmatched-endpoint case is shown in Figures 4.26 and 4.27. The input waveform for this case is a 2-1/2 cycle 2 MHz burst as shown in Figure 4.26a. The spectral magnitude of the burst shows considerably more leakage and thus, more energy in the area of resonance for the film. Therefore, the results of Figure 4.27 are no surprise. The step change in voltage at the ends of the applied burst waveform give rise to the spikes shown. The spikes represent a portion of the transducer's response to a voltage step input--the launching of a unipolar pulse waveform. The

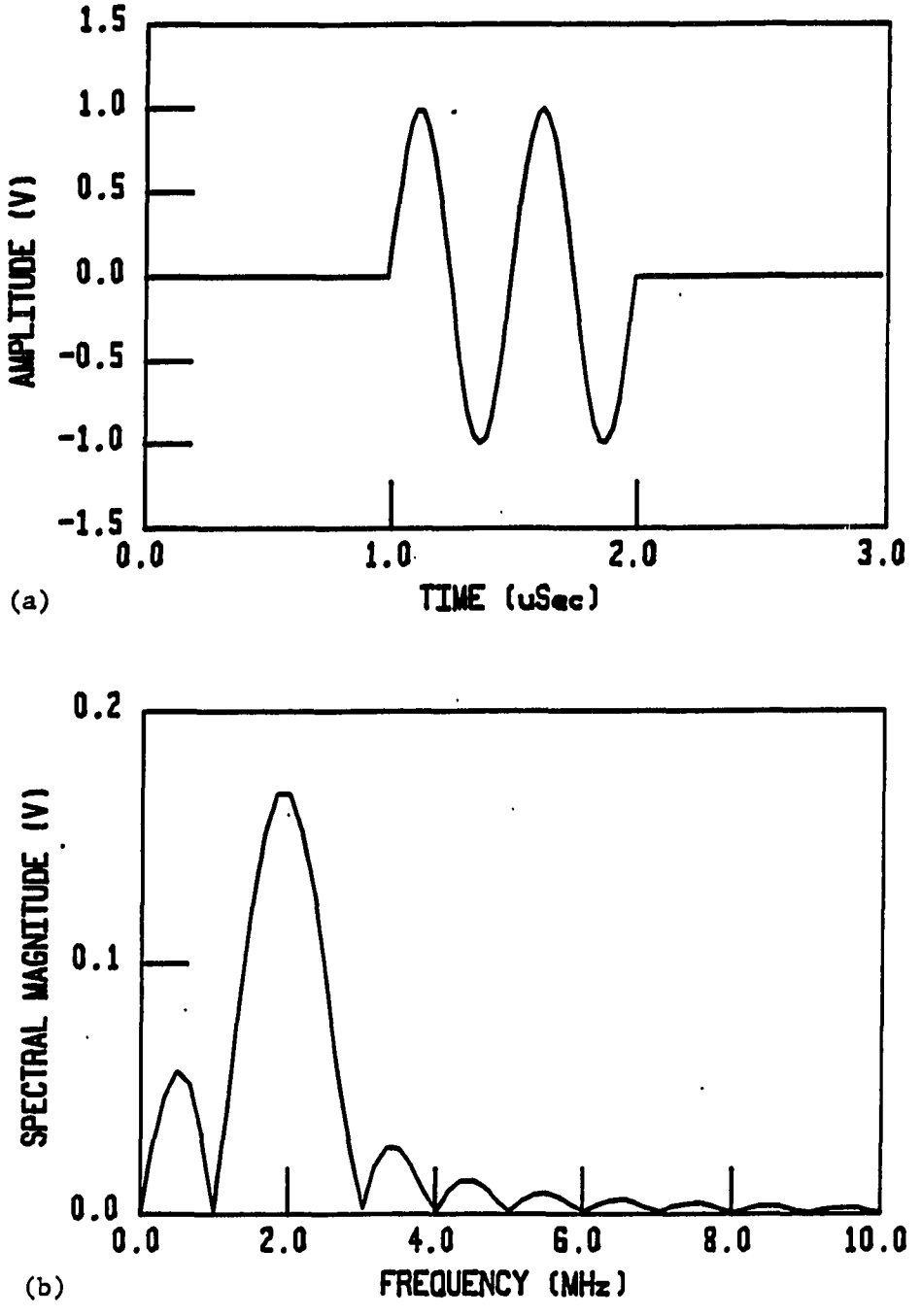

FIGURE 4.24. The 2-cycle 2 MHz input burst waveform with matched-zero endpoints: (a) input time domain voltage waveform and (b) FFT spectral magnitude of the applied burst waveform

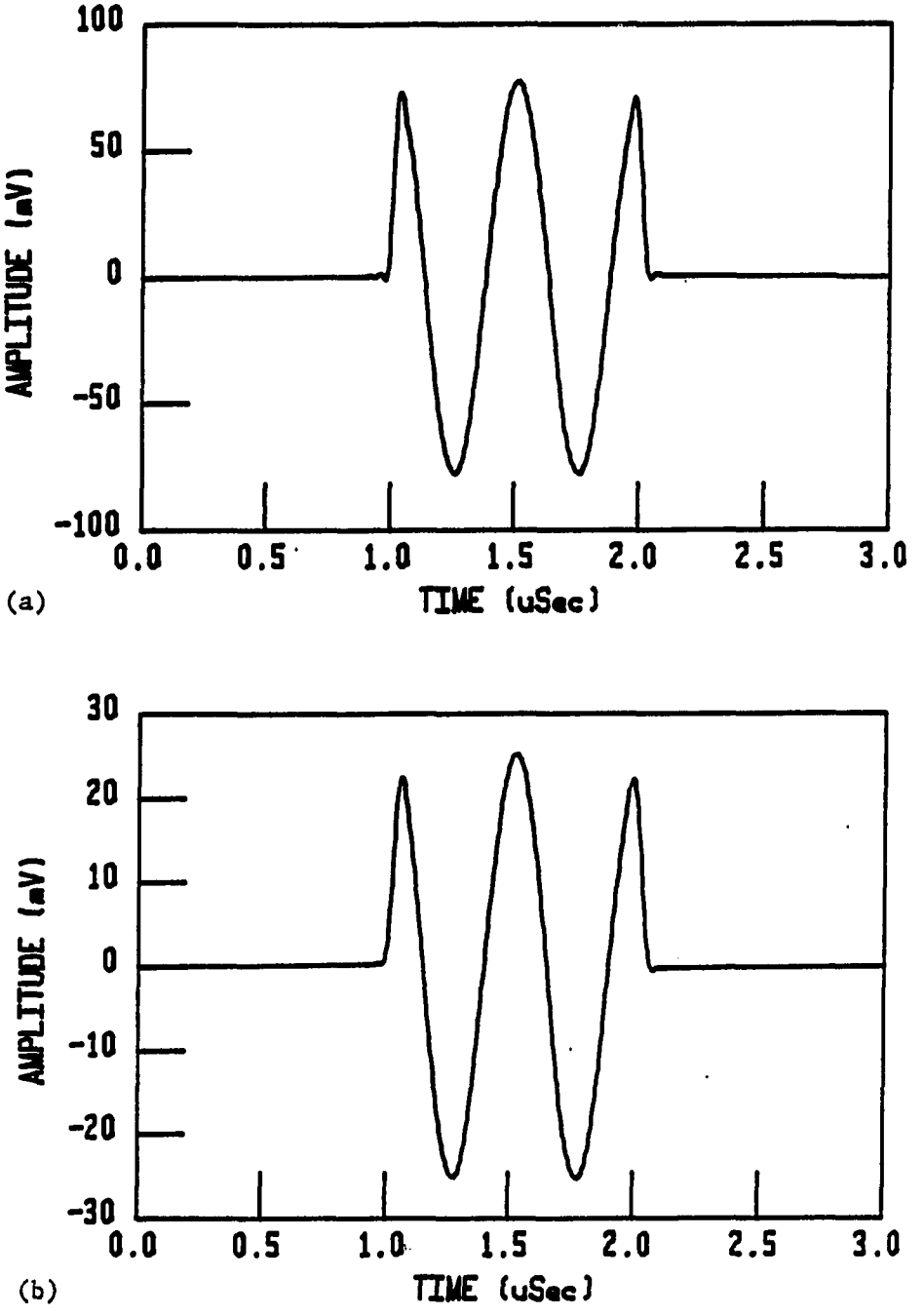

FIGURE 4.25. Simulated time domain burst response waveforms for the matched-zero endpoints case: (a) XMTR waveform and (b) pulse-echo waveform

unipolar waveshape is quickly obscured as the transient response gives way to the derivative of the burst waveform and a smooth sinusoidal response is noted. It is clear that the step voltage change at the ends of the burst caused the transducer to ring at its natural resonant frequency.

The simulation program thus provides valuable insight for the simulation and design of sinusoidal burst piezo film ultrasound transducers. With the option to simulate many matched and tuned designs, nearly any transducer design may be tested for its sinusoidal burst performance.

5. Ideal quarter-wavelength resonating/tuning simulations

Two methods of mechanical matching and tuning may be utilized in the simulation program. The first method involves the use of a quarter-wavelength matching layer on the front face of the transducer. This technique was used in all of the previously shown fully matched simulations. Since the user may specify the acoustic impedance of the backing material, one can specify a large enough value to cause the piezoelectric material to resonate at its quarter-wavelength resonant frequency instead of the usual half-wavelength value. Both of these techniques may be employed to enhance ultrasound transducer performance.

To better understand the concept of quarter-wavelength matching, Figure 4.28 shows the circuit representation for a

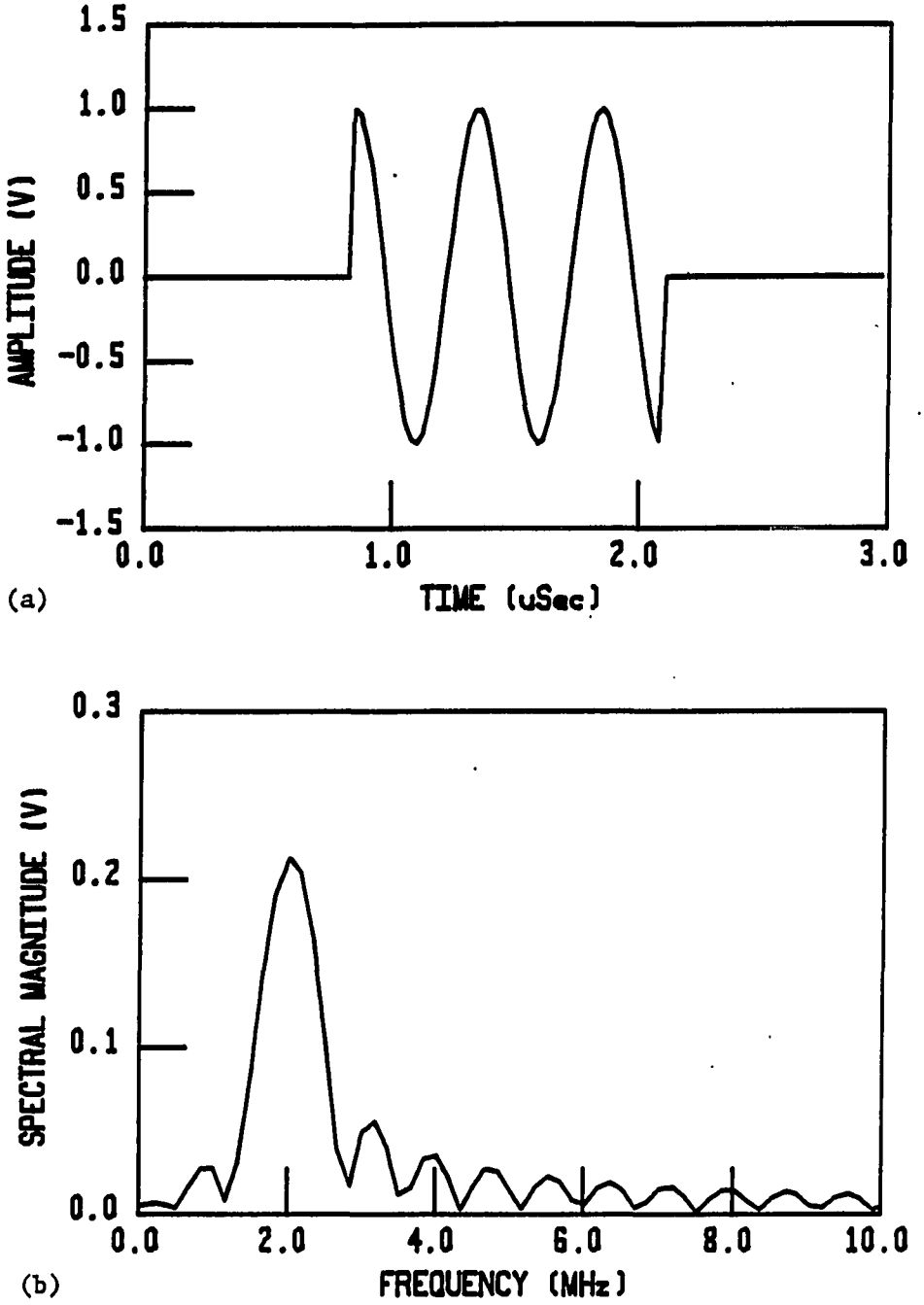

FIGURE 4.26. The 2-1/2-cycle 2 MHz input burst waveform with unmatched endpoints: (a) input time domain voltage waveform and (b) FFT spectral magnitude of the applied burst waveform

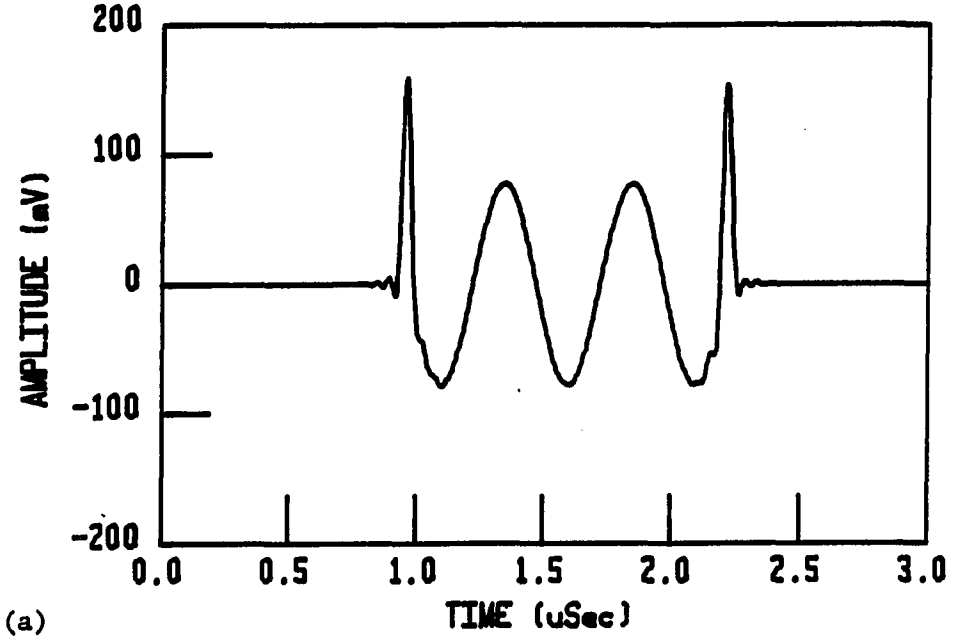

(a)

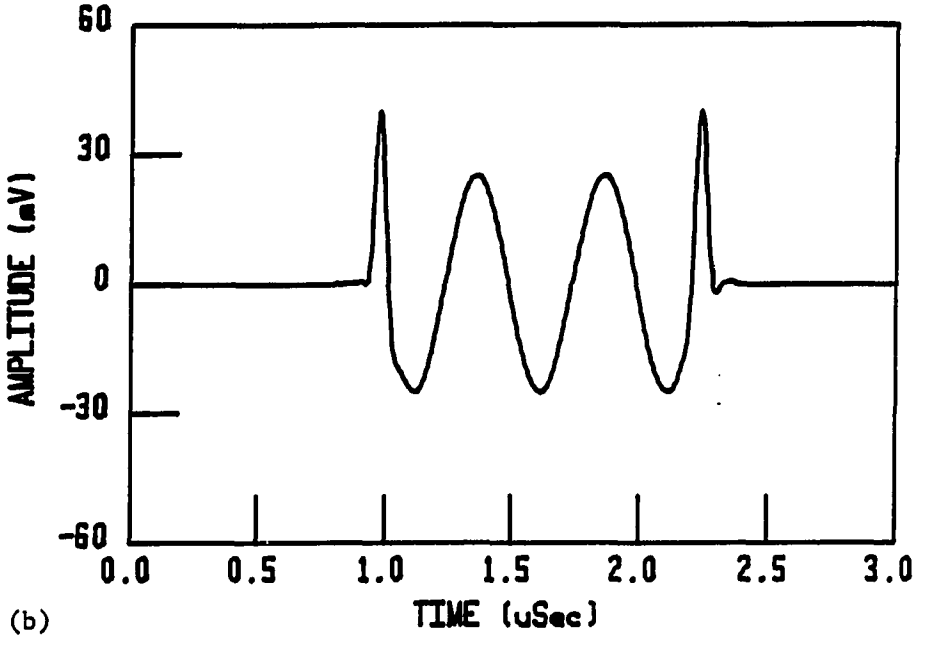

(b)

FIGURE 4.27. Simulated time domain burst response waveforms for the unmatched endpoints case: (a) XMTR waveform and (b) pulse-echo waveform

layer (i.e., bonding or electrode layer, etc.) as presented in Chapter II.

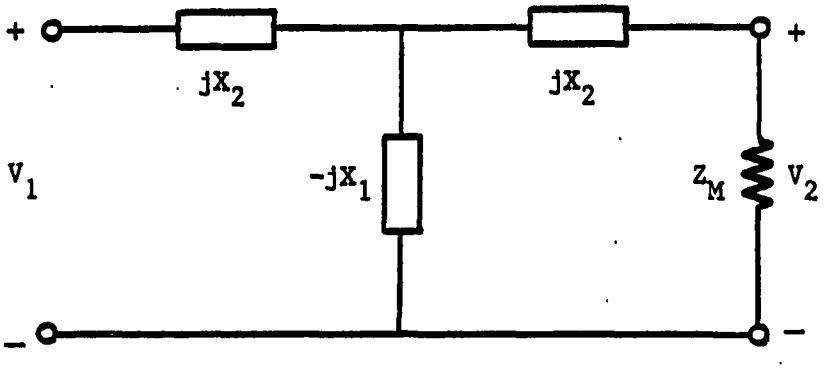

FIGURE 4.28. Circuit model for a layer

The parameters of the circuit are given by:

$$X_1 = Z_L/\sin(\theta_L) \tag{4.20}$$

$$X_2 = Z_L\mathrm{Tan}(\theta_L) \tag{4.21}$$

$$\theta_L = 2\pi f d_L/v_L \tag{4.22}$$

where Z_M = acoustic impedance of the front medium

Z_L = acoustic impedance of the layer

d_L = thickness of the layer

v_L = acoustic velocity of the layer

f = frequency (Hz)

The input impedance of the circuit (from the transducer side) is seen to be:

$$Z_{in} = jX_1 + \frac{-jX_1(Z_M + jX_2)}{Z_M + jX_2 - jX_1} \tag{4.23}$$

If d_L is chosen as the quarter-wavelength thickness of the layer, $\lambda_L/4$, then:

$$\theta_L = 2\pi f(1/4)(V_L/f_s)/V_L \tag{4.24}$$

$$\Rightarrow \theta_L = 2\pi f/f_s \tag{4.25}$$

Table 4.1 shows the values for X_1, X_2, and Z_{in} for the $d_L=\lambda_L/4$ case.

TABLE 4.1. Impedance values for $d_L=\lambda_L/4$

f (Hz)	X_1	X_2	Z_{in}
0	∞	0	Z_m
f_s	Z_1	Z_1	Z_L^2/Z_m

Thus, if Z_L is chosen to be $(Z_M Z_o)^{1/2}$, then $Z_{in}=Z_o$, the impedance of the piezoelectric resonator. Therefore, perfect acoustic matching of the load is achieved at the quarter-wavelength frequency. Normally, a quarter-wavelength matching layer is added to a transducer to match the acoustic medium to the piezoelectric material at the resonant frequency of the transducer. However, one can also choose to vary the thickness of this layer and obtain ideal matching at other frequencies if desired.

Figures 4.29 and 4.30 show the effects of quarter-wavelength matching the front layer to f_s, $f_s/2$, $f_s/4$, and $f_s/8$ on the voltage impulse response. After comparing these to Figures 4.4 and 4.5, the effects of front layer matching are obvious. One can "peak up" the response at any desired frequency. Just as important, however, is the fact that by including this option in the simulation program, a user can observe the effects of not only matching layers on acoustic performance, but also bonding and protecting layers. Obviously, every layer on a transducer will have its own characteristic quarter-wavelength matching frequency. If the layer is for bonding or protecting only, the designer must insure that the layer's matched frequency does not have adverse effects on the transducer's performance. A thick layer, as in the $f_s/8$ case of Figure 4.30b, causes a very "different" characteristic response than for the thin layer cases.

Figure 4.2 showed the assigned impedance values in the modified Mason's model. Parallel resonance occurs when $Im\{Z_1\}=0$. When both faces of the transducer are equally loaded ($Z_F=Z_B$) the condition that gives parallel resonance, f_p, is:

$$Im\{Z_1\} = 0 = -jX_1 + jX_2/2 \qquad (4.26)$$

$$\text{or} \quad X_1 = X_2/2 \qquad (4.27)$$

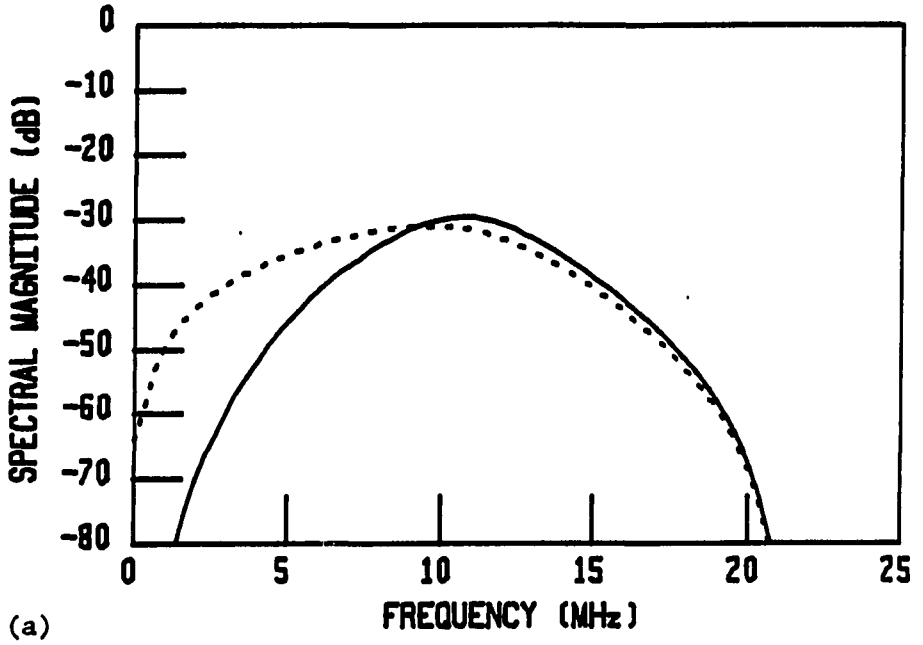

(a)

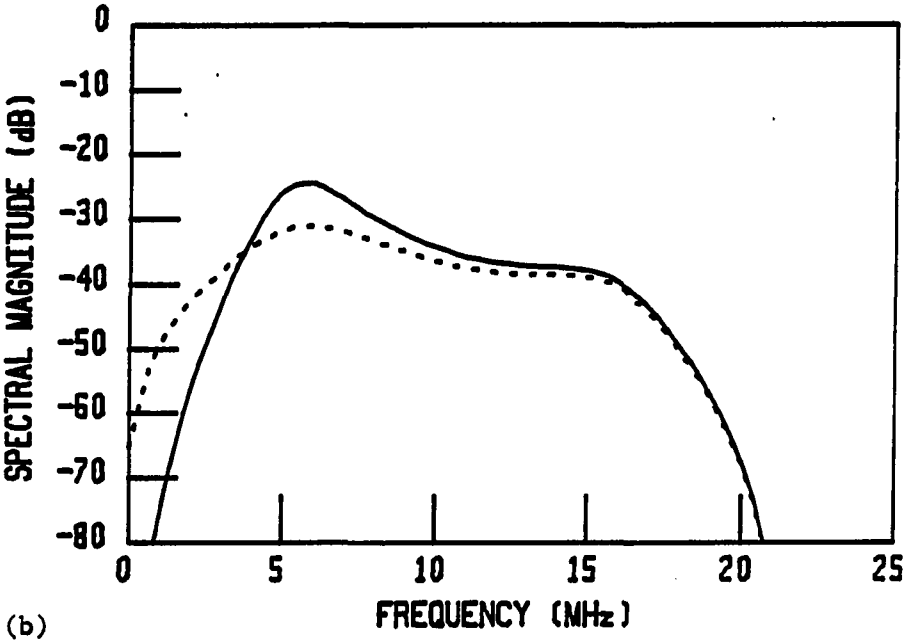

(b)

FIGURE 4.29. Simulated voltage impulse response for pulse-echo performance of untuned (broken line) and shunt-tuned to f_s (solid line) transducers: (a) front-matched f_s and (b) front-matched to $f_s/2$

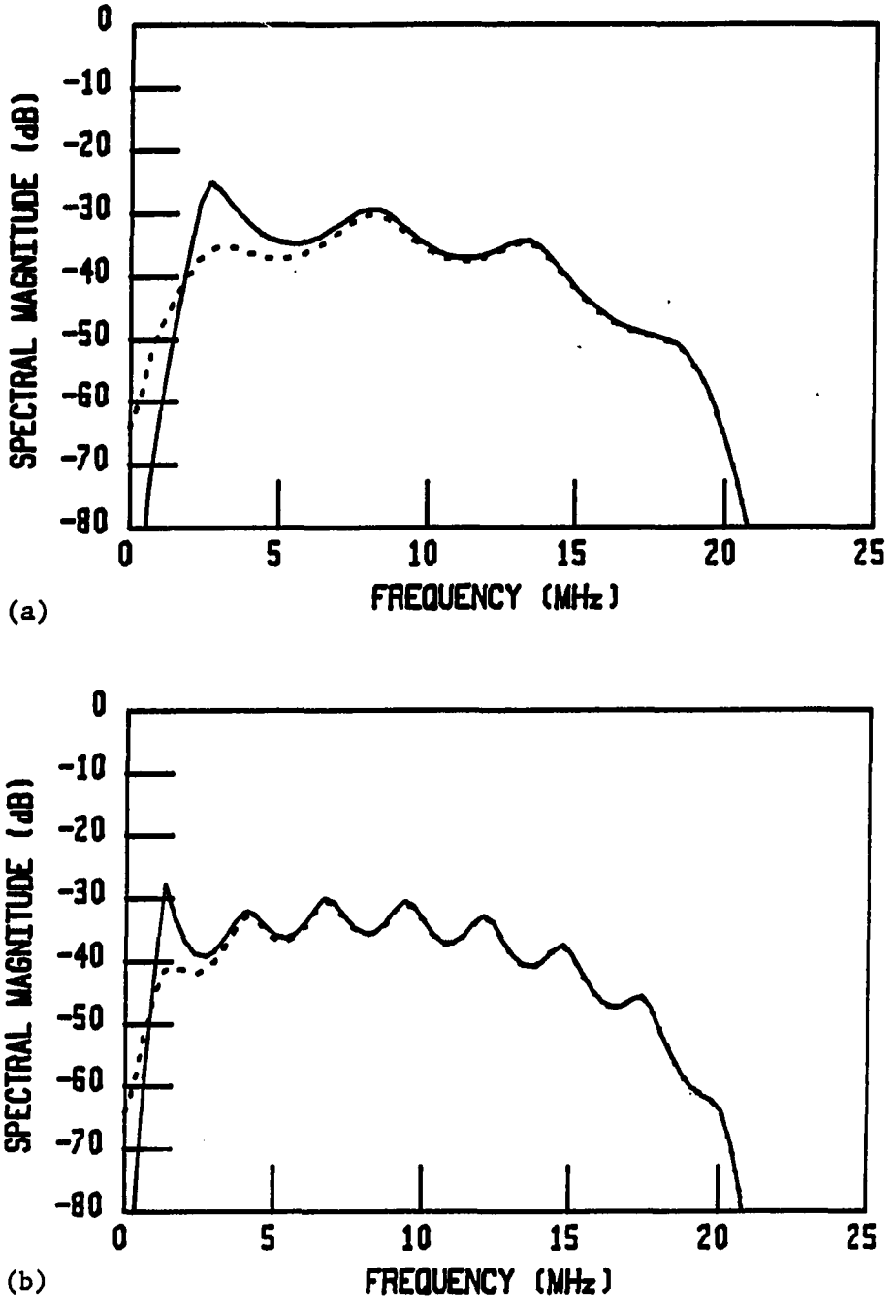

FIGURE 4.30. Simulated voltage impulse response for pulse-echo performance of untuned (broken line) and shunt-tuned to $f_s/4$ (solid line) transducers: (a) front-matched to f_s and (b) front-matched to $f_s/8$

The 1/2 factor for X_2 arises since the equal front and rear mechanical impedance branches are in parallel. If one should instead terminate the rear face of the transducer with an open circuit (i.e., $Z_B >> Z_F$), the shunt combination gives twice the impedance. Thus, $Im\{Z_1\}$ will resonate at half the original f_p, the quarter-wavelength frequency of the resonator.

Since the simulation program allows a user to specify the acoustic impedance at the back face, the user can simulate the design of a quarter-wavelength resonator transducer. Thus, a 110 micron piezo film transducer would resonate at about 5 MHz instead of 10 MHz. After testing many such simulations, a minimum ratio of about 5 in Z_B/Z_o was noted to give adequate quarter-wavelength resonant behavior. In practical transducer designs, a brass backing gives a ratio of about 9.5 for the piezo films.

Figures 4.31 and 4.32 show the voltage impulse (transfer function) pulse-echo response of the 110.6 micron $P(VF_2-VF_3)$ with various values of Z_B/Z_o. The dotted lines represent the untuned case and the solid lines represent the results of adding inductively shunt tuning. The back-matched case ($Z_B/Z_o=1$) in Figure 4.31a shows the characteristic broadband response centered about the half-wavelength resonant frequency of the piezo film ($\simeq$10.5 MHz). Figure

4.31b shows the quarter-wavelength response for the Z_B/Z_O=4.5 case which corresponds to an aluminum backing material. The results show peaked responses at the quarter-wavelength frequency of about 5 MHz, and at the next odd multiple of this frequency, about 15 MHz.

The results are even more prominent in Figure 4.32 which shows the Z_B/Z_O=9.5 (brass backing) and Z_B/Z_O=26 (drawn tungsten backing) cases. The shunt tuning results all show a "peaking up" of the pulse-echo response at the tuned quarter-wavelength frequency (half-wavelength frequency for the back-matched case in Figure 4.31a), and a loss of bandwidth--consistent with all previous simulation results.

It is clear that both methods of mechanical matching and tuning of ultrasound transducers allow the designer great versatility in performance. It is also clear that "subtleties" such as bonding layers and backing materials must be carefully considered in the design of useful ultrasound transducers. The use of the simulation program XFER.FOR allows one to account for these characteristics in simulated testing of prototype transducer designs.

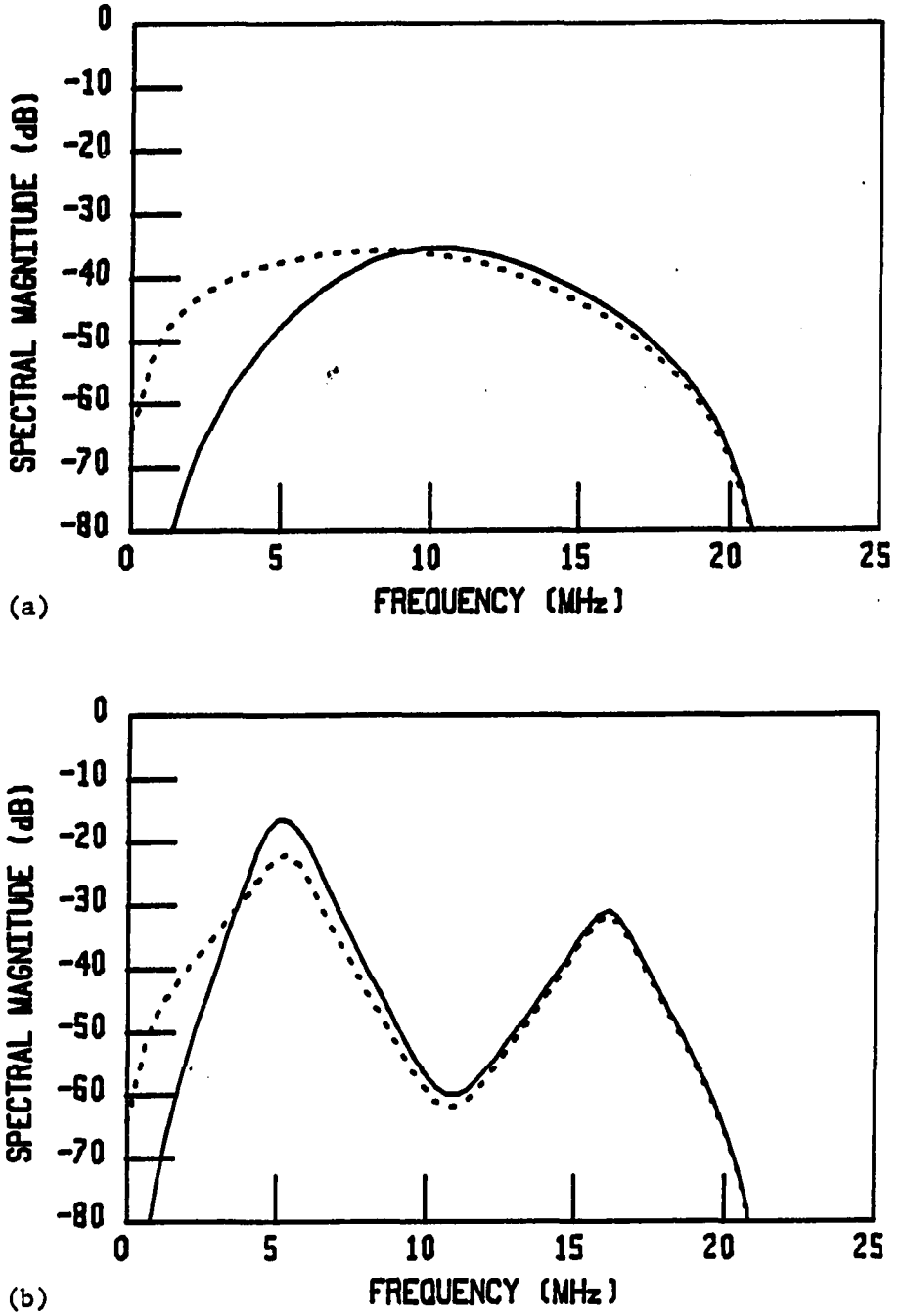

FIGURE 4.31. Pulse-echo spectral magnitude response of simulated ideal voltage impulse input for (a) Z_B/Z_O=1 and (b) Z_B/Z_O=4.5. Broken line is for untuned case, solid line is for shunt-tuned case

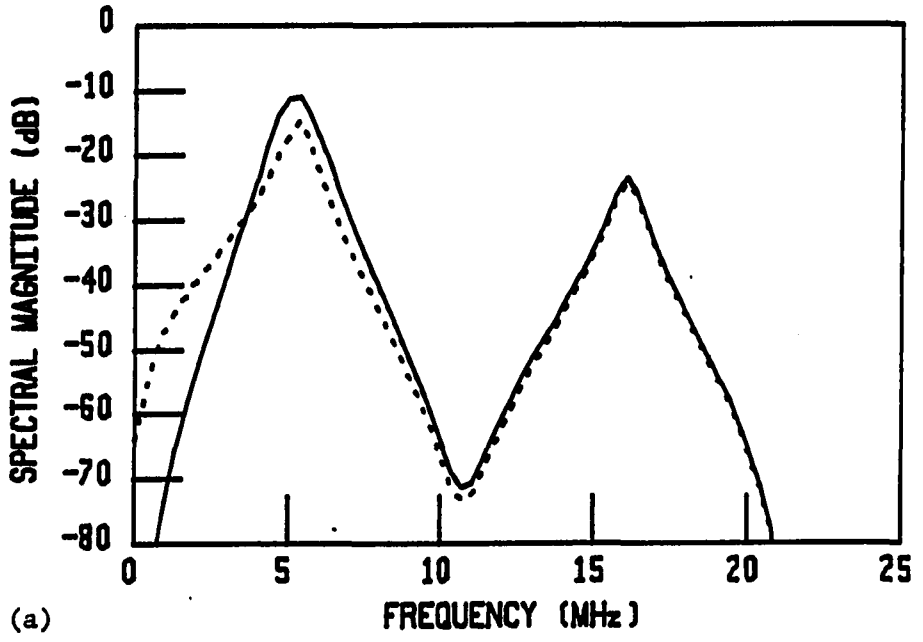

(a)

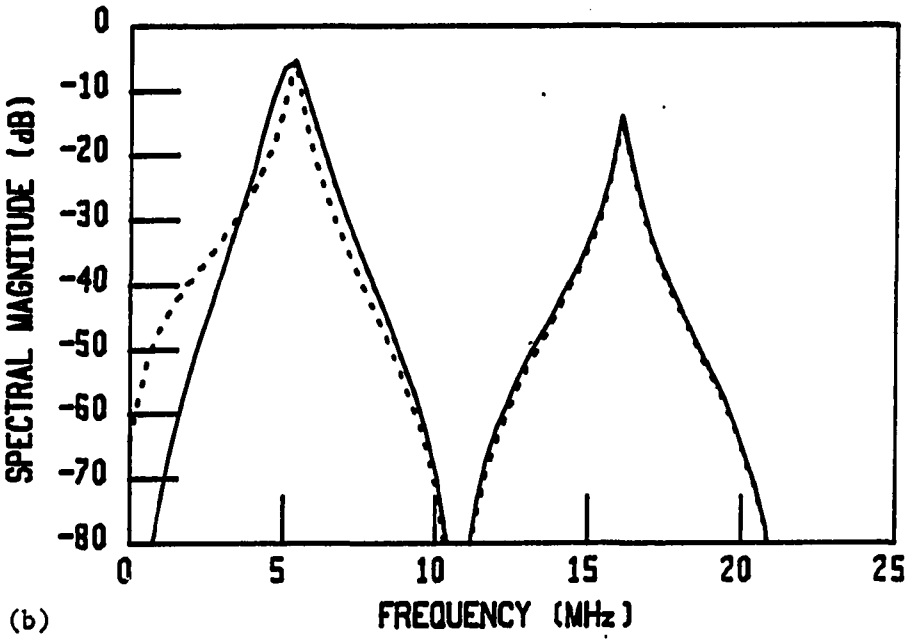

(b)

FIGURE 4.32. Pulse-echo spectral magnitude response of simulated ideal voltage impulse input for (a) Z_B/Z_O=9.5 and (b) Z_B/Z_O=26. Broken line is for untuned case, solid line is for shunt-tuned case

D. Comparison of PVF_2 and $P(VF_2-VF_3)$ Simulated Performance

After analyzing many PVF_2 and $P(VF_2-VF_3)$ film samples, it was clear that the copolymer had a higher electromechanical coupling coefficient, k_t, and lower dielectric losses. It seemed natural to assume that since the copolymer still retained a low Q_m value, that its acoustic performance was superior to PVF_2. However, the only way to verify such an assumption was through side-by-side performance tests that allow quantitative comparisons between the two films for XMTR, RCVR, and XMTR/RCVR operation. It was desired to develop a method for comparing PVF_2 and $P(VF_2-VF_3)$ ultrasound transducers of identical design and tuning. The simulation program provided the means for such analyses.

Such quantitative comparisons would reveal whether one material was distinctly "better" than the other, or whether the "better" material depends on the particular application. The results would be of great interest to the manufacturer, too. Why strive for improvements in processing two different films for ultrasound if one has a distinct advantage over the other in all applications?

The film specifications for three previously analyzed piezo films were used for the comparisons: (1) 31.75 micron PVF_2 (MM86093), (2) 51.58 micron PVF_2 (MM86005), and (3) 30

micron P(VF_2-VF_3) (MM87070). All comparisons were made between a PVF_2 and P(VF_2-VF_3) transducer of identical design. Quantitative comparisons were made and tabulated for sensitivity, 3 dB bandwidth (BW_{3dB}), 3 dB quality factor (Q_{3dB}), and 2 MHz burst amplitude response. These acoustic performance values can be best understood by referring to the sketch of an acoustic performance test shown in Figure 4.33.

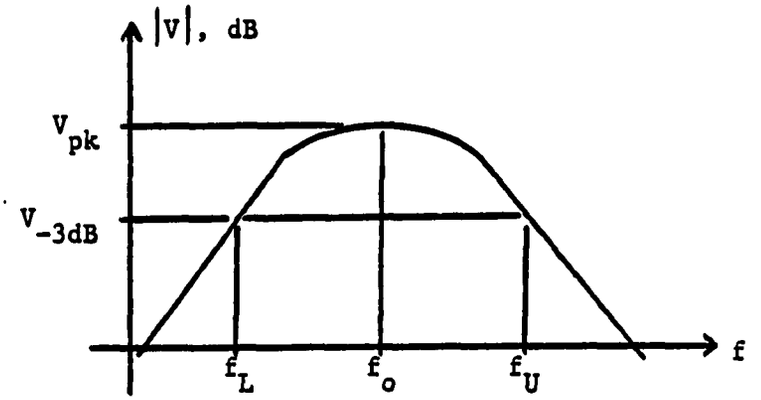

FIGURE 4.33. Sketch of a simulated acoustic performance

Sensitivity is found by noting the value of V_{pk}, the peak response, which is normally noted at the resonant frequency of the transducer. The frequency values where the response is 3 dB below V_{pk} mark the upper and lower 3 dB bandwidth. Q_{3dB} is defined as the ratio of BW_{3dB} to f_o:

$$BW_{3dB} = f_U - f_L \tag{4.28}$$

$$Q_{3dB} = BW_{3dB}/f_o \tag{4.29}$$

The simulations were analyzed for (1) untuned water-loaded transducer, (2) inductively shunt tuned to f_s water-loaded transducer, (3) inductively shunt tuned to f_s back-matched, water-loaded front transducer, and (4) inductively shunt tuned to f_s, back-matched and quarter-wavelength matched front layer (to water) transducer. In some of the untuned simulations an unpeaked (i.e., decaying) response was noted. In those cases f_o was assumed to be that value obtained for the shunt-tuned case. More than 1000 simulations were completed in a comprehensive study of the piezo films. A summary of many of these results is included in Appendix L.

The results were clear. For all designs, the $P(VF_2\text{-}VF_3)$ outperformed PVF_2 in virtually every test of XMTR, RCVR, and XMTR/RCVR performance. In general, the copolymer displayed (1) more sensitivity, (2) a lower Q_{3dB}, and (3) a larger bandwidth. It was clear that the copolymer was superior to PVF_2 in all thickness-mode ultrasound transducer applications. The simulation results and the conclusions were also forwarded to the piezo film manufacturer. The simulation program thus supplied not only useful theoretical insight on prototype transducer designs, but also a valuable method of making quantitative comparisons between piezo film materials.

E. Conclusions

Because of the complexity of the modified Mason's models and the nonlinear properties of the components, it was necessary to evaluate the models with a "custom" computer program. Classical frequency domain circuit analysis techniques were used to evaluate acoustic performance with the models. The previously derived circuit models were hence implemented in a user-friendly interactive design/simulation program.

The program allows a user to evaluate the (1) voltage impulse response, (2) voltage step response, (3) current impulse response, and (4) sinusoidal burst response of a transducer using the modified simple Mason's model (no electrodes), or full Mason's model (with electrodes and/or quarter-wavelength matching front layer). The user can also elect to inductively shunt tune and/or acoustically match the back face of any transducer design. Graphics files are created for the spectral magnitude, spectral phase, and time domain responses of the selected test. This provides the user with a means for "seeing" the performance results.

With the use of this program, a detailed study was carried out which compared side-by-side, the acoustic performance of PVF_2 and $P(VF_2\text{-}VF_3)$. The results of the study gave overwhelming evidence that the copolymer was superior in all transducer designs considered.

It would simply not be possible to build and test a prototype ultrasound transducer of every conceivable design. Yet, a user can easily evaluate and record the results for the 180 basic types of simulation analyses in a few hours. Therefore, the value of the simulation program is obvious. Since the derived circuit models provided the first broad-band modeling of piezo film ultrasound performance, the simulation program provided an accurate method for evaluating the acoustic performance of a prototype piezo film transducer design. Thus, the second main objective of this research was achieved. A question still remained concerning the modified Mason's models, "How well would the simulation program predict the spectral magnitude and time domain responses of a real transducer involved in an actual experiment?". It was this question which prompted the need for the third part of this research.

V. DESIGN AND TESTING OF P(VF_2-VF_3) ULTRASOUND TRANSDUCERS

The development of the electromechanical models and their implementation in a computer simulation program would both be of little value if one could not verify their accuracy. The best method of verification is that of comparing the acoustic performance of actual piezo film ultrasound transducers with the performance predicted with the models under known experimental conditions. At this stage of the research it was not known how to construct piezo film ultrasound transducers of sufficient quality to allow any meaningful assessment of acoustic performance. Thus, the third major part of this research focussed on two main objectives.

The first objective was to develop a prototype piezo film ultrasound transducer that could be used for accurate testing of acoustic performance. It was desirable to design a probe which was capable of both contact operation (like medical probes) and submersible operation (like NDE probes). The second major objective was to compare the acoustic performance of the probes with that predicted (simulated) with the modified Mason's models. All work related to these objectives is presented in this chapter.

This chapter begins by reviewing other piezo film ultrasound transducer designs and describes the work that led to the development of successful piezo film ultrasound

transducers. The special testing facilities and detailed assessment of acoustic performance are discussed for both series and shunt tuned $P(VF_2-VF_3)$ ultrasound probes. This chapter also contains figures that compare plots of actual and predicted acoustic electromechanical waveforms. As before, an effort has been made to group the figures in a manner that provides insight without "overwhelming" the reader.

A. Review of Previous Piezo Film Ultrasound Transducer Designs

At present there are only three commercial producers of piezo films in the world: one in Europe, one in Japan, and one in the U.S. (Pennwalt Corporation, Valley Forge, PA). All three producers manufacture only bulk film with metalized electrode layers, not commercial ultrasound probes. To test actual piezo film transducer performance, investigators have had to design and construct their own test probes. Since the films are so thin and flexible and cannot be readily soldered to, most successful designs have been the result of much experimental "trial and error".

There are many publications describing applications and testing of piezo film (PVF_2) ultrasound transducers, however, most publications lack sufficient detail to permit a "novice" to actually construct working piezo film probes.

This section describes many of the piezo film ultrasound transducer designs that have been reported in technical literature.

1. Hydrophone probe designs

Because of their broadband acoustic performance and close acoustic match to water, the piezo films offer superior performance for hydrophone probe applications. Acoustic hydrophone probes are miniature transducer receivers used for intensity measurements of ultrasonic acoustic fields. Such measurements are often used to derive a 3-dimensional image of the acoustic beam produced by an ultrasound transducer under test.

Early work with PVF_2 hydrophones was reported by Schotten et al., 1980. A hydrophone was constructed from a 4 mm diameter sheet of 25 micron PVF_2, supported by a Plexiglas ring of approximately 100 mm in diameter. The film leads were connected to a 50 Ω coax cable with conductive epoxy bonding. The probe provided excellent broadband reception in the 0.5-15 MHz frequency range. The authors also used a thin (12 micron) film design which provided excellent reception of frequencies as high as 40 MHz.

Another PVF_2 hydrophone design was reported by Lewin (1981). Lewin's published work featured a schematic drawing of the construction of his miniature hydrophone probes. The

probes were constructed with a 25 micron PVF_2 element, 0.6-1 mm in diameter. Electrical connections were again made with the use of conductive adhesives and the probe was housed in stainless steel hypodermic tubing for shielding. The probe showed excellent broadband performance (±1.6 dB for 1-10 MHz).

Another well described PVF_2 hydrophone design was reported by Platte (1985). The investigator constructed and tested a needle-like PVF_2 hydrophone with a 20 micron thickness. The probe design was used for extremely broadband (1-20 MHz) small diameter (i.e., 0.3 mm) hydrophones. However, the publication contained less technical details of the construction than the previously described hydrophone probe designs.

The problems reported in the hydrophone probe designs were noted and later considered useful in the experimental probe designs.

2. Imaging transducer designs

Since multiple transducer elements can be produced on a single sheet of piezo film, many investigators have constructed piezo film arrays for imaging applications. An interesting imaging design was reported by Swartz and Plummer (1980b). The investigators bonded PVF_2 elements to a silicon substrate and, using conventional microelectronics

techniques, formed an integrated structure called a piezo-electric-oxide-semiconductor field effect transistor, or "POSFET". Many schematic drawings were included which detailed the authors' design.

Sessler (1981) published a summary of PVF_2 applications which included schematic drawings of various ultrasound transducers. His work included a moderate amount of detail for a PVF_2 headphone, microphone, variable-focus ultrasound transducer, and a multi-element imaging array. His work described basic construction techniques for many ultrasound transducer designs, however, it lacked many of the details needed for an unfamiliar investigator to repeat the work.

Other PVF_2 imaging arrays are described in moderate detail by Foster et al. (1984) and Foster et al. (1983). The authors described PVF_2 imaging arrays that were used in an ultrasound macroscope for imaging breast tissue. Again, only gross details of the designs were presented.

3. Medical and NDE transducer designs

Medical and NDE ultrasound transducer designs were of the most interest. Carome et al. (1979) described brass-backed 25 micron PVF_2 ultrasound transducers that were tested at the Ginzton Laboratory at Stanford University. The PVF_2 was bonded to a brass backing (which produced quarter-wavelength resonance) with a viscous epoxy, and clamped

in a jig which used a hard rubber ball to push the excess epoxy and trapped air out from under the film element. The rubber ball technique was first reported by Papadakis (1972). Little detail was given concerning the electrical connections, except that the metalized electrode layer was etched away from the edges to prevent arcing.

Another quarter-wavelength resonance design was described by Swartz and Plummer (1980b). Their design featured a 30 micron PVF_2 element bonded to a silicon backing material with a 5 micron thickness of epoxy. A 1 micron layer of parylene was used to protect the front (exposed) face. Prototype transducers showed excellent broadband acoustic performance.

Hunt et al. (1983) reported one of the most complete works on PVF_2 transducer designs for medical applications. They described the entire design of the probe, the tuning circuit, testing procedures, and test results. Their work described a focussed PVF_2 transducer which used a 30 micron PVF_2 disc (13 mm in diameter) mounted on an aluminum backing with a 2-part bonding epoxy. Gold electrode layers were used to overcome the poor conductivity and corrosion problems of the aluminum.

Finally, Saitoh et al. (1985) discussed the design of PVF_2 medical probes and methods of analysis to determine the

values for k_t and Q_m of the piezo film. However, no details for their probe design were included in their reported work.

Many of the inherent design problems associated with piezo film ultrasound transducers are not explicitly addressed in technical literature. Few publications are aimed specifically at describing the design and construction of piezo film ultrasound transducers for medical and NDE applications. One of the most complete descriptions of piezo film transducer construction is given in the M.S. thesis of Brown (1986).

4. Previous transducer designs

Brown's M.S. research focussed on the design of wide-band ultrasound instrumentation for tissue characterization. Part of that research included the design and testing of submersible PVF_2 ultrasound transducers. Many prototype designs were constructed and tested in an attempt to develop reliable methods for bonding a film element to a backing material and making reliable electrical connections. Figure 5.1 shows a sketch of the PVF_2 probe design. An exploded view is given in Figure 5.2.

The PVF_2 film element was bonded to a Plexiglas backing material with a 2-sided acrylic adhesive strip (Adhesives Research #6209). Copper shims, with soldered lead wires, were tightened against the Ni-Al metalized layers of the

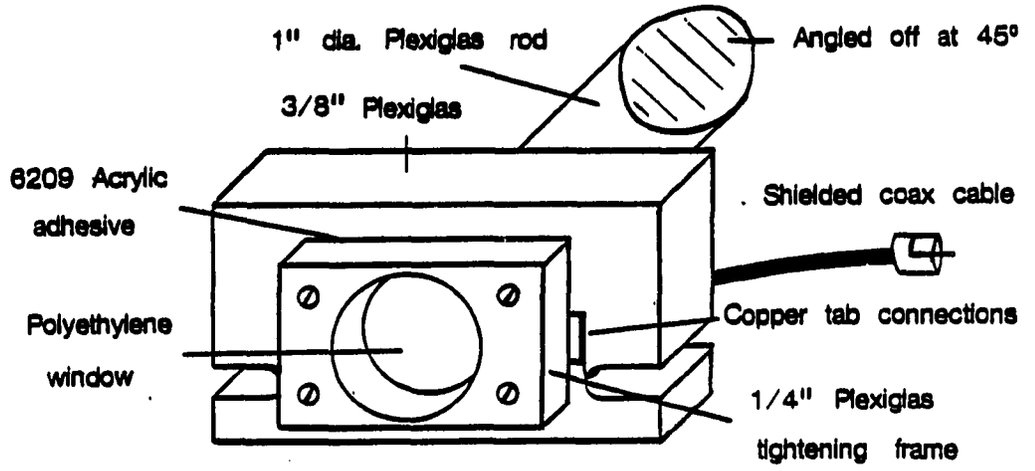

FIGURE 5.1. Sketch of PVF_2 ultrasound transducer design used in Brown's M.S. research

film element for electrical connection. Tests on prototypes of this design showed excellent broadband frequency response and ruggedness. Sinusoidal bursts of more than 1000 volts (peak) were applied to many such prototypes.

The design was not without problems. The acoustic mismatch of the Plexiglas backing material caused unwanted reflections. The trapped air and "cushion" effects of the acrylic adhesive severely reduced the sensitivity of the design. The tightening frame also prevented direct contact of the film element with a desired target material (i.e., the skin), making the design suited only for submerged (NDE) applications. The Ni-Al metallization severely corroded in the water-filled scanning tanks so a polyethylene protective layer was placed over the film element. The protective

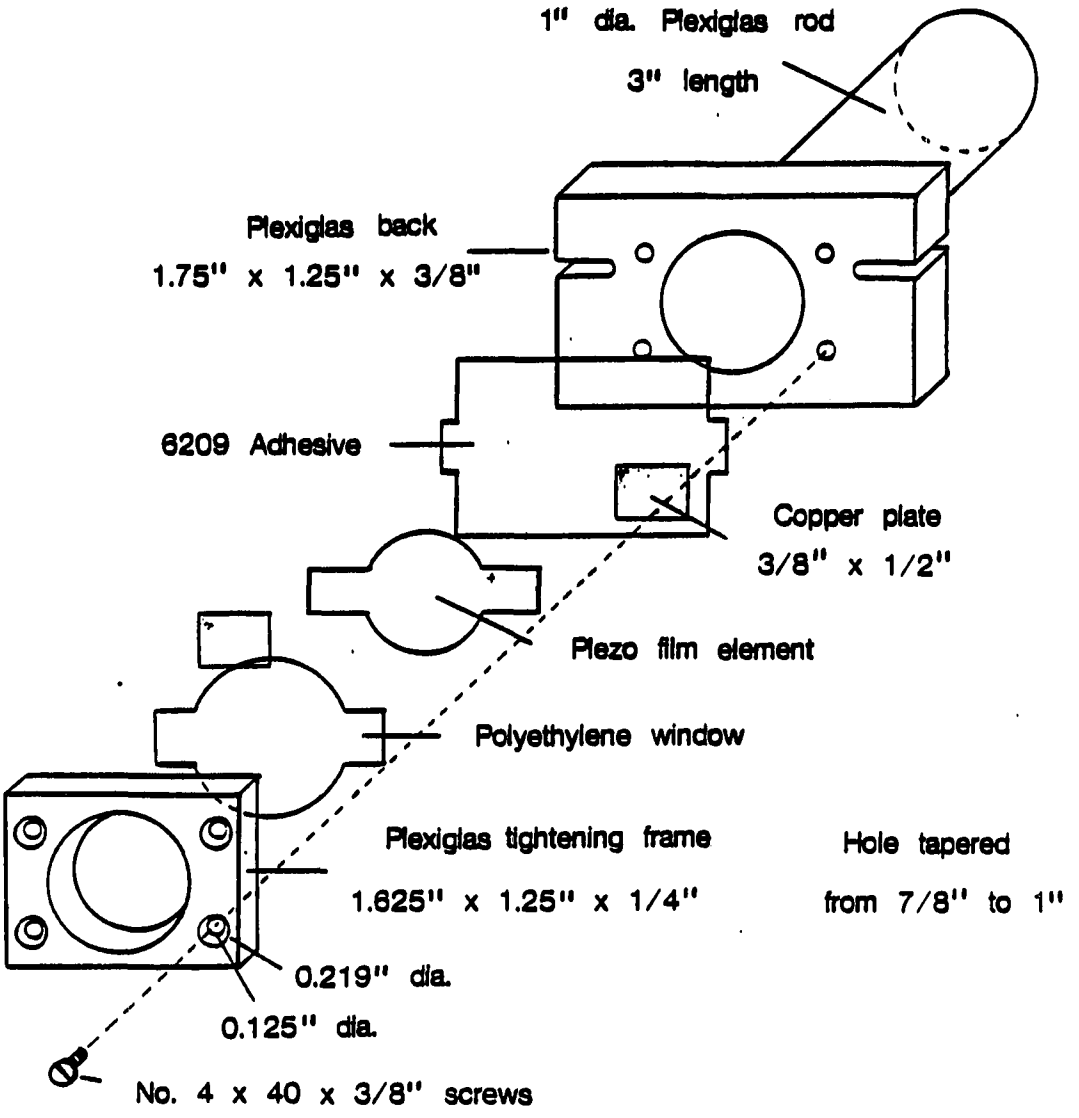

FIGURE 5.2. Exploded view of Brown's PVF_2 transducers

layer prevented corrosion but also introduced a bandpass filter effect on the transducer response.

This design was "scrapped" and a new prototype design was pursued which would eliminate the previously discussed problems. It was clear that little help would be gained from other publications and that further experimental design would be required.

B. Development of Successful P(VF_2-VF_3) Transducer Prototypes

At the start of the third part of this research, the best available design for a piezo film ultrasound transducer was the submersible NDE probe described in Figures 5.1 and 5.2. Because of the many problems associated with unmatched backing, film bonding techniques, electrical connections, and metallization corrosion, it was decided to seek a completely new design. The lack of explicit design details in most technical publications meant that little, if any, help would be gained from other reported works. This implied that more experimental design work was needed to develop a prototype which would be suitable for accurate testing of the piezo films for comparison of actual and predicted acoustic performance.

After carefully considering the desirable applications and methods for testing a piezo film ultrasound transducer, the following list of criteria was established for an acceptable design:

1. The probe must be submersible. Any accurate tests of acoustic performance would have to be done in a known non-dispersive low-loss medium such as water.

2. The piezo film element must be on the front plane of the transducer, not recessed as in previous designs. This would permit contact-type medical applications where the transducer must be maintained in contact with the skin.

3. The electrical connections must be rugged, reliable over a long period of time, and waterproof.

4. The design must be capable of providing an acoustically matched backing for broadband acoustic performance.

5. The design must include a noncorrosive metalized electrodes, or a protective layer that doesn't noticeably degrade acoustic performance.

6. The probe must be capable of including electrical tuning components (i.e., inductors, resistors).

7. The design must be economical and simple enough to achieve with limited funds and existing equipment facilities.

It was clear that to achieve a successful design would require careful attention to solving the problems and limitations of the previous efforts. It was believed that a successful working prototype would "evolve" only after careful attention to solving the previous problems associated with bonding the film, electrical lead connections, matched-

backing materials, and metallization corrosion. This section describes the evolution of the design which satisfied the aforementioned criteria.

1. First prototype, #P1

Rather than attempt a single design that would address all of the previous problems, it was decided to first address the problem of electrical connections to the film's metalized electrodes. Previous attempts with 2-part conductive epoxies failed when the epoxies caused fracturing of the metallization while curing. After discussing the problem with technical personnel at Pennwalt Corporation, a brand name for a compatible epoxy was suggested.

The first prototype design, #P1, would thus be used for testing a new electrical connection to the piezo film electrodes. Figure 5.3 shows a sketch of the first prototype.

A Plexiglas block was again used as the backing material. A vertical milling machine was used to countersink a small copper-clad circuit board which had been previously etched to produce a conductive strip for contact with one side of a film element. The film was again bonded to the Plexiglas backing with a 2-sided acrylic adhesive (Adhesives Research #6209). The rectangular element had two tabs that were meant for clamped-epoxy connections. After adhering the film element into position, a drop of 2-part silver

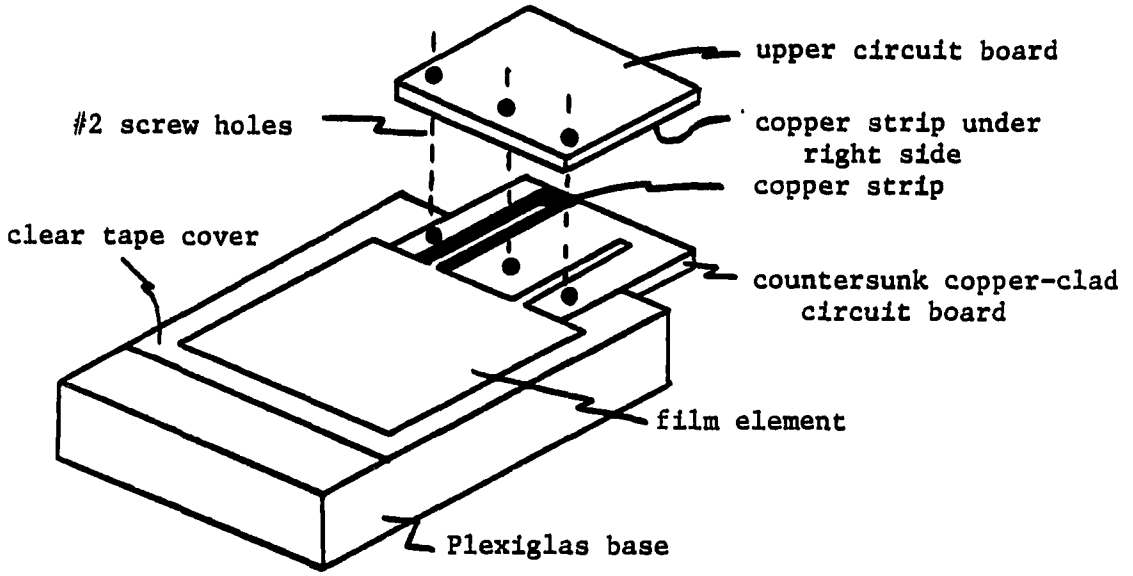

FIGURE 5.3. Sketch of prototype #P1

conductive epoxy[5] was placed on each copper conductive strip and the upper circuit board was tightened onto the countersunk circuit board. Care was taken to prevent electrical short-circuiting of the film element as excess conductive epoxy was forced from the clamped connections. Finally, a clear protective acrylic adhesive tape[6] was applied to the front of the film element and a silicon sealant was used to seal around the edges of the circuit board connections. Lead wires were soldered to the circuit boards to allow connection to a transducer pulser and oscilloscope.

---

[5]ACME E-Solder No. 3021 Conductive Epoxy, ACME Division, Allied Products Corp., New Haven, CT.

[6]Manco CS-11 Clear Carton Sealing Tape, Manco Inc., Cleveland, OH.

After allowing 48 hours for the epoxies to cure, the prototype was submerged in a water tank and connected to transducer pulse-echo unit (Sperry Reflectoscope, type UM) and an oscilloscope. Return echoes from a small metal plate were noted on the oscilloscope. The return echoes, although small ($\simeq$1 mv), exhibited broadband properties. The test transducer was left connected and submerged, and continuously pulsed for more than one hour without any failures noted. Because of the high voltage output of the Sperry unit, this was considered a good test of the electrical connections. It was then decided to address some of the other problems.

2. Second prototype, #P2

Next, the clamped conductive epoxy connections were applied to a design that located the piezo film element on the front plane of the transducer housing. Figure 5.4 shows a sketch of the approach used on the second prototype, #P2.

A short length of 1.25" diameter Plexiglas rod was used to produce shoulders that were tapered at 10° and 20° angles as shown in the figure. Small copper-clad circuit boards were countersunk and glued into position on the lower shoulders and holes were drilled and tapped for #2 screws that would tighten the upper circuit board onto the countersunk circuit boards. The film element had to have sufficiently

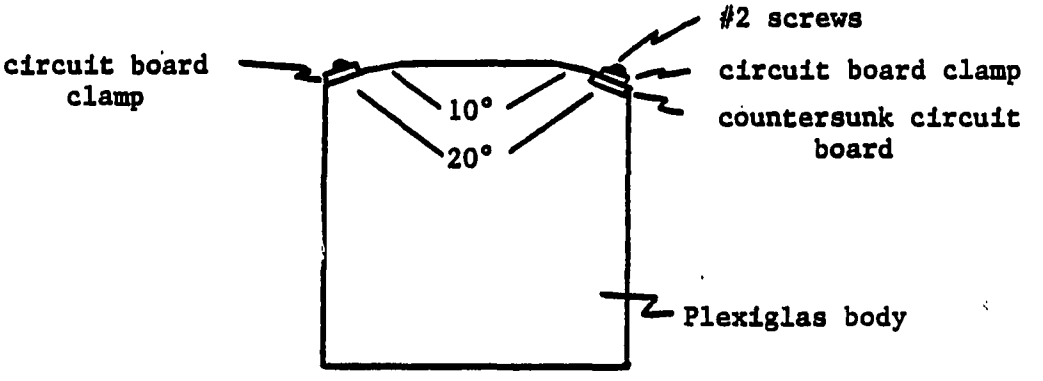

FIGURE 5.4. Sketch of prototype #P2

long tabs to reach the clamped connections. In previous designs it was noted that bending the film over any appreciable edge caused easy metallization fracture, thus, the tapered shoulders were lightly filed and sanded to make the bends as smooth as possible.

The design failed to work. The 10° tapered shoulders were not sufficient to keep the screw heads and upper circuit boards behind the front plane without using extremely long film tabs. It was believed that if round shoulders were used, the film tabs could be shortened. Thus, prototype #P2 was scrapped.

3. Third prototype, #P3

Rather than try to machine round shoulders on a suitable backing material, it was decided to begin with a round material from which to machine the remainder of the housing.

A 1" thick slice of 2.5" diameter Plexiglas rod was cut and milled as shown in Figure 5.5.

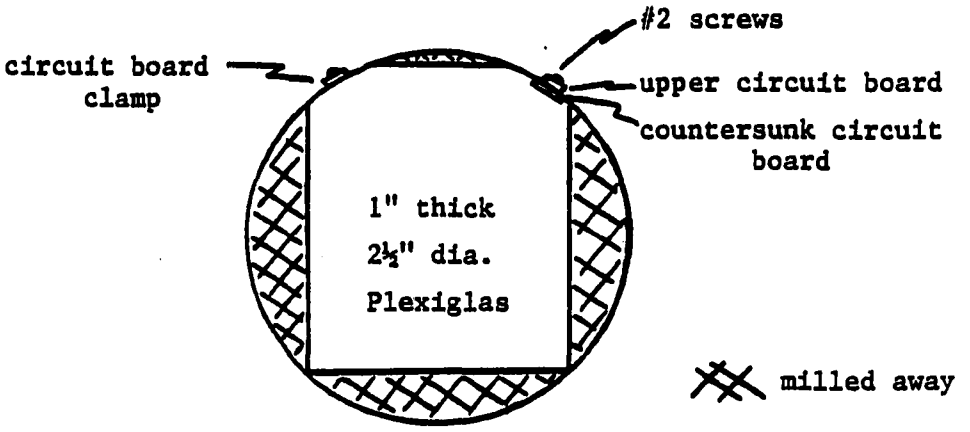

FIGURE 5.5. Sketch of prototype #P3

Lower copper-clad circuit boards were again countersunk into the shoulders of the housing and upper circuit boards were cut and tightened into place with #2 screws.

This design also failed to work. Even the gradual taper of the 2.5" diameter shoulders was considered insufficient to prevent metallization fracture at the borders along the front plane. The design also required exceptionally long piezo film element tabs to reach the clamped connections, if the connections were to remain recessed from the front plane of the transducer. As a result, the use of clamped electrical connections was dismissed as a possibility for any further designs.

4. Fourth prototype, #P4

Next, a modification of the design used for #P2 was pursued. However, instead of using copper-clad circuit boards, which are thick and bulky, copper foil "sandwiches" which contained a drop of conductive epoxy were instead used. The design, again based on a 1.25" diameter Plexiglas rod backing, is sketched in Figure 5.6.

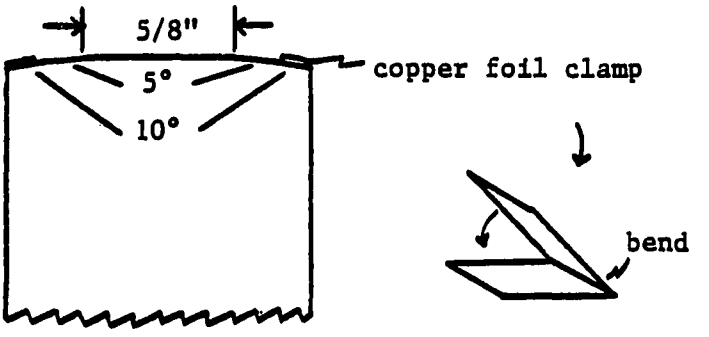

FIGURE 5.6. Sketch of design for prototype #P4

Since screws were not used, the shoulders could be tapered at 5° angles instead of 10°. A significant change was made in the method of bonding the piezo film element to the Plexiglas backing. The film element was bonded directly to the Plexiglas with a drop of 2-part optical bonding epoxy (Isochem EO-1548; Isochem Products Comp., Lincoln, RI). The excess epoxy and air were gently pushed out from under the

5/8" diameter piezo film element and the film tabs were placed in the copper sandwiches. To prevent shorting the two sides of the film, the Ni-Al metallization was etched away from the side of the film tab opposite the desired electrical connection. A concentrated aqueous solution of ferric chloride was used for the etching. After adding a drop of the ACME conductive epoxy, the copper sandwiches were folded over and carefully squeezed shut. The excess conductive epoxy was carefully removed to prevent short circuits.

Finally, a drop of the Isochem bonding epoxy was placed on top of the piezo film element and covered with a protective layer of adhesive tape (Scotch brand Magic Tape). A flat cylinder was then placed on top and clamped against the Plexiglas backing with a 5" C-clamp. The clamped probe was then placed in a fabricated drying oven for 14 hours and cured at 42°.

After proper curing, the probe was unclamped and its leads, previously soldered to the copper sandwich clamps, were connected to an audio oscillator. An audible tone in the 10-15 kHz range verified the integrity of the electrical connections. However, subsequent tests on the Sperry Reflectoscope caused an immediate failure of the electrical connections. The resulting open circuit was believed to be

caused by a fracture of the metallization along the boundary of the front plane and shoulders. Microscopic inspection failed to verify this belief, however, the visual inspection was impeded by a protective layer of silicone glue placed around the electrical connections.

In all previous prototypes where metallization fracture occurred during high voltage pulse tests, the failures occurred where the film elements incurred a bend. It was clear that the most reliable design would be one in which the entire piezo film element, including the tabs, was kept flat. This approach would be used in all future designs.

5. Fifth prototype, #P5

In order to maintain a flat piezo film element on the front plane of the transducer, the electrical connections would have to extend slightly beyond the front plane. It was believed that if the extension was only slight, such a design could still permit contact use for medical applications. Instead of using clamps of any kind, it was decided to simply bond the piezo film tabs to flat copper shims with a conductive epoxy. Figure 5.7 shows a sketch of the technique used for the fifth prototype, #P5.

The piezo film element was bonded to the 1.25" Plexiglas backing using the same method previously described for #P4. Before the film was bonded to the backing, a copper

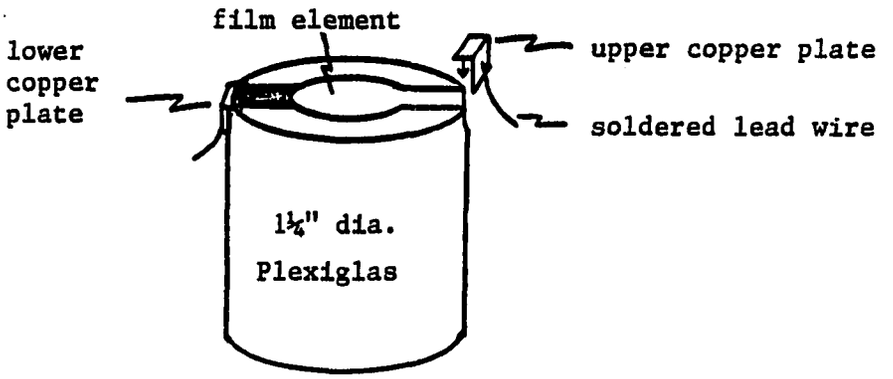

FIGURE 5.7. Sketch of design for prototype #P5

foil shim (with lead wire) was glued onto one side of the front plane and a small drop of the ACME conductive epoxy was placed on the shim. After carefully squeezing out the excess bonding epoxy and clamping a protective adhesive layer over the film, the clamped assembly was cured at 42° for 14 hours. Then, a second copper foil shim (with lead) was bonded to the front surface of the opposite film tab and also glued to the side of the Plexiglas backing with a quick-drying cyanoacrylate adhesive.[7]

After curing at room temperature for 24 hours, the transducer was partially submerged in a water-filled scanning tank and the wire leads were connected to the Sperry Reflectoscope pulser. Broadband return echoes were noted from the bottom of the scanning tank and the 114 micron

---

[7]Permabond 910, Permabond International Division, Englewood, NJ.

$P(VF_2-VF_3)$ appeared to possess good acoustic performance. The thick Ni-Al metallization was relatively poor and severely reduced the sensitivity of the probe. However, the sensitivity was clearly superior to any piezo film ultrasound transducer previously tested in this work. Considering the mismatched Plexiglas backing, acoustically thick front protective layer, and poor metallization, the design appeared to provide reliable methods for lead attachment and bonding the piezo film to a backing material. Next, it was decided to address the remaining criteria.

6. Matched-backing materials

It was next desirable to attain an acoustically matched backing for the piezo films. By bonding the piezo film to a material of the same acoustic impedance, acoustic energy would freely propagate from the rear face, giving broadband acoustic performance (refer to Chapter IV). To prevent unwanted reflections from the rear of the backing material, it is desirable to use a material with a high acoustic attenuation coefficient. The ideal acoustic match would occur with a backing material of precisely the same acoustic impedance of the piezo film and of sufficient thickness and attenuation to prevent any rearward reflections from being returned to the rear face of the film.

Such natural occurring materials are rarely found. However, a classical approach is to use a mixture of casting epoxy and powdered material which gives the desired acoustic impedance. The powdered material, usually tungsten, scatters and thus attenuates acoustic waves that travel through the material. When this approach is used for PZT ceramics, the mixture must contain a tremendous amount of powdered metal in order to match the low acoustic impedance of most epoxies with the high acoustic impedance of the PZT materials. Since tungsten has an extremely high density and is readily available, it is commonly used for in backing materials for the PZT materials.

The problem with using tungsten-epoxy mixtures for the piezo films is that most of the casting epoxies have acoustic impedances that are already close to the piezo films and only a small amount of tungsten could be used. As a result, the attenuation of such a backing material would be unacceptably low. Thus, a very thick matching layer would be required to sufficiently attenuate acoustic waveforms that enter the backing material. However, the use of a lighter metal would require a higher ratio of metal to epoxy, increasing the attenuation. Another problem encountered in using powdered tungsten is that because of the low viscosity of the Isochem casting epoxy, the tungsten failed to

uniformly settle in test castings. This resulted in severely nonlinear graded acoustic impedances which also lacked sufficient attenuation.

Other mixtures of tungsten and rubber, aluminum, and zinc were analyzed. Zinc was by far the best suited material for use with the Isochem casting epoxy. Like most of the powdered metals, zinc is pyrophoric, however it is not known to be carcinogenic like nickel which has comparable properties and was also available. Thus, mixtures of epoxy and powdered zinc were cast and analyzed for acoustic impedance. The procedure is outlined below:

1. A mixture of 2-part casting epoxy (Isochem EP-1548) was carefully weighed and mixed.
2. The mixture was heated on a hot plate to approximately 80° to lower the viscosity of the epoxy and allow air bubbles to leave.
3. A carefully weighed portion of powdered zinc dust was added, which increased the weight of the epoxy mixture by a noted factor.
4. The mixture was stirred and again heated to provide a uniform mixture with little trapped air.
5. The mixture was then poured into a 5 dram plastic cylinder which served as a mold.
6. The cylinder was then placed in a drying oven and cured at 42° for 14 hours.
7. After curing, the plastic cylinder was broken away from the material and the ends of the casting were milled away, sanded, and polished. This was necessary to remove a layer of slag at the top surface and insure a smooth reflection surface for the acoustic performance tests.

8. The casting was measured, weighed, engraved with a serial number, and tested.

The density of a casting was determined from measurements of its volume (measured with the Craftsman caliper) and weight (measured with a precision balance: Mettler H31AR, #329222). The acoustic velocity was determined by using an oscilloscope to measure the propagation time through the measured length of the casting.

Increasing the ratio of zinc to epoxy causes an increase in density and decrease in acoustic velocity. Thus, numerous ratios were tested to determine the correct mixture. The weight increase factor, W_F, represents the factor by which the weight of the pure epoxy was increased after powdered zinc was added. Thus, a W_F=1.5 casting is one in which the weight of the combined epoxy-zinc mixture is 1.5 times greater than the epoxy before any zinc was added. Table 5.1 summarizes the results of epoxy-zinc castings that were subsequently analyzed.

A plot of acoustic impedance as a function of W_F is given in Figure 5.8. From the plot, a suitable value of W_F to match the acoustic impedance of PVF_2 ($3.916 \cdot 10^6$ Rayl) is 1.88. Actually this value would also work well for $P(VF_2-VF_3)$ too, since the resulting reflection coefficient (using Z=4.28 for $P(VF_2-VF_3)$) is about 4%. Extrapolating the plot to Z=4.28 gives W_F=2.06. The epoxy-zinc casting

TABLE 5.1. Analysis results of epoxy-zinc test castings

W_F	v_o (m/s)	ρ (g/cm^3)	Z (10^6Rayl)
∞[a]	4210	7.1	29.8910
1.00[b]	2518	1.056	2.6595
1.38	2387	1.358	3.2415
1.50	2305	1.500	3.4575
1.75	2300	1.6155	3.7157
1.90	2149	1.8370	3.9477

[a]Properties of zinc only. Results from CRC Book of Chemistry and Physics, 61st edition, 1980-1981.

[b]Properties of epoxy only (no zinc).

data showed that a suitable backing material could be manufactured for the piezo films.

7. Matched-backing prototypes, #P6 and #P7

The next logical step in the development of a successful piezo film ultrasound transducer was to somehow combine the previously developed methods of bonding the film and making electrical connections with the technique for producing a matched-backing material. A convenient method was used to combine these technologies. This section describes the step-by-step construction of the first high performance copolymer transducers. To aid in the description, Figure 5.9 shows the process at various numbered steps from start to finish. The steps are explained below:

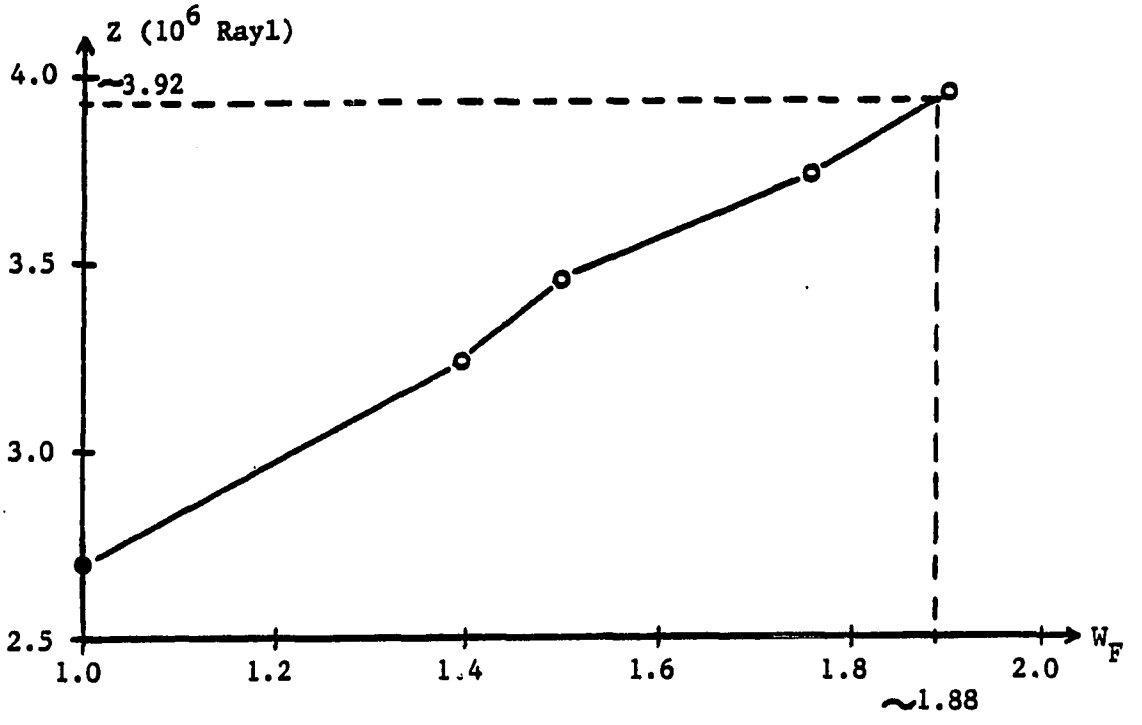

FIGURE 5.8. Plot of W_F effects on acoustic impedance of the epoxy-zinc castings

1. A 2.5" length of 1.25" diameter Plexiglas rod was cut and the ends milled flat on a vertical milling machine.

2. A lathe was then used to bore a 5/8" diameter hole, 2" deep, in the center of the rod. A standard tapered drill bit was used so as to produce a rear surface that was unlikely to produce return echoes toward the front surface.

3. A heated (≃60°) mixture of epoxy and zinc was poured into the 5/8" diameter hole and the probe housing was placed upright in a drying oven for 14 hours at 42°C.

4. After curing, the top 1/4" of the housing and epoxy was milled away to remove the uppermost layer that contained bubbles and slag. A 3/4" x 3/4" box end was milled 1/4" deep as shown. The

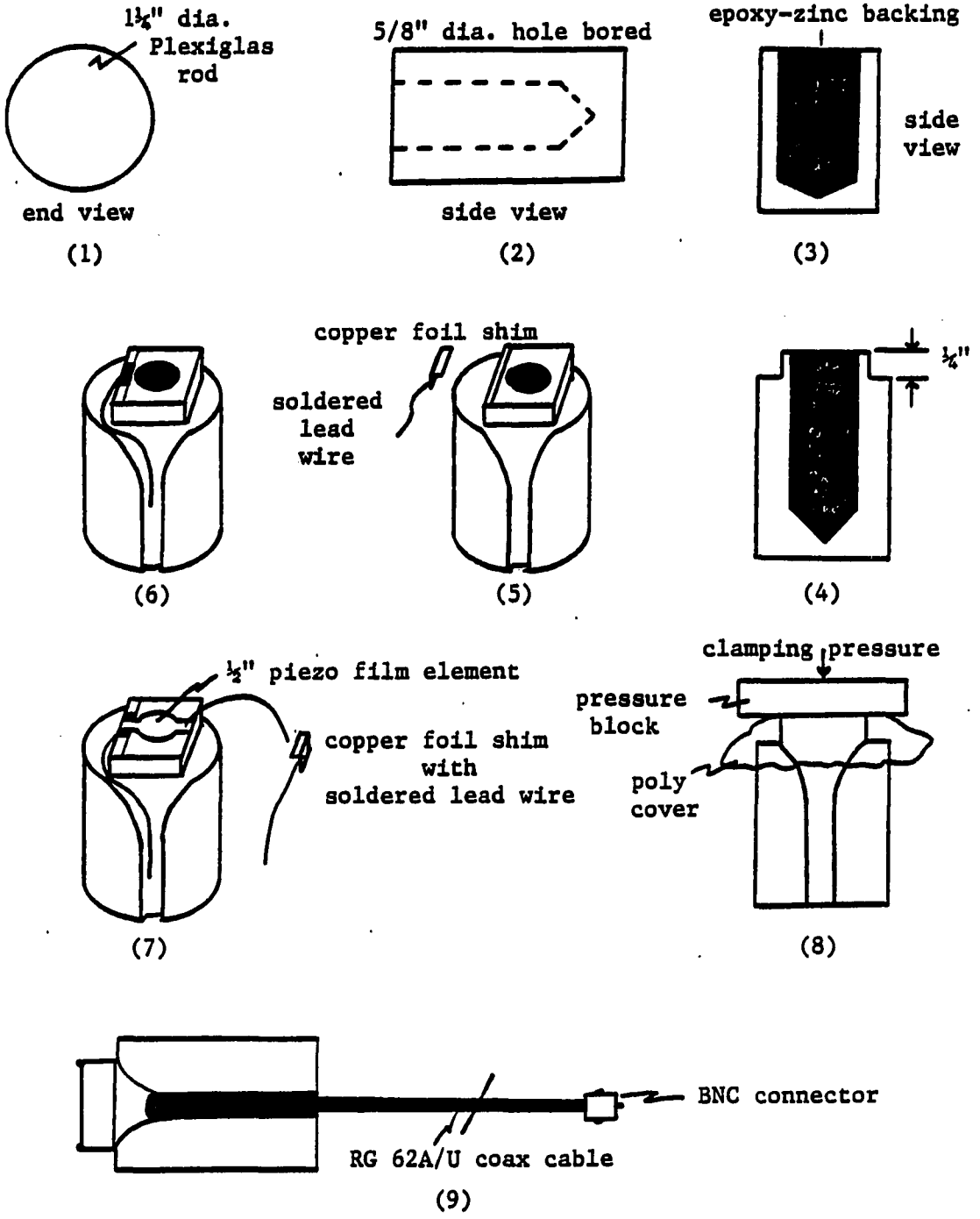

FIGURE 5.9. Step-by-step construction of #P5 and #P6 copolymer ultrasound transducers

front bonding surface was then sanded and buffed to a highly polished surface.

5. The housing was clamped on its side and a cable channel was milled along the length of the housing. The channel was milled sufficiently large near the front to permit electrical connections and tuning components to be placed. A 0.005" channel was cut along the left side and a copper foil shim, with lead wire, was glued into position.

6. With the left side (+) copper shim in position, a drop of the 2-part casting epoxy was placed on the center of the front surface, and a small drop of conductive epoxy was placed on the copper shim.

7. A 1/2" diameter piezo film element (with 1/8" film tabs) was placed on top of the front surface and the excess epoxy carefully pushed out by hand. The film tab surfaces opposite the desired electrical connection were etched free of metallization. The second copper foil shim (-) was bonded into position after applying a drop of conductive epoxy to the tab.

8. A drop of the 2-part casting epoxy was placed on the front surface of the piezo film and a clear acrylic cover was placed over the box end of the probe housing. A pressure block was clamped to the housing which was then placed in the drying oven for 14 hours at 42°C.

9. A coax cable, with male BNC connector, was then soldered to the lead wires and epoxied into the channel with a 2-part industrial epoxy (GC 10-347). The soldered connections were first insulated with heat-shrink tubing and then covered with the GC epoxy. The same epoxy was also used to coat the copper shims so that the only exposed conductive surface was that of the front surface (ground) of the piezo film.

The procedure was used to produce two more prototype transducers, #P6 and #P7. The 114 micron $P(VF_2-VF_3)$ with Ni-Al

metallization was used. Subsequent testing of these probes on the Sperry Reflectoscope showed excellent sensitivity and reliable operation for both submerged and contact use. Because the Sperry unit was extremely narrowband and a high speed sampling system was not available, no real quantitative analysis could be performed at the available facilities.

However, special arrangements were made to use the ultrasound testing facilities of the Ames Lab Center for NDE at Iowa State University. Each transducer was connected to the pulse-echo connector of a Panametrics 5052PR pulser and submerged in a water-filled scanning tank as shown in Figure 5.10.

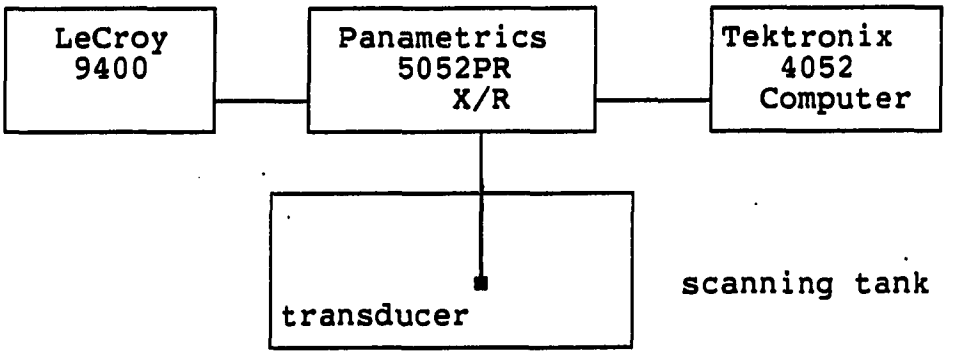

FIGURE 5.10. Test setup for testing transducers at the Center for NDE

The receiver output of the Panametrics pulser was applied to a LeCroy high speed (100 MHz) digital oscilloscope as shown. The entire data acquisition was controlled by software in the Tektronix computer. The system is capable of capturing and averaging 100 consecutive return echoes and displaying either the time domain echo or its FFT spectral magnitude.

Tests of #P6 and #P7 showed excellent, though somewhat narrowband, acoustic performance. Both transducers exhibited nearly identical responses in both the time and frequency domain, with a center frequency of about 4.5 MHz. Since the transducers were untuned and of low capacitance, their response was severely "at the mercy" of the 7 feet of RG58A/U cable capacitance. Later analysis also revealed that the front protective layer and the input impedance of the Panametrics pulser also severely altered the acoustic performance of the probes.

Despite the lack of bandwidth, the transducers showed good sensitivity and reliable performance when either submerged or when placed in contact with the body. The many hours of subsequent testing proved the reliability of this latest prototype design.

8. Conclusions

The results of this section show that a successful transducer design was achieved which satisfied all of the desired criteria. The successful design came as a result of more than two months of experimental design and two years of previous experience in the design of piezo film transducers. This same basic design is used to date, with only slight modifications.

It was clear, from resistance measurements, that the Ni-Al metallization was a poor choice for the piezo films. The metallization was suspected of causing at the least, poorer sensitivity and at the worst, a nonlinear distribution of the electric field over the piezo film which would cause a distorted acoustic waveform. Pennwalt Corporation agreed to send new copolymer films with gold metallization. It was believed that since the gold metallization would not have the corrosion problems of Ni-Al, the thick front cover could be omitted. The front cover tends to act as a quarter-wavelength resonator for a particular frequency (determined by the layer's thickness) which alters the performance of a probe.

It is impossible to assess the quantitative acoustic performance of an ultrasound transducer without a sophisticated high-speed data acquisition system. Thus, the testing

facilities of the Center for NDE would be needed for the analyses. It was also clear that in order to compare the actual and predicted acoustic performance of an ultrasound transducer, special consideration would have to be given to the transducer's cable capacitance and the transducer pulser's input impedance.

C. Quantitative Analysis of the Ultrasound Transducers' Performance

One of the objectives of the third part of this research was to compare the actual acoustic performance of piezo film ultrasound transducers, with the performance predicted with the previously derived electromechanical circuit models. In order to make any meaningful comparisons, the transducers would have to be tested under known experimental conditions which would have to be accounted for in the simulation of the experiment. Such comparisons require high speed data acquisition and storage equipment. This section describes the experiments used to analyze the piezo film ultrasound transducers' performance, and the data acquisition equipment used at the facilities at the Center for NDE.

1. Computer simulation of pulse-echo ultrasound experiments

A simple pulse-echo ultrasound experiment was designed from which the results could be used for quantitative comparisons of actual and predicted acoustic performance. The particular parameters of interest for such comparisons were sensitivity, bandwidth (BW_{3dB}), and Q_{3dB}. The computer simulation program discussed in Chapter IV, XFER.FOR, was capable of computing the theoretical values for pulse-echo acoustic performance. The output results of the program are the time and frequency domain values for voltage/force (XMTR) operation, force/voltage (RCVR) operation, and voltage/voltage (XMTR/RCVR) operation. The XMTR/RCVR results represent the ideal pulse-echo ultrasound performance of a piezo film ultrasound transducer when subjected to a unit voltage impulse input. These results are also for a lossless medium (i.e., no diffraction, no attenuation, and perfect reflection).

Instead of using the unit voltage impulse input, the actual driving voltage of a transducer under test was sampled and applied to the input of the simulation model. The simulation program could then be used to compute the output voltage for pulse-echo (XMTR/RCVR) response and this waveform could be compared to the actual waveform obtained in the experiment. To compare actual and theoretical pulse-

echo performance then, a method was needed for acquiring both the input driving voltage waveform and the pulse-echo output waveform of the transducer under test.

A simple pulse-echo experiment involving reflection from a known submerged target could be used. To accurately predict the pulse-echo acoustic performance, the simulation program would also have to account for the diffraction and reflection of the acoustic waveform in water. The effects of diffraction on a propagating waveform are extremely nonlinear and complex. A common approach to the problem is based on modeling the diffraction effects as a high-pass radiation transfer function (Rhyne, 1977). This radiation transfer quantity is a function of frequency, transducer diameter, and distance. For a fixed diameter and distance, a table of radiation transfer function magnitudes can be computed for desired frequencies. One can then deconvolve the effects of diffraction from an acoustic waveform. Rhyne's work was used as a reference since it contained tabulated values of the radiation filter magnitude which were normalized to fixed values of transducer diameter and target distance. The relationship between the radiation filter and a return pulse-echo waveform from a target are given by:

$$|T(\omega)| = \frac{V_{RCVR}(\omega)}{V_{XMTR}(\omega)\Gamma F(d,a,f)} \qquad (5.1)$$

where $T(\omega)$ = pulse echo XMTR/RCVR transfer function

$V_{RCVR}(\omega)$ = received acoustic waveform magnitude

$V_{XMTR}(\omega)$ = transmitted acoustic waveform magnitude

Γ = reflection coefficient of water/target

$F(d,a,f)$ = radiation filter function for water

The simulation results can thus be corrected for diffraction and reflection by applying Equation 5.1 and multiplying the model's transfer function by $\Gamma F(d,a,f)$. The relevant reflection coefficient and an array of $F(d,a,f)$ values were used on the simulation program to correct for the experimental diffraction and reflection. Figure 5.11 shows a plot of the high-pass filter properties of diffraction in water for a target distance of d=3.25 cm, and a transducer diameter of 0.5".

A fused quartz target was used for known reflection at a distance of 3.5 cm. For a 0.5" diameter piezo film element, a table of radiation filter magnitudes could be used in the 0-20 MHz range. This was desirable for a 110 micron film thickness which has a resonant frequency of about 10.5 MHz. The data acquisition equipment of the Center for NDE would have to be used to capture the actual driving voltage waveform which would later be used in the simulation program. It was clear that the simulation program would also have to include the effects of a trans-

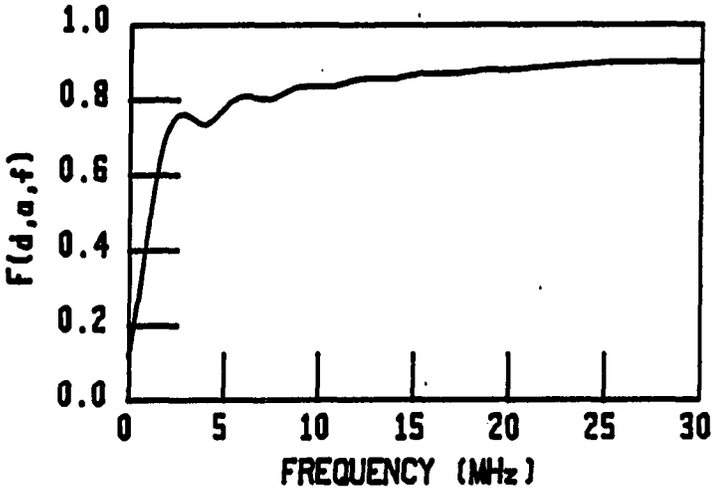

FIGURE 5.11. High-pass effects of acoustic diffraction in water

ducer's cable capacitance and the input impedance and gain of the receiver used to amplify the pulse-echo waveforms.

2. Data acquisition for the experiments

To prevent damage to the data acquisition system and minimize the cable capacitance of the setup, a 10:1 voltage divider probe was used to sample the driving voltage waveform as shown in the sketch of Figure 5.12.

A coax T-connector and 10:1 oscilloscope probe were used to allow sampling and acquiring of the actual driving voltage waveform under the load of the transducer under test. Both the pulse-echo and driving voltage waveforms could be sampled (100 MHz) and 512 samples stored on magnetic tape for later analysis.

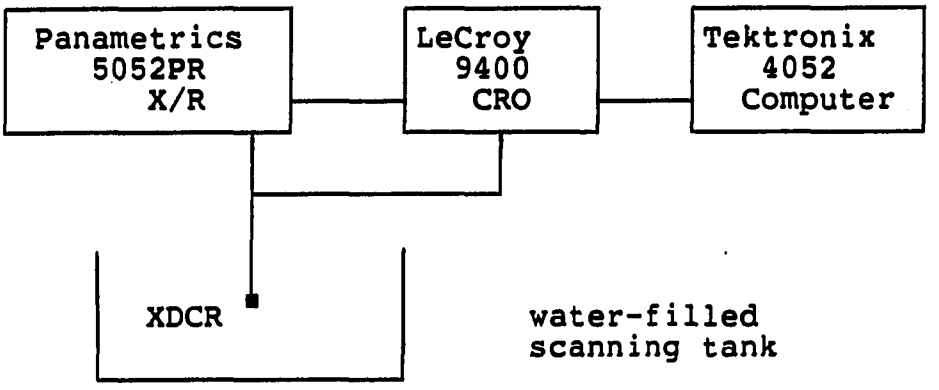

FIGURE 5.12. Diagram of the experimental setup

For the computer simulations, the sampled input voltage waveform was fast Fourier transformed and the simulation analysis completed in the frequency domain in the same manner described in Chapter IV. The simulated pulse-echo response was corrected for diffraction and reflection and the resulting XMTR/RCVR response was written to a graphics file. This approach proved extremely valuable in comparing actual and predicted pulse-echo performance of many copolymer ultrasound transducers.

D. Design and Testing of Series-tuned P(VF_2-VF_3) Transducers

After developing a successful transducer design, a pair of series-tuned high sensitivity test probes was constructed. Such probes, though narrowband in acoustic performance, can be tuned for exceptionally high sensitivity

at a desired frequency. A probe with high sensitivity at around 2 MHz,a frequency commonly used in medical pulse-echo ultrasound applications, was desired. These probes would also be used for the first comparisons of actual and predicted (simulated) acoustic performance.

This section first describes the probe design and series tuning for the test transducers. Performance tests of the probes are then compared with the predicted response of the simulation program. A great deal of insight was gained in both the design of series-tuned probes and in simulating their acoustic performance.

1. The probe design

A modified version of that used for prototypes #P6 and #P7 was used for the probe design. A sample of 110.6 micron $P(VF_2-VF_3)$ (film number VA110G00) was used. After analyzing the performance of #P6 and #P7 it was clear that the problems associated with the protective front layer, poor metallization, and high cable capacitance would all have to be addressed. Since this newest copolymer film had gold metallization (300 Å) the corrosion problems were assumed to be solved.

To reduce the effects of high cable capacitance, 5' length RG58A/U coax cables were used. The shorter cables of the previous transducers prevented their connection to the

test equipment while submerged, without the use of an extension cable and adaptor. The 5' lengths would be shorter and still allow connection to the test equipment.

A new design was required for the front protective layer. The thick epoxy-tape layer of #P6 and #P7 acted as a quarter-wavelength matching layer which tuned the acoustic performance to an undesired low frequency. An extremely thin uniform layer was desired. Many film materials were considered for bonding to the front film surface but most were considered too thick. However, a sample of commercial plastic food wrap showed a measured thickness of 0.0002" or about 5 microns. Such a material would be acoustically transparent in the 0-20 MHz frequency range of interest. A transducer, #P8, was then constructed in the same manner described for #P6 and #P7 except that a large drop of heated bonding epoxy ($\simeq$40°C) was placed on the front surface of the film. A large smooth piece of the poly food wrap material was then draped over the front surface. After carefully pushing out the excess air and epoxy, a flat Plexiglas block and section of pencil eraser were clamped to the probe housing as shown in Figure 5.13.

After curing the clamped assembly for 14 hours at 42°C, the block and eraser were removed and a very smooth bonded front layer was observed, except for a few small wrinkles

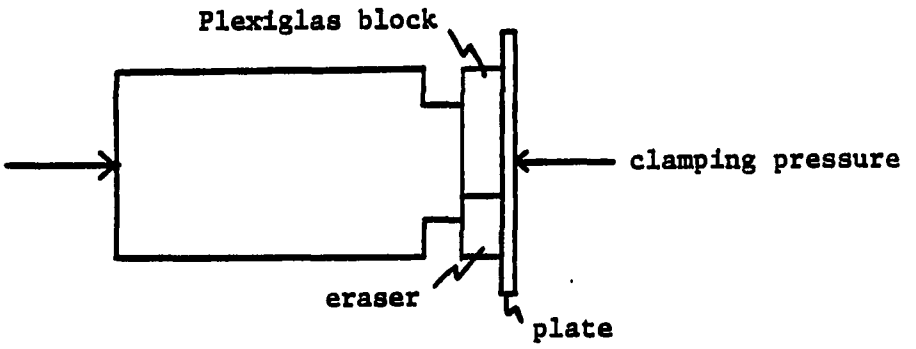

FIGURE 5.13. Clamping of poly cover to front surface of #P8.

located near the side of the piezo film element. The excess poly cover was next trimmed away from around the front surface. While gently brushing a finger over the front surface, more bubbles appeared under the poly cover. It was apparent that the cover was not bonded to the epoxy. All of the cover was subsequently removed, leaving behind a smooth, ultra thin layer of epoxy on the front face of the transducer. Since the gold metallization would not corrode, a modification of this approach was used for all future transducers.

This solution was highly desirable since it would be extremely difficult to precisely model the nonuniform epoxy layer and cover on the front surface. With neither present, the simulation model would be more accurate. In all subsequent designs, no epoxy was applied to the front surface of

the piezo film element. Instead, the surface was cleaned, covered with a poly cover, and clamped with a larger eraser as shown in Figure 5.14.

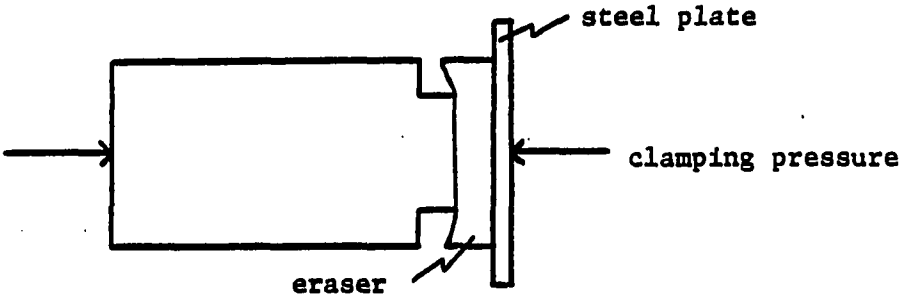

FIGURE 5.14. Method of clamping remainder of transducers

The eraser maintained even pressure on the film element and electrode connections. After curing in the drying oven, the clear poly cover was removed and the electrical connectors and cable added.

Thus, the problems encountered in the previous designs had all been addressed and a successful probe design was completed. The procedure was used to "mass produce" seven more probe bodies that would be used for several tuned designs.

2. The series-tuned design

In an effort to "peak up" the acoustic response of the transducers, the capacitance of the cable and film was tuned out by by including a series inductance, L_s, as shown in Figure 5.15.

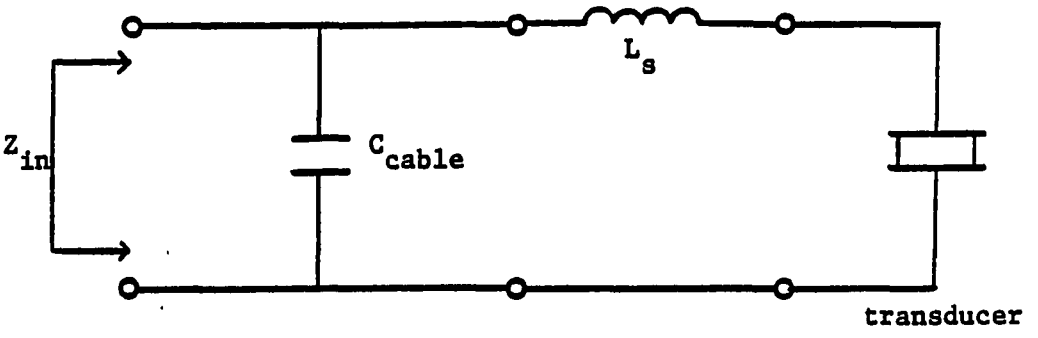

FIGURE 5.15. Schematic of series-tuned circuit

If L_s is chosen to properly resonate with the capacitance of the circuit, the input impedance can be made resistive (or nearly so) at the tuned frequency. Because of the relatively large cable capacitance located between the inductor and film capacitance, it was known that the electrically tuned resonant circuit would exhibit a high-Q narrowband response. By writing an equation for the input impedance one can solve for the value of L_s which minimizes the magnitude of the reactive part of Z_{in}. A real-valued

inductor does not exist for all circuits which will completely eliminate the input reactance, however, by minimizing the magnitude of the input reactance, a "best match" condition can be achieved.

The derivation for this value of L_s was so cumbersome that an easier solution was used. The circuit in Figure 5.15, including the transducer's impedance values near resonance, were analyzed in a PCAP program.[8] At the desired tuned frequency, L_s was varied and a hardcopy and plots of the input impedance were used to determine the value which gave the "best" tuning. The results showed that inductances of 5.5 μH and 150 μH should tune the transducers to 10.7 MHz and 2 MHz respectively.

Two of the new copolymer probes were then used to construct a 2 MHz probe (#P10) and a 10.7 MHz probe (#P13). After construction, preliminary testing of the probes on the Sperry Reflectoscope showed higher sensitivity than any previously tested piezo film ultrasound transducers. The probes were then ready for more accurate performance testing at the facilities of the Center for NDE.

---

[8]Princeton Circuit Analysis Program, maintained on the ISU VAX computer system.

3. Test results for #P10 and #P13

The two transducers were tested at the Center for NDE using the same experimental setup presented in Figure 5.12. A target distance of 3.25 cm was used since this was the distance selected for the diffraction correction in the simulation program. All acquired waveforms were stored on a magnetic tape (Scotch DC300A) via the Tektronix 4052 computer.

Each transducer was carefully focussed for normal incidence on the fused quartz target at the prescribed distance. Next, the LeCroy digital oscilloscope sampled (at 100 MHz) the desired waveforms and 512-point sample arrays were recorded on magnetic tape. Both the input driving voltage and return pulse-echo voltage were recorded for analysis. The results for #P10 and #P13 are shown in Figures 5.16-5.19.

Figure 5.16 shows an interpolated plot of the 512-point sampled input driving voltage and its FFT spectral magnitude for #P10. The spectral magnitude plot shows relatively flat spectral content above 8 MHz. The "hump" at approximately 2 MHz was due to the effects of the series tuning. The time domain pulse-echo waveform and spectral magnitude results, given in Figure 5.17, show a very narrowband high-Q response, peaked at approximately 1.5 MHz. The same results

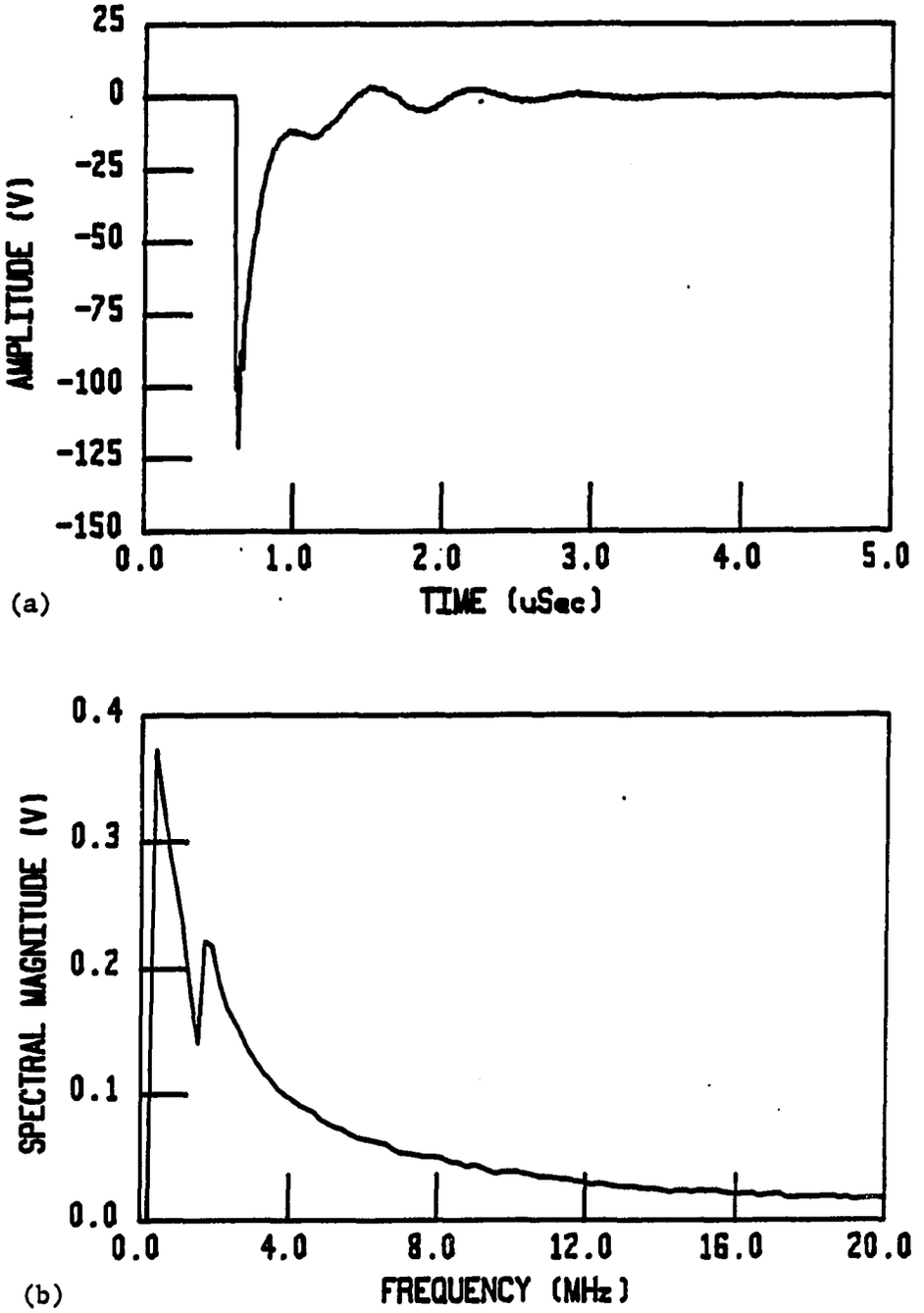

FIGURE 5.16. Actual driving voltage for #P10 P(VF_2-VF_3) transducer: (a) time domain waveform and (b) spectral magnitude

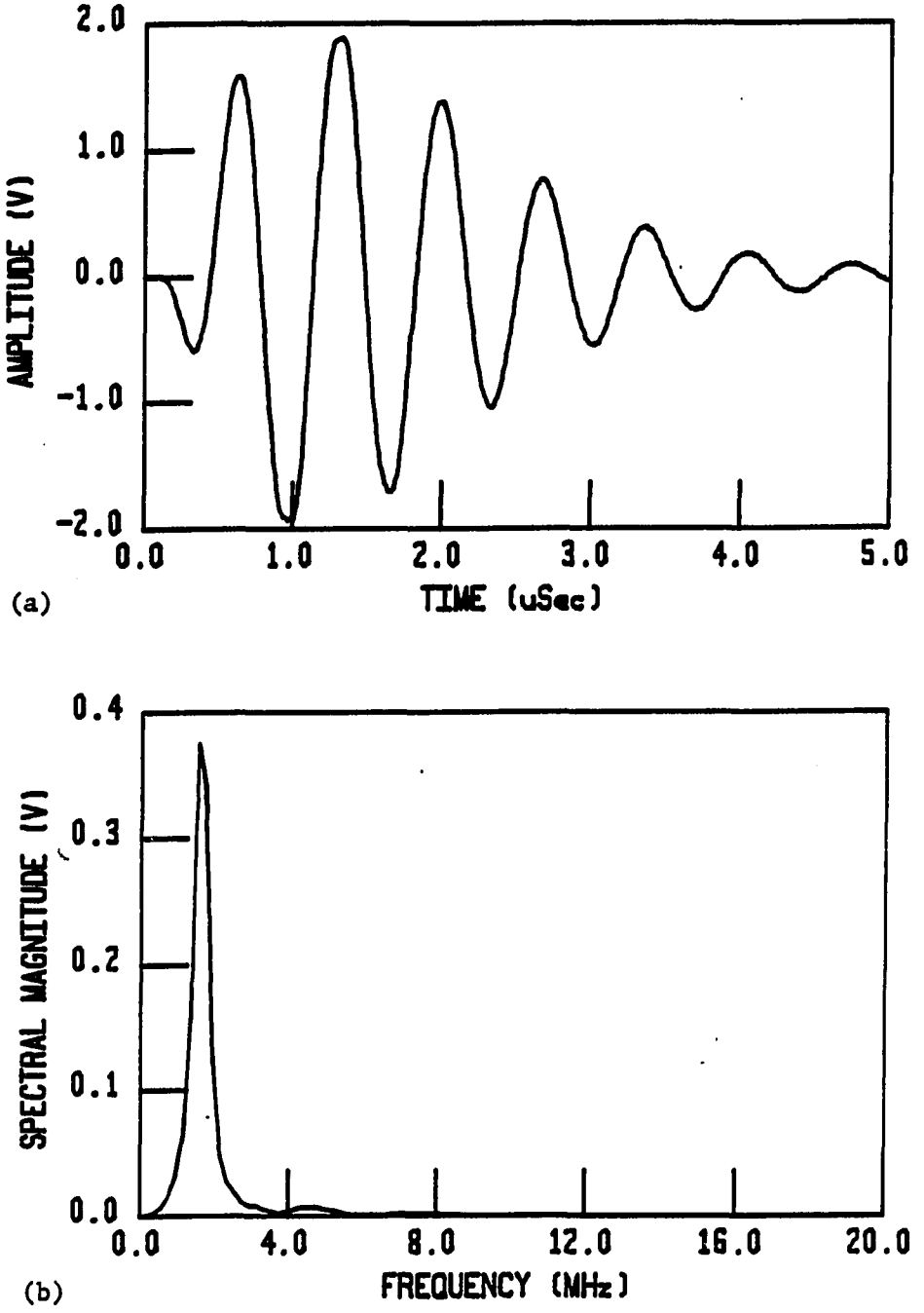

FIGURE 5.17. Actual pulse-echo return waveform for #P10 $P(VF_2\text{-}VF_3)$ transducer: (a) time domain waveform and (b) spectral magnitude

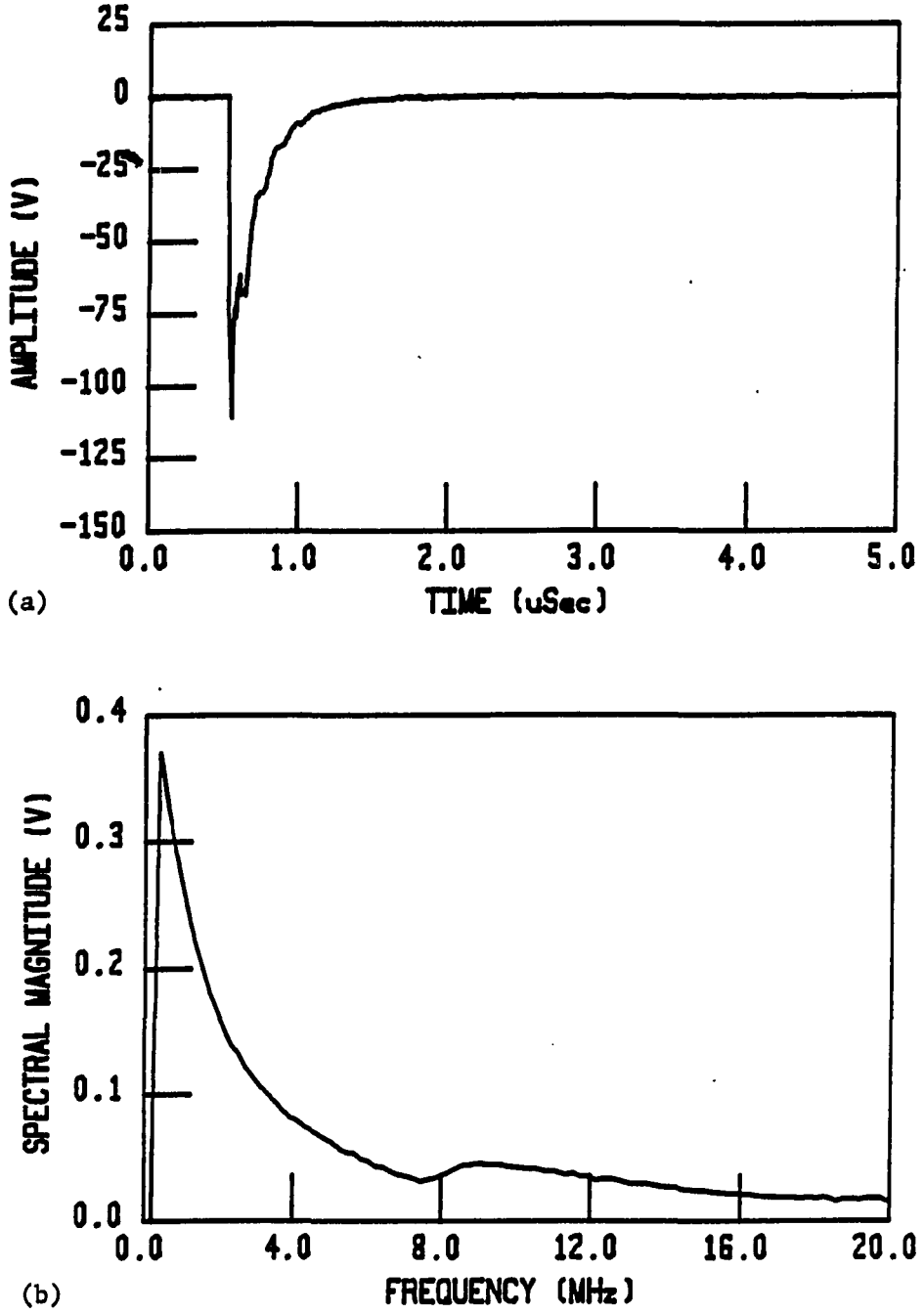

FIGURE 5.18. Actual driving voltage for #P13 P(VF_2-VF_3) transducer: (a) time domain waveform and (b) spectral magnitude

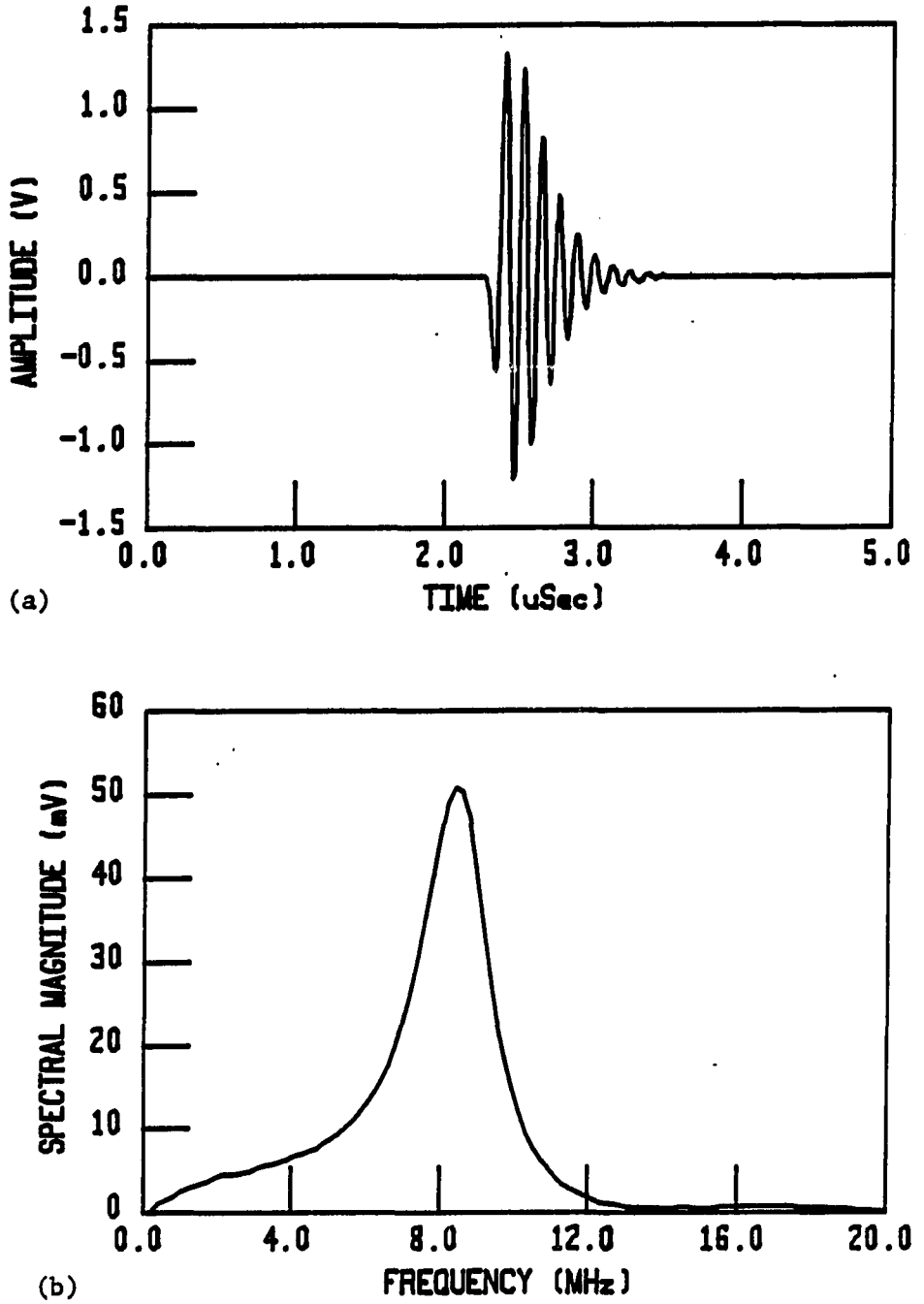

FIGURE 5.19. Actual pulse-echo return waveform for #P13 $P(VF_2\text{-}VF_3)$ transducer: (a) time domain waveform and (b) spectral magnitude

for #P13 are given in Figures 5.18 and 5.19. Again, the results showed a narrowband response which was peaked at a lower frequency than that theoretically tuned for. It was clear that there were other factors at play that had not been properly considered in the series-tuned design. Subsequent simulation analyses of the experiments later revealed the oversights.

4. Simulation results for #P10 and #P13

The 512-point time domain arrays of the actual driving voltages were read into the simulation program, XFER.FOR, and the predicted responses were computed. To account for the electrical input impedance of the Panametrics 5052PR, a value of 250 Ω in parallel with 30 pF of capacitance was used. The 250 Ω resistance was specified as the input resistance of the Panametrics unit with the damping control set to minimum. As for the capacitance, a conservative "guess" was made since actual impedance measurements of the unit had not yet been made. Figures 5.20 and 5.21 show the simulation program's results.

Figure 5.20 shows the predicted results for #P10 which show a more narrowband peaked response, at a slightly higher frequency than the actual results. Both the time and frequency domain results show similarities in characteristic shape but there are clearly some quantitative differences.

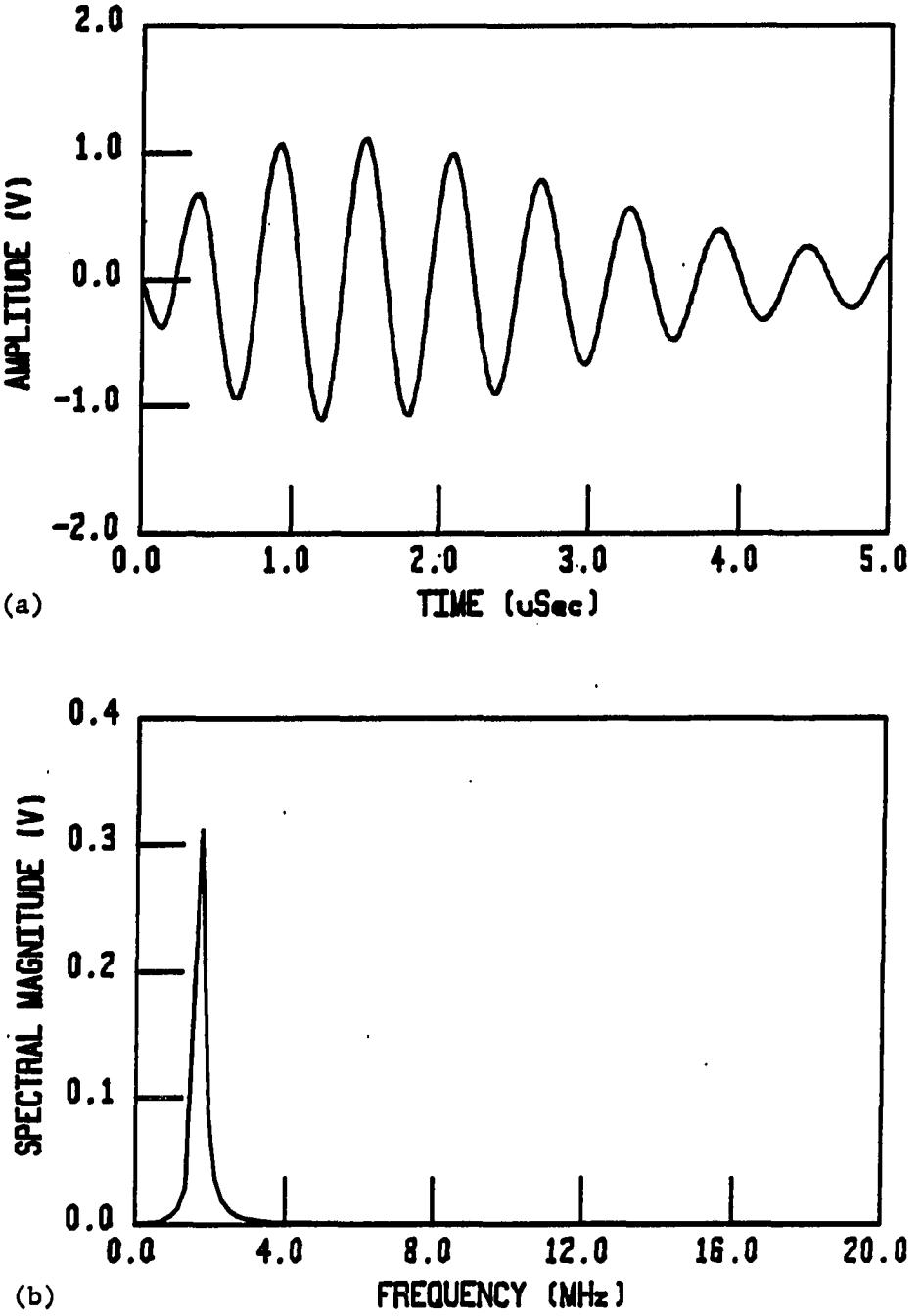

FIGURE 5.20. First simulation results of pulse-echo performance for #P10: (a) time domain results and (b) spectral magnitude results

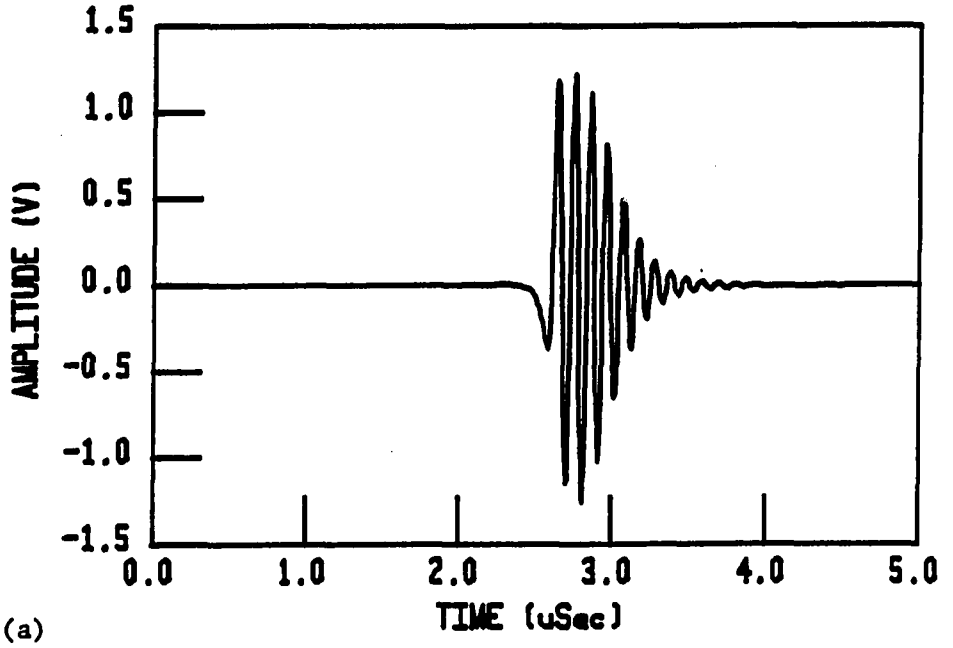

(a)

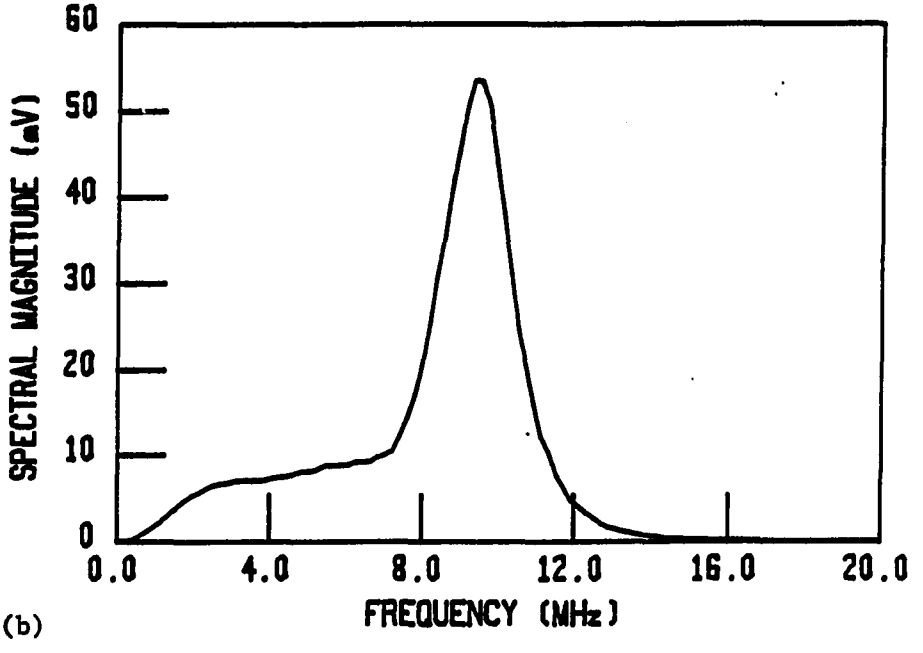

(b)

FIGURE 5.21. First simulation results of pulse-echo performance for #P13: (a) time domain results and (b) spectral magnitude results

The same is true of the predicted results for #P13 shown in Figure 5.21. Although the characteristic shapes of the actual and predicted results are similar, it is clear that the predicted results show a response that is peaked at a higher frequency. Thus, the predicted results for both #P10 and #P13 showed a more narrowband response which was peaked at a higher than the actual observed response. Both the actual and predicted responses were peaked at lower frequencies than designed for.

5. Discussion of results

It was clear from comparisons of simulated and actual test results of #P10 and #P13 that not all of the stray capacitance and impedance had been accounted for. The input capacitance of the Panametrics unit was responsible. The previous PCAP results, used for the series-tuned designs, showed that the series tuning was very sensitive to the cable capacitance. In an effort to assess the sensitivity of the simulated results to the cable capacitance, the predicted pulse-echo responses for an untuned copolymer transducer were analyzed with various cable lengths.

Figures 5.22 and 5.23 show the results. Figure 5.22 shows the input driving waveform and frequency spectrum for the Panametrics pulser with no load connected (i.e., open circuit). This "ideal" waveform was used in the simulation

program to predict the pulse-echo performance of 1/2" diameter copolymer transducers of the same design and experiment as #P10 and #P13, except that a series inductor was not included. Figure 5.23 shows these results. The figure shows a response which is peaked at about 3 MHz for the 5' coax cable case, and 8 MHz for the case where no cable is included. The response is seen to be much more broadband and sensitive when no coax cable is included in the design. The results of these simulation showed that the design is extremely sensitive to the effects of cable capacitance and thus, the previously used value of 30 pF for the Panametrics pulser was now in question. Clearly, both the actual and simulated pulse-echo results were acutely sensitive to all impedances associated with the electrical circuit.

6. Conclusions

The new construction techniques used for transducers #P10 and #P13 satisfied all of the original design criteria. The transducers were rugged, could be used for both submerged (NDE) and contact (medical) applications. The gold metallization solved the severe corrosion problems encountered with the previous designs with Ni-Al metallization.

The series-tuned designs showed very high sensitivity and a narrowband response. It was discovered that the

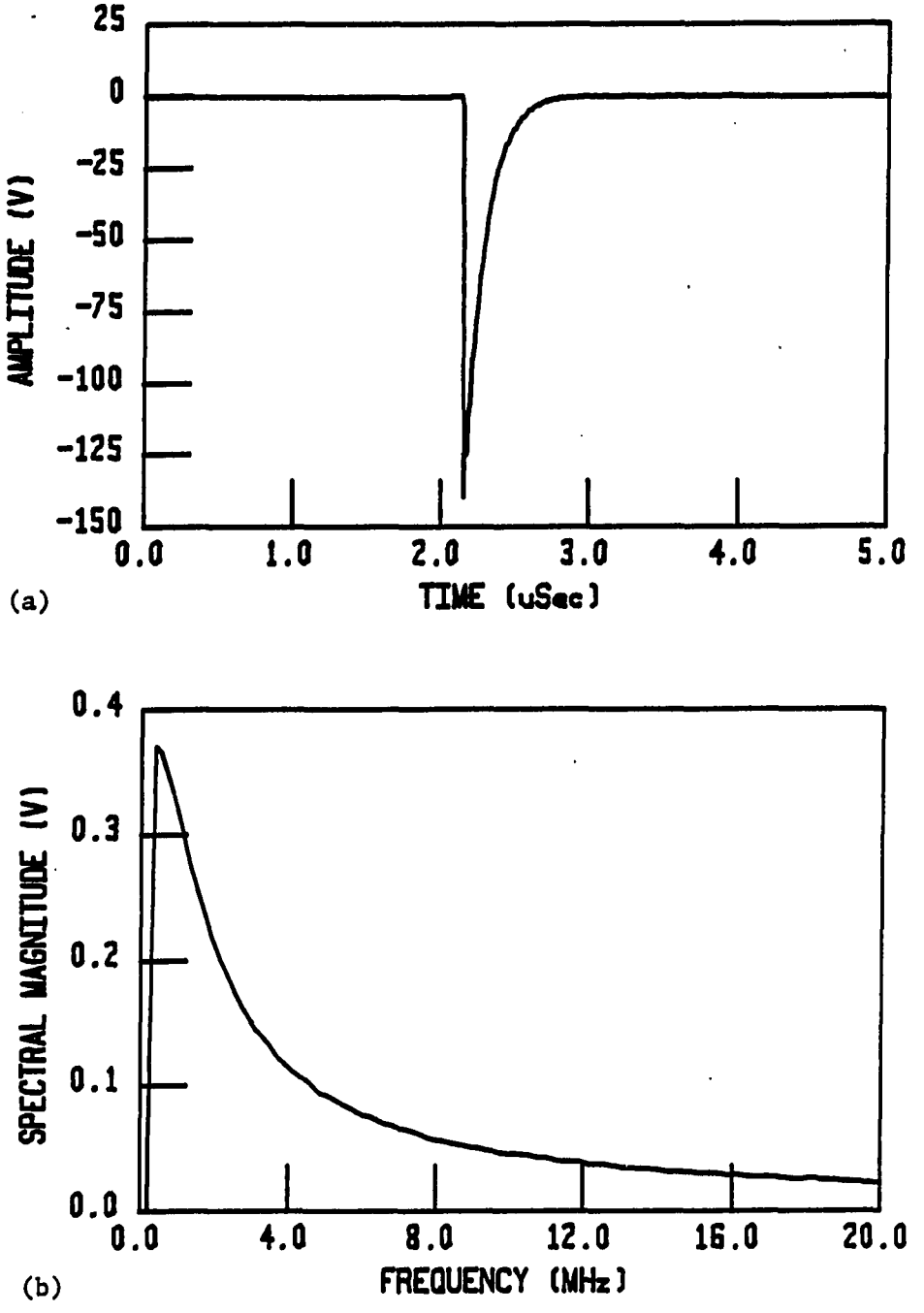

FIGURE 5.22. Actual unloaded driving voltage of Panametrics 5052PR pulser: (a) time domain waveform and (b) frequency spectrum

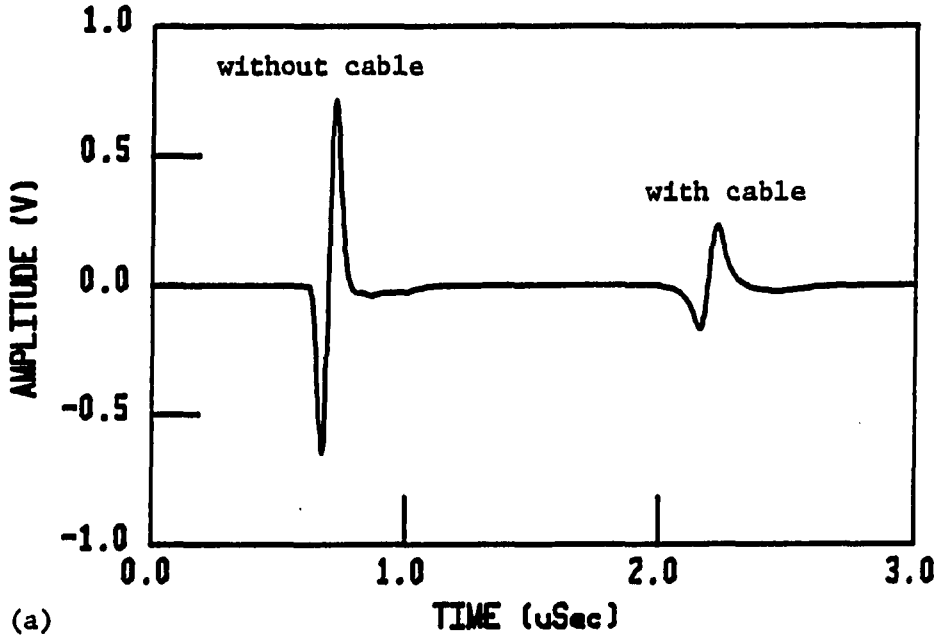

(a)

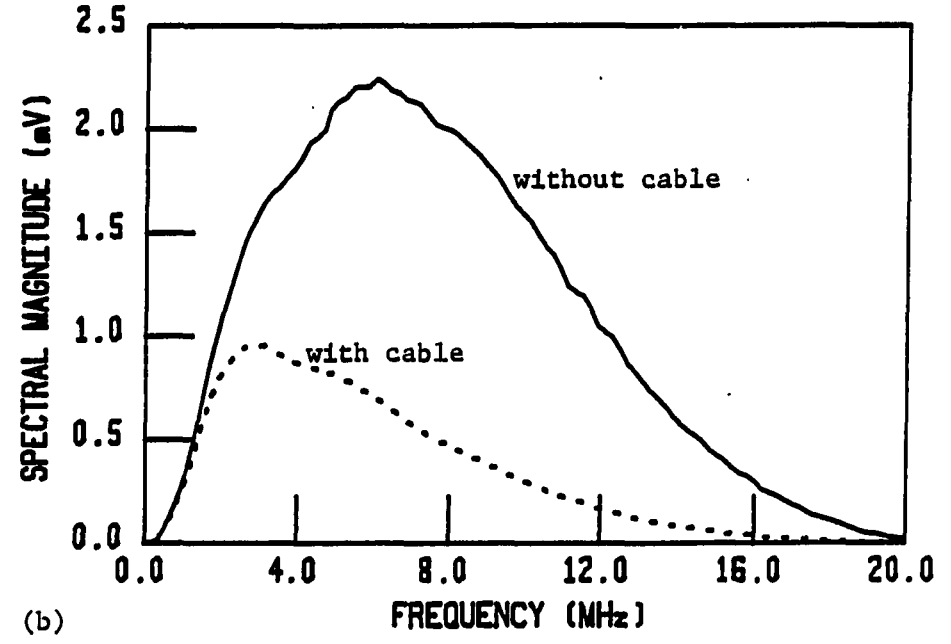

(b)

FIGURE 5.23. Simulated pulse-echo performance of untuned copolymer transducer with and without a 5-foot RG58A/U coax cable: (a) time domain waveform and (b) frequency spectrum

capacitance of the Panametrics pulser and coax cable greatly affected the Q and center frequency of the response. Because there were still discrepancies in the actual and predicted pulse-echo responses, it could not yet be proven that the models provided reliable simulation of acoustic performance. However, since the general appearance of the actual and predicted waveforms were so similar, good correlation was expected if the impedance of the Panametrics unit were more accurately modeled.

The testing and simulation work on #P10 and #P13 demonstrated a powerful method for modeling acoustic performance. Using the actual driving waveform for a transducer was considered much more accurate than modeling the pulser's waveform with a simple mathematical function as others had done (Hayward and Jackson, 1984a and Hutchens and Morris, 1984).

E. Design and Testing of Shunt-tuned P(VF_2-VF_3) Transducers

It was next desired to construct a set of broadband P(VF_2-VF_3) ultrasound transducers. It is after all, the broadband properties of the piezo films that make them attractive for ultrasound applications, thus, a probe which clearly demonstrated these properties was desired. It was also hoped that by carefully considering the details of the

design, the simulation program would show better prediction of pulse-echo acoustic performance.

This section describes the design and testing of four such shunt-tuned P(VF_2-VF_3) probes. Considerable insight was gained in the design of these transducers. Plots of actual and predicted pulse-echo waveforms are included.

1. The design

To further reduce the effects of cable capacitance that were previously encountered, a shorter length of low capacitance RG62A/U coax cable was used. A shunt inductance was used to resonate with the cable, oscilloscope, and piezo film capacitances at series resonance, 10.513 MHz. Four such transducers, #P17cz-#P20cz, were constructed.

The coax cable lengths were cut to precise lengths to give the capacitance necessary to resonate with the actual measured values of shunt inductance. In addition, the Qs of the inductors were measured at several frequencies and used in the simulation program for the predicted responses.

The cable lengths required for the designs were 3-3.5', and at 13.2 pF/ft, the RG62A/U coax cable provided less than half the capacitance of the RG58A/U. The same 110.6 micron P(VF_2-VF_3) was used, as well as the same probe construction used for #P10 and #P13. With such a design, the transducers would provide a more broadband pulse-echo response.

2. First tests of the shunt-tuned transducers

The shunt-tuned transducers were tested at the Center for NDE using the same pulse-echo experiment as in all previous tests. Results for #P17cz are shown in Figure 5.24. The results were disappointing.

The time domain pulse-echo waveform showed considerable ringing. The spectral magnitude showed a narrowband response that was centered at approximately 7 MHz. These results were consistent (nearly identical) for all four transducers. Despite the attempts to carefully tune the transducers for broadband performance centered at 10.5 MHz, the results were still narrowband and peaked at a significantly lower frequency. It was only after a long and careful study of the design that the solution to the problem was discovered.

3. A new approach to the shunt-tuned design

The first test results of #P17cz-#P20cz clearly showed incorrect shunt tuning in transducer design. The solution to the problem came as a result of considering the efficient transfer of power in a circuit with second-order complex impedances as shown in Figure 5.25.

It is well known (Nilsson, 1983) that maximum real power is delivered from the source to the complex load impedance if $Z_L=Z_i^*$. Under such conditions $jX_L=-jX_i$ and a

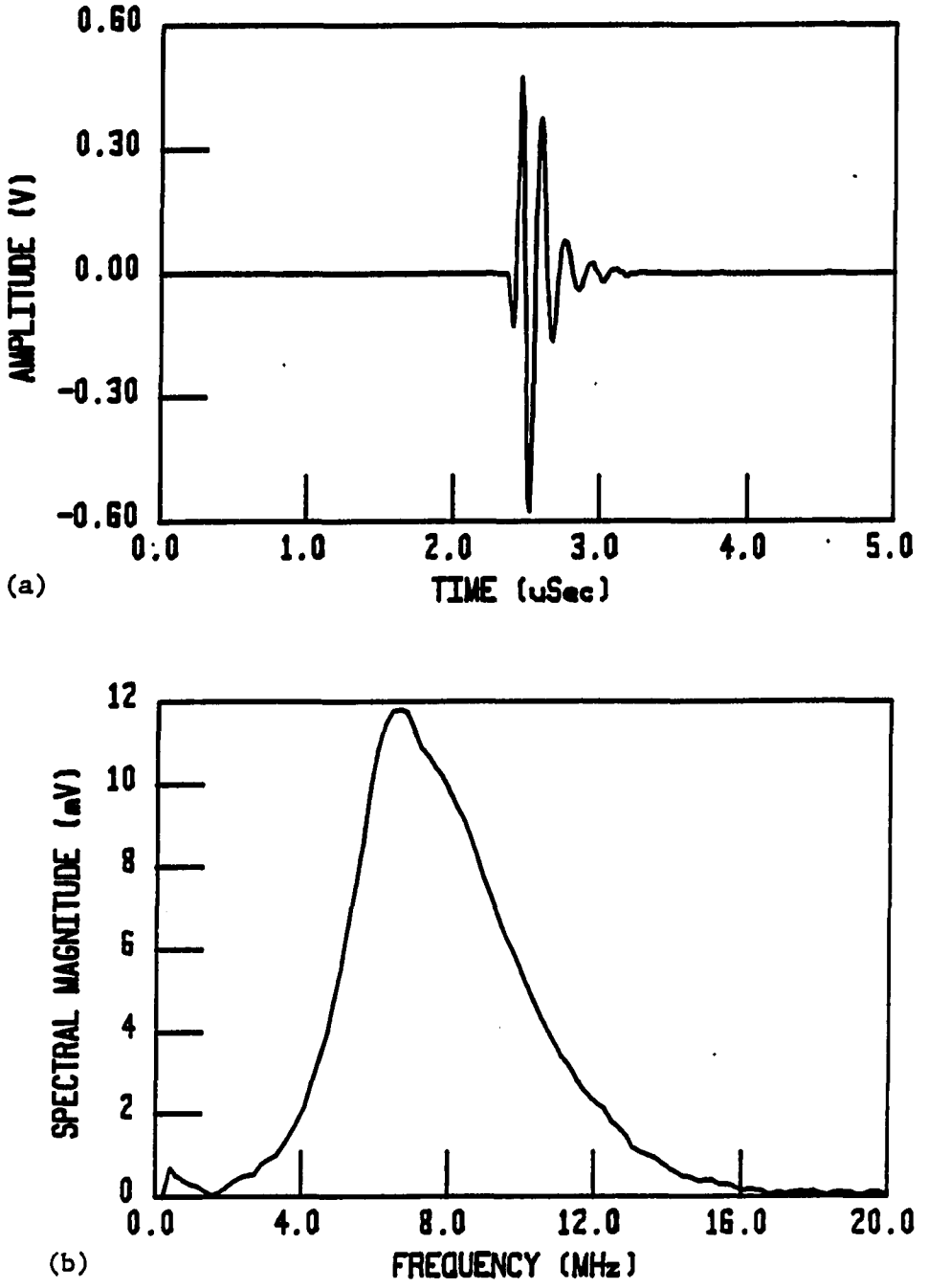

FIGURE 5.24. Actual pulse-echo waveforms from first tests of #P17cz: (a) time domain waveform and (b) frequency spectrum

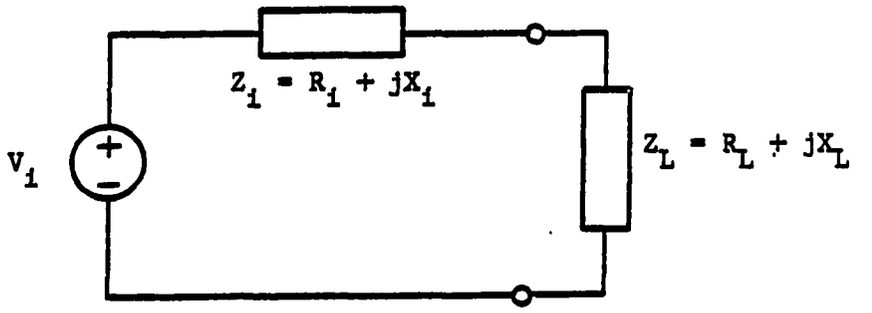

FIGURE 5.25. A circuit terminated in a complex load impedance

matched circuit is achieved for optimum power delivered to R_L. However, for the case where $jX_L \neq -jX_i$, optimum power transfer obviously cannot be achieved. In this case, if it is desired to obtain maximum power transfer centered about some frequency; f_o, R_L must be chosen to match the Q of the complex source impedance with that of the complex load impedance at f_o. That is, R_L must be chosen such that $Q_i = Q_L$. After considering the equivalent circuit for an ultrasound transducer, it was clear that this approach must be used for broadband shunt-tuning.

The equivalent circuit model of a shunt-tuned ultrasound transducer for transmit operation can be represented as a parallel RLC electrical circuit as shown in Figure 5.26.

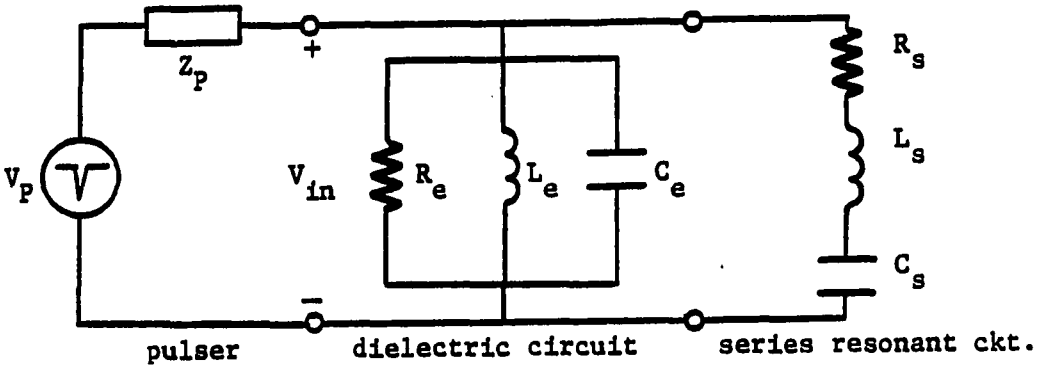

FIGURE 5.26. Circuit model of a shunt-tuned ultrasound transducer in transmit operation

The "s" subscripted variables represent the series resonant impedance components for the water-loaded piezo film case. The "e" subscripted variables represent the shunt equivalent quantities of the dielectric circuit. At series resonance, f_s, it is desirable to match Q_s with Q_e (Silk, 1984). These quantities are given by:

$$Q_e = 2\pi f_s R_e C_e \tag{5.2}$$

and

$$Q_s = 1/(2\pi f_s R_s C_s) \tag{5.3}$$

The simulation program was used to print out the water-loaded Z_s impedance values. Using the previously derived procedure for computing the Z_s components (Chapter III), the results were C_s=1.855 pF, R_s=7652 Ω, and Q_s=1.068.

In the dielectric circuit, a value of 2.2 μH was used for L_e since this was the value used for #P17cz-#P20cz. The

total shunt capacitance for the cable and film element was 92.6 pF. The program results showed R_o=2593 Ω at f_s, thus, Q_e=15.8 was computed using Equation 5.2. This was indeed a severe mismatch! To match Q_e to Q_s required a shunt resistance of:

$$R_e = \frac{1.068}{2\pi(10.513\ \text{MHz})(92.6\ \text{pF})} \tag{5.4}$$

$$R_e = 174.8\ \Omega \tag{5.5}$$

The shunt resistance required to cause R_e=174.8 Ω is given by:

$$174.8\ \Omega = \frac{R(2593\ \Omega)}{R + 2593\ \Omega} \tag{5.6}$$

$$\Rightarrow R = 187.4\ \Omega \tag{5.7}$$

Thus, a shunt resistance of R=187.4 Ω should match Q_e to Q_s and increase the bandwidth for transmission operation.

In the receive mode of operation, an internal switching (diode) circuit of the Panametrics pulser switches the receiver circuit "on" and the transmitter circuit "off". The impedance of the receive circuit thus alters the circuit representation of Figure 5.26. The circuit schematic of the

pulser unit shows that the impedance of the receiver circuit includes (at the least) 250 Ω in shunt with approximately 130 pF of capacitance. This increase in C_e of 130 pF gives a Q_e of 38.1 for the previously discussed shunt-tuned transducers! The large capacitance also causes the dielectric circuit to be tuned at a frequency much lower than the intended f_s value of 10.5 MHz, since the tuned frequency is $1/(L_s C_e)^{1/2}$. The value of resistance required to match Q_e to Q_s for the extra 130 pF of capacitance is 107 Ω.

Although there are two different resistor values required for the matching, 100 Ω was used since using a resistor of higher value than that which matches Q_e to Q_s results in poor bandwidth. Further reducing the shunt resistance to a value lower than that which matches Q_e to Q_s does not further significantly enhance the bandwidth, but instead reduces the sensitivity (spectral amplitude response). Thus, the four shunt-tuned transducers, #P17cz-#P20cz, were retested while shunting each with a 100 Ω resistor.

4. Second testing of the shunt-tuned transducers

The pulse-echo experiments of #P17cz-#P20cz were repeated at the facilities of the Center for NDE. With an added shunt resistance of 100 Ω, the transducers showed greatly improved broadband acoustic performance. Figures

5.27-5.30 show the time domain and spectral magnitude results. The increase in bandwidth is clearly seen by comparing Figure 5.24 with Figure 5.27. As expected, a loss in sensitivity was another result of the matched-Q tuning. All four transducers exhibited the same broadband pulse-echo acoustic performance.

Figure 5.31 shows the effects of adding an epoxy-backed polyethylene cover over the front face of #P17cz. The cover lowered the peak performance and reduced the overall sensitivity. From each of the spectral magnitude plots, BW_{3dB} and Q_{3dB} were computed and are summarized in Table 5.2.

TABLE 5.2. Summary of actual shunt-tuned pulse-echo acoustic performance

TRANSDUCER	F_{Peak} (MHz)	BW_{3dB} (MHz)	Q_{3dB}
#P17cz	6.8	4.0	1.70
#P18cz	7.9	4.5	1.68
#P19cz	7.9	5.0	1.58
#P20cz	6.5	5.0	1.30
#P17cz[a]	5.5	4.1	1.34

[a]With adhesive-backed poly cover over front face of transducer.

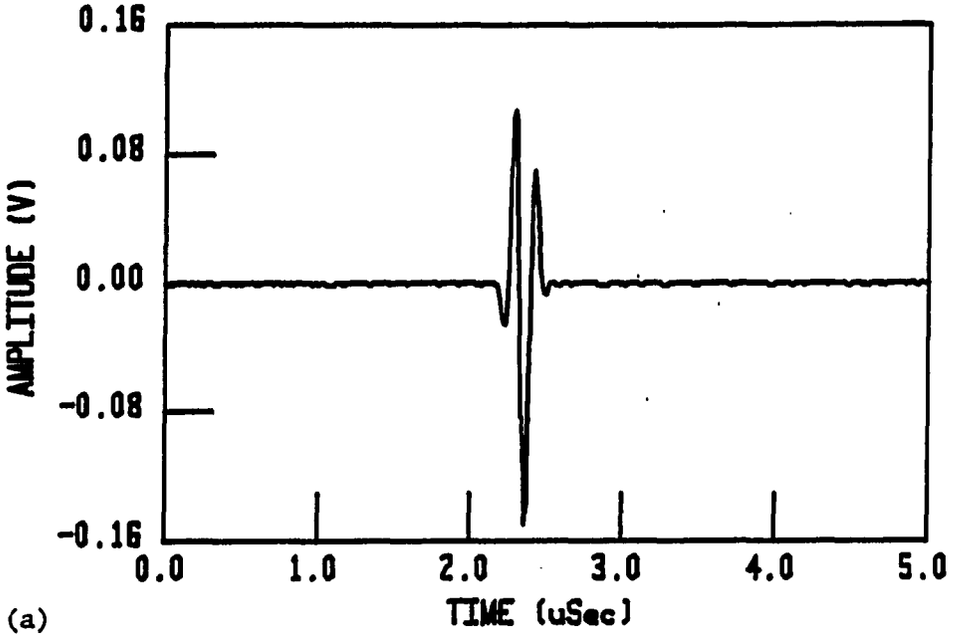

(a)

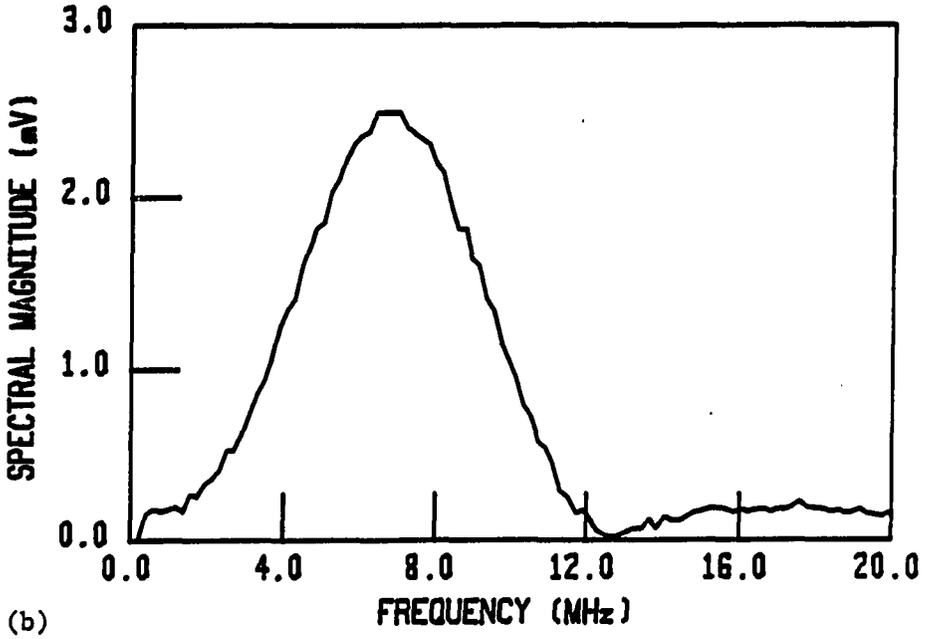

(b)

FIGURE 5.27. Actual pulse-echo waveforms for #P17cz $P(VF_2\text{-}VF_3)$ transducer: (a) time domain waveform and (b) spectral magnitude

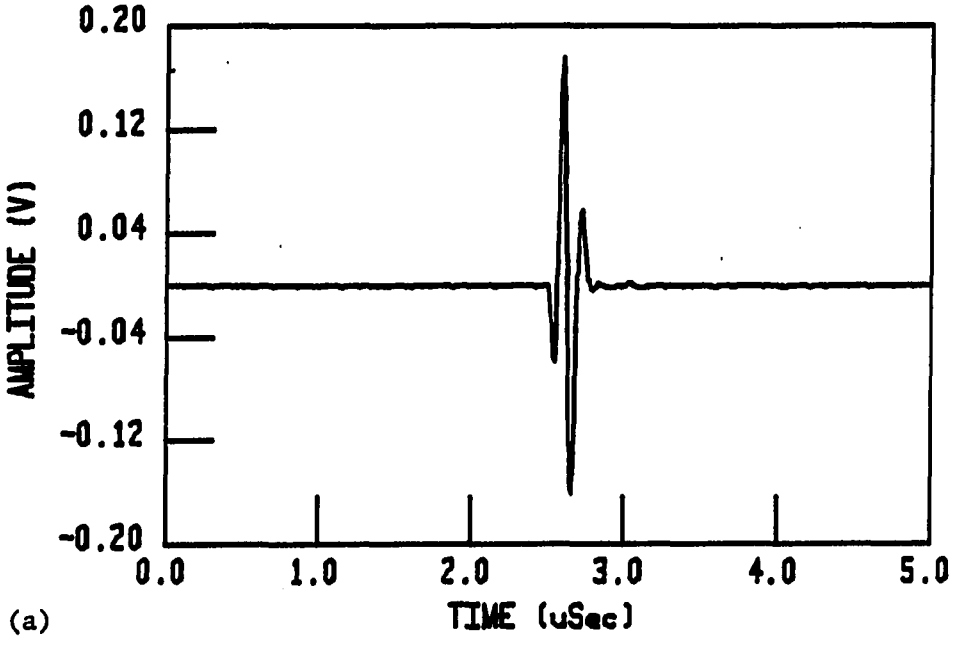

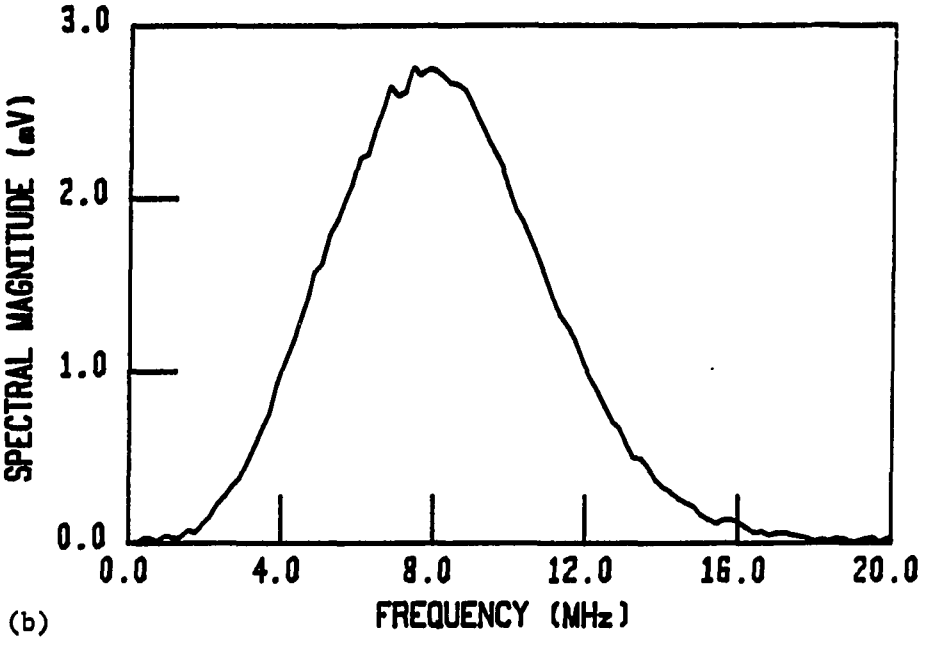

FIGURE 5.28. Actual pulse-echo waveforms for #P18cz $P(VF_2-VF_3)$ transducer: (a) time domain waveform and (b) spectral magnitude

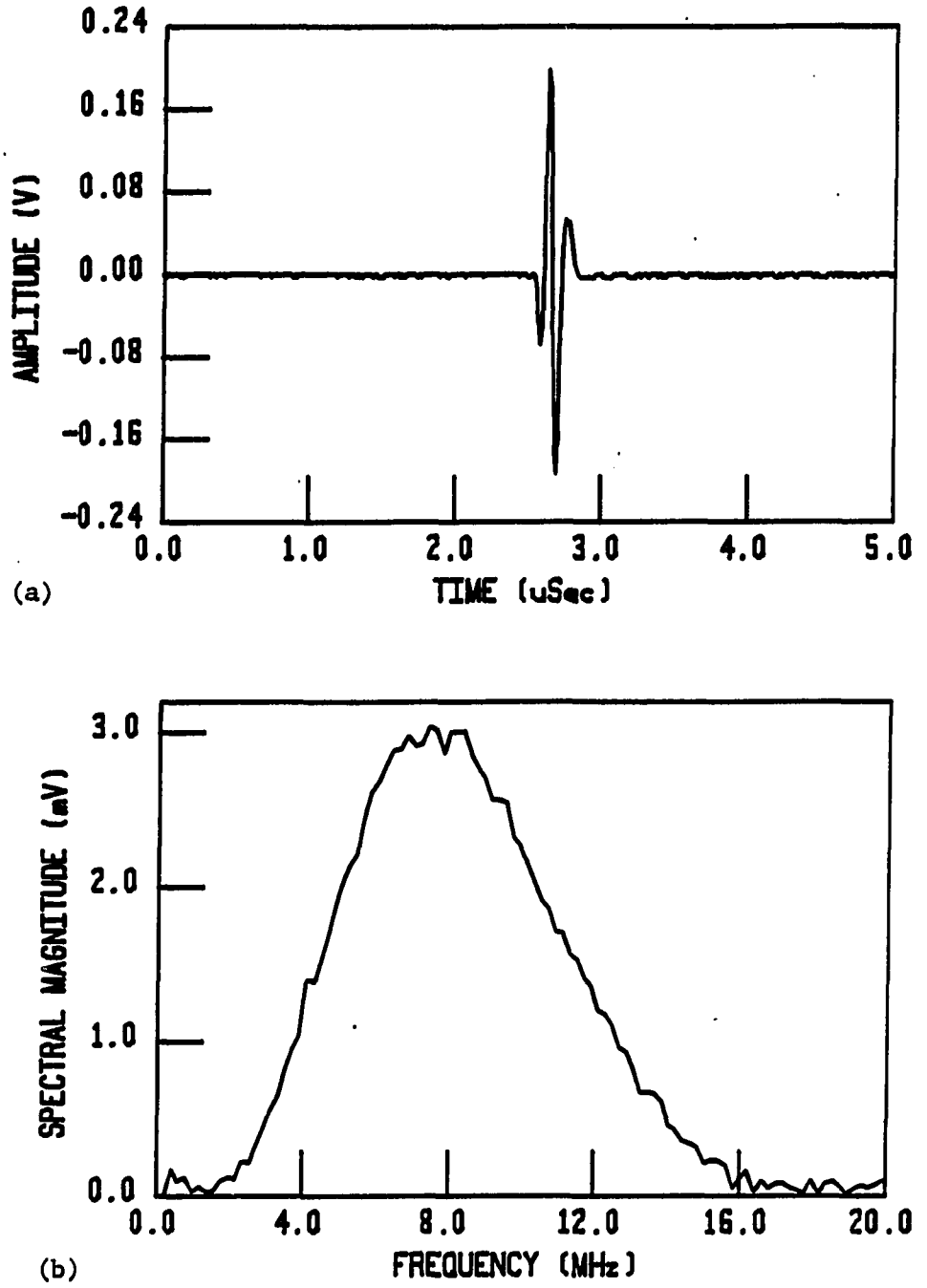

FIGURE 5.29. Actual pulse-echo waveforms for #P19cz $P(VF_2\text{-}VF_3)$ transducer: (a) time domain waveform and (b) spectral magnitude

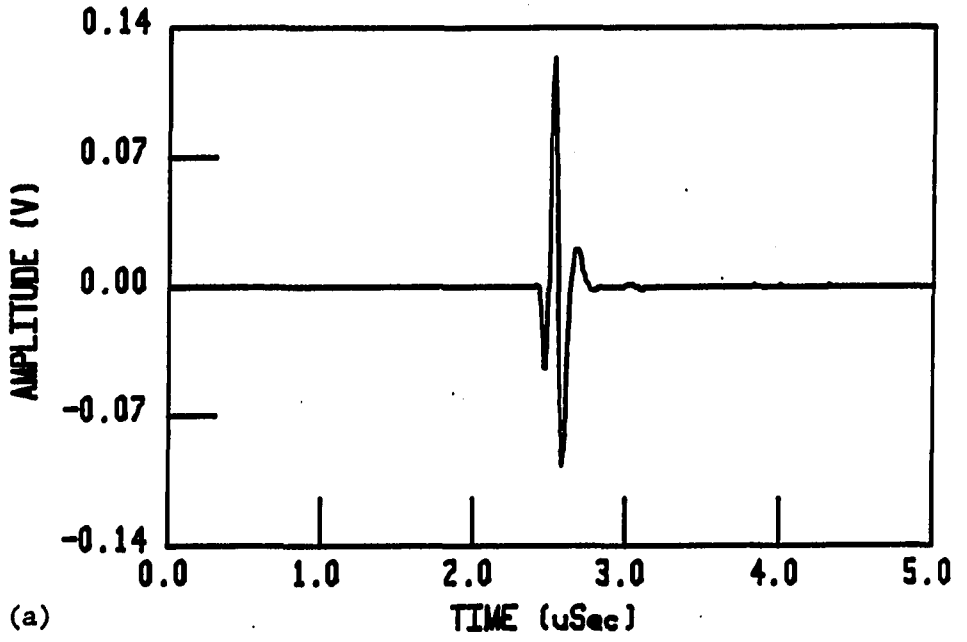

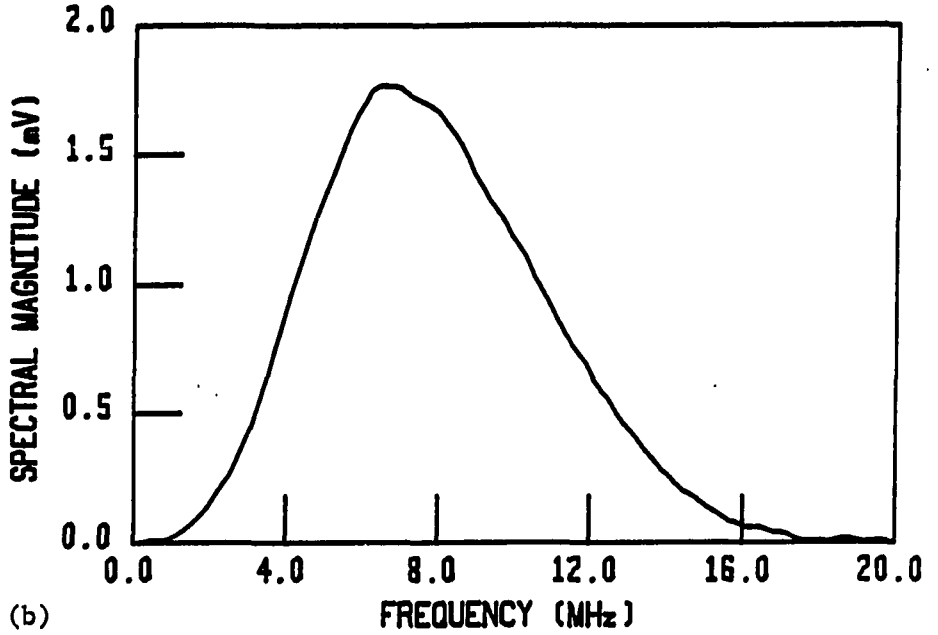

FIGURE 5.30. Actual pulse-echo waveforms for #P20cz $P(VF_2\text{-}VF_3)$ transducer: (a) time domain waveform and (b) spectral magnitude

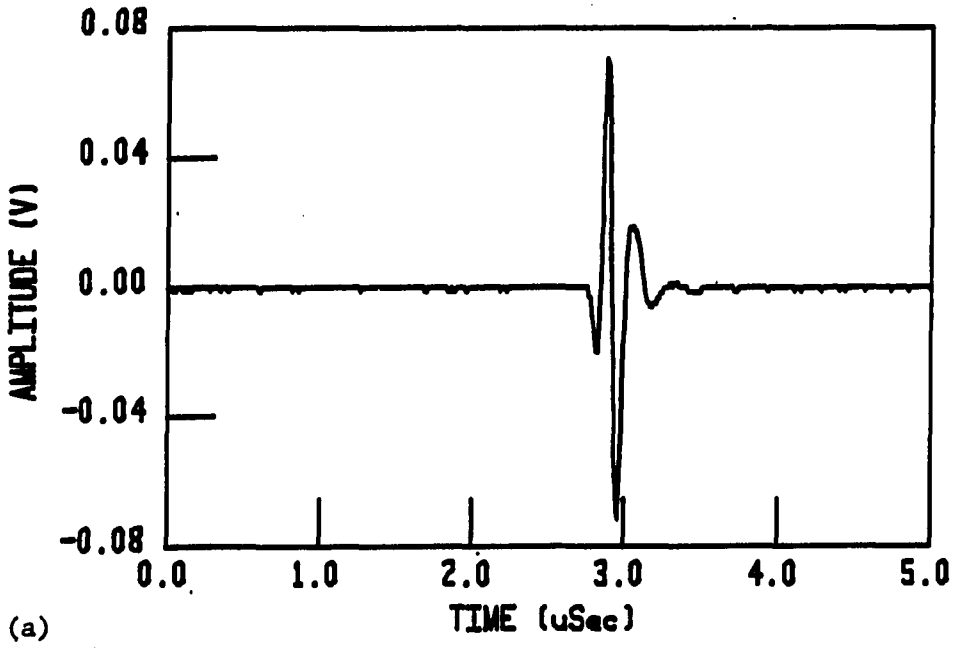

(a)

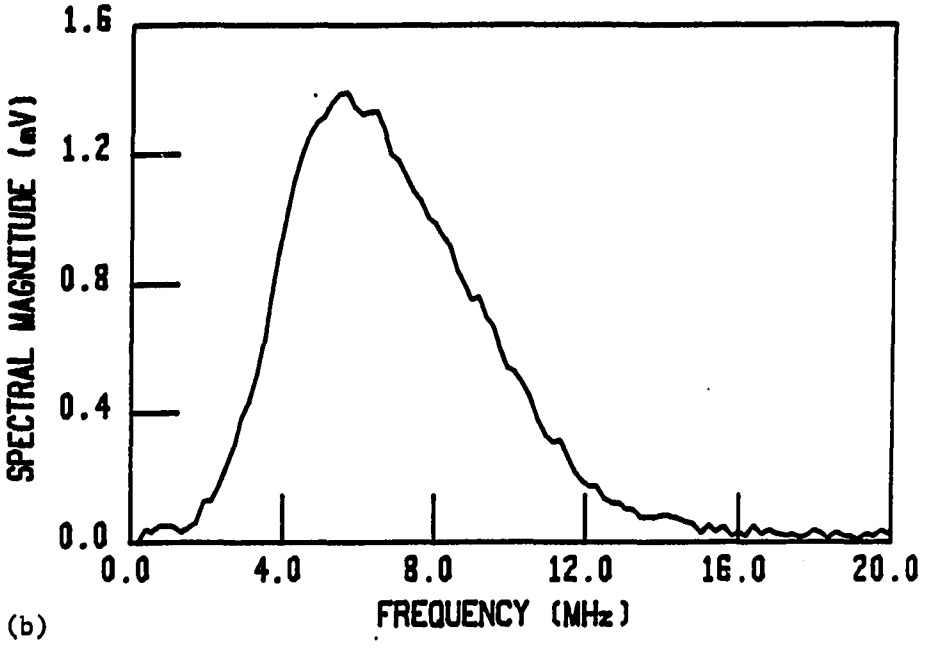

(b)

FIGURE 5.31. Actual pulse-echo waveforms for #P17cz with poly cover over front face: (a) time domain waveform and (b) spectral magnitude

The actual pulse-echo acoustic performance of the transducers was considerably improved when properly shunt tuned with matched Q_e and Q_s. It was still apparent however, that the pulse-echo response was peaked at a much lower frequency than expected. In reviewing the previous shunt tuning equivalent circuits it was apparent that the only means for this phenomenon was for the impedance of the dielectric circuit to be more complicated than that previously considered. The simulation program would later verify this assumption.

5. Simulation results of shunt-tuned transducers

The simulation program XFER.FOR was used to simulate the pulse-echo acoustic performance of the shunt-tuned transducers #P17cz-#P20cz. The program simulations, designed for the same pulse-echo experiments as the actual tests, included the additional 100 Ω shunt resistance and assumed an input impedance of 250 Ω in shunt with 130 pF capacitance for the Panametrics receiver. The simulation results for #P20cz are shown in Figure 5.32. Although the time domain waveform is similar in shape to the actual waveform (Figure 5.30), the spectral magnitude plots for the two are distinctly different. The simulated pulse-echo performance showed a much higher center frequency (9 MHz compared to 6.5 MHz) and lower Q_{3dB}. It was overwhelmingly clear

that these effects were still due to the failure to properly model the impedance of the Panametrics receiver.

The impedance of the Panametrics receiver was clearly more capacitive than previously accounted for. Because the Panametrics pulser also contains many switching diodes, the receiver's input impedance is also very nonlinear. It was more than ever clear that actual impedance measurements of the Panametrics pulser would need to be made and accounted for in future simulations.

The simulation program was extremely useful in verifying the improvements in BW_{3dB} and Q_{3dB} by matching Q_e and Q_s. Figure 5.33 illustrates the effects of the shunt tuning resistance on receiver performance. The figure shows the simulated pulse-echo performance of #P17cz both with and without a shunt resistance of 100 Ω during receive operation. The results show the benefits of a matched-Q dielectric circuit to pulse-echo performance. The matched-Q circuit of the receive operation shows a larger amplitude, more broadband pulse-echo response. Thus, both BW_{3dB} and Q_{3dB} are improved with the addition of the 100 Ω matching resistor. Further reducing the shunt resistance to 50 Ω gave a lower amplitude response than the original simulation. The results show that there is an optimum shunt resistance value for the matching. It can also be seen in

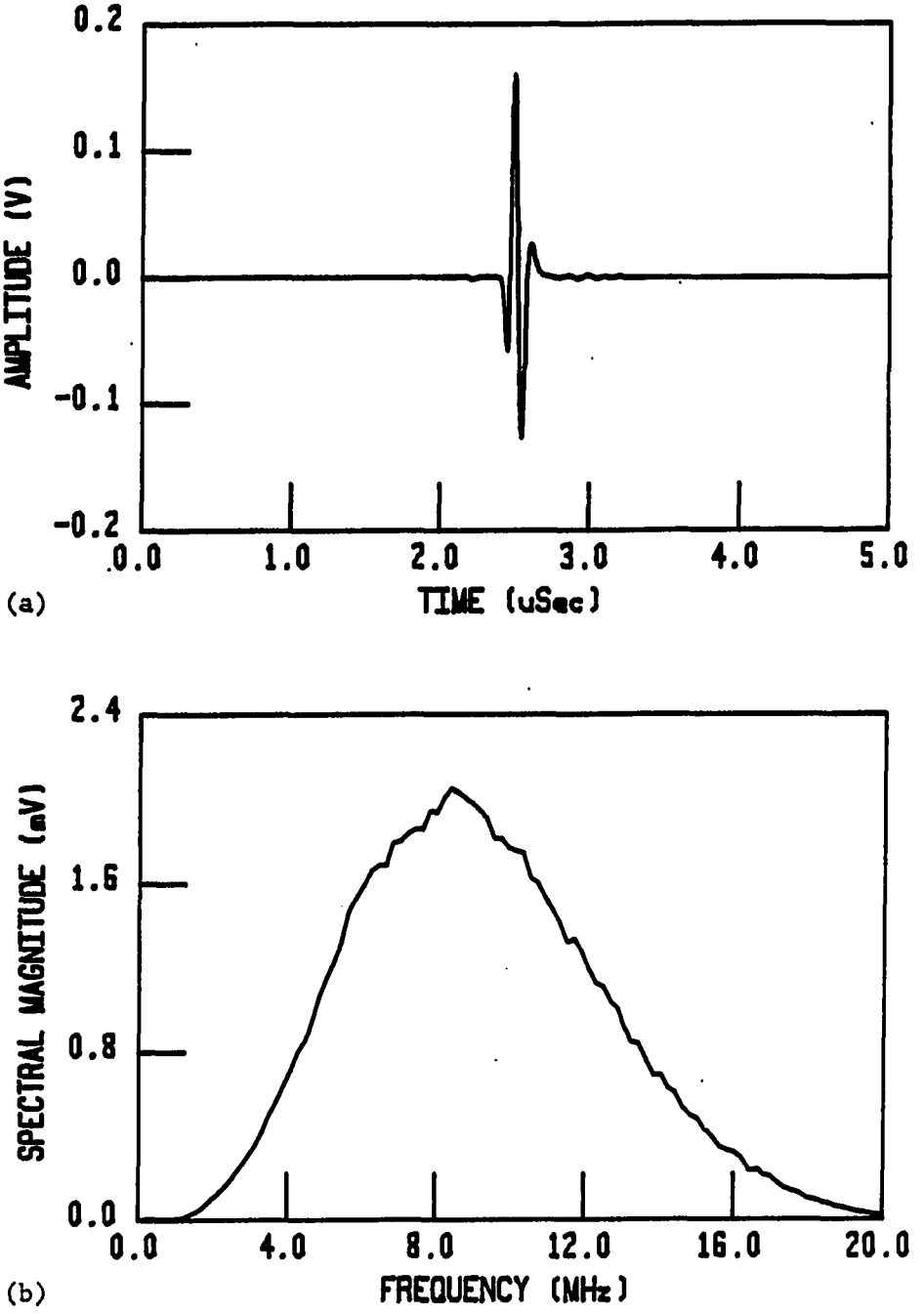

FIGURE 5.32. Simulated pulse-echo performance of #P20cz $P(VF_2-VF_3)$ transducer with a 100 Ω shunt resistance: (a) time domain waveform and (b) spectral magnitude response

the figures that adding the shunt resistance also shifts the peak of the spectral response upward, as desired. It was clear that with more precise knowledge of the Panametrics pulser's impedance during receive operation, a more broadband design could be achieved.

Conclusions

The insight gained in the shunt-tuned transducer design was significant. When properly shunt tuned and matched, the $P(VF_2-VF_3)$ transducers provided broadband pulse-echo performance with significant sensitivity.

The considerations for optimum-bandwidth power transfer led to a successful method of shunt tuning the transducers for greater bandwidth and sensitivity. The fact that this was also illustrated with the simulation program (Figure 5.33) verified the matched-Q tuning approach.

Despite the fact that the shunt-tuned copolymer transducers provided excellent broadband performance, the accuracy of the simulation program's predicted response still remained questionable. The unknown impedance of the Panametrics pulser could clearly be used to justify a difference in the actual and predicted acoustic performance. However, the accuracy of the predicted acoustic performance could only be assessed with better knowledge of the estimated Panametrics input impedance.

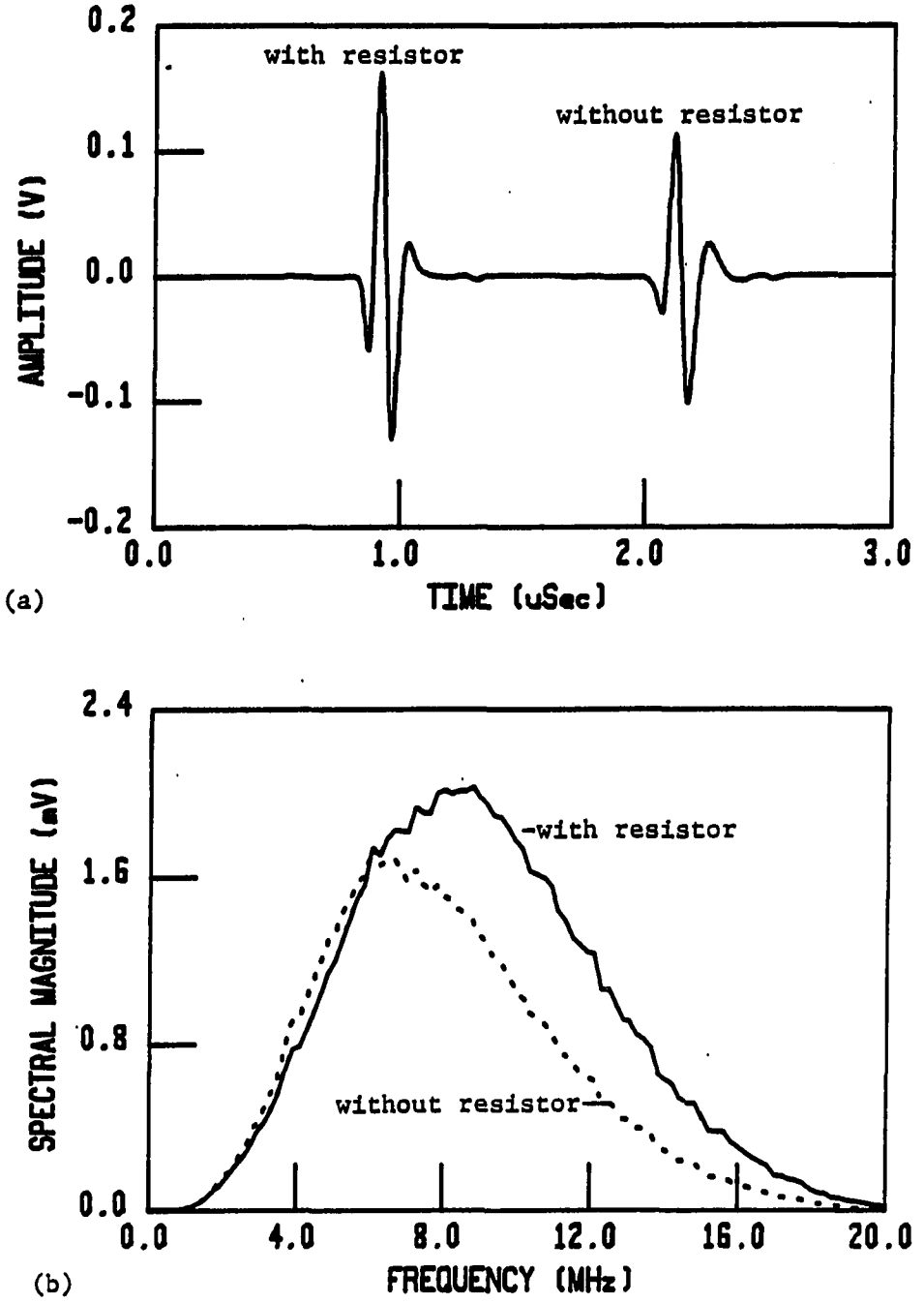

FIGURE 5.33.. Simulated pulse-echo performance of #P17cz $P(VF_2-VF_3)$ transducer with/without a 100 Ω shunt resistance: (a) time domain waveform and (b) spectral magnitude response

F. Final Analysis of the Transducer Tests and Simulated Pulse-Echo Performance

It was clear from the earlier comparisons of actual and predicted acoustic performance that the input impedance of the Panametrics 5052PR receiver would have to be better characterized in the simulation program. Earlier attempts to measure the input capacitance of the unit failed because the pulser circuit's switching diodes interfered with the measurement devices' analyses. This problem was solved when a more powerful measurement device was located.

This section presents the impedance measurement results of the Panametrics pulser, and the subsequent reanalysis of the shunt-tuned copolymer transducers. It was this final comparison of actual and simulated acoustic performance that was used to consider the validity and accuracy of the entire electromechanical modeling and simulation results of this research.

1. Analyzing the Panametrics 5052PR receiver input impedance

The Panametrics 5052PR pulser uses switching diode circuits to turn "on" the receiver circuit and turn "off" the transmitter circuit, following the excitation pulse of

the transmitter circuit. These diodes interfere with the capability of a device to measure the input impedance of the receiver circuit since a diode's impedance varies with the amplitude and polarity of an applied voltage. Many capacitance and impedance meters were incapable of measuring the Panametrics' input impedance. However, the Center for NDE had a device which was capable of making such measurements. The instrument, a Hewlett Packard 4194A Impedance/Gain-Phase Analyzer (no. 26167J00867) with test fixture 16047D, is capable of making 400 discrete impedance measurements (magnitude and phase) over a frequency range of 1 kHz-40 MHz, in seconds. The results may be plotted, stored in memory for processing, etc.

This device was used to measure the input impedance of the receiver jack of the same Panametrics 5052PR previously used, with the controls all set as in the experiments (10 dB of receiver gain, 0 damping). The results were extremely nonlinear and could not be accurately modeled with any of the third-order RLC models of the HP 4194A. This was no doubt due to the presence of the many switching diodes.

The impedance measurements were corrected for the cable capacitance used in the measurement setup and the effects of the 500 Ω shunt resistance of the transmit circuit's damping were added. A FORTRAN program, used for the processing,

printed out the resulting receive-mode input impedance of the pulser, neglecting the remaining impedance of the switched-off transmitter circuit. These results are summarized in Table 5.3.

TABLE 5.3. Summary of corrected receive-mode input impedance of the Panametrics pulser

F (MHz)	$\|Z_{in}\|$ (Ω)	Arg$\{Z_{in}\}$ (°)	Re$\{Z_{in}\}$ (Ω)	Im$\{Z_{in}\}$ (Ω)
0.0	250.00	0.00	250.00	0.00
4.0	237.54	-6.23	236.14	-25.76
8.0	215.76	-14.43	208.95	-53.77
12.0	170.95	-23.64	156.61	-68.54
16.0	136.62	-29.61	118.77	-67.51
20.0	81.59	-42.59	60.17	-55.22
24.0	54.77	-40.71	41.51	-35.72
28.0	27.57	-32.30	23.30	-14.73
32.0	16.31	-10.34	16.05	-2.93
36.0	9.65	33.07	8.08	5.26
40.0	12.66	62.10	5.92	11.19

The results gave an input resistance of 250 Ω at DC as specified by the manufacturer for "0" damping. An additional 120 pF of shunt capacitance was also included to account for the transmitter circuit's impedance during the receive time. Again, this was only an estimate. A 100 pF shunt capacitance was evident in the schematic but the effects of the additional switching diodes of the transmit circuit probably make the transmitter's impedance nonlinear

also. This estimated capacitance value was used since the only way of measuring the actual impedance would be to internally disconnect the discharge circuit from the transmitter, and then measure the impedance looking back into the transmit/receive jack.

The Panametrics impedance values were implemented in the simulation program XFER.FOR. A cubic spline interpolation of the values in Table 5.3 was used at each of the desired frequencies required for the pulse-echo simulations.

2. Reanalyzing the shunt-tuned transducers #P17cz-#P20cz

After incorporating the new impedance values for the Panametrics pulser, the simulations of pulse-echo acoustic performance of the shunt-tuned transducers #P17cz-#P20cz were repeated. It was hoped that these results would finally confirm the accuracy of the modified Mason's models and simulation program.

Figures 5.34-5.37 show the simulation results for the four shunt-tuned copolymer transducers. The results clearly show excellent correlation with the actual waveforms of Figures 5.27-5.30. Table 5.4 summarizes the actual and predicted pulse-echo performance data. The results show good agreement in Q_{3dB}, BW_{3dB}, and sensitivity, especially for the averaged results. The characteristic shapes of both the time and frequency domain results for the predicted

performance simulations are obviously well correlated with the actual measured results.

TABLE 5.4. Comparison of actual and predicted pulse-echo ultrasound performance for #P17cz-#P20cz

XDCR #	BW_{3dB}, (MHz)	Q_{3dB}	Time Dom. Pk. (v)[a]
P17cz (actual)	4.04	1.55	0.150
P17cz (model)	5.63	1.42	0.148
P18cz (actual)	4.93	1.41	0.176
P18cz (model)	5.33	1.54	0.146
P19cz (actual)	4.87	1.47	0.198
P19cz (model)	5.54	1.41	0.147
P20cz (actual)	4.96	1.25	0.124
P20cz (model)	5.40	1.52	0.146
Average (actual)	4.70	1.42	0.162
Average (model)	5.50	1.47	0.147

[a]Positive peak value of time domain pulse-echo waveform.

The impedance values for the Panametrics pulser were indeed responsible for the poor correlation in the previous analyses. The predicted frequency spectrums show nearly the same BW_{3dB} and Q_{3dB} as the observed waveforms. Probably even better correlation would result if one could obtain the actual input impedance values for the transmit circuit of the Panametrics unit. By accounting for the exact input

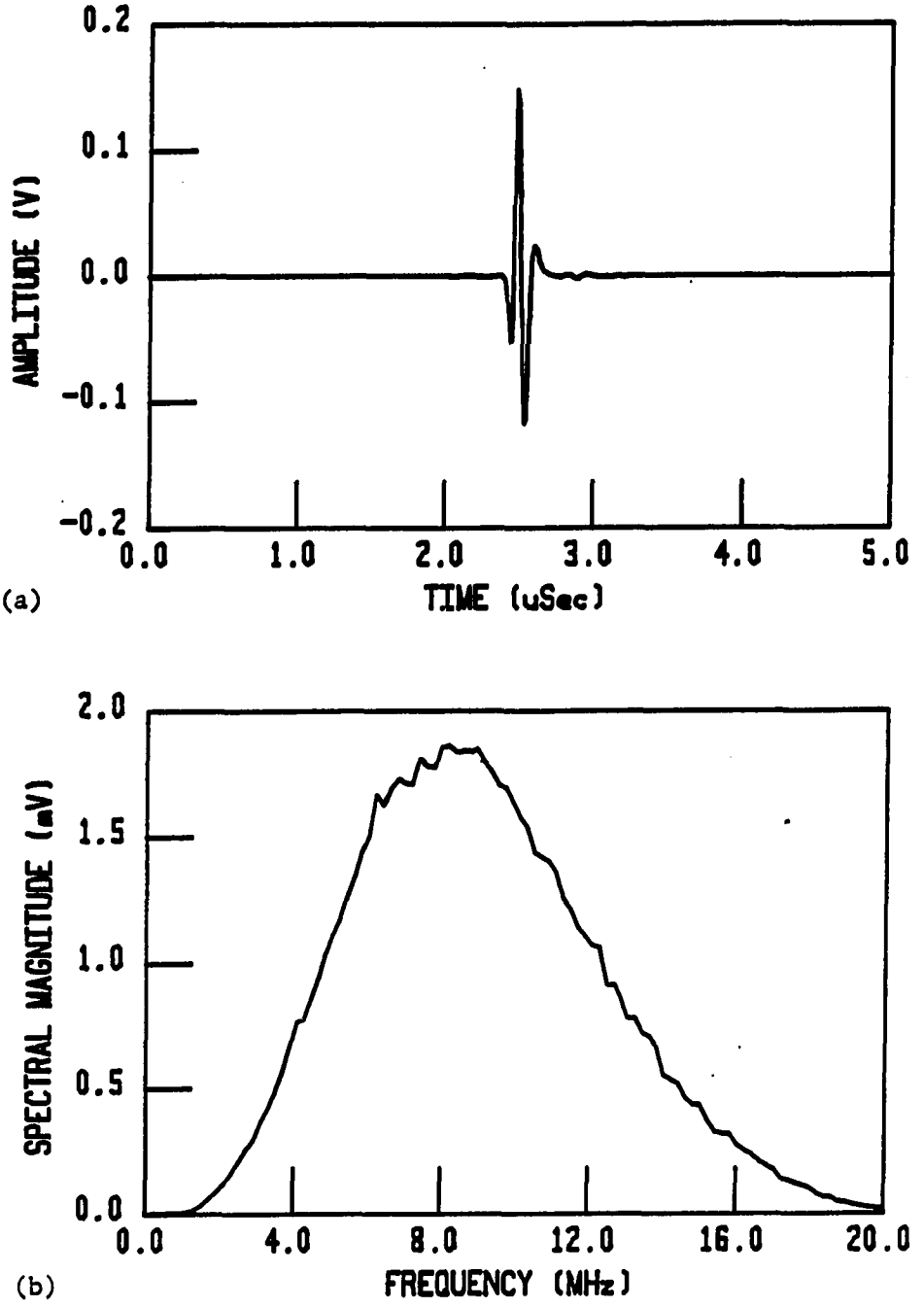

FIGURE 5.34. Predicted pulse-echo acoustic performance of #P17cz P(VF_2-VF_3) transducer: (a) time domain waveform and (b) spectral magnitude

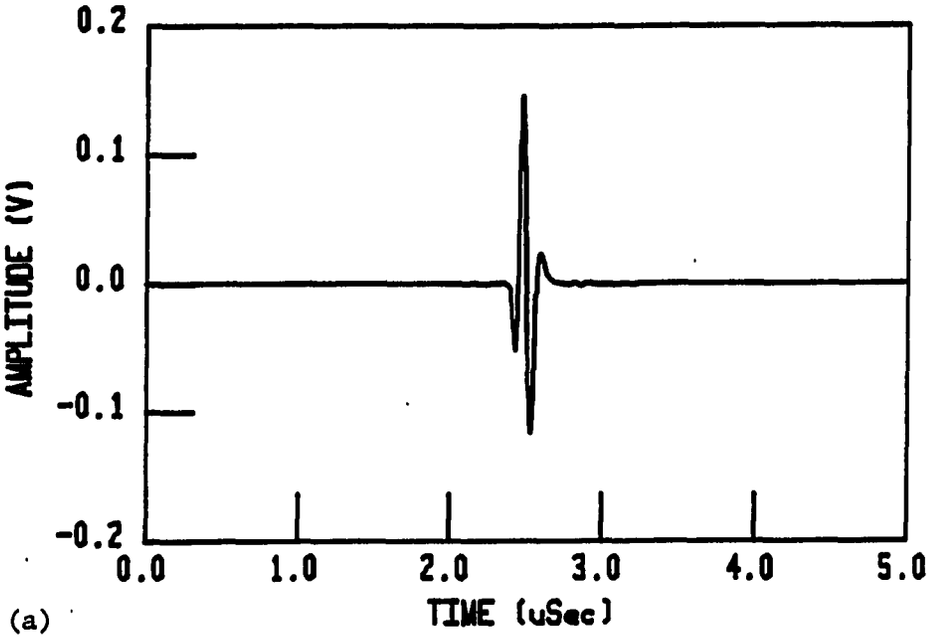

(a)

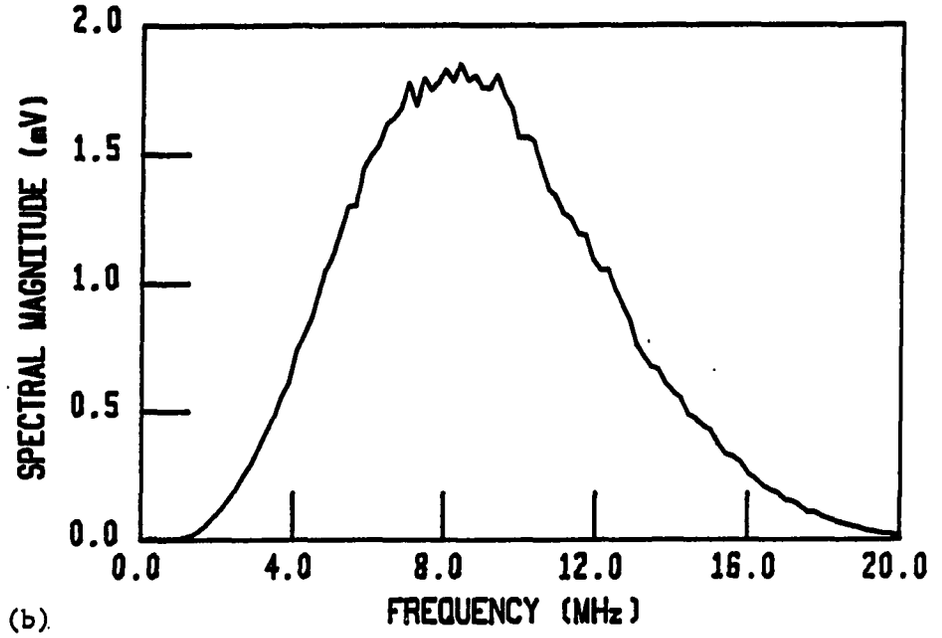

(b)

FIGURE 5.35. Predicted pulse-echo acoustic performance of #P18cz P(VF_2-VF_3) transducer: (a) time domain waveform and (b) spectral magnitude

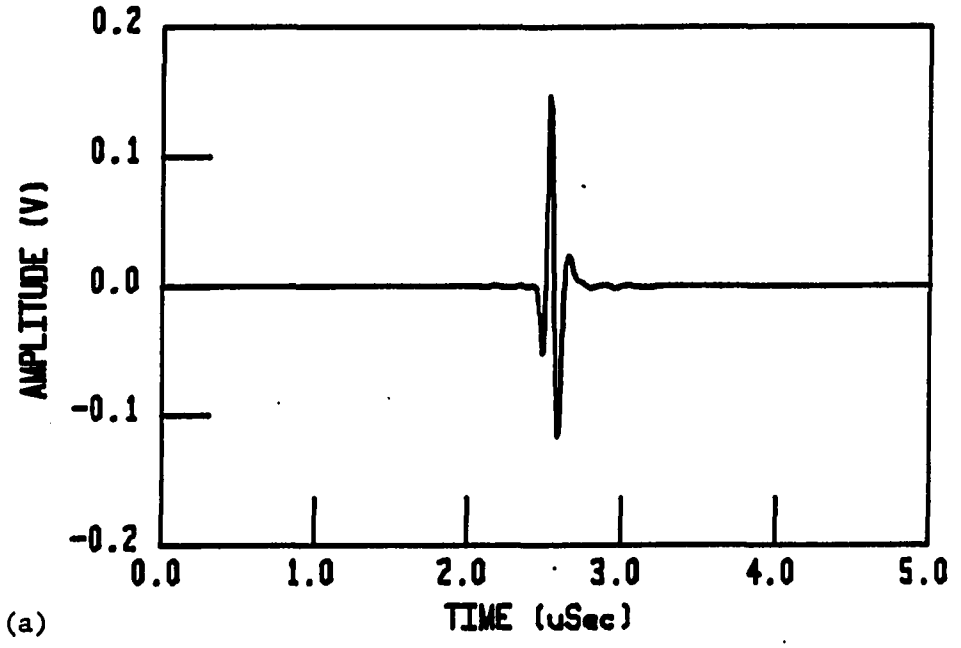

(a)

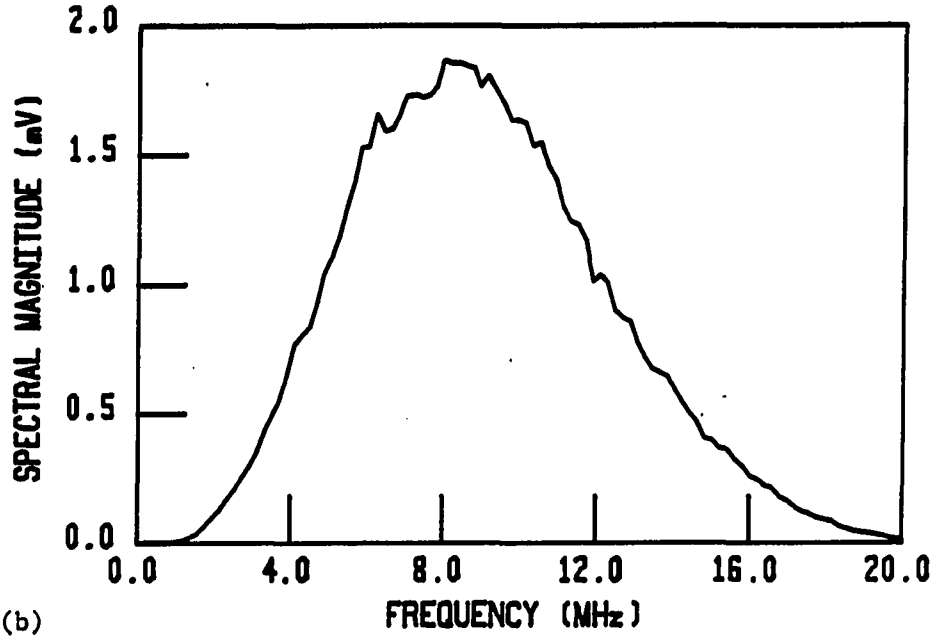

(b)

FIGURE 5.36. Predicted pulse-echo acoustic performance of #P19cz P(VF_2-VF_3) transducer: (a) time domain waveform and (b) spectral magnitude

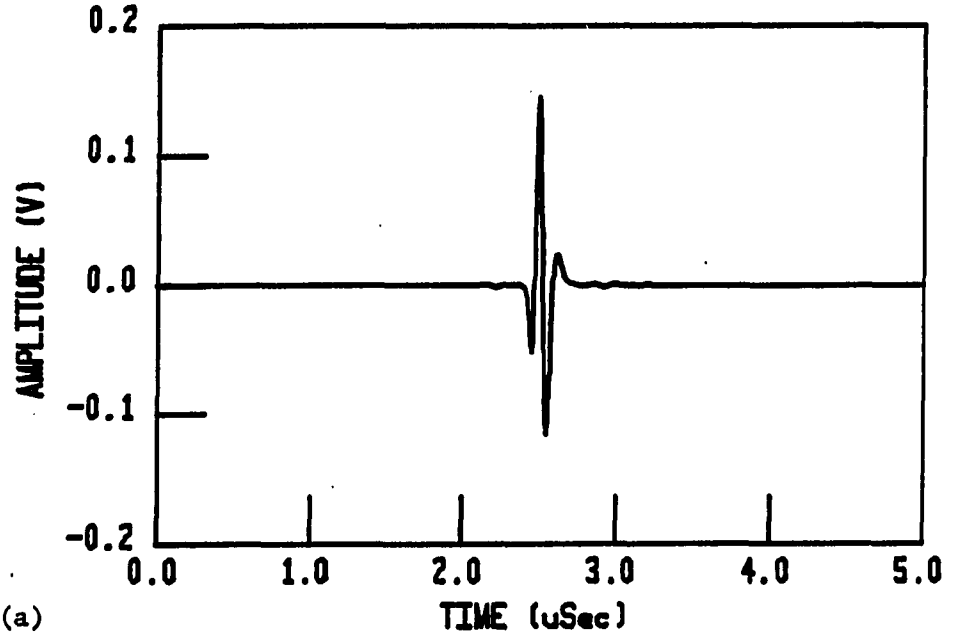

(a)

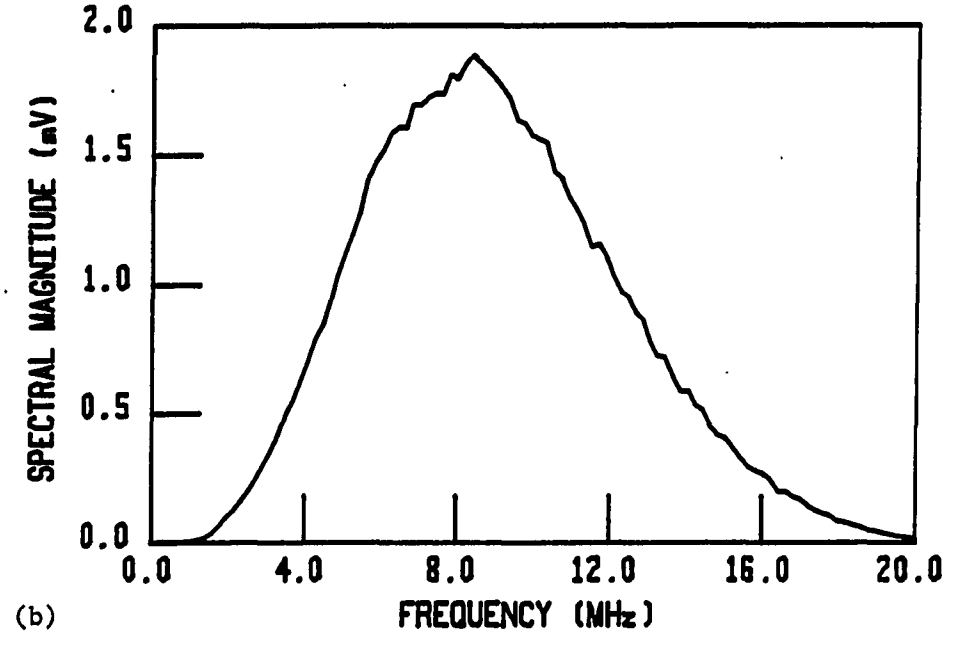

(b)

FIGURE 5.37. Predicted pulse-echo acoustic performance of #P20cz P(VF_2-VF_3) transducer: (a) time domain waveform and (b) spectral magnitude

impedance of the Panametrics 5052PR, and the reflection/ transmission of the return incident echo on the front face, the most accurate simulation results would occur. Since the differences in actual and predicted acoustic performance were primarily in amplitude, the results were considered sufficient to confirm the accuracy of the modeling and simulation techniques.

3. Conclusions

It was clear that the Panametrics 5052PR severely affected the pulse-echo acoustic performance in the receive mode of operation. The results for this section showed that by properly accounting for this impedance, much more accurate predictions of acoustic performance are possible. From better knowledge of this impedance, one can design copolymer ultrasound transducers with excellent sensitivity and bandwidth.

The results of the last simulations finally confirmed the accuracy of the work in the first two parts of this research: the derivation of electromechanical circuit models for piezo film ultrasound transducers, and their simulation in a computer program.

These results not only confirmed the accuracy of the simulation models, but also pointed out the sensitivity of the copolymer transducers to commercial ultrasound equipment.

G. Conclusions

The objectives of the third part of this research were achieved. The successful design of broadband P(VF_2-VF_3) ultrasound transducers permitted quantitative comparisons of pulse-echo acoustic performance with that predicted in simulations using the modified Mason's models.

The quantitative tests were possible only after achieving a successful transducer design. The back-matched design of the transducers permits both submersible (NDE) and contact (medical) applications. Even with the completion of the probe designs, considerable experimental and theoretical work was needed to successfully tune the transducer designs for sufficient bandwidth and sensitivity. Performance tests of the transducers at the Center for NDE were used to analyze the actual performance of all designs.

The test results showed that the use of gold metallization not only provides more reliable electrode conductivity, but also provides a corrosion-resistant front covering for the films. The actual test results also showed that the piezo films can be successfully tuned for enhanced narrowband response (series tuning) or broadband response (shunt tuning). Simulation results for the transducers showed that accurate prediction of acoustic performance demands accurate accounting for all impedances present in an experiment. In

particular, the transducer pulser unit and coax cable impedances can severely alter the performance of the low capacitance piezo film transducers. However, the results showed that by properly accounting for all such considerations, the modified Mason's models and simulation techniques indeed provide accurate prediction of pulse-echo acoustic performance. Thus, the objectives of this final part of the research were achieved.

Some additional significant insight was gained in accomplishing this part of the research. The successful method of matching the electrical and mechanical Q (Q_e=Q_s) for optimum bandwidth and sensitivity is extremely important for any broadband design. The results (transducer #P17cz-#P20cz) showed that when correctly matched, both bandwidth and sensitivity are enhanced.

One of the most significant observations from the pulse-echo acoustic performance tests/simulations was that because of the low capacitance of the piezo film materials (46.6 pF for the 1/2" diameter 110.6 micron $P(VF_2-VF_3)$) the acoustic performance of the transducers is inherently susceptible to modification by the cables and equipment with which they are used. Although this may at first appear to be a significant disadvantage to using piezo film ultrasound transducers, the otherwise excellent properties of these

materials warrants the use of special techniques to minimize the effects of the cable and equipment impedances. For instance, by locating an FET source-follower near the piezo film element (i.e., in the probe housing) these effects could be eliminated.

The final pulse-echo simulations of transducers #P17cz-#P20cz demonstrated the validity and accuracy of the entire research--from the electromechanical modeling, to the computer simulation techniques used. Equally important was the fact that at last a reliable design was developed for broadband piezo film ultrasound transducers. The results of this research would now permit the design of broadband piezo film ultrasound transducers to be conducted scientifically rather than by trial and error.

Further analysis of the transmitter portion of the Panametrics pulser's input impedance could even further improve the simulation program results. The excellent results obtained from an estimate of the impedance were sufficient to verify the modeling and simulation research for the piezo films. The research work was thus considered complete.

VI. RESEARCH APPLICATIONS

To demonstrate the power of the results of this research work, the results were used for the design of copolymer ultrasound transducers that would have significant value for medical and NDE applications. Using the previously derived modeling results for the 110.6 micron $P(VF_2-VF_3)$ (film number VA110G00), transducer designs were considered for two distinct applications. The use of the modified Mason's models and simulation program for the development and testing of new transducer designs is clearly demonstrated in this chapter. The simulation program XFER.FOR was used for both the design of the transducers and for simulating their pulse-echo acoustic performance.

The first section of this chapter describes the use of the simulation program in designing extremely broadband copolymer ultrasound transducers. The second section describes the use of copolymer transducers for unipolar acoustic pulse applications.

A. Broadband Ultrasound Transducer Design/Simulations

Since the accuracy of the modified Mason's models and simulation were verified in the third part of the research, it was desirable to make use of these tools for assessing several broadband ultrasound transducer designs. This section describes the design and pulse-echo performance

simulations of both passive and active broadband probe designs. In addition, the effects of increased electromechanical coupling, k_t, are demonstrated. All pulse-echo simulations were modeled after the same experiments used to test all previous transducers at the Center for NDE: normal reflection from a fused quartz target in water at a distance of 3.25 cm.

1. Passive designs

The previous test results of transducers #P17cz-#P20cz and the a priori knowledge of a better estimate for the input impedance of the Panametrics 5052PR receiver circuit were used in several transducer designs. A transducer with improved bandwidth and sensitivity was thus expected. The simulation results of Chapter IV showed that maximum bandwidth could be achieved without using any inductive tuning. Although the untuned designs generally offer somewhat less sensitivity, it was decided to investigate the performance of untuned passive designs which may offer superior ultrasound performance. With the demonstrated accuracy of the simulation program, the designs would be tested without having to construct an actual prototype.

Using the Panametrics receiver input impedance values, (Table 5.3) the interpolated value for the impedance at the series resonant frequency (10.5 MHz) is (176.24-j63)Ω. The

shunt capacitance of the transmitter (130 pF) was combined with this impedance, as was the capacitance of a 3.5' length of RG62A/U coax cable, and that of a 1/2" diameter $P(VF_2-VF_3)$ element. The entire dielectric circuit was then modeled as a parallel RLC circuit with C=140 pF. A shunt inductance of 1 μH is required to resonate this capacitance at 10.5 MHz. To match the Q_e of this circuit with that of the transducer's mechanical value, Q_s, the simulation program was needed to print out the series resonant impedance of the modified Mason's model, Z_s, near f_s.

The series resonance components needed for the design, determined as in Chapter III, were R_s=7652 Ω and C_s=1.855 pF. These values gave a water-loaded Q_s of 1.068. A shunt resistance of 106 Ω was required to match Q_e of the dielectric circuit to this value, thus a value a 100 Ω was used as for transducers #P17cz-#P20cz.

To simulate the pulse-echo acoustic performance, an unloaded Panametrics pulser waveform was used in the simulation program (Figure 5.22). Figures 6.1 and 6.2 show simulation results for the tuned passive design. Figure 6.1 shows the extremely broadband transmitted pulse waveform. The pulse-echo waveforms, uncorrected for reflection and diffraction, are given in Figure 6.2. The simulation results indeed show a more broadband pulse-echo response

than any of those simulated for #P17cz-#P20cz. Analysis of the spectral magnitude plot gave Q_{3dB}=1.20, BW_{3dB}=6.04 MHz, and a time domain pulse-echo peak value of 0.434 volts. Thus, the sensitivity, bandwidth, and Q were all improved over the previous designs.

The performance of the same design, without the shunt inductance, was also simulated. The results, shown in Figure 6.3, show improvement in BW_{3dB}, Q_{3dB}, and the peak value of the time domain pulse-echo waveform. The untuned design indeed provided superior performance to any previous designs studied.

These results verified the earlier assumptions that with further a priori knowledge of the receiver's input impedance, a more broadband pulse-echo acoustic response can be designed. To investigate the benefits of an infinite receiver input impedance on pulse-echo performance, an active design was also considered.

2. Active designs

The adverse effects of the cable and receiver impedance on the ultrasonic performance of the piezo film ultrasound transducers can be addressed by considering an active design. One solution is to incorporate an FET source-follower circuit as close to the piezo film element as possible.

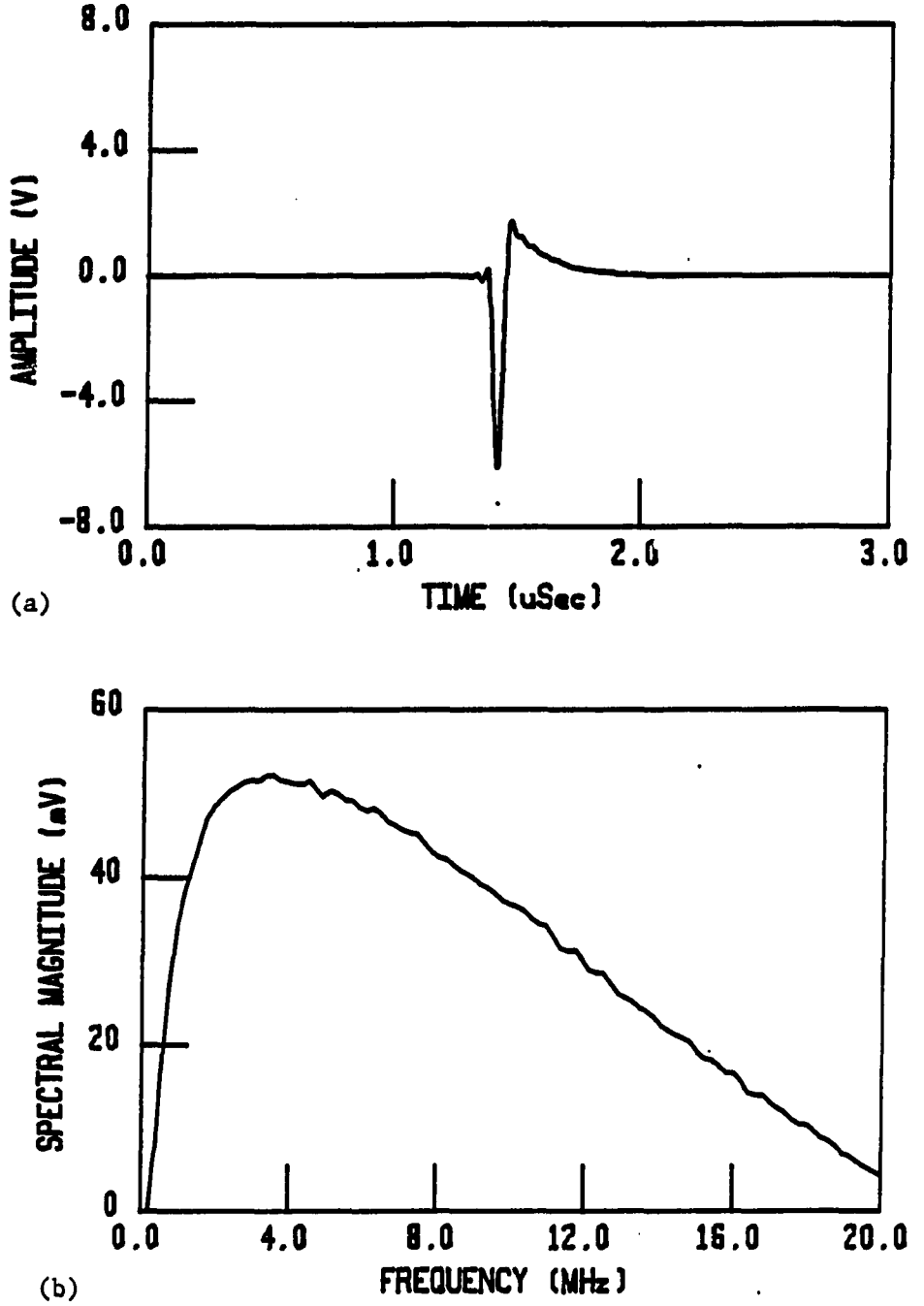

FIGURE 6.1. Simulated transmit-mode ultrasound performance of P(VF_2-VF_3) transducer, shunt-tuned passive design: (a) time domain waveform and (b) spectral magnitude response

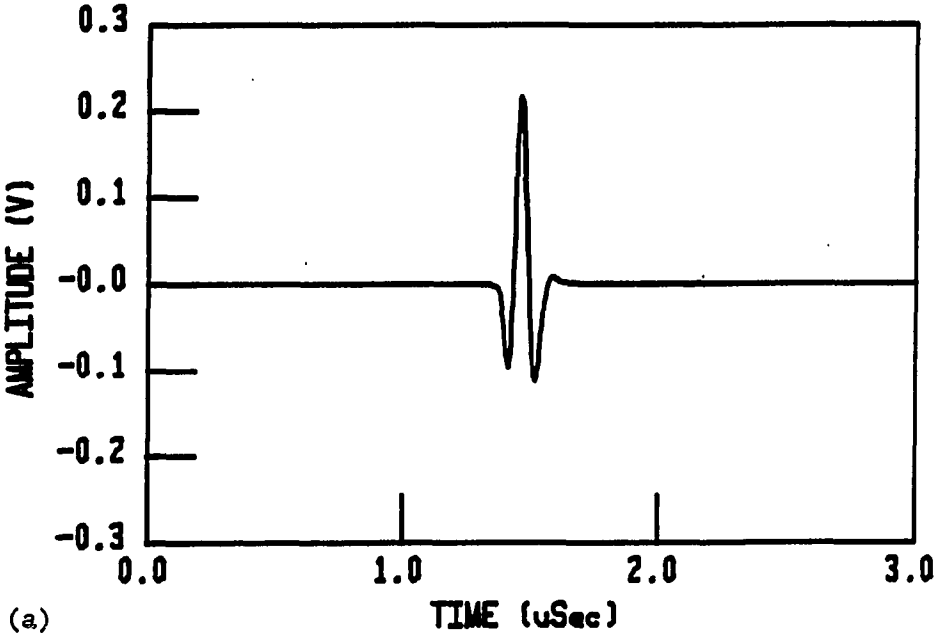

(a)

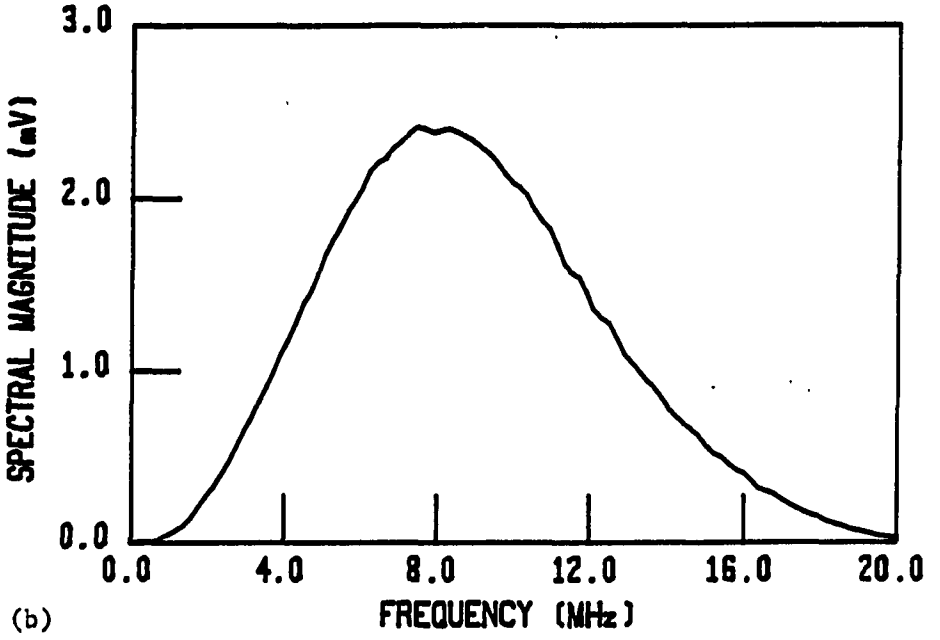

(b)

FIGURE 6.2. Simulated pulse-echo ultrasound performance of $P(VF_2\text{-}VF_3)$ transducer, shunt-tuned passive design: (a) time domain waveform and (b) spectral magnitude response

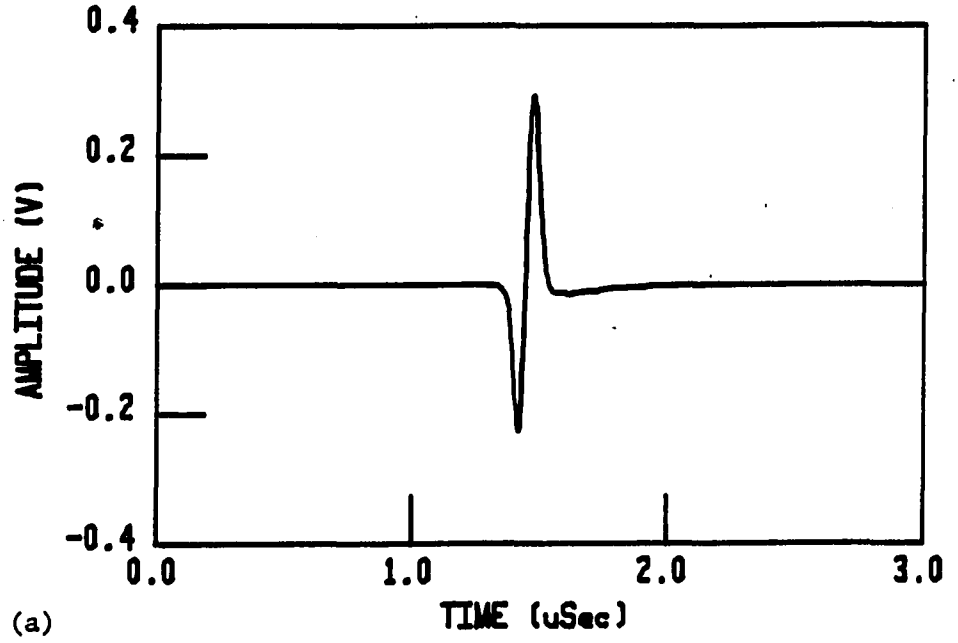

(a)

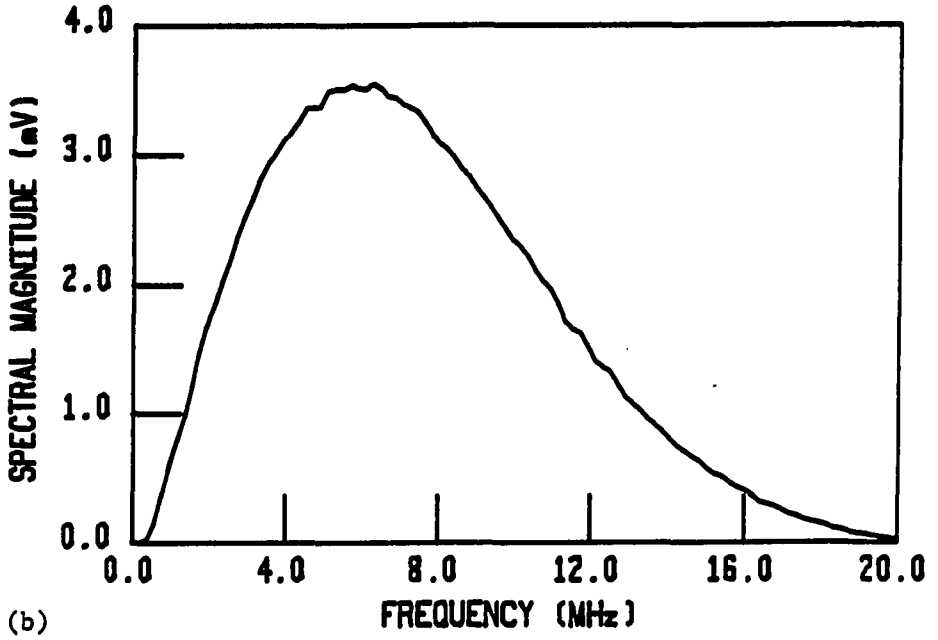

(b)

FIGURE 6.3. Simulated pulse-echo ultrasound performance of $P(VF_2-VF_3)$ transducer, untuned passive design: (a) time domain waveform and (b) spectral magnitude response

The FET circuit, powered by an added DC power supply, could be mounted inside the rear of the probe housing. Since the circuit has an "infinite" input impedance and extremely low output impedance, it acts as a buffer to isolate the undesirable effects of cable and receiver impedance from the transducer. Of course supplying power to the FET and protecting the circuit from the excitation pulse of the pulser require additional design considerations, but are not presently seen as major problems.

To simulate such a design one can simply open-circuit the dielectric circuit in the receive mode and consider only the shunt-tuning inductance and resistance. Thus, the impedances of the receiver and cable are omitted. Since the total capacitance of the dielectric circuit is then lower, a higher value of shunt-tuning inductance is required.

For comparison, a design similar to that previously used was considered, but included a new shunt inductance of 4.66 μH for the tuning. A shunt resistance of 100 Ω was again used for the design, thus the simulation results would reveal the effects of cable and receiver impedance on ultrasonic performance.

The results for the pulse-echo simulations are given in Figure 6.4. In comparing this design to the passive design, the improvements in ultrasonic performance are obvious. The

active design produced a Q_{3dB} of 0.98 and time domain peak value of 1.47 volts. Thus, the FET design provided more than three times the sensitivity of the tuned passive design, with a significantly improved bandwidth.

The tuned active design was also superior to the untuned passive design. Thus, the next logical step was to pursue an untuned active design. The performance of an active untuned design (no shunt inductance, 100 Ω shunt resistance) was then simulated. Figure 6.5 shows the simulated pulse-echo results. As expected, the results showed the most broadband low-Q performance of any previously studied design. A slightly lower sensitivity was also noted for the untuned case. This was expected since previous simulation results showed that a shunt inductance "peaks up" the load impedance of the receive-mode circuit, causing increased sensitivity and a narrower bandwidth.

These results showed that an active design indeed warrants future consideration where maximum bandwidth is desired. Using an FET source-follower circuit would also permit the same ultrasonic performance of a piezo film ultrasound transducer when used with any pulser unit, or any coax cables or connectors. Thus, a designer would not require knowledge of the pulser unit's receiver input impedance to design broadband transducers if an active design were used.

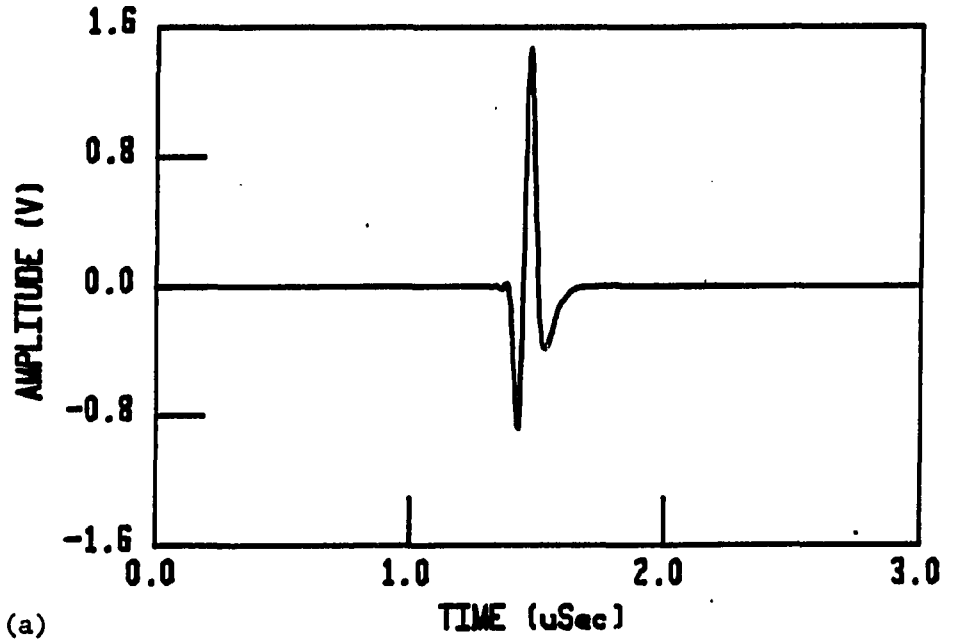

(a)

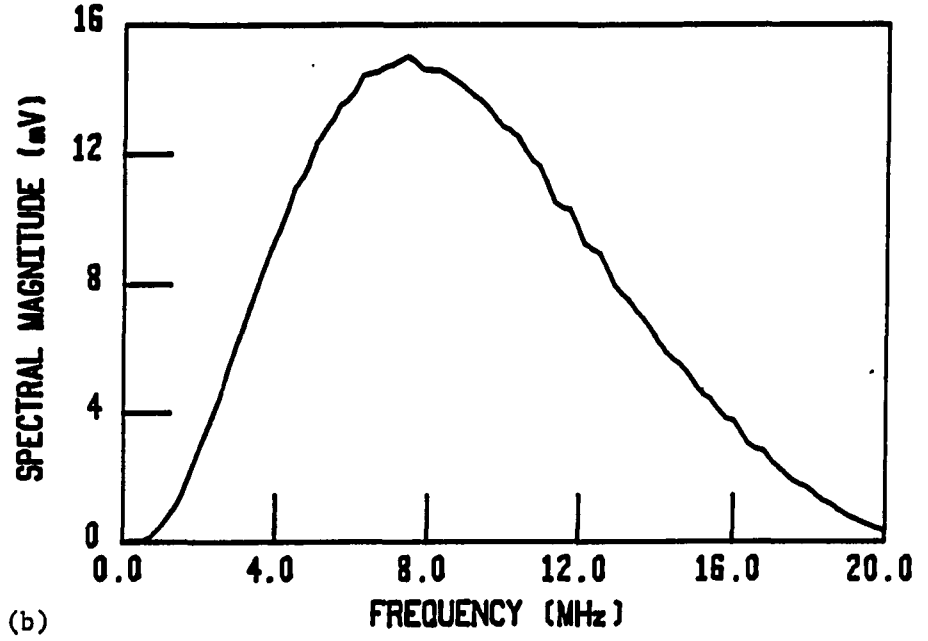

(b)

FIGURE 6.4. Simulated pulse-echo ultrasound performance of $P(VF_2\text{-}VF_3)$ transducer, tuned active design: (a) time domain waveform and (b) spectral magnitude response

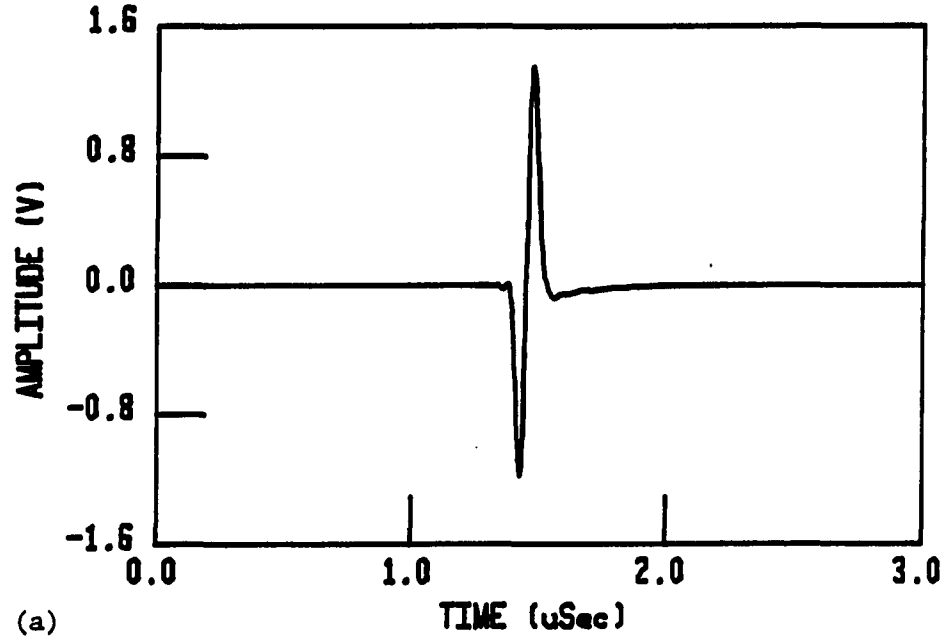

(a)

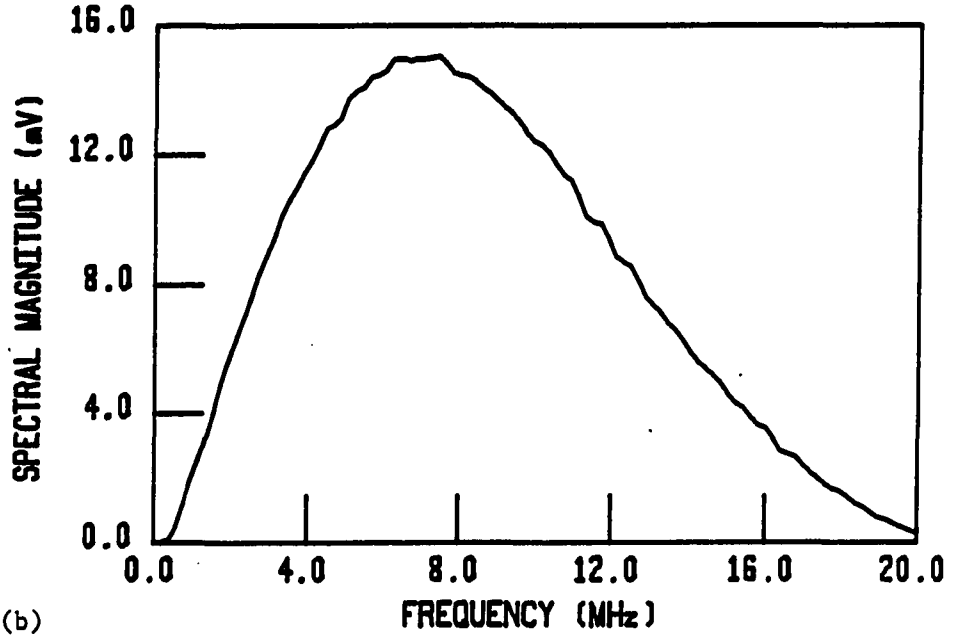

(b)

FIGURE 6.5. Simulated pulse-echo ultrasound performance of $P(VF_2\text{-}VF_3)$ transducer, untuned active design: (a) time domain waveform and (b) spectral magnitude response

Again, the previously derived modeling and simulation results were extremely useful in assessing the theoretical performance for prototype transducer designs, without having to construct and test an actual transducer.

3. Enhanced film designs

The early tests of $P(VF_2-VF_3)$ ultrasound transducers showed greatly increased sensitivity over earlier PVF_2 designs (Chapter V). A great deal of this difference was no doubt due to the much higher electromechanical coupling, k_t, of the $P(VF_2-VF_3)$. The $P(VF_2-VF_3)$ samples that were analyzed showed k_t values of about 22%, compared to 12% for PVF_2. Technical personnel at Pennwalt Corporation expect to attain a k_t of 30% for $P(VF_2-VF_3)$. This roughly 50% increase should give a 1.5^2 increase in pulse-echo sensitivity since electromechanical energy conversion is proportional to k_t ($\phi=k_t[v_oC_oZ_o/T_o]^{1/2}$).

The previous tuned and untuned passive and active designs were repeated using k_t=30%. As expected, all designs showed a 1.5^2 increase in pulse-echo sensitivity. All other elements (shunt inductance and shunt resistance) were the same as in the previous simulations. Because the increased k_t slightly changed the mechanical impedance of the transducer, the designs were no longer optimized (i.e., $Q_s \neq Q_e$). Thus, increasing k_t to 30% greatly enhanced sensi-

tivity but in some cases also caused slightly lower BW_{3dB} and higher Q_{3dB}. Table 6.1 summarizes the ultrasonic pulse-echo performance of all passive and active designs studied.

TABLE 6.1. Comparison of ultrasound performance for active and passive $P(VF_2-VF_3)$ transducer designs

XDCR DESIGN	BW_{3dB}, (MHz)	Q_{3dB}	Time Dom. Pk. (V)[a]
k_t = 21.7%:			
Passive, tuned	6.04	1.20	0.217
Passive, untuned	6.47	0.94	0.292
Active, tuned	7.40	0.98	1.470
Active, untuned	8.02	0.90	1.350
k_t = 30%:			
Passive, tuned	5.76	1.26	0.485
Passive, untuned	7.53	0.80	0.625
Active, tuned	6.90	1.05	3.150
Active, untuned	7.75	0.89	2.814

[a]Positive peak value of time domain pulse-echo waveform.

The simulation results clearly show the benefits of the active and untuned designs. It is also clear that sizable increases in k_t would permit significant increases in sensitivity and bandwidth. By properly matching Q_e to Q_s, the broadband ultrasonic properties of the piezo films can be utilized.

4. Conclusions

The power of the simulation models was demonstrated in the study of the latest passive and active broadband ultrasound transducers. The simulation program allowed new designs to be accurately tested without having to build actual test transducers.

The simulation results were useful in demonstrating two approaches a designer may use to address the adverse effects of cable and receiver impedance on the ultrasonic performance of piezo film ultrasound transducers. One can either precisely account for all of the impedances and incorporate them into the probe design, or eliminate their effects with an active design. The active design offers advantages in bandwidth and sensitivity, and such a probe can be used with any cable or receiver. It has the disadvantage of requiring a switching circuit, DC power supply, and separate output cable. Where maximum bandwidth is desired, the simulation results showed that an untuned design is superior. The results showed that the best performance (Q_{3dB}, BW_{3dB}, and sensitivity) was with the untuned active design.

B. P(VF_2-VF_3) Probes for Unipolar Ultrasound Applications

The use of broadband unipolar ultrasonic stress pulses has been shown to be of great use in flaw sizing problems

and for the measurement of graded material properties (Thompson and Hsu, 1988). Tests with unipolar ultrasonic pulses have also been shown to provide a method for determining "fuzzy" boundaries. This technique could have great use in both medical and NDE applications. The detection and measurement of fat and tissue layers may be greatly enhanced with the use of unipolar ultrasound.

The ISU Center for NDE has been pursuing research in the generation and detection of unipolar ultrasound pulses. One of the major challenges of this technique is in the generation of the unipolar pulse waveform. A high power step-voltage driver is required, as is a very broadband ultrasound transducer. The $P(VF_2-VF_3)$ transducers used in this research were tested and at the time of this writing, the results look promising.

This section illustrates both actual and simulated unipolar ultrasonic waveforms, and discusses some of the problems associated with their generation and detection.

1. Test results

The application of a step-voltage waveform to a broadband ultrasound transducer causes the front face of the piezoelectric element to likewise move forward (or backward) and come to a momentary stop. This movement generates an ultrasonic pulse of unipolar pressure. Because the low

frequency components of the waveform readily diffract, the unipolar waveshape is maintained for only a short distance. In water, the unipolar waveshape quickly degrades to a tripolar waveform in a matter of millimeters. The successful generation of the unipolar pulse is dependent on the very broadband response of the transducer since any tendency for the transducer to ring, quickly destroys the unipolar waveshape.

The successful reception and reproduction of a unipolar pulse offers a different challenge. Most ultrasound transducers appear to respond to a unipolar waveform by producing an output voltage which is similar to the derivative of the incident unipolar waveshape. A bipolar output waveform is thus the result. More research is needed regarding the tuning requirements of a transducer to faithfully reproduce unipolar waveshapes in the receive mode of operation. The copolymer transducers #P17cz-#P20cz have been shown to be capable of generating unipolar ultrasonic pulses, however, their pulse-echo waveforms failed to reproduce a unipolar waveshape.

Figure 6.6 shows the computer simulated ultrasonic performance of transducer #P18cz for an ideal step input voltage waveform. The figure shows an exceptionally broadband transmitted unipolar pulse waveform. However, the

pulse-echo waveform (omitting the effects of diffraction and reflection) shows a tripolar waveshape. The shunt-tuned design of #P18cz caused the noted distortion of the unipolar waveform in receive operation. A series-tuned active design may permit undistorted reception of the unipolar waveshape. Figure 6.8 shows the results of a pitch-catch experiment at the Center for NDE. The experiment involved using #P18cz as a transmitter and a broadband PZT transducer[9] as the receiver. The received waveforms, from a few millimeters, verified that the copolymer transducer indeed produced a unipolar ultrasonic pulse.

2. Conclusions

Piezo films could play an important role in future unipolar ultrasound technology. The results of this research show that the broadband properties of the films make them well suited for generation of unipolar ultrasound waveforms. The problems associated with faithful reproduction of the unipolar waveshape during reception, demand further study. However, a series-tuned active design may be the solution to successfully preventing the natural tendency of a piezo film ultrasound transducer to differentiate a unipolar waveform during receive operation. Because piezo films can be formed into complex shapes, future transducer

---

[9]Panametrics V110 5MHz, 1/4" planar contact transducer.

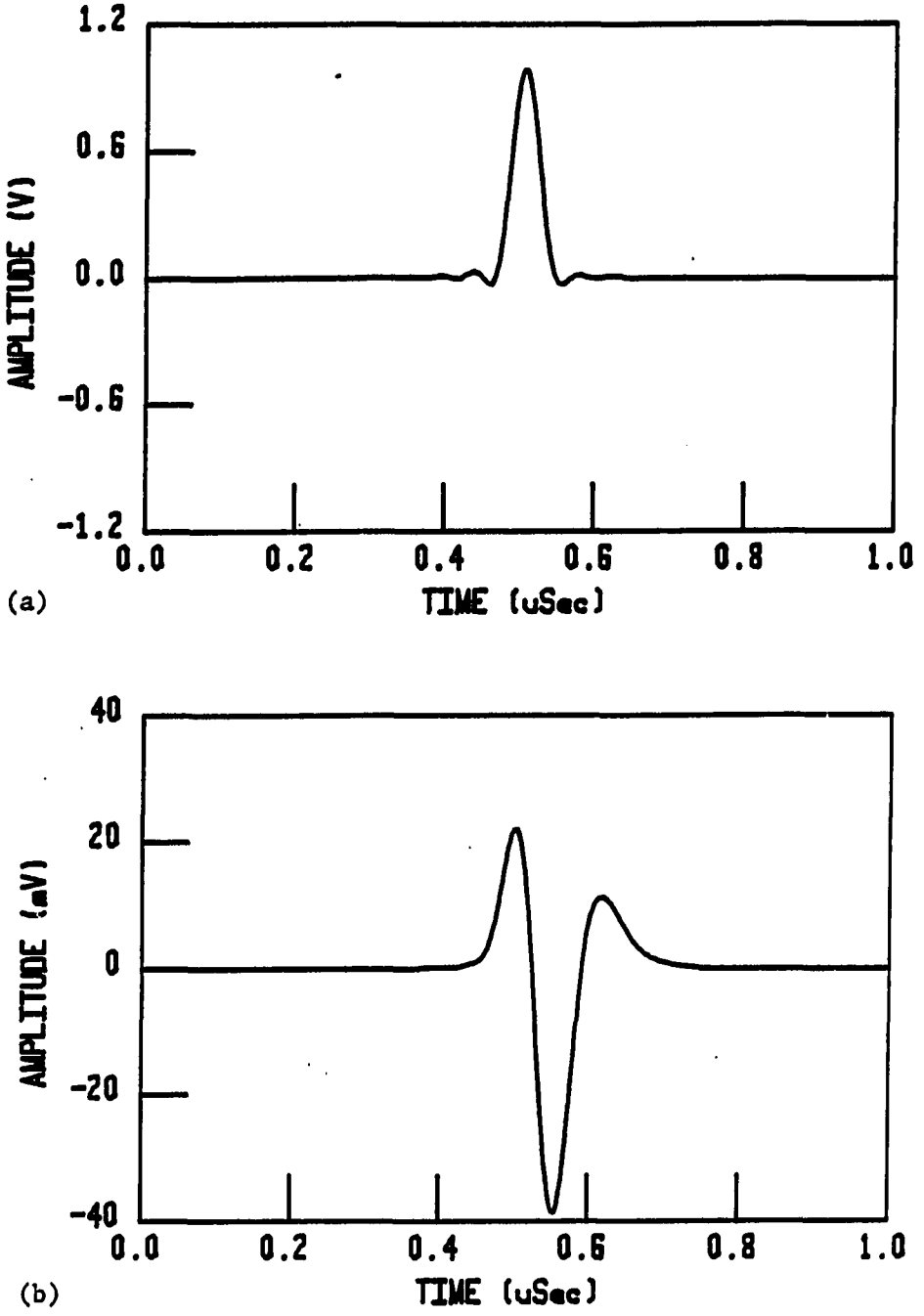

FIGURE 6.6. Simulated ultrasound performance of #P18cz $P(VF_2\text{-}VF_3)$ transducer for an ideal step-voltage input: (a) transmitted unipolar pulse and (b) pulse-echo tripolar waveform

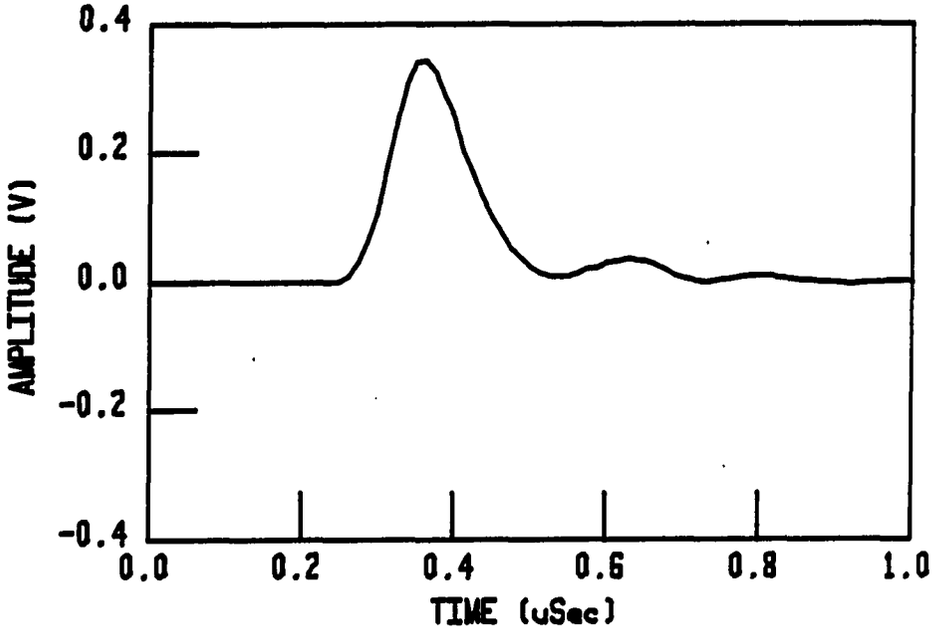

FIGURE 6.7. Pitch-catch waveform of #P18cz (transmitter) and 5 MHz PZT (receiver)

film geometries may be derived which will minimize the effects of diffraction on unipolar pulse propagation in water and tissue.

C. Conclusions

The applications work described in this chapter clearly demonstrates the power of the results of this research. Using the previously derived computer simulation models, ultrasound transducer designs for two applications were studied. The modified Mason's models and electrical tuning

techniques were useful in deriving theoretical designs for both passive and active transducers that would be well suited for broadband applications. It was the computer simulation program that really provided valuable insight for this work. The theoretical designs used in simulated experimental tests allow a designer to "see" the results.

The simulation results showed that by omitting the inductance of the shunt designs, and matching Q_e to Q_s, a transducer's bandwidth can be enhanced with little effect on sensitivity. Computer simulation results also showed that an active transducer design (FET source-follower receiver circuit) not only yields superior bandwidth and sensitivity, but also provides the same broadband performance with any pulser/receiver unit or coax cable length. The receiver load isolation capabilities of the active circuit design can thus make piezo film ultrasound transducers as versatile as their PZT ceramic counterparts.

The research results were also useful in investigating the potential for piezo films to play an important role in unipolar pulse ultrasound applications. Both simulation and actual test results confirmed the ability of a piezo ultrasound transducer to generate a high quality unipolar ultrasonic pulse. The problem of producing a differentiated (bipolar) waveform in response to an impinging unipolar

ultrasonic pulse, is being studied in an ongoing research project. However, a series-tuned active design may solve the differentiation problems. The results of this research will no doubt play a key role in solving such problems and enhancing designs for unipolar pulse-echo performance.

VII. SUMMARY OF RESULTS

The first part of this research, described in Chapter III, was devoted to the derivation of electromechanical circuit models used for piezo film ultrasound transducers. The frequency-dependent lossy properties of PVF_2 and $P(VF_2\text{-}VF_3)$ films prohibit the direct application of classical electromechanical circuit models. A method was derived for determining the piezoelectric constants and the frequency-dependent dielectric properties for the polymers from analysis of air-loaded broadband impedance measurements. These frequency dependent lossy properties were accounted for in a simple electrical impedance circuit model, and a modified version of Mason's classical circuit. The models showed excellent prediction of the electrical input impedance and piezoelectric parameters for many piezo film samples.

The modified Mason's models provided much new insight into the effects of high dielectric and mechanical losses on ultrasonic transducer performance. In addition, the models are needed to provide the impedance information required for the accurate design of broadband ultrasound transducers. The successful development of the circuit models has thus provided the means for new research concerning piezo film ultrasound applications.

After the development of the electromechanical circuit models, the second part of this research (discussed in Chapter IV) was devoted to implementing the models in a user-friendly interactive design/simulation program. The simulation program makes full use of the power of the electromechanical models. The program allows a user to design and test a piezo film ultrasound transducer under nearly any conceivable conditions. Thus, an investigator can quantitatively assess the ultrasonic performance of a prototype transducer without having to actually construct and test it. The power of this, of course, is that a user can optimize the design of a transducer for a particular application and "see" the results on a computer.

The third part of this research (discussed in Chapter V) involved the design, construction, and testing of $P(VF_2-VF_3)$ ultrasound transducers. Performance tests of the copolymer transducers showed excellent correlation with the performance predicted with the modified Mason's models via the simulation program. The successful design of the broadband probes came as a result of much experimental design and the use of the simulation program to derive an optimally tuned design. Thus, the third part of this research made practical use of the previous results. When tests of the actual transducers verified the accuracy of the simulation technique, the research was considered complete.

Chapter VI discussed some applications of this research. The broadband ultrasonic properties of the new $P(VF_2-VF_3)$ films show much promise for medical and NDE applications. The superior acoustic matching to tissue and water, and flexible properties of the piezo films will no doubt be useful in many future applications in medicine and materials science. The full potential of the piezo films will be realized only with the use of active transducer designs. Future improvements in the properties of the piezo films will further enhance their exciting broadband ultrasound performance, allowing new and unique applications to be studied. The results of this research will no doubt play a role in the future study of piezo films for ultrasound applications.

The results of this research have opened the doors for much new theoretical work for piezo film ultrasound applications. The modified Mason's models allow many unanswered questions to now be considered.

Nearly all published work concerning transducer design has been based on the use of a lossless piezoelectric material. These results, although sufficiently accurate for PZT materials and quartz, may not be valid for the piezo films. The modified Mason's models will provide the means for further study of lossy piezoelectric resonators. A

great deal of insight concerning optimum back-matching conditions and bandwidth enhancement could come as a result of studying the electromechanical transfer functions of the models. It is only through the study of such accurate models that the conditions for optimized designs will be known. It is conceivable that an entire thesis or dissertation research project could be directed to such a detailed theoretical study.

It is also hoped that improved designs for piezo film ultrasound transducers will be developed. The author's method of bonding, acoustic back matching, and electrical connections have been proven reliable. Future designs should include a shielded metal housing to reduce the effects of noise. The results of Chapter VI also showed that active probe designs will ultimately provide the highest sensitivity and most broadband ultrasound performance, provided one can develop a successful circuit design which could be housed in the probe.

A quarter-wavelength resonator should also be considered for future designs. A high acoustic impedance backing material, like brass, would permit quarter-wavelength resonance, and a piezo film element could be easily bonded to such a backing. Thus a shorter probe could be constructed without the need for manufacturing an acoustically matched backing material.

Finally, it is hoped that this research will lead to more interest in applying piezo films to medical ultrasound applications. This research showed that the new P(VF_2-VF_3) films possess sufficient properties to warrant interest in many medical applications. This research shows that piezo film ultrasound transducers should be considered for medical pulse-echo measurements--i.e., fat and thickness measurements, and imaging applications. Flexible transducers and arrays could be constructed for such applications. Enough details are now known concerning the piezo films to warrant serious consideration for any broadband ultrasound application.

VIII. BIBLIOGRAPHY

Alais, P.; Houchangnia, Z.; and Larmande, M. Th. "Analog Electrical Simulation of the Transient Behavior of Piezoelectric Transducers." In Acoustical Imaging, Vol. 10, pp. 731-750. Edited by P. Alais and A. F. Metherell. New York: Plenum Press, 1980.

Augustine, L. J.; and Andersen, J. "An Algorithm for the Design of Transformerless Broadband Equalizers of Ultrasonic Transducers." Journal of Acoustic Society of America, 66, No. 3 (September 1979):629-635.

Ballato, A.; Bertoni, H. L.; and Tamir, T. "Systematic Design of Stacked-Crystal Filters by Microwave Network Methods." IEEE Trans. on Microwave Theory and Techniques, MTT-22, No. 1 (January 1974):14-25.

Brown, L. F. Design of Wideband Ultrasound Instrumentation for Tissue Characterization. M.S. thesis. Iowa State University, Ames, Iowa, 1986.

Bui, L. N.; Shaw, H. J.; and Zitelli, L. T. "Study of Acoustic Wave Resonance in Piezoelectric PVF_2 Film." IEEE Trans. on Sonics and Ultrasonics, SU-24, No. 5 (September 1977):331-336.

Callerame, J.; Tancrell, R. H.; and Wilson, D. T. "Comparison of Ceramic and Polymer Transducers for Medical Imaging." Proceedings of IEEE Ultrasonics Symposium, Cat. CH1344-1/78, (1978):117-121.

Carome, E.; Shaw, H. J.; Weinstein, D.; and Zitelli, L. T. "PVF_2 Transducers for NDT." IEEE Ultrasonics Symposium (1979):346-349.

Challis, R. E.; and Harrison, J. A. "Transmission Circuits for Thick-Transducer Ultrasound Transmission Test Systems." Ultrasonics, 22, No. 3 (May 1984):103-109.

Chatigny, J. V. "Piezo Film Yields Novel Transducers." Electronics Week, 57, No. 17 (August 6, 1984):74-77.

Committee on Piezoelectric Crystals. "Standards on Piezoelectric Crystals, 1949." Proceedings of the IRE, 49 (December 1949):1378-1395.

Committee on Piezoelectric Crystals. "IRE Standards on Piezoelectric Crystals--The Piezoelectric Vibrator: Definitions and Methods of Measurement, 1957." Proceedings of the IRE, 57 (March 1957):353-358.

Committee on Piezoelectric and Ferroelectric Crystals. "IRE Standards on Piezoelectric Crystals: Determination of the Elastic, Piezoelectric, and Dielectric Constants--The Electromechanical Coupling Factor, 1958." Proceedings of the IRE, 58 (April 1958):764-777.

Committee on Piezoelectric and Ferroelectric Crystals. "IRE Standards on Piezoelectric Crystals: Measurements of Piezoelectric Ceramics, 1961." Proceedings of the IRE, 61 (July 1961):1161-1169.

Cromwell, L.; Weibell, F. J.; and Pfeiffer, E. A. Biomedical Instrumentation and Measurements. 2nd ed. Englewood Cliffs, New Jersey: Prentice-Hall, 1980.

Desilets, C. S.; Fraser, J. D.; and Kino, G. S. "The Design of Efficient Broad-Band Piezoelectric Transducers." IEEE Trans. on Sonics and Ultrasonics, SU-25, No. 3, (May 1978):115-125.

Dotti, D. "A New Model of a Piezoelectric Transducer for Direct Impulse Evaluation." IEEE Trans. on Sonics and Ultrasonics, SU-22, No. 3 (May 1975):202-205.

Filipczynski, L. "Transients, Equivalent Circuit and Negative Capacitance of a Piezoelectric Transducer Performing Thickness Vibrations." Journal of Technical Physics, 16, No. 2 (February 1975):121-135.

Foster, F. S.; Arditi, M.; Patterson, M. S.; Lee-Chahal, D.; and Hunt, J. W. "Breast Imaging With a Conical Array Hybrid Scanner." Ultrasound in Medicine and Biology, 9, No. 2 (1983):151-164.

Foster, F. S.; Strban, M.; and Austin, G. "The Ultrasound Macroscope: Initial Studies of Breast Tissue." Ultrasonic Imaging, 6, No. 3 (July 1984):243-162.

Gerber, E. A.; and Koerner, L. F. "Methods of Measurement of the Parameters of Piezoelectric Vibrators." Proceedings of the IRE, 58 (October 1958):1731-1737.

Goll, J. H.; and Auld, B. A. "Multilayer Impedance Matching Schemes for Broadbanding of Water Loaded Piezoelectric Transducers and High Q Electric Resonators." IEEE Trans. on Sonics and Ultrasonics, SU-22, No. 1 (January 1975):52-53.

Haumschild, D. J. An Ultrasonic Bragg Scattering Technique for the Quantitative Characterization of Marbling in Beef. Ph.D. dissertation, Iowa State University, Ames, Iowa, 1981.

Haumschild, D. J.; and Carlson, D. L. "An Ultrasonic Bragg Scattering Technique for the Quantitative Characterization of Marbling in Beef." Ultrasonics, 21, No. 5 (September 1983):226-233.

Hayward, G. "Using a Block Diagram Approach for the Evaluation of Electrical Loading Effects on Piezoelectric Reception." Ultrasonics, 24, No. 3 (May 1986):156-163.

Hayward, G. "A Systems Feedback Representation of Piezoelectric Transducer Operational Impedance." Ultrasonics, 22, No. 4, (July 1984):153-162.

Hayward, G.; and Jackson, M. N. "The use of z-Transforms in Modelling Piezoelectric Transducers." IEEE Ultrasonics Symposium (1983):883-886.

Hayward, G.; and Jackson, M. N. "Discrete-Time Modeling of the Thickness Mode Piezoelectric Transducer." IEEE Trans. on Sonics and Ultrasonics, SU-31, No. 3 (May 1984):137-150.

Hayward, G.; Gillies, D.; and Durrani, T. S. "A Multidimensional Linear Systems Model of the Piezoelectric Transducer." IEEE Ultrasonics Symposium (1984): 790-793.

Highmore, P. J. "Impedance Matching at Ultrasonic Frequencies Using Thin Transition Layers." Ultrasonics International Conference Proceedings (1973):112-118.

Houze, M.; Gazalet, M. G.; Rouvaen, J. M.; Nongaillard, B.; and Bridoux, E. "Adjustment of Piezoelectric Transducer Parameters for Bandwidth Enhancement." Ultrasonics, 23, No. 6 (November 1985):276-280.

Hsu, D. K. "Ultrasonic Scattering From a High Symmetry Fiber Composite Model." In Review of Progress in Quantitative Nondestructive Evaluation, Vol. 2A, pp. 965-74. Edited by Donald O. Thompson and Dale E. Chimenti. New York: Plenum Publishing Corporation, 1984.

Hue, J.; Ghazaleh, C.; Bruneel, C.; and Torguet, R. "Optimization Criterions for the Piezoelectric Transducers used in Acoustical Imaging." In Acoustical Imaging, Vol. 10, pp. 751-759. Edited by P. Alais and A. F. Metherell. New York: Plenum Press, 1980.

Hunt, J. W.; Arditi, M.; and Foster, F. S. "Ultrasound Transducers for Pulse-Echo Medical Imaging." IEEE Trans. on Biomedical Engineering, BME-30, No. 8 (August 1983):453-481.

Hutchens C. G.; and Morris, S. A. "A Three Port Model for Thickness Mode Transducers Using SPICE II." IEEE Ultrasonics Symposium (1984):897-902.

Jackson, M. N.; and Hayward, G. "A New Three-Port Model of the Thickness Mode Piezoelectric Transducer." IEEE Ultrasonics Symposium (1983):878-882.

Kazys, R.; and Lukosevicius, A. "Optimization of the Piezoelectric Transducer Response by Means of Electrical Correcting Circuits." Ultrasonics, 15, No. 3 (May 1977):111-116.

Kimura K.; and Ohigashi, H. "Ferroelectric Properties of Poly (vinylidenefluoride-trifluorothylene) Copolymer Thin Films." Journal of Applied Physics Letters, 43, No. 9 (November 1983):834-836.

Kossoff, G. "The Effects of Backing and Matching on the Performance of Piezoelectric Ceramic Transducers." IEEE Trans. on Sonics and Ultrasonics, SU-13, No. 1 (March 1966):20-31.

Kossoff, G.; Robinson, D. E.; and Garrett, W. J. "The C.A.L. Abdominal Echoscope." No. 31, Commonwealth Acoustic Laboratories, Commonwealth of Australia Department of Health, Sydney, Australia, March 1965.

Krimholtz, R.; Leedom, D. A.; and Matthaei, G. L. "New Equivalent Circuits for Elementary Piezoelectric Transducers." Electronics Letters, 6, No. 13 (June 25, 1970):398-399.

Lancee, C. T.; Souquet, J.; Ohigashi, H.; and Bom, N. "Ferro-electric Ceramics Versus Polymer Piezoelectric Materials." Ultrasonics, 23, No. 3 (May 1985): 138-142.

Leedom, D. A.; Krimholtz, R.; and Matthaei, G. L. "Equivalent Circuits for Transducers Having Arbitrary Even- or Odd-Symmetry Piezoelectric Excitation." IEEE Trans. on Sonics and Ultrasonics, SU-18, No. 3 (July 1971): 128-141.

Lewin, P. A. "Miniature Piezoelectric Polymer Ultrasonic Hydrophone Probes." Ultrasonics, 19, No. 5 (September 1981):213-216.

Lewin, P. A. "Miniature Piezoelectric Polymer Hydrophones in Biomedical Ultrasonics." Ferroelectrics, 60 (1984):127-139.

Lewis, G. K. "A Matrix Technique for Analyzing the Performance of Multilayered Front Matched and Backed Piezoelectric Ceramic Transducers." In Acoustical Imaging, Vol. 8 pp. 395-416. Edited by A. F. Metherell. New York: Plenum Press, 1978.

Low, G. C.; and Jones, R. V. "Design and Construction of Short Pulse Ultrasonic Probes for Nondestructive Testing." Ultrasonics, 22, No. 2 (March 1984):85-95.

Mason, W. P. Electromechanical Transducers and Wave Filters. 2nd ed. New York: Van Nostrand, 1948.

Mason, W. P. "Use of Piezoelectric Crystals and Mechanical Resonators in Filters and Oscillators." In Physical Acoustics, Vol. 1A, pp. 336-417. Edited by Warren P. Mason. New York: Academic Press, 1964.

Meeker, T. R. "Thickness Mode Piezoelectric Transducers." Ultrasonics, 10, No. 1 (January 1972):26-36.

Morris, S. A.; and Hutchens, C. G. "Implementation of Mason's Model on Circuit Analysis Programs." IEEE Trans. on Ultrasonics, Ferroelectrics, and Frequency Control, UFFC-33, No. 3 (May 1986):295-298.

Nilsson, J. W. Electric Circuits. Reading, MA: Addison-Wesley, 1983.

Ohigashi, H. "Electromechanical Properties of Polarized Polyvinylidene Fluoride Films as Studied by the Piezoelectric Resonance Method." Journal of Applied Physics, 47, No. 3 (March 1976):949-955.

Ohigashi, H.; and Koga, K. "Ferroelectric Copolymers of Vinylidenefluoride and Trifluoroethylene with a Large Electromechanical Coupling Factor." Japanese Journal of Applied Physics, 21, No. 8 (August 1982): L445-L457.

Papadakis, E. P. "Nonuniform Pressure Device for Bonding Thin Slabs to Substrates." Journal of Adhesion, 3, No. 3 (1972):181-194.

Patterson, P. E.; and Brown, L. F. "Biomechanical Waveform Analysis in the Frequency Domain." IEEE Trans. on Engineering in Medicine and Biology, 6, No. 3 (September 1987):12-16.

Pennwalt Corporation. Kynar Piezo Film Technical Manual. Pennwalt Corp., King of Prussia, PA, 1983.

Pennwalt Corporation. Methods and Applications of Piezo Plastic in Ultrasonics. Kynar Piezo Group, Pennwalt Corp., King of Prussia, PA, February 1986.

Pennwalt Corporation. Kynar Piezo Film Technical Manual. Pennwalt Corp., King of Prussia, PA, 1987.

Persson, H. W.; and Hertz, C. H. "Acoustic Impedance Matching of Medical Ultrasound Transducers." Ultrasonics, 23, No. 2 (March 1985):83-89.

Platte, M. "A Polyvinylidene Fluoride Needle Hydrophone for Ultrasonic Applications." Ultrasonics 23, No. 3 (May 1985):113-118.

Plonus, M. A. Applied Electromagnetics. New York: McGraw-Hill, 1978.

Ravinet, P.; Hue, J.; Volluet, G.; Hartemann, P.; Broussoux, D.; and Micheron, F. "Acoustic and Dielectric Loss Processes in PVF_2." IEEE Ultrasonics Symposium (1980):1017-1022.

Redwood, M. "Determination of the Parameters of a Piezoelectric Transducer from the Decay of Resonant Vibrations." Journal of the Acoustic Society of America, 34, No. 7 (July 1962):895-902.

Rhyne, T. L. "An Improved Interpretation of Mason's Model for Piezoelectric Plate Transducers." IEEE Trans. on Sonics and Ultrasonics, SU-25, No. 2 (March 1978): 98-103.

Rhyne, T. L. "Acoustic Instrumentation and Characterization of Lung Tissue." In Ultrasound In Biomedicine-Volume Two edited by D. N. White. Forest Grove, OR: Research Studies Press, 1977.

Saitoh, S.; Honda, H.; Kaneko, N.; Izumi, M.; and Suzuki, S. "The Method of Determining k_t and Q_m for Low Q Piezoelectric Materials." IEEE Ultrasonics Symposium (1985):620-623.

Sayers, C. M.; and Tait, C. E. "Ultrasonic Properties of Transducer Backings." Ultrasonics, 22, No. 2 (March 1984):57-60.

Schotton, K. C.; Bacon, D. R.; and Quilliam, R. M. "A PVDF Membrane Hydrophone for Operation in the Range 0.5 MHz to 15 MHz." Ultrasonics, 18, No. 3 (May 1980): 123-126.

Seitchik, J. A. "The Determination of Transducer Coupling Coefficients by Time Domain Analyses." IEEE Trans. on Sonics and Ultrasonics, SU-19, No. 1 (January 1972): 23-27.

Selfridge, A. R.; and Gehlbach, S. "KLM Transducer Model Implementation Using Transfer Matrices." IEEE Ultrasonics Symposium (1985):875-877.

Sessler, G. M. "Piezoelectricity in Polyvinylidenefluoride." Journal of Acoustic Society of America, 70, No. 6 (December 1981):1596-1608.

Silk, M. G. Ultrasonic Transducers for Nondestructive Testing. Bristol: Adam Hilger Ltd, 1984.

Sittig, E. K. "Transmission Parameters of Thickness-Driven Piezoelectric Transducers Arranged in Multilayer Configurations." IEEE Trans. on Sonics and Ultrasonics, SU-14, No. 4 (October 1967):167-174.

Stanke, F. E.; and Lang, S. W. "Automated System for Measuring the Constants of Low-Q Piezoelectric Materials." IEEE Ultrasonics Symposium (1985):656-661.

Swartz, R. G.; and Plummer, J. D. "On the Generation of High-Frequency Acoustic Energy with Polyvinylidene Fluoride." IEEE Trans. on Sonics and Ultrasonics, SU-27, No. 6 (November 1980a):295-302.

Swartz, R. G.; and Plummer, J. D. "Monolithic Silicon-PVF_2 Piezoelectric Arrays for Ultrasonic Imaging." In Acoustical Imaging, Vol. 8, pp. 69-95. Edited by A. F. Metherell. New York: Plenum Press, 1980b.

Thompson, D. O.; and Hsu, D. K. "Technique for Generation of Unipolar Ultrasonic Pulses." IEEE Trans. on Ultrasonics, Ferroelectrics, and Frequency Control, to be published in 1988.

Thompson, D. O.; Wormley, S. J.; Rose, J. H.; and Thompson, R. B. "Elastic Wave Scattering From Multiple Voids (Porosity)." In Review of Progress in Quantitative Nondestructive Evaluation, Vol. 2A, pp. 867-82. Edited by D. O. Thompson and D. E. Chimenti. New York: Plenum Publishing Corporation, 1983.

Thompson, R. B.; and Gray, T. A. "A Model Relating Ultrasonic Scattering Through Liquid-Solid Interfaces to Unbounded Medium Scattering Amplitudes." Journal of Acoustic Society of Acoustic Society of America, 74, No. 4 (1983):1279-1290.

Thijssen, J. M.; Verhoef, W. A.; and Cloostermans, M. J. "Optimization of Ultrasonic Transducers." Ultrasonics, 23, No. 1 (January 1985):41-46.

Tiersten, H. F. "Electromechanical Coupling Factors and Fundamental Material Constants of Thickness Vibrating Piezoelectric Plates." Ultrasonics, 8, No. 1 (January 1970):19-23.

Turner, C. W.; and Ishrak, S. O. "Comparison of Different Piezoelectric Transducer Materials for Optically Scanned Acoustic Imaging." In Acoustical Imaging, Vol. 10, pp. 761-78. Edited by P. Alais and A. F. Metherell. New York: Plenum Press, 1982.

van Kervel, S. J. H.; and Thijssen, J. M. "A Calculation Scheme for the Optimum Design of Ultrasonic Transducers." Ultrasonics, 21, No. 3 (May 1983):134-140.

van Randeraat, J,; and Setterington, R. E., ed. Piezoelectric Ceramics, 2nd ed. Eindhoven, The Netherlands: N. V. Philips' Gloeilampenfabrieken, 1974.

Webster, J. G., ed. Medical Instrumentation - Application and Design. Boston: Houghton Mifflin, 1978.

Wells, P. N. T. Physical Principles of Ultrasonic Diagnosis. New York: Academic Press, 1969.

Wells, P. N. T. Biomedical Ultrasonics. New York: Academic Press, 1977.

IX. ACKNOWLEDGEMENTS

I would like to express my gratitude to my major professors Dr. David L. Carlson and Dr. Curran S. Swift. I am very grateful for their confidence in me and support of my research desires, and could not have had better leadership for this work. Thanks for the freedom when I wanted it and the advice when I needed it! I am also deeply appreciative of the interest and enthusiasm shown by my graduate committee: Dr. R. G. Brown, Dr. F. C. Parrish, and Dr. D. F. Young.

I would like to express my gratitude for the technical and material assistance of Isochem Products (Lincoln, NE) and Pennwalt Corporation Piezo Film Group (Valley Forge, PA). In particular, I am especially grateful to Kumar Ogale of Pennwalt for supplying the many high quality piezo films used in this research.

I also want to thank Dr. Steve Russell of the Electrical Engineering Department for helping arrange for the loan of the HP4815A RF Impedance Meter from Rockwell International (Cedar Rapids, IA). A special thanks also goes to Rockwell International, especially to Dave Wilken.

I am also deeply indebted to the Biomedical Engineering Department, especially Dr. Mary H. Greer, for helping support my research. A special thanks also goes to Mike

Anderson who helped "turn" many Plexiglas transducer probe housings.

I would not have been able to continue my Ph.D. research without the generous support of Dr. J. O. Kopplin and the Electrical Engineering Department. I am also indebted to the Department of Electrical and Computer Engineering Endowment Advisory Board for my support through the Ruth and Murray Harpole Endowment Fund Graduate Fellowship. This generous support will always be remembered and appreciated, as I hope that one day I can somehow help others as you helped me.

I also wish to express my sincere gratitude to the personnel of the Center for NDE at the Ames Lab--Dr. D. Hsu, Dr. M. Hughes, Dr. D. O. Thompson, and S. Wormley. I am especially indebted to Dave Hsu for his personal interest and enthusiasm shown toward my research. I would also like to thank Don Thompson for the generous use of the Center's facilities for completing all of the performance tests of the piezo film transducers. I also look forward to further collaboration with Mike Hughes concerning unipolar ultrasound transducer designs.

I would also like to thank my parents for their undying support and confidence in me which has always inspired me to strive for excellence. Thanks for teaching me that any job

that is worth doing is worth doing well. I also want to thank my wife's parents for the many visits that cheered us up during some very long semesters.

A very special thanks goes to the most important people of my life--my family. In spite of the many difficult times during the last 8 years, I will always cherish the closeness of my family in these times. Danelle and I and our children, Karissa, Teresa, Jessica, and Andrea, have learned that having health and each other is having everything that counts.

Finally, I want to thank my grandparents, Lewis R. and Garnyth D. Brown. Mere words cannot express my love and admiration for them, nor my gratitude for their living and inspiring honesty and fairness. I dedicate this dissertation to the most honest upstanding person I have ever met, and a person who always has, and always will inspire me, my Grandpa Brown.

X. APPENDIX A: ZTRANSCR.FOR PROGRAM

```
C ***************************************************************************
C *                                                                         *
C *            LEW BROWN    26 MARCH 1987     ZTRANSCR.FOR                 *
C *                                                                         *
C *      General purpose program for reading in frequency, magnitude,      *
C *    and phase angle of HP 4815A impedance measurements and writing       *
C *    them out to a file.  Be sure to use a FORTRAN ASSIGN                 *
C *    statement for the desired file name.                                 *
C *                                                                         *
C *      The program prompts the user for the frequency, impedance          *
C *    magnitude, and impedance phase values for each reading.  To          *
C *    prevent writing erroneous data to the file, all entries are          *
C *    echoed back to the screen for confirmation.  Program                 *
C *    execution terminates when a 0 frequency value is entered.            *
C *                                                                         *
C ***************************************************************************
C
1     FORMAT(' ',F6.2,3X,F10.3,3X,F10.3)
C
C
      DO 1000 K=1,150
100      PRINT*,'ENTER F (MHz) , Z-MAG (Ohms) , Z-ANG (Deg)'
         READ*,F,ZM,ZA
         PRINT*,F,ZM,ZA
         PRINT*,'< ENTER 1 = CORRECT , 0 = INCORRECT >'
         READ*,NC
       IF(NC.EQ.0)GO TO 100
       IF(F.EQ.0)GO TO 1100
1000   WRITE(9,1)F,ZM,ZA
1100  STOP
      END
```

XI. APPENDIX B: ZCORRECT.FOR PROGRAM

```
C ***************************************************************************
C *              LEW BROWN  29 MARCH 1987  ZCORRECT.FOR                     *
C *                                                                         *
C *                                                                         *
C *      PROGRAM TO CORRECT HP4815A RF VECTOR IMPEDANCE READINGS.           *
C *                                                                         *
C *     This program is used to correct the raw HP 4815A impedance          *
C *   measurements for stray impedances.  The open circuit and short        *
C *   circuit impedances of the film test fixture are used to derive        *
C *   the shunt capacitance, and lead and contact resistance and            *
C *   inductance.  These values are removed from the measured               *
C *   impedance values to derive the corrected measurements of the          *
C *   piezo film air-loaded input impedance values.  Two different          *
C *   methods of correction are used.  On early sets of data, the           *
C *   short circuit and open circuit impedance values were explicitly       *
C *   read into the program and used for the correction.  At later          *
C *   dates, the open circuit and short circuit impedance values were       *
C *   used to derive the component values for shunt capacitance and         *
C *   lead impedance, and these values were written into the program.       *
C *   Both methods are shown (one is commented out).                        *
C *                                                                         *
C *     If using the actual open circuit and short circuit readings,        *
C *   you must remember to run the following sequence of file               *
C *   commands before running the program:                                  *
C *                                                                         *
C *                     D7                                                  *
C *                     ASSIGN (ZSC file) FOR007                            *
C *                     D8                                                  *
C *                     ASSIGN (ZOC file) FOR008                            *
C *                     D9                                                  *
C *                     D10                                                 *
C *                     ASSIGN ZFRAW_.DAT FOR009   where _ = file #         *
C *                     ASSIGN ZFILM_.DAT FOR010   "     "                  *
C *                                                                         *
C *                     HC_.DAT data is written to OUT.DAT via FOR006       *
C *                                                                         *
C *      Note: the raw (uncorrected values) are read in via FOR009,         *
C *   and a data file of the corrected results is written via FOR010.       *
C *   A comprehensive hardcopy file is created via FOR006.                  *
C *                                                                         *
C ***************************************************************************
C
      IMPLICIT REAL*8(A-H,O-Z)
      COMPLEX ZRAW(210),ZSC(210),ZOC(210),YRAW,YHAT,ZHAT,ZFILM,ZE,YOC,ZA
     +DD
      DIMENSION F(210)
      PI=3.141592654
```

```
5     FORMAT(' ','F(MHz)',3X,'MAG(ZFILM),Ohms',3X,'ARG(ZFILM),Deg',3X,'R
     +e(ZFILM),Ohms',3x,'Im(ZFILM),Ohms',3X,'Re(YIN),Mhos',3x,'Im(YIN),M
     +hos')
10    FORMAT(' ',2X,F5.1,5X,F8.2,12X,F6.1,9X,F9.3,7X,F9.3,6x,F9.5,6X,F9.
     +5)
11    FORMAT(' ',F6.2,3X,F9.3,3X,F9.3)
12    FORMAT(' ','CF=Correction Factor: Re{CF} = ',F7.4,3X,'Im{CF} = ',F
     +7.4)
C
C     GET THE DATA IN...
C
      PRINT*,'ENTER THE NUMBER OF VALUES '
      READ*,N
C      DO 100 K=1,N
C      READ(7,*)FREQ,ZM,ZA
C      F(K)=FREQ
C      ZRE=ZM*DCOS(ZA*PI/180.)
C      ZIM=ZM*DSIN(ZA*PI/180.)
C100   ZSC(K)=DCMPLX(ZRE,ZIM)
C
C
C
C      DO 200 K=1,NP1
C      READ(8,*)FREQ,ZM,ZA
C      ZRE=ZM*DCOS(ZA*PI/180.)
C      ZIM=ZM*DSIN(ZA*PI/180.)
C200   ZOC(K)=DCMPLX(ZRE,ZIM)
C
      Lsc=62.3E-9            ! The short circuit inductance 1-27-88.
      Rsc=0.724              ! The short circuit resistance 1-27-88.
      Coc=12.92E-12          ! The open circuit capacitance 1-27-88.
C
      DO 300 K=1,N
         READ(9,*)FREQ,ZM,ZA
         F(K)=FREQ
C
         ZOCIM=-1./(2.*PI*FREQ*1.E6*Coc)
         ZOC(K)=DCMPLX(ZERO,ZOCIM)
         ZSCIM=2.*PI*FREQ*1.E6*Lsc
         ZSC(K)=DCMPLX(Rsc,ZSCIM)
C
         ZRE=ZM*DCOS(ZA*PI/180.)
         ZIM=ZM*DSIN(ZA*PI/180.)
         ZRAW(K)=DCMPLX(ZRE,ZIM)
300   CONTINUE
C
C
         RE=0.            ! The electrode resistance
C
C     The correction factor is for differences in contact resistance
```

```
C     between samples from the same piezo film.
C
      PRINT*,'ENTER CORRECTION FACTOR TO ADD TO ZFILM,(Re,Im)'
      READ*,ADDRE,ADDIM
      ZADD=DCMPLX(ADDRE,ADDIM)
      WRITE(6,12)ADDRE,ADDIM
      WRITE(6,5)
C
C     Now ready to correct all the measurements...
C
      DO 1000 K=1,N
         YRAW=1./ZRAW(K)
         YOC=1./ZOC(K)
         ZERO=0.
         ZE=DCMPLX(RE,ZERO)
         YHAT=YRAW-YOC
         ZHAT=1./YHAT
         ZFILM=ZHAT-ZSC(K)-ZE+ZADD
         ZFMAG=CABS(ZFILM)
         ZFRE=REAL(ZFILM)
         ZFIM=AIMAG(ZFILM)
         ZFANG=ATAN2(ZFIM,ZFRE)*180./PI
         YFMAG=1./ZFMAG
         YFANG=-ZFANG
         YFRE=YFMAG*DCOS(YFANG*PI/180.)
         YFIM=YFMAG*DSIN(YFANG*PI/180.)
        WRITE(6,10)F(K),ZFMAG,ZFANG,ZFRE,ZFIM,YFRE,YFIM
       WRITE(10,11)F(K),ZFMAG,ZFANG
1000  CONTINUE
      STOP
      END
```

XII. APPENDIX C: ZFAVERAG.FOR PROGRAM

```
C ***************************************************************************
C *                                                                         *
C *          LEW BROWN  2 APRIL 1987    ZFAVERAG.FOR                        *
C *                                                                         *
C *                                                                         *
C *    Program to average HP4815A RF corrected impedance readings.          *
C *   This program is used to read in and average the three sets            *
C *   of broadband impedance values for a piezo film sample.                *
C *   The three files of impedance magnitude and phase are read in,         *
C *   averaged, and written to two files: a data file (via FOR010),         *
C *   and a comprehensive hardcopy file (via FOR006).                       *
C *                                                                         *
C *    The input files must be assigned to FOR021, FOR022, and              *
C *   FOR023.                                                               *
C *                                                                         *
C ***************************************************************************
      IMPLICIT REAL*8(A-H,O-Z)
      PI=3.141592654
4     FORMAT(' ','CF=Correction Factor: Re{CF} = ',F7.4,5X,' Im{CF} = ',
     +F7.4)
5     FORMAT(' ','F(MHz)',3X,'MAG(ZFILM),Ohms',3X,'ARG(ZFILM),Deg',3X,'R
     +e(ZFILM),Ohms',3x,'Im(ZFILM),Ohms',3X,'Re(YIN),Mhos',3x,'Im(YIN),M
     +hos')
10    FORMAT(' ',2X,F5.1,5X,F8.2,12X,F7.2,9X,F9.3,7X,F9.3,6X,F9.5,6X,F9.
     +5)
11    FORMAT(' ',F6.2,3X,F9.3,3X,F9.3)
C
C     If a correction factor for contact impedance was used for
C     for the corrections in ZCORRECT.FOR, print out that value
C     for the hardcopy printout.
C
      PRINT*,'ENTER CORRECTION FACTOR FOR PRINTOUT, Re{CF},Im{CF}'
      READ*,ADDRE,ADDIM
      WRITE(6,4)ADDRE,ADDIM
      WRITE(6,5)
C
C     Go get the data to be averaged...
C
      PRINT*,'ENTER NUMBER OF POINTS TO READ IN AND AVERAGE'
      READ*,N
      DO 100 K=1,N
        READ(21,*)F1,ZM1,ZA1
        READ(22,*)F2,ZM2,ZA2
        READ(23,*)F3,ZM3,ZA3
         FREQ=F1
         ZM=(ZM1+ZM2+ZM3)/3.
         ZA=(ZA1+ZA2+ZA3)/3.
```

```
          ZMRE=ZM*DCOS(ZA*PI/180.)
          ZMIM=ZM*DSIN(ZA*PI/180.)
          YM=1./ZM
          YA=-ZA
          YMRE=YM*DCOS(YA*PI/180.)
          YMIM=YM*DSIN(YA*PI/180.)
        WRITE(6,10)FREQ,ZM,ZA,ZMRE,ZMIM,YMRE,YMIM
        WRITE(10,11)FREQ,ZM,ZA
100   CONTINUE
      STOP
      END
```

XIII. APPENDIX D: ZDIELECT.FOR PROGRAM

```
C ***************************************************************************
C *                                                                         *
C *          LEW BROWN  15 MAY 1987     ZDIELECT.FOR                        *
C *                                                                         *
C *    Program to convert permittivity E(f), and dielectric loss            *
C *  tangent, DLOSS(f), from corrected piezo film impedance                 *
C *  measurements.  The user is prompted for the film thickness,            *
C *  and number of points.  The program creates a comprehensive             *
C *  hardcopy file, and two graphics files: one for the permittivity        *
C *  and one for the loss tangent.                                          *
C *                                                                         *
C *    Before running the program, assign  the following                    *
C *  FORTRAN devices for the appropriate files:                             *
C *                                                                         *
C *        ASSIGN inputfile.dat FOR020                                      *
C *        ASSIGN agraphfile.per FOR021    ( for permit. )                  *
C *        ASSIGN agraphfile.los FOR022    ( for loss tang. )               *
C *                                                                         *
C ***************************************************************************
C
      IMPLICIT REAL*8(A-H,O-Z)
1     FORMAT(' ','FREQ(MHz)',5X,'DLOSS(f)',5X,'REL. PERMIT',5X,'CAP.(pF)
     +',5X,'RO(Ohms)')
3     FORMAT(' ' )
4     FORMAT(' ','DIELECTRIC COMPUTATIONS FOR PVF2 FILM')
5     FORMAT(' ','DIELECTRIC COMPUTATIONS FOR P(VF2-VF3) FILM')
6     FORMAT(' ','FILM THICKNESS(Microns)= ',F6.2,4X,'K**2= ',F7.5,5X,'A
     +REA(m**2)= ',F11.9)
2     FORMAT(' ',F5.1,9X,F8.6,7X,F6.3,8X,F7.2,5X,F9.2)
10    FORMAT(' ','T RELATIVE DIELECTRIC PERMITTIVITY',5X,I3,2X,'POINTS')
11    FORMAT(' ','X FREQUENCY (MHz)')
12    FORMAT(' ','Y REL. PERMIT.')
13    FORMAT(' ',5X,I3,5X,'1')
14    FORMAT(' ',F10.6,5X,F10.6)
15    FORMAT(' ','T DIELECTRIC LOSS TANGENT',5X,I3,2X,'POINTS')
16    FORMAT(' ','X FREQUENCY (MHz)')
17    FORMAT(' ','Y LOSS TANGENT')
C
        PRINT*,'ENTER 1 = PVF2 , 2 = P(VF2-VF3)'
        READ*,NTYPE
        PRINT*,'ENTER NUMBER OF POINTS TO PROCESS'
        READ*,N
        PRINT*,'DO YOU WANT AGRAPH PLOTS ? 1 = YES , 0 = NO'
        READ*,NPLOT
      IF(NPLOT.NE.1)GO TO 70
        WRITE(21,10)N
        WRITE(21,11)
```

```
        WRITE(21,12)
        WRITE(21,13)N
        WRITE(22,15)N
        WRITE(22,16)
        WRITE(22,17)
        WRITE(22,13)N
70      PRINT*,'ENTER FILM THICKNESS IN MICRONS'
        READ*,THICK
         T=THICK*1.E-6
        PRINT*,'ENTER AREA OF FILM IN SQUARE METERS'
        READ*,AREA
        PRINT*,'ENTER K-squared FOR THIS FILM SAMPLE'
        READ*,AK2
C
      IF(NTYPE.EQ.2)GO TO 30
        WRITE(6,4)
      GO TO 40
30      WRITE(6,5)
40      WRITE(6,6)THICK,AK2,AREA
        WRITE(6,3)
        WRITE(6,1)
C
         A=1-AK2
         PI=3.141592654
         E0=8.854E-12
C
C
      DO 100 K=1,N
        READ(20,*)F,ZM,ZA
         FREQ=F*1.E6
         DLOSS=-A/DTAN(ZA*PI/180.)
         ROOT=DSQRT(1 + (A/DLOSS)**2 )
         C0=A/(ZM*ROOT*2.*PI*FREQ*DLOSS)
         PERMIT=C0*T/(E0*AREA)
         R0=A/(2.*PI*FREQ*C0*DLOSS)
         C=C0/1.E-12
        WRITE(6,2)F,DLOSS,PERMIT,C,R0
      IF(NPLOT.EQ.0)GO TO 100
        WRITE(21,14)F,PERMIT
        WRITE(22,14)F,DLOSS
100   CONTINUE
      STOP
      END
```

XIV. APPENDIX E: ZF0.FOR PROGRAM

```
C ***************************************************************************
C *                                                                         *
C *              LEW BROWN      14 JAN 1988       ZF0.FOR                  *
C *            #####     Program set for VA110G00     #####                 *
C *                                                                         *
C *                                                                         *
C *     This program reads in the impedance magnitude and phase data        *
C *   for a piezo film, and computes the resonant input impedances          *
C *   for the film.  Both Zs and Zp are printed out at user-specified       *
C *   frequencies, so that Fs and Fp may be computed.  The user may         *
C *   also elect to write graphics files for the relative dielectric        *
C *   permittivity and dielectric loss tangent.  A comprehensive            *
C *   hardcopy output file is written via FOR006.   Also note               *
C *   that the cubic spline subroutine CSPIN must be linked to the          *
C *   main program from the ISU PORTLIB: utility.                           *
C *                                                                         *
C *     Assign input file via ASSIGN (INFILE) FOR020                        *
C *     Hardcopy output is to OUT.DAT;* via FORTRAN WRITE device #6.        *
C *     ASSIGN (perm. plot) FOR030                                          *
C *     ASSIGN (dloss(f) plot) FOR031                                       *
C *                                                                         *
C ***************************************************************************
C
      IMPLICIT REAL*8(B-H,O-Z)
      DIMENSION AXD(14),AXE(13),AYD(14),AYE(13),AF(1),AER(1),ADLOSS(1)
      COMPLEX ZFILM,YFILM,Z2,Z3,Y3,ZC0,ZR0,YR0,YC0,YR0C0,ZR0C0,ZRES
C
C     INPUT THE DLOSS(F) AND Er(F) DATA VALUES TO INTERPOLATE...
C
      DATA AXE/.5,1.0,1.5,2.0,3.0,4.0,5.0,6.0,8.,10.,12.,15.,20./
      DATA AXD/.5,.75,1.0,1.5,2.0,3.0,4.0,5.0,6.0,8.,10.,12.,15.,20./
      DATA AYE/5.92,5.5,5.28,5.13,4.97,4.83,4.75,4.66,4.55,4.49,4.41,4.3
     +6,4.08/
      DATA AYD/.099,.106,.109,.113,.114,.115,.117,.118,.120,.123,.1255,.
     +128,.133,.140/
      ND=14
      NE=13
C
        PRINT*,'ENTER 1 = PLOT FILES FOR DIEL. DATA , 0 = NO FILES'
        READ*,NDPLOT
        PRINT*,'ENTER 1 = HARDCOPY FILE , 0 = NO HARDCOPY'
        READ*,NHARD
C
C
1     FORMAT('1 ',26X,'ZF0.FOR SIMULATION')
2     FORMAT(' ','PVDF SIMULATION : DIM (cm) = ',F8.4,' X ',F8.4,2X,'THI
     +CKNESS (Microns) = ',F8.4)
```

```
3     FORMAT('0' )
4     FORMAT(' ','   FREQ.',2X,'Mag(ZR0C0)',1X,'Arg{ZR0C0}',2X,'Re{Z3}',
     +5X,'Im{Z3}',5X,'Re{Z2}',3X,'Im{Z2}',3x,'Xa/Ra')
25    FORMAT(' ','  (MHz)',5X,'(Ohms)',5X,'(Deg)',5x,'(Ohms)',5x,'(Ohms
     +)',5X,'(Ohms)',3X,'(Ohms)')
5     FORMAT(' ',F7.3,4X,F7.2,3X,F7.2,3X,F8.2,3X,F8.2,3X,F8.2,1X,F9.2,1X
     +,F8.5)
40    FORMAT(' ',F7.2,5X,F12.6)
9     FORMAT(' ',' K**2 = ',F7.5)
C
50    FORMAT(' ','T INT. POLYNOMIAL PLOT OF Er(f) - ',I3,' Points')
51    FORMAT(' ','T INT. POLYNOMIAL PLOT OF DLOSS(f) - ',I3,' Points')
52    FORMAT(' ','Y REL. DIELECTRIC PERMITTIVITY')
53    FORMAT(' ','Y LOSS TANGENT ')
54    FORMAT(' ','X FREQUENCY (MHz)')
55    FORMAT(' ',2X,I4,5X,'1')
C
C     FIRST, GET THE INPUT DATA SPECS.....
C
      PI=3.1415926535
C90    PRINT*,'ENTER THE DIMENSIONS OF RECTANGLE - L(cm) , W(cm)'
90    CONTINUE
C        READ*,DL,DW
         DL=1.01885
         DW=1.
         DAREA=DL*DW*.0001
C        PRINT*,'ENTER THE THICKNESS OF THE PVDF FILM (Microns)'
C        READ*,DD
         DD=110.6
         T0=DD*1.E-6
        PRINT*,'ENTER THE NUMBER OF POINTS TO READ IN'
        READ*,N
C
C     NOW PRINT OUT THE SPECIFICATIONS....
C
      IF(NDPLOT.EQ.0)GO TO 88
        WRITE(30,50)N
        WRITE(31,51)N
        WRITE(30,52)
        WRITE(31,53)
        WRITE(30,54)
        WRITE(31,54)
        WRITE(30,55)N
        WRITE(31,55)N
C
88      WRITE(6,1)
        WRITE(6,2)DL,DW,DD
C
C *********************************************************************
C     HERE ARE THE PIEZOELECTRIC CONSTANTS NEEDED FOR THE
```

```
C     ANALYSIS...
C
         DAK2=0.
        WRITE(6,9)DAK2
        WRITE(6,3)
        WRITE(6,4)
        WRITE(6,25)
        WRITE(6,3)
        PRINT*,'ENTER MULT. FACTOR FOR PERMIT.'
        READ*,EFACT
        PRINT*,'ENTER MULT. FACTOR FOR DLOSS'
        READ*,DFACT
C
C*************************************************************************
C      HERE IS THE MAIN FREQUENCY LOOP.
C*************************************************************************
C
      NINT=1
      DO 100 I=1,N
        READ(20,*)FREQ,ZMAG,ZANG
         THETA=ZANG*PI/180.
         ZINRE=ZMAG*DCOS(THETA)
         ZINIM=ZMAG*DSIN(THETA)
         ZFILM=DCMPLX(ZINRE,ZINIM)
         YFILM=1./ZFILM
C
C     Now call the cubic spline interpolating routine..
C
         AF(1)=FREQ
      CALL CSPIN(AXE,AYE,NE,AF,AER,NINT)
      CALL CSPIN(AXD,AYD,ND,AF,ADLOSS,NINT)
         PERMIT=EFACT*AER(1)
         DL=DFACT*ADLOSS(1)
      IF(NDPLOT.EQ.0)GO TO 77
        WRITE(30,40)FREQ,PERMIT
        WRITE(31,40)FREQ,DL
77       C0=PERMIT*8.854E-12*DAREA/T0
         R0=(1.-DAK2)/(2.*PI*FREQ*1.E6*C0*DL)
         ZERO=0.
         ZR0=DCMPLX(R0,ZERO)
         ZC0=DCMPLX(ZERO,-1./(2.*PI*FREQ*1.E6*C0))
         YR0=1./ZR0
         YC0=1./ZC0
         YR0C0=YR0 + YC0
         ZR0C0=1./YR0C0
         ZR0C0RE=REAL(ZR0C0)
         ZR0C0IM=AIMAG(ZR0C0)
         ZR0C0MG=CABS(ZR0C0)
         ZR0C0AG=DATAN2(ZR0C0IM,ZR0C0RE)*180./PI
         Y3=YFILM - YR0C0
```

```
      Z3=1./Y3              ! Note, Z3 is the same as Zs.
      Z3RE=REAL(Z3)
      Z3IM=AIMAG(Z3)
      Z2=Z3 + ZC0           ! Note, Z2 is the same as Zp.
      Z2MAG=CABS(Z2)
      Z2RE=REAL(Z2)
      Z2IM=AIMAG(Z2)
C
      ZRES=ZFILM - ZC0
      RA=REAL(ZRES)
      XA=AIMAG(ZRES)
    IF(RA.GT.1.E-10)GO TO 999
      RA=1.E-10
999   RATIO=XA/RA
    IF(NHARD.EQ.0)GO TO 100
      WRITE(6,5)FREQ,ZR0C0MG,ZR0C0AG,Z3RE,Z3IM,Z2RE,Z2IM,RATIO
100 CONTINUE
    STOP
    END
```

XV. APPENDIX F: ZDEV.FOR PROGRAM

```
C ***************************************************************************
C *                                                                         *
C *         LEW BROWN      19 JUNE 1987     ZDEV.FOR                       *
C *                                                                         *
C *      Program to read in impedance simulation data from ZSIMP.FOR        *
C *   ZSEC.FOR, ZIN.FOR, and compare their percent deviations from the      *
C *   actual film impedance measurements.  The results are written out      *
C *   to a hardcopy file (via FORTRAN device #6) to file OUT.DAT;*.         *
C *   Graphics files for the deviations are also created.                   *
C *                                                                         *
C *   Assign the following device commands:                                 *
C *                                                                         *
C *   ASSIGN ZF____.DAT FOR020       Actual film results                    *
C *   ASSIGN ZSIMP_.DAT FOR021       ZSIMP.FOR results                      *
C *   ASSIGN ZSEC__.DAT FOR022       ZSEC.FOR results                       *
C *   ASSIGN ZIN___.DAT FOR023       ZIN.FOR results                        *
C *   ASSIGN DVPLOT.MAG FOR030      % Deviation plot of magnitude           *
C *   ASSIGN DVPLOT.PHS FOR031      % Deviation plot of phase               *
C *                                                                         *
C ***************************************************************************
C
      IMPLICIT REAL*8(A-H,O-Z)
1     FORMAT(' ',20X,'ZDEV.FOR RESULTS')
2     FORMAT(' ',' FREQ  *    Z(Measured)  *   Z(ZSIMP.FOR)',5X,'Z(ZSEC.
     +FOR)'5X,'Z(ZIN.FOR)')
3     FORMAT(' ',' (MHz) *    Mag   Phase  *   Mag    Phase',5X,'Mag   P
     +hase',5X,'Mag  Phase')
4     FORMAT(' ',1X,F5.2,' * ',F7.2,1X,F6.2,'  *  ',F6.3,2X,F6.3,3X,F6.3
     +,2X,F6.3,2X,F6.3,2X,F6.3)
5     FORMAT(' ','*************************************************
     +******************')
k     FORMAT(' ','NOTE: MAG is in Ohms , PHASE is in Degrees.')
7     FORMAT(' ',' Percent deviation of associated model data from actua
     +l measured value')
10    FORMAT(' ','T COMPARISON OF MODEL IMPEDANCE MAGNITUDES')
11    FORMAT(' ','Y IMPEDANCE MAGNITUDE DEVIATION (%)')
12    FORMAT(' ','X FREQUENCY (MHz)')
13    FORMAT(' ','T COMPARISON OF MODEL IMPEDANCE PHASES')
14    FORMAT(' ','Y PHASE DEVIATION (%)')
15    FORMAT(' ',I3,5X,'3')
16    FORMAT(' ',F7.2,3X,F12.6,3X,F12.6,3X,F12.6)
C
C
        PRINT*,'ENTER NUMBER OF POINTS TO PROCESS'
        READ*,N
        PRINT*,'ENTER 1 = DEVIATION PLOTS , 0 = NO PLOT'
        READ*,NPLOT
```

```
      IF(NPLOT.EQ.0)GO TO 50
        WRITE(30,10)
        WRITE(30,11)
        WRITE(30,12)
        WRITE(30,15)N
        WRITE(31,13)
        WRITE(31,14)
        WRITE(31,12)
        WRITE(31,15)N
50    CONTINUE
        WRITE(6,1)
        WRITE(6,2)
        WRITE(6,3)
        WRITE(6,5)
C
      DO 100 K=1,N
        READ(20,*)F,ZTRUE,PHSTRUE
        READ(21,*)F,ZSIMP,PHSSIMP
        READ(22,*)F,ZSEC,PHSSEC
        READ(23,*)F,ZIN,PHSZIN
C
         DZSMP=(ZSIMP*100./ZTRUE)-100.
         DPHSMP=100.-100.*(PHSSIMP/PHSTRUE)
C
         DZSC=(ZSEC*100./ZTRUE)-100.
         DPHSC=100.-100.*(PHSSEC/PHSTRUE)
C
         DZIN=(ZIN*100./ZTRUE)-100.
         DPHSZIN=100.-100.*(PHSZIN/PHSTRUE)
C
        WRITE(6,4)F,ZTRUE,PHSTRUE,DZSMP,DPHSMP,DZSC,DPHSC,DZIN,DPHSZIN
      IF(NPLOT.EQ.0)GO TO 100
        WRITE(30,16)F,DZSMP,DZSC,DZIN
        WRITE(31,16)F,DPHSMP,DPHSC,DPHSZIN
100   CONTINUE
        WRITE(6,5)
        WRITE(6,6)
        WRITE(6,7)
      STOP
      END
```

XVI. APPENDIX G: ZPLOT.FOR PROGRAM

```
C ***************************************************************************
C *                                                                         *
C *          LEW BROWN      23 MAY 1987        ZPLOT.FOR                   *
C *                                                                         *
C *    This program is for reading in piezo film data files and             *
C *   writing graphics files for plotting the impedance magnitude,          *
C *   impedance phase, and circular impedance and admittance plots.         *
C *                                                                         *
C *              YOU CAN ASSIGN DEVICE NUMBERS FOR:                         *
C *                                                                         *
C *          ASSIGN (input file name to read from) FOR010                   *
C *          ASSIGN (output filename 1, ie mag) FOR020                      *
C *          ASSIGN (output filename 2, ie phase) FOR021                    *
C *          ASSIGN (circular Z filename ) FOR023                           *
C *          ASSIGN (circular Y filename ) FOR024                           *
C *                                                                         *
C ***************************************************************************
C
1     FORMAT(' ','T PVF2 INPUT IMPEDANCE MAG. (ACTUAL) ',I3,' POINTS')
2     FORMAT(' ','T PVF2 INPUT IMPEDANCE PHASE (ACTUAL) ',I3,' POINTS')
3     FORMAT(' ','Y IMPEDANCE MAG. (Ohms)')
4     FORMAT(' ','Y IMPEDANCE PHASE (Deg)')
5     FORMAT(' ','X FREQUENCY (MHz)')
6     FORMAT(' ',3X,I3,5X,'1')
10    FORMAT(' ',F13.6,5X,F13.6)
20    FORMAT(' ','T CIRCULAR IMPEDANCE PLOT ',I3,' Points')
21    FORMAT(' ','T CIRCULAR ADMITTANCE PLOT ',I3,' Points')
22    FORMAT(' ','Y REACTANCE (Ohms)')
23    FORMAT(' ','X RESISTANCE (Ohms)')
24    FORMAT(' ','Y ADMITTANCE (Siemens)')
25    FORMAT(' ','X CONDUCTANCE (Siemens)')
C
      PI=3.141592654
        PRINT*,' ENTER NUMBER OF POINTS TO READ IN'
        READ*,N
        WRITE(20,1)N
        WRITE(21,2)N
        WRITE(20,3)
        WRITE(21,4)
        WRITE(20,5)
        WRITE(21,5)
        WRITE(20,6)N
        WRITE(21,6)N
        WRITE(23,20)N
        WRITE(23,22)
        WRITE(23,23)
        WRITE(23,6)N
```

```
      WRITE(24,21)N
      WRITE(24,24)
      WRITE(24,25)
      WRITE(24,6)N
    DO 1000 K=1,N
      READ(10,*)A,B,C
      WRITE(20,10)A,B
      WRITE(21,10)A,C
       ZINRE=B*COS(C*PI/180.)
       ZINIM=B*SIN(C*PI/180.)
      WRITE(23,10)ZINRE,ZINIM
       YIN=1./B
       YINRE=YIN*COS(C*PI/180.)
       YINIM=-YIN*SIN(C*PI/180.)
      WRITE(24,10)YINRE,YINIM
1000  CONTINUE
      STOP
      END
```

XVII. APPENDIX H: ZSIMP.FOR PROGRAM

```
C ***********************************************************************
C *                                                                     *
C *              LEW BROWN   14 JAN 1988      ZSIMP.FOR                 *
C *           #####     Program set for VA110G00      #####             *
C *                                                                     *
C *      This program is used to evaluate the simplified electrical     *
C *    impedance circuit model for a piezo film ultrasound transducer.  *
C *    An area of 1 cm x 1 cm is assumed, but also be changed as         *
C *    desired.  The relative dielectric permittivity and dielectric    *
C *    loss tangent values are are interpolated via a cubic spline      *
C *    interpolation routine (CSPIN) from the ISU VAX PORTLIB:          *
C *    utility.  The user must link the program's object code with the  *
C *    the PORTLIB: subroutine.                                         *
C *                                                                     *
C *      The user is prompted for (1) the number of points, (2) the     *
C *    lower frequency of interest, and (3) the upper frequency of      *
C *    interest.  The program computes the electrical input impedance   *
C *    of the simplified model.  The program creates output graphics    *
C *    files for (1) the input impedance magnitude, and (2) input       *
C *    impedance phase angle.                                           *
C *                                                                     *
C *       A comprehensive hardcopy file is written to OUT.DAT via       *
C *    FORTRAN device FOR006.  The graphics files are written using     *
C *    device numbers listed below:                                     *
C *                                                                     *
C *               Impedance magnitude:   FOR007                         *
C *                  Impedance phase:   FOR008                          *
C *                                                                     *
C ***********************************************************************
C
      IMPLICIT REAL*8(B-H,O-Z)
      DIMENSION  AXD(14),AXE(13),AYD(14),AYE(13),AF(1),AER(1),ADLOSS(1)
      COMPLEX ZR0,ZC0,ZIN,ZSEC,YIN,YSEC,YR0,YC0
C
C     INPUT THE DLOSS(F) AND Er(F) DATA VALUES TO INTERPOLATE ...
C
      DATA AXE/.5,1.0,1.5,2.0,3.0,4.0,5.0,6.0,8.,10.,12.,15.,20./
      DATA AXD/.5,.75,1.0,1.5,2.0,3.0,4.0,5.0,6.0,8.,10.,12.,15.,20./
      DATA AYE/5.92,5.5,5.28,5.13,4.97,4.83,4.75,4.66,4.55,4.49,4.41,4.3
     +6,4.08/
      DATA AYD/.099,.106,.109,.113,.114,.115,.117,.118,.120,.123,.1255,.
     +128,.133,.140/
      ND=14
      NE=13
C
1     FORMAT('1 ',26X,'ZSIMP.FOR SIMULATION')
3     FORMAT('0' )
```

```
4     FORMAT(' ','FREQ.',5X,'ZMAG',3X,'ARG(ZIN)',5X,'Re{Zin}',5x,'Im{Zin
     +}',5X,'Re{Z3}',5x,'Im{Z3}')
25    FORMAT(' ','(MHz)',4X,'(Ohms)',3x,'(Deg)',7x,'(Ohms)',6x,'(Ohms)',
     +6X,'(Ohms)',5x,'(Ohms)')
5     FORMAT(' ',F7.3,1X,F8.2,2X,F6.2,4x,F7.2,4X,F12.2,3X,F7.2,2X,F12.2)
26    FORMAT(' ',F7.3,3X,F8.2)
27    FORMAT(' ',F7.3,3X,F6.2)
2     FORMAT(' ',F8.3,3X,F12.6,3X,F12.6)
10     FORMAT(' ','R  (Ohms) = ',F7.2,5X,'C (pF) = ',F9.4,5X,'L (uH) = '
     +,F7.3)
40    FORMAT(' ','T SIMPLIFIED  MODEL INPUT IMPEDANCE - ',I3,' Points')
41    FORMAT(' ','Y IMPEDANCE MAGNITUDE (Ohms)')
42    FORMAT(' ','X FREQUENCY (MHz)')
43    FORMAT(' ','Y IMPEDANCE PHASE (Deg)')
44    FORMAT(' ',2X,I4,5X,'1')
45    FORMAT(' ',F7.2,5X,F10.6)
      PI=3.1415926535
        PRINT*,'ENTER THE NUMBER OF COMPUTATION POINTS DESIRED'
        READ*,N
         NP1=N+1
        PRINT*,'ENTER THE LOWER FREQUENCY LIMIT FOR ANALYSIS (MHz)'
        READ*,FLOW
        PRINT*,'ENTER THE UPPER FREQUENCY LIMIT FOR ANALYSIS (MHz)'
        READ*,FHIGH
         DELTAF=(FHIGH-FLOW)/FLOAT(N)
C
C     PRINT OUT THE PLOTTING TITLES FIRST...
C
        WRITE(7,40)NP1
        WRITE(7,41)
        WRITE(7,42)
        WRITE(7,44)NP1
C
        WRITE(8,40)NP1
        WRITE(8,43)
        WRITE(8,42)
        WRITE(8,44)NP1
C
C     NOW PRINT OUT THE SIMULATION SPECIFICATIONS...
C
        WRITE(6,1)
         C = 1.306E-12          ! Actual results for
         DL = 175.46E-6         !  film number
         R = 855.17             !    VA110G00.
         DK2=0.
         CC=C/1.E-12
         AAL=DL/1.E-6
         DAREA=1.01885E-4       ! The actual area for VA110G00
         T0=110.6E-6            ! The actual thickness for VA110G00
        WRITE(6,10)R,CC,AAL
```

```
        WRITE(6,4)
        WRITE(6,25)
90     CONTINUE
C
C*************************************************************************
C                HERE IS THE MAIN FREQUENCY LOOP                         *
C*************************************************************************
C
          NINT=1
       DO 100 I=1,NP1
          ZIM1=FLOAT(I-1)
          FREQ=FLOW+ZIM1*DELTAF
          AF(1)=FREQ
       CALL CSPIN(AXE,AYE,NE,AF,AER,NINT)
       CALL CSPIN(AXD,AYD,ND,AF,ADLOSS,NINT)
          PERMIT=AER(1)
          DLOSS=ADLOSS(1)
          C0=PERMIT*8.854E-12*DAREA/T0
          R0=(1.-DAK2)/(2.*PI*FREQ*1E6*C0*DLOSS)
          ZERO=0.
          ZC0=DCMPLX(ZERO,-1./(2.*PI*FREQ*1.E6*C0))
          ZR0=DCMPLX(R0,ZERO)
          YC0=1./ZC0
          YR0=1./ZR0
          XL=2.*PI*FREQ*1.E6*DL
          XC=1./(2.*PI*FREQ*1.E6*C)
          ZSEC=DCMPLX(R,XL-XC)
          ZSECRE=R
          ZSECIM=XL-XC
          YSEC=1./ZSEC
          YIN=YR0 + YC0 + YSEC
          ZIN=1./YIN
          ZINMAG=CABS(ZIN)
          ZINRE=REAL(ZIN)
          ZINIM=AIMAG(ZIN)
          ZINANG=DATAN2(ZINIM,ZINRE)*180./PI
        WRITE(6,5)FREQ,ZINMAG,ZINANG,ZINRE,ZINIM,ZSECRE,ZSECIM
        WRITE(7,26)FREQ,ZINMAG
        WRITE(8,27)FREQ,ZINANG
        WRITE(9,2)FREQ,ZINMAG,ZINANG
100    CONTINUE
       STOP
       END
C *************************************************************************
```

XVIII. APPENDIX I: ZSEC.FOR PROGRAM

```
C ***************************************************************************
C *                                                                         *
C *            LEW BROWN      ZSEC.FOR        14 JAN 1987                   *
C *          #####     Program set up for VAl10G00    #####                 *
C *                                                                         *
C *     This program is used to evaluate the simplified modified            *
C *   Mason's model for a piezo film ultrasound transducer.  The            *
C *   program use the PORTLIB: subroutine CSPIN to cubic spline             *
C *   interpolate the relative dielectric permittivity and dielectric       *
C *   loss tangent.  The PORTLIB subroutine must be linked with the         *
C *   object code of this program for execution.                            *
C *                .                                                        *
C *     The program prompts the user (1) for the number of points,          *
C *   (2) the low frequency of interest, and (3) the high frequency         *
C *   of interest.  The program than computes the electrical input          *
C *   impedance and prints out several graphics and hardcopy files.         *
C *   A comprehensive hardcopy file is created with FORTRAN device          *
C *   FOR006.  The graphics files are written with the devices              *
C *   outlined below:                                                       *
C *                                                                         *
C *          input impedance magnitude:  FOR007                             *
C *          input impedance phase:      FOR008                             *
C *          output deviation file:      FOR009                             *
C *                                                                         *
C *     The deviation file includes the model's computer values             *
C *   for frequency, impedance magnitude, and impedance phase at            *
C *   each point.  The file is then used by program ZDEV.FOR to             *
C *   compare actual and modeled impedance results.                         *
C *                                                                         *
C *     The simplified model does not include any electrode layers,         *
C *   thus it is the simplest modified Mason's model for a piezo            *
C *   film thickness mode resonator.                                        *
C *                                                                         *
C *     The hardcopy output file is used in analyzing film samples          *
C *   to determine the needed piezoelectric constants.  The values of       *
C *   frequency, Zs, Zp, etc. are used to compute the needed                *
C *   constants.                                                            *
C *                                                                         *
C ***************************************************************************
C
      IMPLICIT REAL*8(B-H,O-Z)
      DIMENSION AXD(14),AXE(13),AYD(14),AYE(13),AF(1),AER(1),ADLOSS(1)
      COMPLEX Z1,Z2,Z3,Y3,ZC0,ZR0,ZRm,Z10,Z20,YIN,ZIN
C
C     INPUT THE INTERPOLATING POLYNOMIAL COEFFICIENTS...
C
      DATA AXE/.5,1.0,1.5,2.0,3.0,4.0,5.0,6.0,8.,10.,12.,15.,20./
```

```
      DATA AXD/.5,.75,1.0,1.5,2.0,3.0,4.0,5.0,6.0,8.,10.,12.,15.,20./
      DATA AYE/5.92,5.5,5.28,5.13,4.97,4.83,4.75,4.66,4.55,4.49,4.41,4.3
     +6,4.08/
      DATA AYD/.099,.106,.109,.113,.114,.115,.117,.118,.120,.123,.1255,.
     +128,.133,.140/
      ND=14
      NE=13
C
1     FORMAT('1 ',26X,'ZSEC.FOR SIMULATION')
2     FORMAT(' ','PVDF SIMULATION : DIM (cm) = ',F8.4,' X ',F8.4,2X,'THI
     +CKNESS (Microns) = ',F8.4)
10    FORMAT(' ','V0  (m/sec) = ',F7.2,5X,' KT**2 = ',F7.5,5X,'Qm = ',F6
     +.3,2X,'Fs (MHz) = ',F9.6)
11    FORMAT(' ','      Km**2 = ',F7.5,7X,'K**2 = ',F7.5,7X,'Z-PVF2 (1.E
     +6 Rayls) = ',F7.5)
3     FORMAT('0' )
4     FORMAT(' ','FREQ.',5X,'ZMAG',3X,'ARG(ZIN)',2X,'RE(ZIN)',4X,'IM(ZIN
     +)',4X,'Re{Z3}',4X,'Im{Z3}',7X,'Im{Z2}')
25    FORMAT(' ','(MHz)',4X,'(Ohms)',3x,'(Deg)',5x,'(Ohms)',4x,'(Ohms
     +)',5X,'(Ohms)',4x,'(Ohms)',7X,'(Ohms)')
5     FORMAT(' ',F7.3,1X,F8.2,2X,F6.2,1X,F7.2,1X,F10.3,1X,F10.2,1X,F10
     +.2,4X,F9.2)
C
40    FORMAT(' ','T ZSEC IMPEDANCE SIMULATION ',I3,' Points')
41    FORMAT(' ','Y IMPEDANCE MAGNITUDE (Ohms)')
42    FORMAT(' ','Y IMPEDANCE PHASE (Deg)')
43    FORMAT(' ','X FREQUENCY (MHz)')
44    FORMAT(' ',2X,I4,5X,'1')
45    FORMAT(' ',F8.3,5X,F9.3)
46    FORMAT(' ',F8.3,3X,F12.6,3X,F10.6)
C
C     FIRST, GET THE INPUT DATA SPECS.....
C
      PI=3.1415926535
90    CONTINUE
      DL=1.01885
      DW=1.
      DAREA=DL*DW*.0001
C
C     COMMENT OUT LINES FOR THE DESIRED ACOUSTIC LOAD IMPEDANCE..
C     AIR = 397.2 , WATER = 1.48E6
C
         ZL=DAREA*397.2
C         ZL=DAREA*1.48E6
        DD=110.6
        T0=DD*1E-6
       PRINT*,'ENTER THE NUMBER OF COMPUTATION POINTS DESIRED'
       READ*,N
        NP1=N+1
       PRINT*,'ENTER THE LOWER FREQUENCY LIMIT FOR ANALYSIS (MHz)'
```

```
        READ*,FLOW
        PRINT*,'ENTER THE UPPER FREQUENCY LIMIT FOR ANALYSIS (MHz)'
        READ*,FHIGH
         DELTAF=(FHIGH-FLOW)/FLOAT(N)
        PRINT*,'ENTER: 1 = AGRAPH PLOTS , 0 = NO PLOTS'
        READ*,NPLOT
      IF(NPLOT.EQ.0)GO TO 60
        WRITE(7,40)NP1
        WRITE(7,41)
        WRITE(7,43)
        WRITE(7,44)NP1
        WRITE(8,40)NP1
        WRITE(8,42)
        WRITE(8,43)
        WRITE(8,44)NP1
C
C     NOW PRINT OUT THE SIMULATION SPECIFICATIONS....
C
60      WRITE(6,1)
        WRITE(6,2)DL,DW,DD
C     NOW,  CALCULATE THE DATA AND PROCEED....
C
C ***************************************************************************
C     HERE ARE THE PIEZOELECTRIC CONSTANTS NEEDED FOR THE
C     ANALYSIS...
C
         DAK2=0.          ! The dielectric frequency constant, k**2
C        PRINT*,'ENTER Kt-squared'
C        READ*,DAKT2      ! The electromech. coupling coefficient, Kt**2
         DAKT2=.0431      ! As of 1 Feb, 1988   see page 1642.
         DAKT=DSQRT(DAKT2)
        PRINT*,'ENTER V0 (m/s)   ( Using 2368.5    1 Feb 1988 )'
        READ*,V0
C         V0=2368.5       ! As of 1 Feb 1988 see pg 438.
         Fs=V0/(2.*T0)
         FSP=Fs/1.E6
         Z0=DAREA*1814.*V0 ! Using measurements of 13 JAN 1988.
         Z00=Z0/(DAREA*1.E6)
        PRINT*,' ENTER VALUE FOR Qm  ( Using 14.048     1 Feb 1988 )'
        READ*,Qm
C         Qm=14.048       ! As of 1 Feb, 1988   see page 1642.
         Cm=1.263E-12     ! Secondary capacitance, 14 Jan 1988.
        WRITE(6,10)V0,DAKT2,Qm,FSP
        WRITE(6,11)DAKM2,DAK2,Z00
        WRITE(6,3)
        WRITE(6,4)
        WRITE(6,25)
        WRITE(6,3)
C
C***************************************************************************
```

```
C      HERE IS THE MAIN FREQUENCY LOOP.
C*************************************************************************
C
          NINT=1
          FREQ=Fs/1.E6
          AF(1)=FREQ
       CALL CSPIN(AXE,AYE,NE,AF,AER,NINT)
          PERMIT=AER(1)
          C0s=PERMIT*8.854E-12*DAREA/T0
          PHIs=DAKT*SQRT(V0*C0s*Z0/T0)
C
       DO 100 I=1,NP1
          ZIM1=FLOAT(I-1)
          FREQ=FLOW+ZIM1*DELTAF
          AF(1)=FREQ
       CALL CSPIN(AXE,AYE,NE,AF,AER,NINT)
       CALL CSPIN(AXD,AYD,ND,AF,ADLOSS,NINT)
          PERMIT=AER(1)
          DLOSS=ADLOSS(1)
          C0=PERMIT*8.854E-12*DAREA/T0
          PHI=DAKT*SQRT(V0*C0*Z0/T0)
          R0=(1.-DAK2)/(2.*PI*FREQ*1E6*C0*DLOSS)
          THETA0=((2.*PI*FREQ*1.E6)/V0)*T0
C
C      MASON MODEL PARAMETERS...
C
          X20=Z0*DTAN(THETA0/2.)
          X10=Z0/DSIN(THETA0)
C
C      NOW CHANGE THE PARAMETERS TO COMPLEX...
C
          ZERO=0.
          Z10=DCMPLX(ZERO,-X10)
          Z20=DCMPLX(ZERO,X20)
          ZR0=DCMPLX(R0,ZERO)
C
C      NOW, FIND THE IMPEDANCE...
C
          ZC0=DCMPLX(ZERO,-1./(2.*PI*FREQ*1.E6*C0))
          Rm=(PHIs**2)/(2.*PI*FREQ*1.E6*Cm*Qm)
          ZRm=DCMPLX(Rm,ZERO)
          Z1=Z10 + Z20/2. + ZL/2. + ZRm
          Z2=Z1/(PHI**2)
          Z2IM=AIMAG(Z2)
          Z3=Z2 - ZC0
          Y3=1./Z3
          YIN=Y3 + 1./ZC0 + 1./ZR0
          ZIN=1./YIN
          ZINMAG=CABS(ZIN)
          ZINRE=REAL(ZIN)
```

```
          ZINIM=AIMAG(ZIN)
          ZINANG=DATAN2(ZINIM,ZINRE)*180./PI
          Z3MAG=CABS(Z3)
          Z3IM=AIMAG(Z3)
          Z3RE=REAL(Z3)
          Z3ANG=DATAN2(Z3IM,Z3RE)*180./PI
        WRITE(6,5)FREQ,ZINMAG,ZINANG,ZINRE,ZINIM,Z3RE,Z3IM,Z2IM
      IF(NPLOT.EQ.0)GO TO 100
        WRITE(9,46)FREQ,ZINMAG,ZINANG
        WRITE(7,45)FREQ,ZINMAG
        WRITE(8,45)FREQ,ZINANG
100   CONTINUE
      STOP
      END
```

XIX. APPENDIX J: ZIN.FOR PROGRAM

```
C ***************************************************************************
C *                                                                         *
C *            LEW BROWN      14 Jan 1988        ZIN.FOR                  *
C *           #####    Program set for VA110G00    #####                    *
C *                                                                         *
C *      This program is used to evaluate the full modified Mason's         *
C *   model for a piezo film ultrasound transducer.  The program uses       *
C *   the ISU VAX system PORTLIB library cubic-spline subroutine to         *
C *   interpolate the needed values for dielectric permittivity and         *
C *   dielectric loss tangent.  The cubic spline routine CSPIN must         *
C *   be linked to the main program's object code before execution.         *
C *                                                                         *
C *      The program prompts the user for (1) the number of points in       *
C *   the analysis, (2) low frequency of interest, (3) high frequency       *
C *   of interest, and (4) piezo film specifications.  When used with       *
C *   the author's algorithm, the hardcopy results (near resonance)         *
C *                                                                         *
C *   be used to determine the piezoelectric constants for a particular     *
C *   piezo film of interest.  The user should take note of the             *
C *   following assignment statements for the graphics files:               *
C *                                                                         *
C *      ASSIGN THE FOLLOWING DEVICES IF NEEDED:                            *
C *                                                                         *
C *   ASSIGN PLOT.MAG FOR007 , For AGRAPH plot of Z magnitude.              *
C *   ASSIGN PLOT.PHS FOR008 , For AGRAPH plot of Z phase angle.            *
C *   ASSIGN PLOT.ADM FOR009 , For AGRAPH plot of circular admittance.      *
C *   ASSIGN PLOT.IMP FOR010 , For AGRAPH plot of circular impedance.       *
C *   ASSIGN ZIN_DV.DAT FOR015, For ZDEV.DAT file.                          *
C *                                                                         *
C *      The deviation file, which includes the model's impedance           *
C *   magnitude, impedance phase, and frequency, is used by the             *
C *   program ZDEV.FOR for computing the percent deviations of the          *
C *   model's impedance values and actual measured data.                    *
C *                                                                         *
C *      The full Mason's model includes the electrode layers, thus         *
C *   the thickness and acoustic specifications for the layers must         *
C *   be included.                                                          *
C *                                                                         *
C *        NOTE: ALL COMPUTATIONS FOR REAL VARIABLES ARE IN                 *
C *                  IMPLICIT DOUBLE PRECISION                              *
C *                                                                         *
C ***************************************************************************
C *
      IMPLICIT REAL*8(B-H,O-Z)
      DIMENSION AXD(14),AXE(13),AYD(14),AYE(13),AF(1),AER(1),ADLOSS(1)
      COMPLEX ZTEMP1,ZTEMP2,ZTEMP3,Z1E,Z2E,Z10,Z20,Z1,Z2,ZC0,ZRm,ZIN,YIN
C #########################################################################
```

```
C #                                                                    #
C #   Input the Er(f) and DLOSS(f) values to interpolate...            #
C #                                                                    #
C #                                                                    #
C ######################################################################
      DATA AXE/.5,1.0,1.5,2.0,3.0,4.0,5.0,6.0,8.,10.,12.,15.,20./
      DATA AXD/.5,.75,1.0,1.5,2.0,3.0,4.0,5.0,6.0,8.,10.,12.,15.,20./
      DATA AYE/5.92,5.5,5.28,5.13,4.97,4.83,4.75,4.66,4.55,4.49,4.41,4.3
     +6,4.08/
      DATA AYD/.099,.106,.109,.113,.114,.115,.117,.118,.120,.123,.1255,.
     +128,.133,.140/
      ND=14
      NE=13
C #                                                                    #
C ######################################################################
C #                                                                    #
1     FORMAT(' ','PVDF SIMULATION : DIA(In)= ',F5.3,'  THICKNESS(Microns
     +)= ',F8.4)
2     FORMAT(' ','PVDF SIMULATION : DIM (cm) = ',F8.4,' X ',F8.4,2X,'THI
     +CKNESS (Microns) = ',F8.4)
19    FORMAT(' ','V0 (m/sec) = ',F7.2,2X,'KT**2 = ',F7.5,2X,'Qm = ',F6.3
     +,2X,'Fp(Theor.) (MHz) = ',F9.6)
22    FORMAT(' ',6X,'K**2 = ',F7.5,3X,'Z-PVF2 (1.E6Rayls) = ',F7.5,' Fp(
     +Damped) (MHz) = ',F9.6)
21    FORMAT('1',26X,'ZIN.FOR SIMULATION')
3     FORMAT('0' )
4     FORMAT(' ','FREQ.',5X,'ZMAG',3X,'ARG(ZIN)',2X,'RE(ZIN)',4X,'IM(ZIN
     +)',4X,'RE(YIN)',4X,'IM(YIN)', 5X,'RE(Z2)',5X,'IM(Z2)')
25    FORMAT(' ','(MHz)',4X,'(Ohms)',3x,'(Deg)',5x,'(Ohms)',4x,'(Ohms
     +)',5x,'(Siem.)',4x,'(Siem.)',5X,'(Ohms)',5x,'(Ohms)')
5     FORMAT(' ',F7.3,1X,F8.2,2X,F6.2,1X,F7.2,2X,F10.3,2X,F10.6,1X,F10.6
     +,3X,F10.3,1X,F10.3)
6     FORMAT(' ','T INPUT IMPEDANCE (MAG) Vs. FREQUENCY ',I3,' Points')
7     FORMAT(' ','T INPUT IMPEDANCE (PHASE) Vs. FREQUENCY ',I3,' Points'
     +)
8     FORMAT(' ','X FREQ (MHz)')
9     FORMAT(' ','Y INPUT IMPEDANCE MAGNITUDE (Ohms)')
10    FORMAT(' ','Y INPUT IMPEDANCE PHASE ANGLE (Deg)')
11    FORMAT(' ',2X,I4,5X,'1')
12    FORMAT(' ',F13.6,5X,F13.6)
13    FORMAT(' ','T INPUT ADMITTANCE DIAGRAM - ',I4,' POINTS')
14    FORMAT(' ','X CONDUCTANCE (Siemens)')
15    FORMAT(' ','Y SUSCEPTANCE (Siemens)')
16    FORMAT(' ','T INPUT IMPEDANCE DIAGRAM - ',I4,' POINTS')
17    FORMAT(' ','X RESISTANCE (Ohms)')
18    FORMAT(' ','Y REACTANCE (Ohms)')
990   FORMAT(' ',F8.3,5X,F12.6,5X,F12.6)
C
C     First. get the design specifications ...
C
```

```
      PI=3.1415926535
      PRINT*,'DO YOU WANT TO SPECIFY DIMENSIONS FOR DISC OR RECTANGLE ?'
      PRINT*,'     < ENTER 0 = RECTANGLE , 1 = DISC >'
      READ*,ISHAPE
      IF(ISHAPE.EQ.1)GO TO 90
      PRINT*,'ENTER THE DIMENSIONS OF RECTANGLE - L(cm) , W(cm)'
      READ*,DL,DW
C      DL=1.01885
C      DW=1.
      DAREA=DL*DW*.0001
      GO TO 95
90    PRINT*,'ENTER THE DIAMETER OF THE TRANSDUCER (Inches) '
      READ*,DIA
      RAD=DIA*.0254/2.
      DAREA=PI*RAD**2.
95    ZE=DAREA*19700.*3240.    ! Gold electrodes
C
C     Comment out lines for the desired acoustic load impedance...
C     AIR = 397.2 , WATER = 1.48E6 , PVF2 = 3.916E6
C
      ZL=DAREA*397.2
C      ZL=DAREA*1.48E6
C      PRINT*,'ENTER THE THICKNESS OF THE PVDF FILM (Microns)'
C      READ*,DD
      DD=110.6
      TO=DD*1E-6
      TE=300.E-10
      PRINT*,'ENTER THE NUMBER OF COMPUTATION POINTS DESIRED'
      READ*,N
      NP1=N+1
      PRINT*,'ENTER THE LOWER FREQUENCY LIMIT FOR ANALYSIS (MHz)'
      READ*,FLOW
      PRINT*,'ENTER THE UPPER FREQUENCY LIMIT FOR ANALYSIS (MHz)'
      READ*,FHIGH
      DELTAF=(FHIGH-FLOW)/FLOAT(N)
C
C     Now, print out the simulation specifications ...
C
      PRINT*,'DO YOU WANT A HARDCOPY OF RESULTS ?'
      PRINT*,'< ENTER 1 = YES , 0 = NO >'
      READ*,NHARD
      IF(NHARD.EQ.0)GO TO 200
      WRITE(6,21)
      IF(ISHAPE.EQ.1)GO TO 96
      WRITE(6,2)DL,DW,DD
      GO TO 97
96    WRITE(6,1)DIA,DD
97    CONTINUE
C
C     Now print out the AGRAPH titles if so desired ...
```

```
C
200   CONTINUE
      PRINT*,'DO YOU WANT AGRAPH PLOTS ? '
      PRINT*,' <  0 = NO , 1 = ALL PLOTS, 2 = ADM. DIAGRAM, 3 = IMP. DIA
     +GRAM >'
      READ*,NPLOT
      IF(NPLOT.EQ.0)GO TO 80
      IF(NPLOT.EQ.2)GO TO 70
      IF(NPLOT.EQ.3)GO TO 60
      WRITE(7,6)NP1
      WRITE(8,7)NP1
      WRITE(7,8)
      WRITE(8,8)
      WRITE(7,9)
      WRITE(8,10)
      WRITE(7,11)NP1
      WRITE(8,11)NP1
60    WRITE(10,16)N
      WRITE(10,17)
      WRITE(10,18)
      WRITE(10,11)NP1
      IF(NPLOT.EQ.3)GO TO 80
70    WRITE(9,13)N
      WRITE(9,14)
      WRITE(9,15)
      WRITE(9,11)NP1
C
C     Now proceed to calculate the impedances ...
C
C ********************************************************************
C     HERE ARE THE PIEZOELECTRIC CONSTANTS NEEDED FOR THE
C     ANALYSIS...
C
80    DAK2=0.                  ! The dielectric frequency constant.
C      PRINT*,'ENTER VALUE FOR KT**2  ( Using .0428   1 FEB 1988)'
C      READ*,DAKT2
      DAKT2=.0428              ! See page 1642.
      DAKT=DSQRT(DAKT2)
C      PRINT*,'ENTER V0 (m/s)  ( Using 2382.5  1 Feb 1988)'
C      READ*,V0
      V0=2382.5                ! See page 1642.
      Fs=V0/(2.*T0)
      FsD=10.707505            ! The damped (observed) Fs - see page 1642.
      FSP=Fs/1.E6
      Z0=1814.*V0*DAREA
C      PRINT*,'ENTER Qm     ( Using 14.039   1 Feb 88 )'
C      READ*,Qm
      Qm=14.039                ! See page 1642.
      IF(NHARD.EQ.0)GO TO 39
      WRITE(6,19)V0,DAKT2,Qm,FSP
```

```
      Z00=Z0/(1.E6*DAREA)
      WRITE(6,22)DAK2,Z00,FsD
      WRITE(6,3)
      WRITE(6,4)
      WRITE(6,25)
39    CONTINUE
      FREQ=Fs/1.E6
      AF(1)=FREQ
      NINT=1
      CALL CSPIN(AXE,AYE,NE,AF,AER,NINT)
      PERMIT=AER(1)
      C0s=PERMIT*8.854E-12*DAREA/T0
      PHIs=DAKT*DSQRT(V0*C0s*Z0/T0)
      Cm=1.263E-12      ! The secondary mechanical capacitance, pg 1642.
C                                                                       *
C ***********************************************************************
C*    HERE IS THE MAIN FREQUENCY LOOP.                                  *
C ***********************************************************************
C                                                                       *
      DO 100 I=1,NP1
      ZIM1=FLOAT(I-1)
      FREQ=FLOW+ZIM1*DELTAF
      AF(1)=FREQ
      CALL CSPIN(AXE,AYE,NE,AF,AER,NINT)
      CALL CSPIN(AXD,AYD,ND,AF,ADLOSS,NINT)
      PERMIT=AER(1)
      DLOSS=ADLOSS(1)
      PRINT*,'FREQ = ',FREQ
      C0=PERMIT*8.854E-12*DAREA/T0
      PRINT*,'C0 = ',C0
      PHI=DAKT*DSQRT(V0*C0*Z0/T0)
C
C     Find the dielectric loss resistance ...
C
      R0=(1.-DAK2)/(2.*PI*FREQ*1.E6*C0*DLOSS)
C
C     Now find the Mason's model input impedance ...
C
      THETA0=((2.*PI*FREQ*1.E6)/V0)*T0
      THETAE=((2.*PI*FREQ*1.E6)/3240.)*TE
C
C     Mason's model parameters ...
C
      X2E=ZE*DTAN(THETAE/2.)
      X1E=ZE/DSIN(THETAE)
      X20=Z0*DTAN(THETA0/2.)
      X10=Z0/DSIN(THETA0)
C
C     Now, change the parameters to complex variables ...
C
```

```
      ZERO=0.
      Z1E=DCMPLX(ZERO,-X1E)
      Z10=DCMPLX(ZERO,-X10)
      Z2E=DCMPLX(ZERO,X2E)
      Z20=DCMPLX(ZERO,X20)
      ZR0=DCMPLX(R0,ZERO)
      ZC0=DCMPLX(ZERO,-1./(2.*PI*FREQ*1.E6*C0))
      Rm=(PHIs**2)/(2.*PI*FREQ*1.E6*Cm*Qm)
      ZRm=DCMPLX(Rm,ZERO)
C
C     Now, find the impedance ...
C
      ZTEMP1=CMPLX(ZL,X2E)
      ZTEMP2=ZTEMP1*Z1E/(ZTEMP1 + Z1E)
      Z1=ZTEMP2 + Z2E + Z20
      Z2=(ZRm+ Z10 + Z1/2.)/(PHI**2.)
      Z2RE=REAL(Z2)
      Z2IM=AIMAG(Z2)
      ZTEMP3=Z2 - ZC0
      ZIN=ZC0*ZTEMP3/(ZC0 + ZTEMP3)
      YIN=1./ZIN
      ZIN = ZIN*ZR0/(ZIN + ZR0)
      YIN=1./ZIN
      ZINMAG=CABS(ZIN)
      ZINRE=REAL(ZIN)
      ZINIM=AIMAG(ZIN)
      SUSCEP=AIMAG(YIN)
      COND=REAL(YIN)
      ZINANG=DATAN2(ZINIM,ZINRE)*180./PI
      WRITE(15,990)FREQ,ZINMAG,ZINANG
      IF(NHARD.EQ.0)GO TO 998
      WRITE(6,5)FREQ,ZINMAG,ZINANG,ZINRE,ZINIM,COND,SUSCEP,Z2RE,Z2IM
998   IF(NPLOT.EQ.0)GO TO 100
      IF(NPLOT.EQ.2)GO TO 50
      IF(NPLOT.EQ.3)GO TO 55
      WRITE(7,12)FREQ,ZINMAG   ! Write out the impedance magnitude
      WRITE(8,12)FREQ,ZINANG   ! Write out the impedance phase
55    WRITE(10,12)ZINRE,ZINIM  ! Write out impedance components
      IF(NPLOT.EQ.3)GO TO 100
50    WRITE(9,12)COND,SUSCEP   ! Write out circular admittance values
100   CONTINUE
      STOP
      END
```

XX. APPENDIX K: XFER.FOR PROGRAM

```
C ************************************************************************
C *                                                                      *
C *              LEW BROWN      XFERG.FOR        15 Jan 1988             *
C *                                                                      *
C *          #####        Program set up for VA110G00   #####          *
C *          #####        110.6 micron P(VF2-VF3)       #####          *
C *                                                                      *
C *                                                                      *
C *    This program is used to simulate the electromechanical           *
C * performance of P(VF2-VF3).  The program makes use of the             *
C * piezoelectric constants and the model values derived from            *
C * ZSEC*.FOR and ZIN*.FOR.  The relative dielectric                     *
C * permittivity, Er(f), and the dielectric loss tangent,                *
C * DLOSS(f), values were extrapolated from 0.5-50.5 MHz to 0-100 MHz    *
C * and the user may elect to obtain AGRAPH graphics plot files for      *
C * either function.  A cubic spline interpolating routine, CSPIN(*),    *
C * from the VAX PORTLIB: library of subroutines is used and thus        *
C * access to the PORTLIB: routines must be specified in the LINKing     *
C * of the object code.                                                  *
C *                                                                      *
C *    The program is capable of computing (1) the voltage impulse       *
C * response, (2) the voltage step response, (3) the current impulse     *
C * response, and/or (4) the sinusoidal burst response of the XMTR,      *
C * RCVR, or XMTR/RCVR, for either the simplified model (no electrodes)* *
C * or the full model (including electrodes).  The user can also         *
C * specify the back-to-front acoustic load impedance ratio and/or       *
C * inductively shunt tune the transducer to any multiple of the series* *
C * resonant frequency, Fs.  In addition, the user may elect to supply   *
C * an actual waveform for application to a specific transducer design   *
C * (selected by serial number).                                         *
C *                                                                      *
C *    The frequency domain sinusoidal steady state response (mag and    *
C * phase) for each simulation frequency is written to a graphics file,* *
C * as well as the inverse FFT time domain results.  All time domain     *
C * values are the results of zero-padding the spectral results (just    *
C * before calling the relevant FFT) to 8 times their original length.   *
C * This insures "smooth" time domain plots without adding any further   *
C * information to the analysis results.  Since it will not always be    *
C * desirable to have such great resolution, the user may choose to      *
C * write out only every Kth value to the time domain graphics files.    *
C *                                                                      *
C *     NOTE: All real variables, except those that begin with "A",      *
C * are in implicit double precision.                                    *
C *                                                                      *
C *    The program uses the following FORTRAN write devices numbers to   *
C * create the output graphics files:                                    *
C *                                                                      *
```

```
C * FORTRAN DEVICE #                GRAPHICS FILE                          *
C *                                                                         *
C *        7              Relative dielectric permittivity, Er(f)          *
C *        8              Dielectric loss tangent, DLOSS(f)                *
C *       10              Voltage impulse response of XMTR (mag)           *
C *       11                    "            "          (phs)              *
C *       12              Voltage impulse response of RCVR (mag)           *
C *       13                    "            "          (phs)              *
C *       14              Voltage impulse response of XMTR/RCVR (mag)      *
C *       15                    "            "                (phs)       *
C *       16              Voltage impulse response of RCVR (mag)           *
C *       17                    "            "          (phs)              *
C *       18              Voltage step response of XMTR (mag)              *
C *       19                    "            "       (phs)                 *
C *       20              Voltage step response of XMTR/RCVR (mag)         *
C *       21                    "            "          (phs)              *
C *       22              Current impulse response of XMTR (mag)           *
C *       23                    "            "          (phs)              *
C *       24              Spectrum of input sinewave burst (mag)           *
C *       25                    "            "          (phs)              *
C *       30              Voltage impulse response of XMTR (time)          *
C *                     or Sinewave burst response of XMTR (time)          *
C *       31              Voltage impulse response of RCVR (time)          *
C *       32              Voltage impulse response of XMTR/RCVR (time)     *
C *                     or Sinewave burst response of XMTR/RCVR (time)     *
C *       33              Voltage step response of XMTR (time)             *
C *       34              Voltage step response of XMTR/RCVR (time)        *
C *       35              Current impulse response of XMTR (time)          *
C *       36              Current impulse response of XMTR/RCVR (time)     *
C *       40              Input sinewave burst waveform                    *
C *                                                                         *
C *    This program is the result of "adding on" to the program ZIN.FOR*
C * and evolved a section at a time.  It was not initially conceived    *
C * that the program would develop into the now complex form.  However,*
C * it is well documented and despite its lack of subroutine structure,*
C * it is easy to follow.                                               *
C *                                                                         *
C *                        It isn't slim,                                   *
C *                        It doesn't "shine";                              *
C *                        But it works great,                              *
C *                        And it's all mine!                               *
C *                                                                         *
C ***************************************************************************
C
      IMPLICIT REAL*8(B-H,O-Z)
C
      DIMENSION AXD(17),AXE(16),AYD(17),AYE(16),AF(1),AER(1),ADLOSS(1),F
     +T(4096),FTCALL(4096),VZLFXIMG(4096),VZLFXIAN(4096),VRCVRIMG(4096),
     +VRCVRIAN(4096),VXMRCIMG(4096),VXMRCIAN(4096),VZLFXSMG(4096),VZLFXS
     +AN(4096),VXMRCSMG(4096),VXMRCSAN(4096),VZLFIIMG(4096),VZLFIIAN(409
```

```
     +6),VXMRIIMG(4096),VXMRIIAN(4096),TEMP1(4096),TEMP2(4096),ACORRECT(
     +1),AFREQRAD(104),ARADCOR(104),APANX(11),APANRe(11),APANIm(11)
C
      COMPLEX Z,Z1,Z2,Z3,Z5,Z6,Z7,Z8,Z9,Z10,ZB,ZBE,ZBET,ZF,ZFE,ZFET,ZINX
     +,ZR0,ZC0,ZR0C0,ZSHUNTL,ZINR,Vin,VPRIX,VSECX,VZ,VZE,VZFE,VZLFXI,VZ3
     +,VZ7,VZ9,VZ10,VSECRI,VPRIRI,VXMRCI,VRCVRI,VZLFXS,VPRIR,VXMRCS,DIin
     +,IZ3,VZLFII,VXMRII,ZMF,ZFM,VZFM,Z11,Z12,Z13,VZ12,ZINLS,ZCABLE,ZINT
     +S,ZRLS,ZR0C0LS,VR0C0LS,ZCPULSER,ZPULSER,PANZR
C
C     INPUT THE INTERPOLATING POLYNOMIAL COEFFICIENTS...
C
      DATA AXE/0.,.01,.5,1.0,1.5,2.0,3.0,4.0,5.0,6.0,8.,10.,12.,15.,20.,
     +50./
      DATA AXD/0.,.01,.5,.75,1.0,1.5,2.0,3.0,4.0,5.0,6.0,8.,10.,12.,15.,
     +20.,50./
      DATA AYE/7.42,7.155,5.92,5.5,5.28,5.13,4.97,4.83,4.75,4.66,4.55,4.
     +49,4.41,4.36,4.08,2.85/
      DATA AYD/.012,.016,.099,.106,.109,.113,.114,.115,.117,.118,.120,.1
     +23,.1255,.128,.133,.140,.1925/
      ND=17
      NE=16
C
      AFREQRAD(1)=0.
      AFREQRAD(2)=0.5
      DO L=1,100
      AFREQRAD(L+2)=.8 + FLOAT(L)*0.2
      END DO
      AFREQRAD(103)=25.
      AFREQRAD(104)=60.
      DATA ARADCOR/.12,.28,.4594,.5317,.5946,.6472,.6895,.7214,.7435,.75
     +67,.7623,.7620,.7575,.7509,.7441,.7387,.7361,.7370,.7415,.7492,.75
     +91,.7702,.7812,.7913,.7994,.8053,.8088,.8101,.8095,.8078,.8056,.80
     +37,.8028,.8031,.8050,.8084,.8129,.8181,.8235,.8285,.8327,.8358,.83
     +78,.8385,.8383,.8374,.8363,.8353,.8349,.8352,.8364,.8385,.8413,.84
     +45,.8478,.8509,.8536,.8555,.8567,.8571,.8569,.8564,.8557,.8551,.85
     +49,.8552,.8561,.8576,.8596,.8618,.8642,.8663,.8681,.8694,.8702,.87
     +04,.8703,.8699,.8694,.8690,.8689,.8693,.8701,.8711,.8727,.8745,.87
     +61,.8778,.8768,.8794,.8804,.8801,.8802,.8801,.8786,.8798,.8773,.88
     +13,.8826,.8797,.8828,.8842,.9,.9/
      NR=104
C
      DATA APANX/0.,4.,8.,12.,16.,20.,24.,28.,32.,36.,40./
      DATA APANRe/250.,236.1,208.9,156.6,118.8,60.1,41.5,23.3,16.,8.1,5.9
     +2/
      DATA APANIm/0.,-25.8,-53.8,-68.6,-67.5,-55.2,-35.7,-14.7,-2.93,5.26
     +,11.19/
      NP=11
C
C ######################################################################
C
```

```
10    FORMAT(' ','T VA110G00 VOLT. IMPULSE RESP. OF XMTR - ',I4,' Points
     +')
11    FORMAT(' ','T VA110G00 VOLT. IMPULSE RESP. OF RCVR - ',I4,' Points
     +')
12    FORMAT(' ','T VA110G00 VOLT. IMPULSE RESP. XMTR/RCVR - ',I4,' Poin
     +ts')
13    FORMAT(' ','T VA110G00 VOLT. STEP RESP. OF XMTR - ',I4,' Points')
14    FORMAT(' ','T VA110G00 VOLT. STEP RESP. OF XMTR/RCVR - ',I4,' Poin
     +ts')
15    FORMAT(' ','Y VOLTAGE MAGNITUDE (dB)')
16    FORMAT(' ','Y VOLTAGE PHASE (Deg)')
17    FORMAT(' ','Y VOLTAGE (Volts)')
18    FORMAT(' ','X FREQUENCY (MHz)')
19    FORMAT(' ','X TIME (Sec)')
20    FORMAT(' ',2X,I4,5X,'1')
21    FORMAT(' ',F18.10,3X,F18.10)
22    FORMAT(' ',E13.6,3X,E13.6)
23    FORMAT(' ','T VA110G00 CURR. IMPULSE RESP. OF XMTR - ',I4,' Points
     +')
24    FORMAT(' ','T VA110G00 CURR. IMPULSE RESP. OF XMTR/RCVR - ',I4,' P
     +oints')
25    FORMAT(' ','T VA110G00 INPUT BURST WAVEFORM - ',I4,' Points')
26    FORMAT(' ','T VA110G00 INPUT BURST SPECTRUM - ',I4,' Points')
27    FORMAT(' ','T VA110G00 XMTR BURST RESPONSE - ',I4,' Points')
28    FORMAT(' ','T VA110G00 XMTR/RCVR BURST RESPONSE - ',I4,' Points')
29    FORMAT(' ','T VA110G00 INPUT PULSE WAVEFORM ',I4,' Points')
30    FORMAT(' ','T VA110G00 INPUT WAVEFORM SPECTRUM ',I4,' Points')
31    FORMAT(' ','T VA110G00 PULSER XMTR WAVEFORM ',I4,' Points')
32    FORMAT(' ','T VA110G00 PULSER XMTR/RCVR WAVEFORM ',I4,' Points')
33    FORMAT(' ','T VA110G00 PULSER XMTR/RCVR RESPONSE ',I4,' Points')
34    FORMAT(' ','T VA110G00 PULSER XMTR SPECTRUM ',I4,' Points')
C
40    FORMAT(' ','T MM86005 PLOT OF ER(f) - ',I4,' Points')
41    FORMAT(' ','T MM86005 PLOT OF DLOSS(f) - ',I4,' Points')
42    FORMAT(' ','Y INTERPOLATED REL. DIEL.PERM.')
43    FORMAT(' ','Y INTERPOLATED LOSS TANGENT')
44    FORMAT(' ','X FREQUENCY (MHz)')
45    FORMAT(' ',2X,I4,3X,'1')
46    FORMAT(' ',F10.6,5X,F10.6)
C
C#####################################################################
C
      PI=3.1415926535
      ZERO=0.
      Or=0.
      DONE=1.
      DINF=-999.9999999999
      D90=90.
      D180=180.
      DA=1.
```

```
C     , DDA=1.0
      DDA=1.29735                ! Area of .506" disc.
      QLs=100.
      NSTUNE=0
      CCABLE=1.E-15
      CPULSER=1.E-15
      RPULSER=1.E15
      CXSTEP=0.
      NPANAM=0
      ROFACT=1.
      PANZR=1.E12
      DAREA=DDA*.0001
      Fs=10.51381E6        ! The series resonant frequency.
C
C     Comment out the lines for the desired acoustic load impedance ...
C     AIR = 397.2 , WATER = 1.48E6
C
      ZAIR=397.2
      ZH2O=1.48E6
C      ZLB=DAREA*ZAIR
C      ZLF=DAREA*ZAIR
      ZLF=DAREA*ZH2O
      ZLB=DAREA*ZH2O
      ZTARGET=2200.*5968. ! Fused silica acoustic impedance, pg 1509.
      TAU=(ZTARGET-ZH2O)/(ZTARGET + ZH2O) ! Refl. coef. of target
      CCABLE=1.E-12
      PRINT*,'ENTER 1 for Z-Back = Z-Front , 0 for Z-Back = A * Z-Front'
      READ*,NZBACK
      IF(NZBACK.EQ.1)GO TO 47
      PRINT*,'ENTER MULT. FACTOR FACTOR, A, FOR Z-Back'
      READ*,FA
      ZLB=FA*ZLB           ! The back acoustic impedance.
47    DD=110.6             ! The film thickness in microns, pg
      TO=DD*1.E-6          !            and now in meters.
      TE=300.E-10           ! The thickness of the metallization.
C
C ######################################################################
C
      PRINT*,'                SIMULATION MENU'
      PRINT*,' '
      PRINT*,'   Enter number for desired simulation test:'
      PRINT*,'(0) Plot of Er(f) and DLOSS(f) only.'
      PRINT*,'(1) Voltage impulse response test of XMTR, RCVR, XMTR/RCVR
     +.'
      PRINT*,'(2) Voltage step response test of XMTR, XMTR/RCVR.'
      PRINT*,'(3) Current impulse response test of XMTR, XMTR/RCVR.'
      PRINT*,'(4) Both (1) and (2).'
      PRINT*,'(5) Both (1) and (3).'
      PRINT*,'(6) All  (1)  -  (3).'
      PRINT*,'(7) Burst test of XMTR, XMTR/RCVR.'
```

```
      PRINT*,'(8) Actual pulser test of XMTR, XMTR/RCVR.'
      READ*,MENU
      PRINT*,'ENTER LOW TIME FOR TIME DOMAIN PLOTS'
      READ*,PLOW
      PRINT*,'ENTER HIGH TIME FOR TIME DOMAIN PLOTS'
      READ*,PHIGH
      PRINT*,'ENTER MODULO TIME INTEGER FOR TIME DOMAIN OUTPUT FILES'
      READ*,MFACT
      IF(MENU.EQ.8)GO TO 39
      PRINT*,'                    MODEL MENU'
      PRINT*,' '
      PRINT*,'(0) Simplified Model - Water loaded'
      PRINT*,'(1) Full Model - Water loaded'
      PRINT*,'(2) Full Model - Matched back, Matched water-loaded front'
      READ*,MODEL
      PRINT*,'DO YOU WANT TO SHUNT TUNE THE XDCR ?'
      PRINT*,'    ENTER:  1 = Yes , 0 = No '
      READ*,NTUNE
      IF(NTUNE.EQ.1)THEN
      PRINT*,'Enter res. freq. factor, A, where tuned resonance is A*Fs'
      READ*,DA
      END IF
      PRINT*,'ENTER THE SIMULATION ORDER (Max=512)'
      READ*,N
      NT8=N*8
      NO2=N/2
      NO2P1=NO2+1
      NO2M1=N/2 - 1
      PRINT*,'ENTER THE LOWER FREQUENCY FOR ANALYSIS (MHz)'
      READ*,FLOW
      PRINT*,'ENTER THE UPPER FREQUENCY LIMIT FOR ANALYSIS (MHz)'
      READ*,FHIGH          ! The folding frequency.
      FSAMPLE=2.*FHIGH*1.E6  ! Sample rate = twice folding frequency.
      DELTAT=1./FSAMPLE    ! The sampling time increment.
      DELTAF=(FHIGH-FLOW)/NO2 ! Frequency resolution of the simulation.
      IF(MENU.NE.7)GO TO 49
C
C   <<<<<<<<<<<<<<<<<<<<<<<< BURST SECTION >>>>>>>>>>>>>>>>>>>>>>>>>>
C
C     This section performs the preliminary calculations required for
C  the sinusoidal burst response tests.  A sinusoidal burst is gen-
C  erated and its FFT is performed.  The FFT results are then used to
C  convolve with the system response of the XMTR and XMTR/RCVR to
C  derive the frequency-domain burst response.  Finally, the frequency
C  domain results are processed with an inverse FFT to obtain a plot
C  of the burst responses.
C
C  NOTE: This option prevents evaluation of the step response and uses
C        the step response arrays VZLFXSMG() and VZLFXSAN() as storage.
C
```

```
      PRINT*,'          ***** BURST RESPONSE SIMULATION *****'
      PRINT*,' '
48    PRINT*,'Enter sinusoidal burst frequency (MHz)'
      READ*,FF
      IF(FF.GE.FHIGH)THEN
      PRINT*,'Burst frequency too high.  Must be less than ',FHIGH
      GO TO 48
      END IF
      F=FF*1.E6
C
      PRINT*,'Enter 0 = burst endpoints both equal 0'
      PRINT*,'      1 = burst endpoints equal +/- 1'
      READ*,NBURST
1     IF(NBURST.EQ.0)THEN
      PRINT*,'Enter integer number of cycles in burst'
      READ*,CNUMBUR
      ELSE
      PRINT*,'Enter (integer + .5) number of cycles in burst'
      READ*,CNUMBUR
      END IF
C
      BP1WIDTH=(CNUMBUR+1)/F
      TOTWIDTH=FLOAT(N)*DELTAT
      IF(BP1WIDTH.GE.TOTWIDTH)THEN
      PRINT*,'Too many cycles to fit in sampling period.'
      GO TO 1
      END IF
C
      NBPOINTS=(CNUMBUR/F)/DELTAT
      NSTART=(N-NBPOINTS)/2
      NEND=NSTART+NBPOINTS
C
C
C     Now print out AGRAPH titles for graphics files...
C
      WRITE(40,25)N      ! Input
      WRITE(40,17)       !       sinewave
      WRITE(40,19)       !                burst
      WRITE(40,20)N      !                     waveform.
C
      WRITE(24,26)NO2M1  ! Spectral
      WRITE(24,17)       !          mag.
      WRITE(24,18)       !               of
      WRITE(24,20)NO2M1  !                  burst (volts).
C
      WRITE(25,26)NO2M1  ! Spectral
      WRITE(25,16)       !          phs.
      WRITE(25,18)       !               of
      WRITE(25,20)NO2M1  !                  burst (deg.).
C
```

```
      WRITE(30,27)NT8      ! XMTR
      WRITE(30,17)         !      output
      WRITE(30,19)         !             burst
      WRITE(30,20)NT8      !                   waveform.
C
      WRITE(32,28)NT8      ! XMTR/RCVR
      WRITE(32,17)         !           output
      WRITE(32,19)         !                 burst
      WRITE(32,20)NT8      !                       waveform.
C
C
      DO K=1,N                          ! Clear
      FTCALL(K)=FLOAT(K-1-NO2)*DELTAT ! the
      FT(K)=FTCALL(K)                   !          arrays
      VZLFXSMG(K)=0.                    !                 for
      VZLFXSAN(K)=0.                    !                     burst
      END DO                            !                           data.
C
      DO K=NSTART,NEND                  ! Now
      IF(NBURST.EQ.0)THEN               !     compute
      VZLFXSMG(K)=DSIN(2.*PI*F*FLOAT(K-NSTART)*DELTAT)
      ELSE                              !              the
      VZLFXSMG(K)=DCOS(2.*PI*F*FLOAT(K-NSTART)*DELTAT)
      END IF                            !                  burst
      END DO                            !                        waveform.
C
      DO L=1,N                          ! Graphics
      V=VZLFXSMG(L)/2.                  !          plot
      WRITE(40,21)FT(L),V               !               of
      END DO                            !                  input burst.
C
C     Set the FFT routine calling parameters..
C
      IMPULSE=0
      KIN=0
      KOUT=1
      INVERT=0
      CALL FFT1(FTCALL,IMPULSE,VZLFXSMG,VZLFXSAN,N,INVERT,KIN,KOUT)
C
      DO J=NO2P1,N                      ! Graphics plots of
      WRITE(24,22)FTCALL(J),VZLFXSMG(J) !       burst spectral mag.,
      WRITE(25,22)FTCALL(J),VZLFXSAN(J) !       and burst spectral phs.
      END DO
C
C
      GO TO 60                          ! Skip rest of graphics outputs.
C
C
C  <<<<<<<<<<<<<<<<<<< ACTUAL DRIVING PULSE ANALYSIS >>>>>>>>>>>>>>>>>>
C
```

```
C     This section, reserved for MENU=8, is for convolution of a
C   user-supplied waveform with the modified Mason's model (full
C   model #1 is used).  The user must assign the input waveform
C   file (512 points) to FORTRAN device number FOR009.
C
C     The user specifies the serial number for a specific transducer
C   for the analysis.  Special designs can be analyzed with #90
C   (cable-less designs) and #91 (30% Kt designs).
C
C     After the transducer selection, this section then performs the
C   512-point FFT on the supplied waveform and uses the frequency
C   domain results for convolution in the simulation.
C
C
39    PRINT*,'*** WILL USE FULL MASONS MODEL FOR SIMULATION ***'
      PRINT*,'ENTER SERIAL NUMBER, **, OF XDCR FOR SIMULATION'
      PRINT*,'               ( ie.  #P**cz)'
      READ*,NXDCR
      NTUNE=1                          ! Shunt tuned design ...
      NSTUNE=0                         ! Flag for series tuning
      DLS=0.
      QLS=30.
      RSHUNT=100.                      ! Shunt resistance use at Ames Lab
      NLSHUNT=1
      NFLAG=0
      NFET=0
      IF(NXDCR.EQ.17)THEN
      SL=2.18E-6                       ! Inductor number 1
      CLENGTH=3.408                    ! Cable length = 3.408 ft.
      NFLAG=1
C
      ELSE IF(NXDCR.EQ.18)THEN
      SL=2.16E-6                       ! Inductor number 3
      CLENGTH=3.555                    ! Cable length = 3.555 ft.
      NFLAG=1
C
      ELSE IF(NXDCR.EQ.19)THEN
      SL=2.2E-6                        ! Inductor number 6
      CLENGTH=3.44                     ! Cable length = 3.44 ft.
      NFLAG=1
C
      ELSE IF(NXDCR.EQ.20)THEN
      SL= 2.2E-6                       ! Inductor number 5
      CLENGTH=3.408                    ! Cable length = 3.408 ft.
      NFLAG=1
C
      ELSE IF(NXDCR.EQ.90)THEN
      SL=1.0E-6                        ! ULTIMATE broadband design ...
      CLENGTH=3.5
      NFLAG=1
```

```
      PRINT*,'ENTER 1 = FET RCVR, 0 = PANAMETRICS RCVR'
      READ*,NFET
      IF(NFET.EQ.1)SL=4.77E-6
C
      ELSE IF(NXDCR.EQ.91)THEN
      SL=1.0E-6                    ! High Kt ( 30%) design ...
      CLENGTH=3.5
      RSHUNT=100.
      NFLAG=1
      PRINT*,'ENTER 1 = FET RCVR, 0 = PANAMETRICS RCVR'
      READ*,NFET
      IF(NFET.EQ.1)SL=4.77E-6
C
C     Must be a series tuned design...
C
      END IF
      IF(NFLAG.NE.1)THEN
      NTUNE=0                      ! Series tuned design ...
      NSTUNE=1                     ! Set series tuning flag.
      RSHUNT=1.E12                 ! Remove RSHUNT for series tuned
      END IF
      IF(NXDCR.EQ.9)THEN
      DLS=5.5E-6
      CLENGTH=5.*(28./13.1)        ! RG58/U coax cable length
      NFLAG=1
C
      ELSE IF(NXDCR.EQ.10)THEN
      DLS=153.E-6
      CLENGTH=5.*(28./13.1)        ! RG58/U coax cable length
      NFLAG=1
C
      ELSE IF(NXDCR.EQ.13)THEN
      DLS=5.6E-6
      CLENGTH=5.*(28./13.1)        ! RG58/U coax cable length
      PRINT*,'DO YOU WANT TO CHANGE THE DEFAULT XDCR DESIGN?'
      PRINT*,'          Enter 0 = No , 1 = Yes'
      READ*,NDD
      IF(NDD.EQ.1)THEN
      PRINT*,'ENTER RG62A/U COAX CABLE LENGTH'
      READ*,CLENGTH
      PRINT*,'ENTER SERIES TUNING INDUCTANCE, Ls'
      READ*,DLS
      END IF
      NFLAG=1
C
      ELSE IF(NXDCR.EQ.15)THEN     ! Go back and start over ...
      DLS=148.6E-6
      CLENGTH=5.*(28./13.1)        ! RG58/U coax cable length
      NFLAG=1
C
```

```
      IF(NFLAG.NE.1)GO TO 39
      END IF
C
      IF(NXDCR.GE.90)THEN
      PRINT*,'ENTER 0 = OMIT Ls , 1 = USE Ls'
      READ*,NLSHUNT
      END IF
C
      CSCOPE=13.1E-12                ! Capacitance of 10:1 probe and CRO.
      CTEE=9.E-12                    ! Capacitance of BNC tee and adaptor.
      CSCOPE=CSCOPE + CTEE
      CCABLE=CLENGTH*13.1E-12        ! Total cable capacitance.
C
C      PRINT*,'ENTER CPULSER IN pF'
C      READ*,CPL
      CPL=130.                       ! Input capacitance of XMTR.
C      CPL=30.
      CPULSER=CPL*1.E-12
      CPULSER=CPULSER + CSCOPE       ! Input capacitance of pulser RCVR.
C      CPULSER=1.E-18
C
      DIAMETER=0.506       ! Film disc diameter in inches.
C
      PRINT*,'ENTER RSHUNT'
      READ*,RSHUNT
      PRINT*,'ENTER 0 = PANZR=ACTIVE , 1 = PANZR=250 Ohms'
      READ*,NPANAM
      DAREA=PI*((DIAMETER*.0254/2.)**2.) ! Disc area in square meters.
C      FA=2.82
      ZLF=ZH2O*DAREA
      ZLB=ZH2O*FA*DAREA
C      PRINT*,'ENTER THE SERIES TUNING INDUCTANCE, (uH)'
C      READ*,DLS
C      DLS=0.
C      PRINT*,'ENTER QLs'
C      READ*,QLs
C      QLS=30.
      QLs=100.
      MODEL=1
      N=512
      NT8=N*8
      NO2=N/2
      NO2P1=N/2 + 1
      NO2M1=N/2 - 1
      FLOW=0.
      FHIGH=21.40          ! Twice the parallel resonance frequency, Fp.
      DELTAT=10.E-9
      DELTAF=100./512.     ! Frequency resolution of the analysis.
      FSAMPLE=100.E6       ! The LeCroy CRO sampling rate.
C
```

```
C     Now print out AGRAPH headers for the graphics files...
C
      WRITE(40,29)N        ! Input
      WRITE(40,17)         !       pulser
      WRITE(40,19)         !              voltage
      WRITE(40,20)N        !                      waveform.
C
      WRITE(24,30)NO2      ! Input
      WRITE(24,17)         !       pulser
      WRITE(24,18)         !              spectrum
      WRITE(24,20)NO2      !                       magnitude.
C
      WRITE(30,31)NT8      ! XMTR
      WRITE(30,17)         !      output
      WRITE(30,19)         !             pulser
      WRITE(30,20)NT8      !                    waveform.
C
      WRITE(10,34)NO2      ! XMTR
      WRITE(10,17)         !      output
      WRITE(10,18)         !             spectral
      WRITE(10,20)NO2      !                      magnitude
      WRITE(10,21)Or,Or    !                                waveform.
C
      WRITE(32,32)NT8      ! XMTR/RCVR
      WRITE(32,17)         !           output
      WRITE(32,17)         !                  pulser
      WRITE(32,20)NT8      !                         waveform.
C
      WRITE(14,33)NO2      ! XMTR/RCVR
      WRITE(14,17)         !           output
      WRITE(14,18)         !                  spectral
      WRITE(14,20)NO2      !                           magnitude
      WRITE(14,21)Or,Or    !                                   waveform.
C
C     Now, read in pulser voltage points and do FFT....
C
      READ(9,*)NHEADER              ! Skip past the file header, N.
      DO K=1,N
      FTCALL(K)=FLOAT(K-1-NO2)*DELTAT ! Set time axis values
      VZLFXSAN(K)=0.                ! Clear imaginary part of input
      READ(9,*)VPROBE               ! Read the 10:1 probe data points.
      VZLFXSMG(K)=10.*VPROBE        ! Correct it and store it for FFT.
      WRITE(40,21)FTCALL(K),VZLFXSMG(K) ! Write it out to graphics file.
      END DO
C
C     Now, set the FFT calling parameters...
C
      IMPULSE=0
      KIN=0
      KOUT=1
```

```
      INVERT=0
C
C       Call the FFT to get the frequency domain representation of the
C  user-supplied actual driving waveform ...
C
      CALL FFT1(FTCALL,IMPULSE,VZLFXSMG,VZLFXSAN,N,INVERT,KIN,KOUT)
      DO J=NO2P1,N                        ! Write FFT magnitude to
      WRITE(24,22)FTCALL(J),VZLFXSMG(J)   !            graphics
      END DO                              !                    file.
C
      GO TO 60                            ! Skip rest of graphics...
C
C
C <<<<<<<<<<<<<<<<<<<<<<<<<<<<<<<***>>>>>>>>>>>>>>>>>>>>>>>>>>>>>>>>>>>>>>>
C
49    IF(MENU.EQ.0)GO TO 55
C
C     Now print out the AGRAPH titles for the graphics files.
C
      IF(MENU.EQ.2.OR.MENU.EQ.3)GO TO 50
      WRITE(10,10)NO2P1    ! Voltage impulse
      WRITE(10,15)         !                  response
      WRITE(10,18)         !                           of
      WRITE(10,20)NO2P1    !                              XMTR,
      WRITE(10,21)Or,DINF  !                                    (Mag).
C
      WRITE(11,10)NO2P1    ! Voltage impulse
      WRITE(11,16)         !                  response
      WRITE(11,18)         !                           of
      WRITE(11,20)NO2P1    !                              XMTR,
      WRITE(11,21)Or,D90   !                                    (Phs).
C
      WRITE(30,10)NT8      ! Voltage impulse
      WRITE(30,17)         !                  response
      WRITE(30,19)         !                           of
      WRITE(30,20)NT8      !                              XMTR, (Time).
C
      WRITE(12,11)NO2P1    ! Voltage impulse
      WRITE(12,15)         !                  response
      WRITE(12,18)         !                           of
      WRITE(12,20)NO2P1    !                              RCVR,
      WRITE(12,21)Or,DINF  !                                    (Mag).
C
      WRITE(13,11)NO2P1    ! Voltage impulse
      WRITE(13,16)         !                  response
      WRITE(13,18)         !                           of
      WRITE(13,20)NO2P1    !                              RCVR,
      WRITE(13,21)Or,Or    !                                    (Phs).
C
      WRITE(31,11)NT8      ! Voltage impulse
```

```
      WRITE(31,17)        !                response
      WRITE(31,19)        !                        of
      WRITE(31,20)NT8     !                           RCVR, (Time).
C
      WRITE(14,12)NO2P1   ! Voltage impulse
      WRITE(14,15)        !                response
      WRITE(14,18)        !                        of
      WRITE(14,20)NO2P1   !                           XMTR/RCVR,
      WRITE(14,21)Or,DINF !                                    (Mag)
C
      WRITE(15,12)NO2P1   ! Voltage impulse
      WRITE(15,16)        !                response
      WRITE(15,18)        !                        of
      WRITE(15,20)NO2P1   !                           XMTR/RCVR,
      WRITE(15,21)Or,Or   !                                    (Phs)
C
      WRITE(32,12)NT8     ! Voltage impulse
      WRITE(32,17)        !                response
      WRITE(32,19)        !                        of
      WRITE(32,20)NT8     !                          XMTR/RCVR, (Time)
C
50    IF(MENU.EQ.1.OR.MENU.EQ.3.OR.MENU.EQ.5)GO TO 51
C
      WRITE(16,13)NO2P1   ! Voltage step
      WRITE(16,15)        !              response
      WRITE(16,18)        !                      of
      WRITE(16,20)NO2P1   !                         XMTR,
      WRITE(16,21)Or,DINF !                               (Mag).
C
      WRITE(17,13)NO2P1   ! Voltage step
      WRITE(17,16)        !              response
      WRITE(17,18)        !                      of
      WRITE(17,20)NO2P1   !                         XMTR,
      WRITE(17,21)Or,D180 !                               (Phs).
C
      WRITE(33,13)NT8     ! Voltage step
      WRITE(33,17)        !              response
      WRITE(33,19)        !                      of
      WRITE(33,20)NT8     !                         XMTR, (Time).
C
      WRITE(18,14)NO2P1   ! Voltage step
      WRITE(18,15)        !              response
      WRITE(18,18)        !                      of
      WRITE(18,20)NO2P1   !                         XMTR/RCVR,
      WRITE(18,21)Or,DINF !                                   (Mag).
C
      WRITE(19,14)NO2P1   ! Voltage step
      WRITE(19,16)        !              response
      WRITE(19,18)        !                      of
      WRITE(19,20)NO2P1   !                         XMTR/RCVR,
```

```
      WRITE(19,21)Or,Or    !                                    (Phs).
C
      WRITE(34,14)NT8      ! Voltage step
      WRITE(34,17)         !              response
      WRITE(34,19)         !                       of
      WRITE(34,20)NT8      !                          XMTR/RCVR, (Time).
C
51    IF(MENU.EQ.1.OR.MENU.EQ.2.OR.MENU.EQ.4)GO TO 60
C
      WRITE(20,23)NO2P1    ! Current impulse
      WRITE(20,15)         !                 response
      WRITE(20,18)         !                          of
      WRITE(20,20)NO2P1    !                             XMTR,
      WRITE(20,21)Or,Dinf  !                                   (Mag).
C
      WRITE(21,23)NO2P1    ! Current impulse
      WRITE(21,16)         !                 response
      WRITE(21,18)         !                          of
      WRITE(21,20)NO2P1    !                             XMTR,
      WRITE(21,21)Or,Or    !                                   (Phs).
C
      WRITE(35,23)NT8      ! Current impulse
      WRITE(35,17)         !                 response
      WRITE(35,19)         !                          of
      WRITE(35,20)NT8      !                             XMTR, (Time).
C
      WRITE(22,24)NO2P1    ! Current impulse
      WRITE(22,15)         !                 response
      WRITE(22,18)         !                          of
      WRITE(22,20)NO2P1    !                             XMTR/RCVR,
      WRITE(22,21)Or,Dinf  !                                      (Mag)
C
      WRITE(23,24)NO2P1    ! Current impulse
      WRITE(23,16)         !                 response
      WRITE(23,18)         !                          of
      WRITE(23,20)NO2P1    !                             XMTR/RCVR,
      WRITE(23,21)Or,Or    !                                      (Phs)
C
      WRITE(36,24)NT8      ! Current impulse
      WRITE(36,17)         !                 response
      WRITE(36,19)         !                          of
      WRITE(36,20)NT8      !                            XMTR/RCVR, (Time)
C
      GO TO 60             ! Skip Er(f) anf DLOSS(f) plots.
C
55    WRITE(7,40)NO2       ! Graphics
      WRITE(7,42)          !          plot
      WRITE(7,44)          !               of
      WRITE(7,45)NO2       !                  Er(f).
C
```

```
      WRITE(8,41)NO2       ! Graphics
      WRITE(8,43)          !          plot
      WRITE(8,44)          !               of
      WRITE(8,45)NO2       !                  DLOSS(f).
C
60    CONTINUE
C
C ######################################################################
C #   Here are the piezoelectric constants needed for the analysis     #
C ######################################################################
C
      DAKT2=.04280         ! As of 1 Feb 1988, see pg 1642.
      IF(MENU.EQ.8.AND.NXDCR.EQ.91)DAKT2=.09  ! Kt = 30% FOR XCDR #91
      DAKT=DSQRT(DAKT2)
      IF(MODEL.EQ.0)THEN
      V0=2368.5            ! As of 14 Jan 1988, see pg 1472.
      ELSE
      V0=2382.5            ! As of 1 Feb 1988, see pg 1642.
      END IF
      VE=3420.             ! Speed of sound in gold metallization.
      VM=1875.0            ! 1/4 Wave matching layer sound velocity.
      Fp=V0/(2.*T0)        ! The parallel resonant frequency.
      IF(MODEL.EQ.2)THEN
      PRINT*,'Enter 1/4 wave matching frequency mult. factor, Af,'
      PRINT*,'      where matched frequency is Af*Fp.'
      READ*,QWF
      ELSE
      QWF=1.
      END IF
      TM=VM/(4.*Fp*QWF)    ! 1/4 Wave matching layer thickness.
      Z0=DAREA*1814.*V0    ! Using measurements of 15 Jan 1988.
      ZE=DAREA*19700.*VE   ! See pg 1475.
      ZM=DAREA*1347.8*VM   ! 1/4 Wave matching layer acoustic impedance.
      IF(MODEL.EQ.2)ZLB=Z0
      Qm=14.039            ! As of 1 Feb 1988, see pg 1642.
      Cm=1.263E-12         ! Secondary capacitance, see pg 1476.
C
C ######################################################################
      NINT=1
      FREQ=Fp/1.E6
      AF(1)=FREQ
      CALL CSPIN(AXE,AYE,NE,AF,AER,NINT)
      PERMIT=AER(1)
      C0p=PERMIT*8.854E-12*DAREA/T0
      PHIp=DAKT*DSQRT(V0*C0p*Z0/T0)
      FT(1+N/2)=0.
      AF(1)=Fs*DA/1.E6
      CALL CSPIN(AXE,AYE,NE,AF,AER,NINT)
      PERMIT=AER(1)
      C0s=PERMIT*8.854E-12*DAREA/T0
```

```
C      PRINT*,'COs = ',COs
       C=COs
       IF(MENU.EQ.2)THEN
       PRINT*,'ENTER FACT. FOR SHUNT CAPACITANCE, CXSTEP = FACT * COs'
       READ*,FACT
       CXSTEP=FACT*COs
       PRINT*,'CXSTEP = ',CXSTEP
       PRINT*,'ENTER FACT. FOR R0, R0 = FACT. * R0'
       READ*,R0FACT
       END IF
       IF(NTUNE.EQ.1)SHUNTL=1./(((DA*Fs*2.*PI)**2)*C) ! Shunt inductance.
       IF(MENU.EQ.8.AND.NSTUNE.EQ.0)SHUNTL=SL
       RL0=2.                                  ! Resistance of the inductor.
       DC0=COs/1.E-12
       DC=C/1.E-12
       DL0=SHUNTL/1.E-6
       RQe=602.3/(DA**2.)  ! Shunt resistance for Qe = Qs, for 1cm X 1cm.
       IF(NTUNE.EQ.1)THEN
       PRINT*,'Shunt tuning frequency is Fs = ',Fs
       PRINT*,'Bulk capacitance, COs (pF) = ',DC0
       PRINT*,'Total tuning capacitance (COs + cable), (pF) = ',DC
       PRINT*,'Tuning inductance, L0 (uH) = ',DL0
       PRINT*,'Shunt resistance (Ohms)  = ',RSHUNT
       END IF
C
       IF(MENU.EQ.8.AND.NLSHUNT.EQ.0)NTUNE=0
C
C*************************************************************************
C************************* MAIN FREQUENCY LOOP ***************************
C*************************************************************************
C****                                                                  ****
       DO 1000 I=1,NO2
C
C        First, get the Mason's model component values ready for the
C      analyses, then perform each transfer function computation as
C      indicated in the separated sections below...
C
C*****START-PRELIM*START-PRELIM*START-PRELIM*START-PRELIM*START-PRELIM**
C                                                                      *
       FREQ=FLOW+FLOAT(I)*DELTAF
       IF(MENU.EQ.8.AND.FREQ.GT.FHIGH)THEN
       II=I                            ! Record the value of I.
       GO TO 1001                      ! Skip around analysis if F > 2Fp.
       END IF
       DOMEGA=2.*PI*FREQ*1.E6
       AF(1)=FREQ
       CALL CSPIN(AXE,AYE,NE,AF,AER,NINT)
       CALL CSPIN(AXD,AYD,ND,AF,ADLOSS,NINT)
       PERMIT=AER(1)
       DLOSS=ADLOSS(1)
```

```
103   C0=PERMIT*8.854E-12*DAREA/T0
C      PRINT*,'FREQ = ',FREQ
C      PRINT*,'C0 = ',C0
      PHI=DAKT*SQRT(V0*C0*Z0/T0)
      R0=R0FACT/(DOMEGA*C0*DLOSS)
      Rm=(PHIp**2)/(DOMEGA*Cm*Qm)
C
      IF(MENU.EQ.8)THEN
      CALL CSPIN(APANX,APANRe,NP,AF,AER,NINT)
      PANReal=AER(1)
      CALL CSPIN(APANX,APANIm,NP,AF,AER,NINT)
      PANImag=AER(1)
      PANZR=DCMPLX(PANReal,PANImag)
      IF(NPANAM.EQ.1)PANZR=CMPLX(250.,0.)
      IF(NFET.EQ.1)PANZR=CMPLX(10000000000.,0.)
      END IF
C
      IF(MENU.NE.0)GO TO 104
      WRITE(7,46)FREQ,PERMIT
      WRITE(8,46)FREQ,DLOSS
      GO TO 1000
C
C     Get Mason's model secondary reactive components ...
C
104   THETA0=DOMEGA*T0/V0
      THETAE=DOMEGA*TE/VE
      THETAM=DOMEGA*TM/VM
      X20=Z0*DTAN(THETA0/2.)
      X10=Z0/DSIN(THETA0)
      X2E=ZE*DTAN(THETAE/2.)
      X1E=ZE/DSIN(THETAE)
      X2M=ZM*DTAN(THETAM/2.)
      X1M=ZM/DSIN(THETAM)
C
C     Now get complex impedances of Mason's model dielectric components.
C
      ZSHUNTL=DCMPLX(RL0,DOMEGA*SHUNTL)
      ZR0=DCMPLX(R0,ZER0)
      C0=C0 + CXSTEP        ! Extra shunt capacitance for step test.
      ZC0=DCMPLX(ZER0,-1./(DOMEGA*C0))
      ZR0C0=ZR0*ZC0/(ZR0+ZC0)     ! Impedance of R0 // C0.
      IF(NTUNE.EQ.0)GO TO 105
      ZR0C0=1./( (1./ZR0) + (1./ZC0) + (1./ZSHUNTL) )
      IF(MENU.NE.8)ZR0C0=ZR0C0*RQe/(ZR0C0 + RQe)
C
105   IF(MODEL.EQ.0)THEN
C
C%%%%%%%%%%%%%%%%%%%%%%%%%%%%%%%%%%%%%%%%%%%%%%%%%%%%%%%%%%%%%%%%%%%%%%%%%%%%%%%%
C     Compute simplified model XMTR impedances, Z1-Z3, and ZINX..
C
```

```
      ZF=DCMPLX(ZLF,X20)
      ZB=DCMPLX(ZLB,X20)
      Z=ZF*ZB/(ZF+ZB)
      Z1=Z + DCMPLX(ZERO,-X10)
      Z2=Z1/(PHI**2) + Rm
      Z3=Z2 - ZC0
      ZINX=ZR0C0*Z3/(ZR0C0+Z3)    ! Zin of simplified model XMTR.
C
C     Compute simplified model RCVR impedances, Z5-Z8, and ZINR..
C
      Z5=ZR0C0 + Rm - ZC0
      Z6=(PHI**2)*Z5 + DCMPLX(ZERO,-X10)
      Z7=ZB*Z6/(ZB+Z6)
      Z8=Z7 + DCMPLX(ZERO,X20)
      ZINR=Z8*ZLF/(Z8+ZLF)        ! Zin of simplified model RCVR.
C
      ELSE
C
C%%%%%%%%%%%%%%%%%%%%%%%%%%%%%%%%%%%%%%%%%%%%%%%%%%%%%%%%%%%%%%%%%%%%%%%%%%%
C     Compute full model XMTR impedances, Z1-Z3, Z, and ZINX..
C
      ZF=DCMPLX(ZLF,X2E)
      ZB=DCMPLX(ZLB,X2E)
      IF(MODEL.EQ.1)GO TO 107     ! Skip unless matching front required.
      ZMF=DCMPLX(ZLF,X2M)
      ZFM=ZMF*DCMPLX(ZERO,-X1M)/(ZMF + DCMPLX(ZERO,-X1M))
      ZF=ZFM + DCMPLX(ZERO,X2M + X2E)
107   ZBE=ZB*DCMPLX(ZERO,-X1E)/(ZB + DCMPLX(ZERO,-X1E))
      ZFE=ZF*DCMPLX(ZERO,-X1E)/(ZF + DCMPLX(ZERO,-X1E))
      ZBET=ZBE + DCMPLX(ZERO,X2E + X20)
      ZFET=ZFE + DCMPLX(ZERO,X2E + X20)
      Z=ZBET*ZFET/(ZBET + ZFET)
      Z1=Z + DCMPLX(ZERO,-X10)
      Z2=Z1/(PHI**2) + Rm
C      PRINT*,'FREQ = ',FREQ
      Z3=Z2 - ZC0
C      PRINT*,'Z3 = ',Z3
C      PRINT*,'C0 = ',C0
C      PRINT*,'R0 = ',R0
      ZINX=ZR0C0*Z3/(ZR0C0 + Z3) ! Zin of full model XMTR.
      R1s=DOMEGA*DLS/QLs                    ! Resistance of Ls.
      IF(R1s.LT.0.3)R1s=0.30                ! DC resistance of cable.

      ZINLS=ZINX + DCMPLX(R1s,DOMEGA*DLS)  ! These are
      ZCABLE=DCMPLX(ZERO,-1./(DOMEGA*CCABLE))  !    modified impedances
      ZCPULSER=DCMPLX(ZERO,-1./(DOMEGA*CPULSER))
      ZPULSER=PANZR*ZCPULSER/(PANZR + ZCPULSER)
      ZPULSER=ZPULSER*RSHUNT/(ZPULSER + RSHUNT)
      ZTERM=ZPULSER*ZCABLE/(ZPULSER + ZCABLE)
      IF(NFET.EQ.1)ZTERM=RSHUNT
```

```
      ZINTS=ZINLS*ZTERM/(ZINLS + ZTERM)     ! for the tuned cable case.
C
C     Compute full model RCVR impedances, Z5-Z10, and ZINR..
C
      ZRLS=ZTERM + DCMPLX(Rls,DOMEGA*DLS)
      ZR0C0LS=ZR0C0*ZRLS/(ZR0C0 + ZRLS)
      IF(MENU.EQ.8)THEN
      Z5=ZR0C0LS + Rm -ZC0
      ELSE
      Z5=ZR0C0 + Rm - ZC0
      END IF
      Z6=(PHI**2)*Z5 + DCMPLX(ZERO,-X10)
      Z7=ZBET*Z6/(ZBET + Z6)
      Z8=Z7 + DCMPLX(ZERO,X20 + X2E)
      Z9=Z8*DCMPLX(ZERO,-X1E)/(Z8 + DCMPLX(ZERO,-X1E))
      Z10=Z9 + DCMPLX(ZERO,X2E)
      ZINR=Z10*ZLF/(Z10 + ZLF)    ! Zin of full model RCVR.
      IF(MODEL.EQ.1)GO TO 108     ! Skip unless matched front required.
      Z11=Z10 + DCMPLX(ZERO,X2M)
      Z12=Z11*DCMPLX(ZERO,-X1M)/(Z11 + DCMPLX(ZERO,-X1M))
      Z13=Z12 + DCMPLX(ZERO,X2M)
      ZINR=ZLF*Z13/(ZLF + Z13)
108   CONTINUE
      END IF
C                                                                      *
C***END-PRELIM*END-PRELIM*END-PRELIM*END-PRELIM*END-PRELIM*END-PRELIM***
C
      IF(MENU.EQ.0)GO TO 1000
      IF(MENU.EQ.2.OR.MENU.EQ.3)GO TO 135
C
C**************** START-XMTR-VOLTAGE-IMPULSE RESPONSE*******************
C                                                                      *
C     In this section, compute the frequency-domain impulse response of
C  the XDCR transmitter.  Using an ideal impulse input voltage, assume
C  an input voltage of 1 at 0 deg. and compute the resulting output
C  voltage (force) at the front face of the transducer.
C     Vin is the input voltage to the transducer.
C     VZLFXI is Voltage across ZLF (front face load impedance) in the
C  Xmit mode of operation, for Impulse input.
C     If MENU = 7, then the complex input voltage, Vin, will instead be
C  the phasor representation (mag and phase) of the input burst FFT
C  results.
C     If MENU = 8, then the complex input voltage will instead be the
C  phasor representation (real and imaginary parts) of the user-
C  supplied driving voltage.
C
      IF(MENU.EQ.7.OR.MENU.EQ.8)THEN
      VinIM=VZLFXSMG(1+N/2-I)*DSIN(-VZLFXSAN(1+N/2-I)*PI/180.)
      VinRE=VZLFXSMG(1+N/2-I)*DCOS(-VZLFXSAN(1+N/2-I)*PI/180.)
      Vin=DCMPLX(VinRE,VinIM)
```

```
      ELSE
      Vin=DCMPLX(DONE,ZERO)       ! The input impulse function voltage.
      END IF
C
      IF(MODEL.EQ.0)THEN          ! Then do simplified model...
C
      VPRIX=Vin*(Z1/(PHI**2))/Z3 ! Voltage across primary side.
      VSECX=VPRIX*PHI             ! Voltage across the secondary side.
      VZ=VSECX*Z/Z1               ! The voltage across impedance "Z".
      VZLFXI=VZ*ZLF/ZF            !** Desired output voltage (force).**
C
      ELSE                        ! Else do full model...
      IF(MENU.EQ.8)Vin=Vin*ZINX/ZINLS
      VPRIX=Vin*(Z1/(PHI**2))/Z3 ! Voltage across primary side.
      VSECX=VPRIX*PHI             ! Voltage across the secondary side.
      VZ=VSECX*Z/Z1               ! The voltage across the impedance "Z".
      VZFE=VZ*ZFE/ZFET            ! The voltage across impedance "ZFE".
      VZLFXI=VZFE*ZLF/ZF          !**Desired output voltage (force).**
      IF(MODEL.EQ.1)GO TO 109     ! Skip unless matching front required.
      VZFM=VZFE*ZFM/ZF            !
      VZLFXI=VZFM*ZLF/ZMF         !
109   CONTINUE
C
      END IF
C
      VZLFXIRE=REAL(VZLFXI)       ! The real part of the voltage.
      VZLFXIIM=AIMAG(VZLFXI)      ! The imaginary part of the voltage.
      VMAG=CABS(VZLFXI)           ! The voltage magnitude.
      VANG=DATAN2(VZLFXIIM,VZLFXIRE)*180./PI  ! The voltage phase (Deg).
      VZLFXIMG(1+N/2-I)=VMAG      ! Set
      VZLFXIAN(1+N/2-I)=-VANG     !     up
      IF(I.EQ.NO2)GO TO 110       !        inverse
      VZLFXIMG(1+N/2+I)=VMAG      !                FFT
      VZLFXIAN(1+N/2+I)=VANG      !                    arrays.
110   CONTINUE
      IF(MENU.EQ.8)WRITE(10,21)FREQ,VMAG
      IF(MENU.EQ.7.OR.MENU.EQ.8)GO TO 111
      VMAGdB=20.*DLOG10(VMAG)     ! Change VMAG to dB
      WRITE(10,21)FREQ,VMAGdB     !             and write
      WRITE(11,21)FREQ,VANG       !                 AGRAPH files.
C                                                                    *
C****************** END-XMTR-VOLTAGE-IMPULSE-RESPONSE ******************
C
C************** START-XMTR/RCVR-VOLTAGE-IMPULSE-RESPONSE ***************
C                                                                    *
C     This section uses the previous XMTR impulse response results to
C  also compute the combined XMTR/RCVR impulse response.  The output
C  voltage represents, VXMRCI, thus represents the frequency-domain
C  Voltage RCVR output for Impulse input to the transducer.
C     If MENU = 7, then the complex input voltage, Vin, will instead be
```

```
C  the phasor representation (mag and phase) of the input burst FFT
C  results.
C     If MENU = 8, the input voltage, Vin, will instead be the results
C  of the previous section's user-supplied waveform for actual
C  pulse-echo analysis.
C
111   IF(MODEL.EQ.0)THEN          ! Then do simplified model...
C
      IF(MENU.EQ.8)VZLFXI=VZLFXI*SQRT(10.)! Mult. by 10 dB of RCVR gain.
      VZ7=VZLFXI*Z7/Z8            ! The voltage across impedance "Z7".
      VSECRI=VZ7*(PHI**2)*Z5/Z6   ! Voltage across secondary (phi) side.
      VPRIRI=VSECRI/PHI           ! Voltage across primary (1) side.
      VXMRCI=VPRIRI*ZROCO/Z5      !**Desired XMTR/RCVR output voltage.**
C
      ELSE                        ! Else do full model...
      IF(MENU.EQ.8)VZLFXI=VZLFXI*SQRT(10.)
      VZ9=VZLFXI*Z9/Z10           ! The voltage across impedance "Z9".
      IF(MODEL.EQ.1)GO TO 118     ! Skip unless matching front required.
      VZ12=VZLFXI*Z12/Z13         !
      VZ9=VZ12*Z9/Z11             !
118   VZ7=VZ9*Z7/Z8               ! The voltage across impedance "Z7".
      VSECRI=VZ7*(PHI**2)*Z5/Z6   ! Voltage across secondary (phi) side.
      VPRIRI=VSECRI/PHI           ! Voltage across primary (1) side.
      IF(MENU.EQ.8)THEN
      VROCOLS=VPRIRI*ZROCOLS/Z5
      VXMRCI=VROCOLS*ZTERM/ZRLS
      AF(1)=FREQ
      CALL CSPIN(AFREQRAD,ARADCOR,NR,AF,ACORRECT,NINT)
      DCORRECT=ACORRECT(1)
      IF(NXDCR.LT.90)THEN
      VXMRCI=VXMRCI*TAU*DCORRECT ! Add diffraction.
       END IF
      ELSE
      VXMRCI=VPRIRI*ZROCO/Z5      !**Desired XMTR/RCVR output voltage.**
      END IF
      END IF
C
      VXMRCIRE=REAL(VXMRCI)       ! The real part of the voltage.
      VXMRCIIM=AIMAG(VXMRCI)      ! The imaginary part of the voltage.
      VMAG=CABS(VXMRCI)           ! The magnitude of the voltage.
      VANG=DATAN2(VXMRCIIM,VXMRCIRE)*180./PI  ! The voltage phase (Deg).
      VXMRCIMG(1+N/2-I)=VMAG      ! Set
      VXMRCIAN(1+N/2-I)=-VANG     !     up
      IF(I.EQ.NO2)GO TO 120       !        inverse
      VXMRCIMG(1+N/2+I)=VMAG      !                FFT
      VXMRCIAN(1+N/2+I)=VANG      !                    arrays.
120   CONTINUE
      IF(MENU.EQ.8)WRITE(14,21)FREQ,VMAG
      IF(MENU.EQ.7.OR.MENU.EQ.8)GO TO 1000
      VMAGdB=20.*DLOG10(VMAG)     ! Change VMAG to dB
```

```
      WRITE(14,21)FREQ,VMAGdB     !              and write
      WRITE(15,21)FREQ,VANG       !                   AGRAPH files.
C                                                                      *
C*************** END-XMTR/RCVR-VOLTAGE-IMPULSE-RESPONSE *****************
C
C***************** START-RCVR-VOLTAGE-IMPULSE-RESPONSE ******************
C                                                                      *
C     This section computes the ideal impulse response of the RCVR
C  only.  The same ideal impulse voltage used for the XMTR section is
C  used.  The output voltage VRCVRI represents the frequency-domain
C  Voltage of the RCVR for the Impulse response analysis.
C
C
      IF(MODEL.EQ.0)THEN          ! Then do simplified model...
C
      VZ7=Vin*Z7/Z8               ! Voltage across impedance "Z7".
      VSECRI=VZ7*(PHI**2)*Z5/Z6   ! Voltage across secondary (phi) side.
      VPRIRI=VSECRI/PHI           ! Voltage across primary (1) side.
      VRCVRI=VPRIRI*ZR0C0/Z5      !**Desired RCVR output voltage.**
C
      ELSE                        ! Else do full model...
      VZ9=Vin*Z9/Z10              ! Voltage across impedance "Z9".
      IF(MODEL.EQ.1)GO TO 121     ! Skip unless matching front required.
      VZ12=Vin*Z12/Z13            !
      VZ9=VZ12*Z9/Z11             !
121   VZ7=VZ9*Z7/Z8               ! Voltage across impedance "Z7".
      VSECRI=VZ7*(PHI**2)*Z5/Z6   ! Voltage across secondary (phi) side.
      VPRIRI=VSECRI/PHI           ! Voltage across primary (1) side.
      VRCVRI=VPRIRI*ZR0C0/Z5      !**Desired output voltage.**
C
      END IF
C
      VRCVRIRE=REAL(VRCVRI)       ! The real part of the voltage.
      VRCVRIIM=AIMAG(VRCVRI)      ! The imaginary part of the voltage.
      VMAG=CABS(VRCVRI)           ! The voltage magnitude.
      VANG=DATAN2(VRCVRIIM,VRCVRIRE)*180/PI  ! The voltage phase (Deg).
      VRCVRIMG(1+N/2-I)=VMAG      ! Set
      VRCVRIAN(1+N/2-I)=-VANG     !     up
      IF(I.EQ.NO2)GO TO 130       !        inverse
      VRCVRIMG(1+N/2+I)=VMAG      !                FFT
      VRCVRIAN(1+N/2+I)=VANG      !                    arrays.
130   CONTINUE
      VMAGdB=20.*DLOG10(VMAG)     ! Change VMAG to dB
      WRITE(12,21)FREQ,VMAGdB     !             and write
      WRITE(13,21)FREQ,VANG       !                  AGRAPH files.
C                                                                      *
C***************** END-RCVR-VOLTAGE-IMPULSE-RESPONSE ********************
C
135   IF(MENU.EQ.1.OR.MENU.EQ.3.OR.MENU.EQ.5)GO TO 155
C
```

```
C***************** START-XMTR-VOLTAGE-STEP-RESPONSE ********************
C                                                                      *
C     This section computes the ideal step response of the XMTR and
C  combined XMTR/RCVR step response.  An input voltage of -1/jw is
C  used for the input voltage (a negative unit step input).  Thus,
C  Vin is 0 + j1/w.
C     The voltage VZLFXS is thus the Voltage output of the xmtr
C  across ZLF of the Xmtr circuit for the Step input analysis.
C
C      Vin=DCMPLX(ZERO,1./DOMEGA) ! The input negative step voltage.
       Vin=DCMPLX(ZERO,-1./DOMEGA) ! The positive step input voltage.
C
       IF(MODEL.EQ.0)THEN          ! Then do simplified model...
C
       VPRIX=Vin*(Z1/(PHI**2))/Z3 ! Voltage across primary side.
       VSECX=VPRIX*PHI            ! Voltage across secondary side.

       VZ=VSECX*Z/Z1              ! Voltage across impedance "Z".
       VZLFXS=VZ*ZLF/ZF           !**Desired output XMTR voltage.**
C
       ELSE                       ! Else do full model...
       VPRIX=Vin*(Z1/(PHI**2))/Z3 ! Voltage across primary side.
       VSECX=VPRIX*PHI            ! Voltage across secondary side.
       VZ=VSECX*Z/Z1              ! Voltage across impedance "Z".
       VZFE=VZ*ZFE/ZFET           ! Voltage across impedance "ZFE".
       VZLFXS=VZFE*ZLF/ZF         !**Desired output XMTR voltage.**
       IF(MODEL.EQ.1)GO TO 137    ! Skip unless matching front required.
       VZFM=VZFE*ZFM/ZF           !
       VZLFXS=VZFM*ZLF/ZMF        !
137    CONTINUE
C
       END IF
C
       VZLFXSRE=REAL(VZLFXS)      ! Real part of the voltage.
       VZLFXSIM=AIMAG(VZLFXS)     ! Imaginary part of the voltage.
       VMAG=CABS(VZLFXS)          ! The magnitude of the voltage.
       VANG=DATAN2(VZLFXSIM,VZLFXSRE)*180./PI  ! The voltage phase (Deg).
       VZLFXSMG(1+N/2-I)=VMAG     ! Set
       VZLFXSAN(1+N/2-I)=-VANG    !     up
       IF(I.EQ.NO2)GO TO 140      !        inverse
       VZLFXSMG(1+N/2+I)=VMAG     !                FFT
       VZLFXSAN(1+N/2+I)=VANG     !                    arrays.
140    CONTINUE
       VMAGdB=20.*DLOG10(VMAG)    ! Change VMAG to dB
       WRITE(16,21)FREQ,VMAGdB    !             and write
       WRITE(17,21)FREQ,VANG      !                 AGRAPH files.
C                                                                      *
C******************* END-XMTR-VOLTAGE-STEP-RESPONSE ********************
C
C***************** START-XMTR/RCVR-VOLTAGE-STEP-RESPONSE ***************
```

```
C                                                                      *
C     Now, apply the voltage to the RCVR circuit and compute the
C  combined XMTR/RCVR step response.  The output voltage, VXMRCS, is
C  the output Voltage of the combined XMtr/RCvr Step response test.
C
C
      IF(MODEL.EQ.0)THEN          ! Then do simplified model...
C
      VZ7=VZLFXS*Z7/Z8            ! The voltage across impedance "Z7".
      VSECR=VZ7*(PHI**2)*Z5/Z6    ! The voltage across secondary (phi).
      VPRIR=VSECR/PHI             ! The voltage across the primary (1).
      VXMRCS=VPRIR*ZROCO/Z5       !**Desired XMTR/RCVR output voltage.**
C
      ELSE                        ! Else do full model...
      VZ9=VZLFXS*Z9/Z10           ! Voltage across impedance "Z9".
      IF(MODEL.EQ.1)GO TO 145     ! Skip unless matched front required.
      VZ12=VZLFXS*Z12/Z13         !
      VZ9=VZ12*Z9/Z11             !
145   VZ7=VZ9*Z7/Z8               ! Voltage across impedance "Z7".
      VSECR=VZ7*(PHI**2)*Z5/Z6    ! Voltage across secondary (phi) side.
      VPRIR=VSECR/PHI             ! Voltage across primary (1) side.
      VXMRCS=VPRIR*ZROCO/Z5       !**Desired XMTR/RCVR output voltage.**
C
      END IF
C
      VXMRCSRE=REAL(VXMRCS)       ! The real part of the voltage.
      VXMRCSIM=AIMAG(VXMRCS)      ! The imaginary part of the voltage.
      VMAG=CABS(VXMRCS)           ! The magnitude of the voltage.
      VANG=DATAN2(VXMRCSIM,VXMRCSRE)*180./PI  ! The voltage phase (Deg).
      VXMRCSMG(1+N/2-I)=VMAG      ! Set
      VXMRCSAN(1+N/2-I)=-VANG     !     up
      IF(I.EQ.NO2)GO TO 150       !        inverse
      VXMRCSMG(1+N/2+I)=VMAG      !                FFT
      VXMRCSAN(1+N/2+I)=VANG      !                    arrays.
150   CONTINUE
      VMAGdB=20.*DLOG10(VMAG)     ! Change VMAG to dB
      WRITE(18,21)FREQ,VMAGdB     !             and write
      WRITE(19,21)FREQ,VANG       !                  AGRAPH files.
C                                                                      *
C***************** END-XMTR/RCVR-VOLTAGE-STEP-RESPONSE *****************
C
155   IF(MENU.EQ.1.OR.MENU.EQ.2.OR.MENU.EQ.4)GO TO 1000
C
C***************** START-XMTR-CURRENT-IMPULSE-RESPONSE ******************
C                                                                      *
C     This section analyzes the response of the RCVR to an input
C  current impulse function.  The resulting output voltage (force),
C  will then be used to drive the RCVR circuit to obtain the combined
C  XMTR/RCVR current impulse response.
C
```

```
      DIin=DCMPLX(DONE,ZERO)     ! The current impulse, 1 + j0.
C
      IF(MODEL.EQ.0)THEN         ! Then do simplified model...
C
      IZ3=DIin*ZR0C0/(ZR0C0+Z3)  ! The current into impedance "Z3".
      VZ3=IZ3*Z3                 ! The voltage across impedance "Z3".
      VPRIX=VZ3*(Z1/(PHI**2))/Z3 ! Voltage across primary side.
      VSECX=VPRIX*PHI            ! Voltage across the secondary side.
      VZ=VSECX*Z/Z1              ! Voltage across impedance "Z".
      VZLFII=VZ*ZLF/ZF           !**Desired output XMTR voltage.**
C
      ELSE                       ! Else do full model...
      IZ3=DIin*ZR0C0/(ZR0C0+Z3)  ! The current into impedance "Z3".
      VZ3=IZ3*Z3                 ! The voltage across impedance "Z3".
      VPRIX=VZ3*(Z1/(PHI**2))/Z3 ! Voltage across the primary side.
      VSECX=VPRIX*PHI            ! Voltage across secondary side.
      VZ=VSECX*Z/Z1              ! Voltage across impedance "Z".
      VZFE=VZ*ZFE/ZFET           ! Voltage across impedance "ZFE".
      VZLFII=VZFE*ZLF/ZF         !**Desired output XMTR voltage.**
      IF(MODEL.EQ.1)GO TO 156    ! Skip unless matched front required.
      VZFM=VZFE*ZFM/ZF           !
      VZLFII=VZFM*ZLF/ZMF        !
156   CONTINUE
C
      END IF
C
      VZLFIIRE=REAL(VZLFII)      ! Real part of the voltage.
      VZLFIIIM=AIMAG(VZLFII)     ! Imaginary part of the voltage.
      VMAG=CABS(VZLFII)          ! The magnitude of the voltage.
      VANG=DATAN2(VZLFIIIM,VZLFIIRE)*180./PI  ! The voltage phase (Deg).
      VZLFIIMG(1+N/2-I)=VMAG     ! Set
      VZLFIIAN(1+N/2-I)=-VANG    !     up
      IF(I.EQ.NO2)GO TO 160      !        inverse
      VZLFIIMG(1+N/2+I)=VMAG     !                FFT
      VZLFIIAN(1+N/2+I)=VANG     !                    arrays.
160   CONTINUE
      VMAGdB=20.*DLOG10(VMAG)    ! Change VMAG to dB
      WRITE(20,21)FREQ,VMAGdB    !             and write
      WRITE(21,21)FREQ,VANG      !                  AGRAPH files.
C                                                                *
C***************** END-XMTR-CURRENT-IMPULSE-RESPONSE ******************
C
C**************** START-XMTR/RCVR-CURRENT-IMPULSE-RESPONSE *************
C                                                                *
C     This section now applies the XMTR output voltage (force) to the
C  face of the RCVR and computes the resulting output voltage across
C  electrodes.  The results give the overall XMTR/RCVR current impulse
C  response.
C
C
```

```
      IF(MODEL.EQ.0)THEN          ! Then do simplified model...
C
      VZ7=VZLFII*Z7/Z8            ! The voltage across impedance "Z7".
      VSECR=VZ7*(PHI**2)*Z5/Z6    ! The voltage across secondary (phi).
      VPRIR=VSECR/PHI             ! The voltage across the primary (1).
      VXMRII=VPRIR*ZR0C0/Z5       ! **Desired XMTR/RCVR output voltage.**
C
      ELSE                        ! Else do full model...
      VZ9=VZLFII*Z9/Z10           ! Voltage across impedance "Z9".
      IF(MODEL.EQ.1)GO TO 166     ! Skip unless matching front required.
      VZ12=VZLFII*Z12/Z13         !
      VZ9=VZ12*Z9/Z11             !
166   VZ7=VZ9*Z7/Z8               ! Voltage across impedance "Z7".
      VSECR=VZ7*(PHI**2)*Z5/Z6    ! Voltage across secondary (phi) side.
      VPRIR=VSECR/PHI             ! Voltage across primary (1) side.
      VXMRII=VPRIR*ZR0C0/Z5       !**Desired XMTR/RCVR output voltage.**
C
      END IF
C
      VXMRIIRE=REAL(VXMRII)       ! The real part of the voltage.
      VXMRIIIM=AIMAG(VXMRII)      ! The imaginary part of the voltage.
      VMAG=CABS(VXMRII)           ! The magnitude of the voltage.
      VANG=DATAN2(VXMRIIIM,VXMRIIRE)*180./PI  ! The voltage phase (Deg).
      VXMRIIMG(1+N/2-I)=VMAG      ! Set
      VXMRIIAN(1+N/2-I)=-VANG     !     up
      IF(I.EQ.NO2)GO TO 170       !        inverse
      VXMRIIMG(1+N/2+I)=VMAG      !                FFT
      VXMRIIAN(1+N/2+I)=VANG      !                    arrays.
170   CONTINUE
      VMAGdB=20.*DLOG10(VMAG)     ! Change VMAG to dB
      WRITE(22,21)FREQ,VMAG       !             and write
      WRITE(23,21)FREQ,VANG       !                  AGRAPH files.
C                                                                      *
C**************** END-XMTR/RCVR-CURRENT-IMPULSE-RESPONSE ***************
C
1000  CONTINUE
1001  CONTINUE
C                                                                     ****
C*********************************************************************
C******************END OF MAIN FREQUENCY LOOP*************************
C*********************************************************************
C
C
      IF(MENU.EQ.8)THEN
      PRINT*,'DO YOU WANT TIME DOMAIN PLOTS?'
      PRINT*,'ENTER 0 = NO , 1 = YES'
      READ*,NTIME
      IF(NTIME.EQ.0)GO TO 10000
      END IF
      IF(MENU.EQ.0.OR.FLOW.NE.0.)GO TO 10000
```

```
1500   CONTINUE
C
C
       IF(MENU.NE.8)GO TO 1750
       DO K=II,NO2                    ! Zero
       FREQ=FLOW + FLOAT(K)*DELTAF    ! out
       VZLFXIMG(1+NO2-K)=ZERO         !     the
       VZLFXIAN(1+NO2-K)=ZERO         !         unused
       VXMRCIMG(1+NO2-K)=ZERO         !               endpoints
       VXMRCIAN(1+NO2-K)=ZERO         !                  of
       IF(K.EQ.NO2)GO TO 1700         !                     the
       VZLFXIMG(1+NO2+K)=ZERO         !                       spectral
       VZLFXIAN(1+NO2+K)=ZERO         !                         arrays
       VXMRCIMG(1+NO2+K)=ZERO         !      for
       VXMRCIAN(1+NO2+K)=ZERO         !         zero-
       WRITE(10,21)FREQ,ZERO          !            padding
       WRITE(14,21)FREQ,ZERO          !               ...
1700   CONTINUE
       END DO
1750   ONE=1     !
C
C
C****START-INVERSE-FFT*****START-INVERSE-FFT*****START-INVERSE-FFT******
C                                                                      *
C      This section calls an inverse FFT and outputs the time domain
C   results for each transfer function section.  Since the FFT routine
C   exchanges the frequency and time domain arrays, the x-axis frequency
C   array must be refreshed before each inverse FFt call.
C      Since the inverse FFT routine assumes unity spacing in the time-
C   domain (for amplitude scaling purposes) the resulting inverse FFT
C   amplitudes will need to be divided by the sampling frequency in Hz.
C
       KIN=1                          ! Specifies polar frequency input.
       KOUT=0                         ! Specifies rectangular time output.
       INVERT=1                       ! Specifies inverse FFT.
       IMPULSE=-1                     ! For 2-sided input/nonperiodic output
       N=N*8                          ! Increase spectral resolution by 8x.
       FSAMPLE=8.*FSAMPLE             ! Increase sampling rate by 8x.
       NO2=N/2
       NO4=N/4
       DO 1800 K=1,NO2                ! Set up the permanent frequency array.
       FREQ=FLOAT(K)*DELTAF
       FT(1+NO2-K)=-FREQ*1.E6         ! First the left side of the array,
       IF(K.EQ.NO2)GO TO 1800
       FT(1+NO2+K)=FREQ*1.E6          !  and now the right side of the array.
1800   CONTINUE
       FT(1+NO2)=0.
C
       IF(MENU.EQ.2.OR.MENU.EQ.3)GO TO 4700
C
```

```
C     First, voltage impulse response test of the XMTR
C           (or burst response of the XMTR).
C
      DO 2000 K=1,N                ! Copy frequency values into the
2000  FTCALL(K)=FT(K)              !     calling frequency array.
      DO 2100 K=1,N                ! Zero out the temporary
      TEMP1(K)=0.                  !     spectral
2100  TEMP2(K)=0.                  !              arrays.
      DO 2200 K=1,NO4              ! Now copy the model's spectral
      TEMP1(K+7*N/16)=VZLFXIMG(K)  !     results to the center of the
2200  TEMP2(K+7*N/16)=VZLFXIAN(K)  !      temporary spectral arrays.
      DO 2300 K=1,N                ! Now copy the zero-padded spectral
      VZLFXIMG(K)=TEMP1(K)         !   results back into the FFT
2300  VZLFXIAN(K)=TEMP2(K)         !     calling spectral arrays.
C
C     Now ready to call inverse FFT subroutines ...
C
      CALL FFT1(FTCALL,IMPULSE,VZLFXIMG,VZLFXIAN,N,INVERT,KIN,KOUT)
      DO 2500 J=1,N
      IF(MOD(J,MFACT).NE.1)GO TO 2500
      IF(FTCALL(J).LT.PLOW.OR.FTCALL(J).GT.PHIGH)GO TO 2500
      Vt=VZLFXIMG(J)/FSAMPLE       ! Correct for unity sampling of FFT
      WRITE(30,22)FTCALL(J),Vt     ! Write out the results
2500  CONTINUE
C
      IF(MENU.EQ.7.OR.MENU.EQ.8)GO TO 3900
C
C     Now the impulse response test of the RCVR.
C
      DO 3000 K=1,N                ! Copy frequency values into the
3000  FTCALL(K)=FT(K)              !     calling frequency array.
      DO 3100 K=1,N                ! Zero out the temporary
      TEMP1(K)=0.                  !     spectral
3100  TEMP2(K)=0.                  !        arrays.
      DO 3200 K=1,NO4              ! Now copy the model's spectral
      TEMP1(K+7*N/16)=VRCVRIMG(K)  !     results to the center of the
3200  TEMP2(K+7*N/16)=VRCVRIAN(K)  !       temporary spectral arrays.
      DO 3300 K=1,N                ! Now copy the zero-padded spectral
      VRCVRIMG(K)=TEMP1(K)         !   results back into the FFT
3300  VRCVRIAN(K)=TEMP2(K)         !     calling spectral arrays.
C
C Now ready to call inverse FFT subroutines ...
C
      CALL FFT1(FTCALL,IMPULSE,VRCVRIMG,VRCVRIAN,N,INVERT,KIN,KOUT)
      DO 3500 J=1,N
      IF(MOD(J,MFACT).NE.1)GO TO 3500
      IF(FTCALL(J).LT.PLOW.OR.FTCALL(J).GT.PHIGH)GO TO 3500
      Vt=VRCVRIMG(J)/FSAMPLE       ! Correct for unity sampling of FFT
      WRITE(31,22)FTCALL(J),Vt     ! Write out the results
3500  CONTINUE
```

```
C
3900  CONTINUE
C
C     Now the impulse response test of the XMTR/RCVR
C             (or burst response of the XMTR/RCVR).
C
      DO 4000 K=1,N                ! Copy frequency values into the
4000  FTCALL(K)=FT(K)              !     calling frequency array.
      DO 4100 K=1,N                ! Zero out the temporary
      TEMP1(K)=0.                  !     spectral
4100  TEMP2(K)=0.                  !        arrays.
      DO 4200 K=1,NO4               ! Now copy the model's spectral
      TEMP1(K+7*N/16)=VXMRCIMG(K)  !    results to the center of the
4200  TEMP2(K+7*N/16)=VXMRCIAN(K)  !      temporary spectral arrays.
      DO 4300 K=1,N                ! Now copy the zero-padded spectral
      VXMRCIMG(K)=TEMP1(K)         !   results back into the FFT
4300  VXMRCIAN(K)=TEMP2(K)         !     calling spectral arrays.
C
C Now ready to call the inverse FFT subroutine ...
C
      CALL FFT1(FTCALL,IMPULSE,VXMRCIMG,VXMRCIAN,N,INVERT,KIN,KOUT)
      DO 4500 J=1,N
      IF(MOD(J,MFACT).NE.1)GO TO 4500
      Vt=VXMRCIMG(J)/FSAMPLE       ! Correct for unity sampling of FFT
      IF(FTCALL(J).LT.(PLOW).OR.FTCALL(J).GT.(PHIGH))GO TO 4500
      WRITE(32,22)FTCALL(J),Vt     ! Write out the results.
4500  CONTINUE
C
      IF(MENU.EQ.7.OR.MENU.EQ.8)GO TO 10000
4700  IF(MENU.EQ.1.OR.MENU.EQ.3.OR.MENU.EQ.5)GO TO 6700
C
C     Now the voltage step response of the XMTR.
C
      DO 5000 K=1,N                ! Copy frequency values into the
5000  FTCALL(K)=FT(K)              !     calling frequency array.
      DO 5100 K=1,N                ! Zero out the temporary
      TEMP1(K)=0.                  !     spectral
5100  TEMP2(K)=0.                  !        arrays.
      DO 5200 K=1,NO4              ! Now copy the model's spectral
      TEMP1(K+7*N/16)=VZLFXSMG(K)  !    results to the center of the
5200  TEMP2(K+7*N/16)=VZLFXSAN(K)  !      temporary spectral arrays.
      DO 5300 K=1,N                ! Now copy the zero-padded spectral
      VZLFXSMG(K)=TEMP1(K)         !    results back into the FFT
5300  VZLFXSAN(K)=TEMP2(K)         !     calling spectral arrays.
C
C Now ready to call the inverse FFT subroutines ...
C
      CALL FFT1(FTCALL,IMPULSE,VZLFXSMG,VZLFXSAN,N,INVERT,KIN,KOUT)
      DO 5500 J=1,N
      IF(MOD(J,MFACT).NE.1)GO TO 5500
```

```
      IF(FTCALL(J).LT.PLOW.OR.FTCALL(J).GT.PHIGH)GO TO 5500
      Vt=VZLFXSMG(J)/FSAMPLE       ! Correct for unity sampling of FFT
      WRITE(33,22)FTCALL(J),Vt     ! Write out the results.
5500  CONTINUE
C
C     Now the voltage step response of the XMTR/RCVR.
C
      DO 6000 K=1,N                ! Copy frequency values into the
6000  FTCALL(K)=FT(K)              !     calling frequency array.
      DO 6100 K=1,N                ! Zero out the temporary
      TEMP1(K)=0.                  !     spectral
6100  TEMP2(K)=0.                  !       arrays.
      DO 6200 K=1,NO4              ! Now copy the model's spectral
      TEMP1(K+7*N/16)=VXMRCSMG(K)  !    results to the center of the
6200  TEMP2(K+7*N/16)=VXMRCSAN(K)  !      temporary spectral arrays.
      DO 6300 K=1,N                ! Now copy the zero-padded spectral
      VXMRCSMG(K)=TEMP1(K)         !    results back into the FFT
6300  VXMRCSAN(K)=TEMP2(K)         !       calling spectral arrays.
C
C Now ready to call the inverse FFT subroutines ...
C
      CALL FFT1(FTCALL,IMPULSE,VXMRCSMG,VXMRCSAN,N,INVERT,KIN,KOUT)
      DO 6500 J=1,N
      IF(MOD(J,MFACT).NE.1)GO TO 6500
      IF(FTCALL(J).LT.PLOW.OR.FTCALL(J).GT.PHIGH)GO TO 6500
      Vt=VXMRCSMG(J)/FSAMPLE       ! Correct for unity sampling of FFT
      WRITE(34,22)FTCALL(J),Vt     ! Write out the results.
6500  CONTINUE
C
6700  IF(MENU.EQ.1.OR.MENU.EQ.2.OR.MENU.EQ.4)GO TO 10000
C
C     Now the current impulse response of the XMTR.
C
      DO 7000 K=1,N                ! Copy frequency values into the
7000  FTCALL(K)=FT(K)              !     calling frequency array.
      DO 7100 K=1,N                ! Zero out the
      TEMP1(K)=0.                  !     spectral
7100  TEMP2(K)=0.                  !       arrays.
      DO 7200 K=1,NO4              ! Now copy the model's spectral
      TEMP1(K+7*N/16)=VZLFIIMG(K)  !    results to the center of the
7200  TEMP2(K+7*N/16)=VZLFIIAN(K)  !      temporary spectral arrays.
      DO 7300  K=1,N               ! Now copy the zero-padded spectral
      VZLFIIMG(K)=TEMP1(K)         !    results back into the FFT
7300  VZLFIIAN(K)=TEMP2(K)         !       calling spectral arrays.
C
C Now ready to call the inverse FFT subroutines ...
C
      CALL FFT1(FTCALL,IMPULSE,VZLFIIMG,VZLFIIAN,N,INVERT,KIN,KOUT)
      DO 7500 J=1,N
      IF(MOD(J,MFACT).NE.1)GO TO 7500
```

```
      IF(FTCALL(J).LT.PLOW.OR.FTCALL(J).GT.PHIGH)GO TO 7500
      Vt=VZLFIIMG(J)/FSAMPLE      ! Correct for unity sampling of FFT
      WRITE(35,22)FTCALL(J),Vt    ! Write out the results.
7500  CONTINUE
C
C     Now the current impulse response of the XMTR/RCVR.
C
      DO 8000 K=1,N               ! Copy frequency values into the
8000  FTCALL(K)=FT(K)             !     calling frequency array.
      DO 8100 K=1,N               ! Zero out the temporary
      TEMP1(K)=0.                 !     spectral
8100  TEMP2(K)=0.                 !       arrays.
      DO 8200 K=1,NO4             ! Now copy the model's spectral
      TEMP1(K+7*N/16)=VXMRIIMG(K) !    results to the center of the
8200  TEMP2(K+7*N/16)=VXMRIIAN(K) !       temporary spectral arrays.
      DO 8300 K=1,N               ! Now copy the zero-padded spectral
      VXMRIIMG(K)=TEMP1(K)        !    results back into the FFT
8300  VXMRIIAN(K)=TEMP2(K)        !       calling spectral arrays.
C
C Now ready to call the inverse FFT subroutines ...
C
      CALL FFT1(FTCALL,IMPULSE,VXMRIIMG,VXMRIIAN,N,INVERT,KIN,KOUT)
      DO 8500 J=1,N
       IF(MOD(J,MFACT).NE.1)GO TO 8500
      IF(FTCALL(J).LT.PLOW.OR.FTCALL(J).GT.PHIGH)GO TO 8500
      Vt=VXMRIIMG(J)/FSAMPLE      ! Correct for unity sampling of FFT
      WRITE(36,22)FTCALL(J),Vt    ! Write out the results.
8500  CONTINUE
C
C
C %%%%%%%%%%%%%%%%%%%%%%%%%%%%%%%%%%%%%%%%%%%%%%%%%%%%%%%%%%%%%%%%%%%%%%%%%%%
10000 CONTINUE          ! %%%%%%%%%%% END OF MAIN PROGRAM %%%%%%%%%%%%%%%
C %%%%%%%%%%%%%%%%%%%%%%%%%%%%%%%%%%%%%%%%%%%%%%%%%%%%%%%%%%%%%%%%%%%%%%%%%%%
      STOP
      END
C                                                                          ###
C##########################################################################
C############ END OF MAIN PROGRAM - START OF FFT ROUTINES ##############
C##########################################################################
C                                                                          ###
C   This FFT program package contains five subroutine subprograms -
c      FFT, FFT1, FFTCENTER, FFTRECT, and FFTPOLAR.
c
c   The main subroutine is FFT. This subroutine is the one that performs
c     FFT calculations.  The other four serve to make FFT more friendly
c     and easier to use.
c
c   Unit 88 must be assigned to be the terminal display screen.  This is
c      done in the E. E. Class Library on execution of command file
c      LLOGIN.COM.
```

```
C                                                                       *
C***********************************************************************
C                                                                       *
                      SUBROUTINE FFT1(FT,IMPULSE,SR,SI,N,INVERT,KIN,KOUT)
      IMPLICIT REAL*8(A-H,O-Z)
c
c           written by A. A. Read,  August 1981
c           modified by L. F. Brown, September, 1987
c
c   See FFT description for all parameters except FT and IMPULSE.
c  This routine permits painless conversion of a signal from the
c    nonperiodic time (or frequency) domain to the periodic frequency
c    (or time) domain or from the periodic time (or frequency) domain
c    to the nonperiodic frequency (or time) domain.  For example the
c    impulse response and the transfer functions of a linear system
c    are nonperiodic in the time and frequency domains respectively.
c    The nonperiodic frequency spectrum of a signal is often known
c    but not the corresponding time signal.  On the other hand, the
c    FFT assumes the signal to be periodic in both the time and the
c    frequency domains.
c
c  The parameter IMPULSE permits the following conversions:
c
c    IMPULSE > 0  Converts a nonperiodic two-sided frequency spectrum
c                 given at a finite number of evenly spaced frequencies
c                 to be transformed into a periodic time response, e.g.,
c                 a transfer function into an impulse response.
c
c            = 0  No conversion.  Use if signal is already periodic
c                 in both time and frequency domains.
c            < 0  Converts periodic time (or frequency) response
c                 back into nonperiodic frequency (or time) domain.
c
c  The array FT on input contains the time (or frequency) sampling
c    points and is returned as frequency (or time) sampled points
c    Only the array values of FT(1) and FT(N) need be supplied in
c    the call to FFT1.
c
c
c  The User's attention is called to the fact address N/2 + 1
c     is taken as the center or zero of the independent variable
c     whether it is time or frequency.
c
      dimension ft(1),sr(1),si(1)
c
c
        dft=(ft(n)-ft(1))/float(n-1)
        fto=dft*float(n)
        call fft(sr,si,n,invert,kin,kout)
      if(fto.eq.0.0) then
```

```
        write(88,510)
510   format(/,'  WARNING: YOUR TIME-FREQUENCY FILE ',
     +'CONTAINS NO USEFUL DATA.',/,5X,'CALCULATION '
     +'PROCEEDING ASSUMING UNIT SPACING BETWEEN SAMPLES')
        fto=1.0
        dft=1.0
      end if
        n2=n/2+1
      if(impulse.lt.0) dft=fto
      do i=1,n
        ft(i)=float(i-n2)/fto
      if(impulse.ne.0) then
        sr(i)=sr(i)*dft
      if(kout.eq.0) si(i)=si(i)*dft
      end if
      end do
      return
      end
c
c                                                                       *
c***********************************************************************
c                                                                       *
       SUBROUTINE FFT(SR,SI,N,INVERT,KIN,KOUT)
       IMPLICIT REAL*8(A-H,O-Z)
c
c  Origin unknown.  Modified and Filed by A. A. Read, November 1979
c                   Further modified by L. F. Brown, September, 1987
c
c  This subroutine implements the Sande-Tukey radix-2 Fast Fourier
c   Transform.  Either the direct or the inverse transform of
c   complex valued inputs can be computed.
c
c   Complex values of the input are given FFT in the vector arrays
c     sr and si.  If the signal is entirely real, all si's are
c     zero and must be given zero values by the calling program.
c     During program execution, the input values are replaced by
c     the transformed values.
c
c   PARAMETERS:
c
c     N       The order of the FFT.  This should be a positive integer
c             power of 2 such as 2,4,....,32,64,128,256,512,1024,2048,
c             .....,65536.  If not, the program will pick the nearest
c             lower positive integer power of 2 with the resultant
c             probability of large calculation errors or of aborted
c             execution.
c
c     INVERT Specifies either the direct or the inverse transform

c             If INVERT  =< 0  compute the direct FFT
```

```
c                INVERT   > 0  compute the inverse FFT
c
c     KIN     Kind of input data format
c             KIN  < 0  sr,si input in polar format in radians
c             KIN  = 0  sr,si input in rectangular format
c             KIN  > 0  sr,si input in polar format in degrees
c
c     KOUT  Kind of output date format desired
c             KOUT < 0  sr,si output in polar format in radians
c             KOUT = 0  sr,si output in rectangular format
c             KOUT > 0  sr,si output in polar format in degrees
c
c   COMMENTS: The FFT performs a two-sided frequency transformation
c     or the inverse.  The independent variables are time or frequency.
c     Values of these independent variables are never supplied FFT.
c     Only sampled values of the signal or its spectrum at evenly
c     spaced independent variable points are given FFT (in arrays
c     sr and si).  The evenly spaced independent variable sampling
c     points are implied, however, by the address locations of the
c     corresponding signal values in arrays sr and si.  In this
c     implementation of the FFT, both t=0 and f=0 are assumed to
c     correspond to address location N/2+1 in arrays sr and si.
c     In the frequency spectrum then, address 1 in sr and si
c     corresponds to the negative N/2 harmonic of the signal window
c     in time while address N in sr and si corresponds to the positive
c     N/2-1 harmonic.  In terms of frequency spectrum,, address N/2+1
c     of sr and si give the dc components of the spectrum.
c
c    The FFT assumes a unit separation between sampling points.  If that
c     is not true, then the transform must be modified in amplitude
c     according to the results of the SIMILARITY Theorem.  Attached
c     subroutine FFT1 takes that into account.  Refer to the comments
c     given in the FFT1 source code.
c
c
c   Subroutines FFTCENTER, FFTPOLAR, and FFTRECT added September
c     1979 so that both x=0 and f=0 are located at array addresses
c     N/2+1 on entry and exit for both direct and inverse transforms
c     and so complex valued variables could be handled more easily.
c
c   This routine assumes x=0,f=0 start at array addresses 1.  To make
c     it easier to use, the subroutine FFTCENTER was added so the signal
c     would be symmetrical about center of the array and more in keeping
c     with most persons visualization of a periodic signal.
c
c     Subroutine FFT1 added August 1981 to facilitate painless
c     application of the Similarity Theorem.
c
c   N should be modulus 2, i.e., 2,4,8,16,.....,2**16(maximum).  If
c     not the routine will pick the next modulus 2 above N to use in
```

```
c     the calculation.  Trouble will develope if the arrays sr,si are
c     not appropriately dimensioned in the calling program or if extra-
c     neous values exist in these additional array positions.
c
c
      dimension sr(1),si(1),ur(15),ui(15)
      logical first
      data first/.true./
      if(.not.first) go to 120
c
c  This routine assumes an exp(-j2 pi n f0) FFT kernal.
c  Here uk=ur(k)+jui(k) and u15=u1**(1/2**15) = [exp(j2pi)]**(1/2**16)
c    Then uk=u15**(16-k)  where ur(1)=cos(pi/2) and ui(1)=sin(pi/2)
c
      ur(1)=0.0
      ui(1)=1.0
      do m=2,15
        ur(m)=DSQRT((1.0+ur(m-1))/2.0)
        ui(m)=ui(m-1)/(2.0*ur(m))
      end do
      first=.false.
120   if(n.gt.0 .and. n.le.2**16) go to 125
      write(88,510),n
510   format(/,'   WARNING:  Your FFT order =',i4,' and is illegal',
     1    /,'   Execution Ceasing.  CHECK YOUR PROGRAM.')
      stop
125   continue
      call fftcenter(sr,si,n)  ! Added 9-10-79 to adjust spectrum
      kkin=kin
      if(kkin.ne.0) call fftrect(sr,si,n,kkin)
c
c   find an N0 => N
c
130   n0=1
      ii=0
140   n0=n0+n0
      ii=ii+1
      if(n0+n0.le.n) go to 140
      i1=n0/2
c
      i3=1
      i0=ii
      do 260 i4=1,ii
        do 250 k=1,i1
          wr=1.0
          wi=0.0
          kk=k-1
          do 230 i=1,i0
            if(kk.eq.0) go to 240
            if(mod(kk,2) .eq.0) go to 230
```

```
            j0=i0-i
            ws=wr*ur(j0)-wi*ui(j0)
            wi=wr*ui(j0)+wi*ur(j0)
            wr=ws
230       kk=kk/2
240     if(invert.eq.0) wi=-wi
        l=k
        do 250 j=1,i3
          ll=l+il
          zr=sr(l)+sr(ll)
          zi=si(l)+si(ll)
          z=wr*(sr(l)-sr(ll))-wi*(si(l)-si(ll))
          si(ll)=wr*(si(l)-si(ll))+wi*(sr(l)-sr(ll))
          sr(ll)=z
          sr(l)=zr
          si(l)=zi
250       l=ll+il
        i0=i0-l
        i3=i3+i3
260   il=il/2
      um=1.0
      if(invert.eq.0) um=1.0/float(n0)
      do 310 j=1,n0
        k=0
        jl=j-1
        do 320 i=1,ii
          k=2*k+mod(jl,2)
320     jl=jl/2
      k=k+1
      if(k.lt.j) go to 310
      zr=sr(j)
      zi=si(j)
      sr(j)=sr(k)*um
      si(j)=si(k)*um
      sr(k)=zr*um
      si(k)=zi*um
310   continue
      call fftcenter(sr,si,n) ! Added 9-10-79 to center spectrum
      kkout=kout
      if(kkout.ne.0) call fftpolar(sr,si,n,kkout)
      return
      end
C                                                                      *
C**********************************************************************
C                                                                      *
      SUBROUTINE FFTCENTER(X,Y,N)
      IMPLICIT REAL*8(A-H,O-Z)
c                      written by A. A. Read, September 1979
c         modified by L. F. Brown, September, 1987
c
```

```
c  A routine to interchange the top half of an array pair with the
c    lower half of the respective arrays.  Such a routine is needed
c    and useful in the FFT routine so that both f=0 and x=0 will be
c    centered in the arrays around the location n/2+1.   For this FFT
c    the arrays are "centered" on exit of the direct transform to
c    center the frequency spectrum and on entry of the inverse transform
c    to move the f=0 to location 1 and f=-n/2 to location n/2+1 as
c    required by the FFT routine.
c
      dimension x(1),y(1)
      m=n/2
      do 50 i=1,m
      j=m+i
      a=x(i)
      x(i)=x(j)
      x(j)=a
      a=y(i)
      y(i)=y(j)
      y(j)=a
50    continue
      return
      end
C                                                                       *
C***********************************************************************
C                                                                       *
      SUBROUTINE FFTRECT(Z,A,N,KIN)
      IMPLICIT REAL*8(A-H,O-Z)
c
c          written by A. A. Read, September 1979
c          modified by L. F. Brown, September, 1987
c
c        If kin   > 0 input in degrees
c        If kin  =< 0 input in radians
c
      dimension z(1),a(1)
      do 50 i=1,n
      ang=a(i)
      if(ang.eq.0.0) go to 50
      if(kin.gt.0) ang=ang/57.29578
      a(i)=z(i)*DSIN(ang)
      z(i)=z(i)*DCOS(ang)
50    continue
      return
      end
C                                                                       *
C***********************************************************************
C                                                                       *
      SUBROUTINE FFTPOLAR(X,Y,N,KOUT)
      IMPLICIT REAL*8(A-H,O-Z)
c         written by A. A. Read, circa 1978
```

```
c         modified by L. F. Brown, September, 1987
c
c        If kout   > 0 return in degrees
c        If kout  =< 0 return in radians
c
      dimension x(1),y(1)
      do i=1,n
C
        IF( DABS(x(i)) .LT. 1.E-15 .AND. x(i) .NE. 0. )x(i)=1.E-15
        IF( DABS(y(i)) .LT. 1.E-15 .AND. y(i) .NE. 0. )y(i)=1.E-15
C     This prevents underflow when squaring to obtain the magnitude. lfb
        a=DSQRT(x(i)*x(i)+y(i)*y(i))
        if(a.eq.0.0) x(i)=1.0    !  This prevents trouble with ATAN2
        y(i)=DATAN2(y(i),x(i))
        x(i)=a
        if(kout.gt.0) y(i)=y(i)*57.29578
      end do
      return
      end
C                                                                       ###
C ########################################################################
C ###################### END OF FFT ROUTINES #############################
C ########################################################################
C
```

XXI. APPENDIX L: PVF_2 - $P(VF_2-VF_3)$ PERFORMANCE SIMULATIONS

Table 21.1. Comparison of untuned performance simulations

PARAMETER	PVF_2	$P(VF_2-VF_3)$
Thickness (microns)	31.75	30.00
f_s (MHz)	36.611	36.970
Air-backed Q_m	13.489	13.589
XMTR Voltage Impulse Response (Untuned, unmatched)		
Frequency of peak (MHz)	36.210	36.300
Magnitude of peak (dB)	-12.395	-8.853
Lower 3-dB freq. (MHz)	27.713	27.304
Upper 3-dB freq. (dB)	44.645	45.183
3-dB Bandwidth (MHz)	16.932	17.879
3-dB Q	2.139	2.030
2 MHz Burst amplitude (mV)	9.500	15.000
RCVR Voltage Impulse Response (Untuned, unmatched)		
Frequency of peak (MHz)	36.050	36.294
Magnitude of peak (dB)	-19.911	-15.294
Lower 3-dB freq. (MHz)	30.465	30.465
Upper 3-dB freq. (MHz)	40.375	40.802
3-dB Bandwidth (MHz)	9.910	10.337
3-dB Q	3.638	3.511
XMTR/RCVR Voltage Impulse Response (Untuned, unmatched)		
Frequency of peak (MHz)	36.100	36.291
Magnitude of peak (dB)	-32.307	-24.147
Lower 3-dB freq. (MHz)	31.869	31.815
Upper 3-dB freq. (MHz)	39.765	40.154
3-dB Bandwidth (MHz)	7.896	8.339
3-dB Q	4.572	4.352
2 MHz Burst amplitude (mV)	0.450	1.280

Table 21.2. Comparison of untuned performance simulations

PARAMETER	PVF_2	$P(VF_2-VF_3)$
Thickness (microns)	31.75	30.00
f_s (MHz)	36.611	36.970
Air-backed Q_m	13.489	13.589
XMTR Voltage Impulse Response (Untuned, back-matched)		
Frequency of peak (MHz)	34.990	34.055
Magnitude of peak (dB)	-17.756	-13.975
Lower 3-dB freq. (MHz)	17.236	16.468
Upper 3-dB freq. (dB)	54.518	55.268
3-dB Bandwidth (MHz)	37.282	38.800
3-dB Q	0.939	0.878
2 MHz Burst amplitude (mV)	13.800	21.900
RCVR Voltage Impulse Response (Untuned, back-matched)		
Frequency of peak (MHz)	34.847	36.206
Magnitude of peak (dB)	-16.674	-12.819
Lower 3-dB freq. (MHz)	16.732	23.365
Upper 3-dB freq. (MHz)	46.580	47.226
3-dB Bandwidth (MHz)	29.848	23.861
3-dB Q	1.167	1.517
XMTR/RCVR Voltage Impulse Response (Untuned, back-matched)		
Frequency of peak (MHz)	25.639	21.892
Magnitude of peak (dB)	-33.434	-24.749
Lower 3-dB freq. (MHz)	12.333	9.999
Upper 3-dB freq. (MHz)	41.848	39.449
3-dB Bandwidth (MHz)	29.515	29.450
3-dB Q	0.869	0.743
2 MHz Burst amplitude (mV)	2.850	10.000

Table 21.3. Comparison of untuned performance simulations

PARAMETER	PVF_2	$P(VF_2-VF_3)$
Thickness (microns)	31.75	30.00
f_s (MHz)	36.611	36.970
Air-backed Q_m	13.489	13.589
XMTR/RCVR Current Impulse Response (Untuned, unmatched)		
Frequency of peak (MHz)	34.350	34.654
Magnitude of peak (dB)	17.930	22.582
Lower 3-dB freq. (MHz)	20.665	20.675
Upper 3-dB freq. (dB)	42.437	42.744
3-dB Bandwidth (MHz)	21.772	22.069
3-dB Q	1.578	1.570
XMTR/RCVR Current Impulse Response (Untuned, back-matched)		
Frequency of peak (MHz)	33.428	32.937
Magnitude of peak (dB)	24.438	28.993
Lower 3-dB freq. (MHz)	0.745	18.239
Upper 3-dB freq. (MHz)	45.555	44.364
3-dB Bandwidth (MHz)	44.810	26.125
3-dB Q	0.746	1.261